UNIVERSIDAD POLITÉCNICA DE MADRID
Escuela Técnica Superior de Ingenieros de Telecomunicación



Conectividad funcional dinámica en Alzheimer: diagnóstico temprano y evolución en el tiempo

D O C T O R A L T H E S I S

Submitted for the degree of Doctor by:

Martín Carrasco Gómez
MSc in Biomedical Engineering

Madrid, 2024




UNIVERSIDAD POLITÉCNICA DE MADRID
Escuela Técnica Superior de Ingenieros de Telecomunicación

Doctoral Degree in Biomedical Engineering

Conectividad funcional dinámica en Alzheimer: diagnóstico temprano y evolución en el tiempo

D O C T O R A L T H E S I S

Submitted for the degree of Doctor by:

Martín Carrasco Gómez
MSc in Biomedical Engineering

Under the supervision of:
Dr. Andrés Santos Lleó

Madrid, 2024

Title: Conectividad funcional dinámica en Alzheimer: diagnóstico temprano y evolución en el tiempo

Author: Martín Carrasco Gómez

Doctoral Programme: Biomedical Engineering

Thesis Supervision:

Dr. Andrés Santos Lleó, full professor and director of the Electric Engineering Department (Departamento de Ingeniería Electrónica) (Supervisor)

External Reviewers:

Thesis Defense Committee:

Thesis Defense Date:

This thesis has been partially supported by the Ministry of Universities through the FPU-00517 grant received by Martín Carrasco Gómez.



A mis abuelos Antonio y Florencia, y a mi bisabuela Visita,
a quienes admiro y me habría gustado conocer mucho más

Agradecimientos

Esta tesis es el producto de mucho esfuerzo, y de una serie de decisiones, coincidencias, éxitos, circunstancias y errores. Pero, sobre todo, es consecuencia del apoyo que he recibido a lo largo de todo este tiempo por parte de muchísimas personas.

En primer lugar, quiero darle las gracias a mi director, Andrés, por su perpetua buena disposición, su confianza en mí, y su optimismo contagioso. Gracias por tu dedicación y por tu apoyo en estos últimos meses estresantes. A mí tutor, José Javier, por su paciencia y por soportar los líos burocráticos (no pocos) vinculados a la tesis. A los miembros del tribunal y a las evaluadoras externas, Maria Grazia y Pilar Garcés, por dedicar su tiempo a esta tesis, que espero hayan disfrutado.

También quiero expresar mi profundo agradecimiento a Fernando por hacerme parte de su maravilloso Centro de Neurociencia Cognitiva y Computacional, por su honestidad y humildad, por su forma única de ayudarnos a crecer, y por toda la confianza que ha depositado en mí. Eres un modelo a seguir, y espero poder continuar aprendiendo mucho más de ti en el futuro.

Y es que lo que hace realmente especial a este centro de investigación son todas las personas bonitas que forman parte del mismo: Bruña, Marcos, Blanca, Lucías (la buena y la mala), Alexo, Echega, Fede, Isa, Soraya, Adelia, Noe, Nacho, Almudena, Héctor, Luis, María, Adri, Dany, Pablo, David, Andrea, Iván, Alberto, Gianluca, Gabi... Mención especial a Jesús y Berto, mis compinches de calambrazos, con los que he compartido viajes y muchos debates, y gracias a los que me he enamorado un poco más de la Ciencia. Y gracias, gracias, gracias a Ale, mi partner in crime, con quien he enfrentado tantos retos, complicaciones, tristezas y éxitos... Eres una científica como la copa de un pino, y me alegro mucho de que nuestros caminos se cruzaran y poder ser tu amigo. ¡Estoy seguro de que seguiremos impulsándonos el uno al otro por mucho tiempo! ¡Me alegro muchísimo de haber hecho el PhD con todos vosotros!

El camino del doctorado ha estado salpicado por otros sucesos y actividades que han traído mucha gente valiosa a mi alrededor. Por un lado, las asociaciones, que aunque han consumido mi tiempo, me han devuelto con creces mi esfuerzo en forma de personas estupendas. En Celera conocí a mi querida G7, de la que estoy superorgulloso, además de otras personas como Alejandro, Víctor, Katya, Marta, Rosa... Y en LFI conocí a Víctor (otra vez??), Óscar, Héctor, Sara, Alberto, Joaquim, Cristian, Mónica... On the other hand, I happened to cross path with some wonderful Houstonian leprechauns that I am proud to call today my American family. Gretchen and Michael, thank you for your infinite generosity, for your trust in this little hobbit, and for your patience and will to teach me and support me. Also for your silliness!! I'm keeping your *"Another day in paradise"* and *"50% namaste 50% fuck off* as axioms in my book of knowledge. Julian... What can I even say? Well, I think I will begin with "¡Cómo eso!" and follow up with "Rest in Pace". Thanks for all those metro conversations, for being such a good listener, and for being so transparent and sharing all your passions and interests with me. I am really looking forward to meet you all again in Houston, and I feel excited and very grateful for the opportunity I have been granted! Onward!

Tengo la suerte también de contar con muchos amigos que han hecho que haya podido disfrutar de todos y cada uno de los tramos de este camino. Pablo y Jesús, mis vatos favoritos... Sé que puedo contar con vosotros estemos donde estemos, y no puedo expresaros lo afortunado que me siento por ello. Gracias por tu autenticidad, Pablo, y esas conversaciones mirando al techo (always in my <3). Gracias por tu infinita amabilidad, Jisus, y por los incontables memes que nos quedan por compartir. Esos Energym (Andrei, Álvaro y Ángel) tienen un hueco especial en mi corazón, y me siento orgullosísimo de cada uno de vosotros, igual que de Patri, César y Nacho. Gabri, mi tocayo de cumple, gracias por enseñarme a disfrutar y por acogerme con el resto de Monkes. Jais, gracias por ser mi mentora de vida, y enseñarme a ver los colores, y muchas otras cosas más, de forma distinta. Katya, I have always admired your open-mindedness and kindness, and I hope you can share with me more of your crazy art in the future. Julia, aka Kolia, tu risa contagiosa y tu honestidad profunda te convierten en un solete portátil. Rocío, tu inesperada amistad me ha alegrado mucho por estos años, y espero que podamos compartir historias (escritas y habladas) por mucho tiempo. Linda and John, thanks for treating me like another member of your lovely family, I'm sure I'll visit shortly!! Por supuesto, a mis hermanos del Alto Mando, a quienes debo mucha parte de ser quien soy, y con quienes me gustaría averiguar de qué va la vida. David, mi faro y mi piedra de toque (y collejero, lamentablemente), sé que puedo contar contigo para lo que sea, y que tu cordura me guiará muchas veces, como ya lo ha hecho antes. Uli, mi granuja eterno, el tío más cachopan que puede existir, gracias por los azotes estilo B.K. y por expresar tanto en una mirada. Sergio, mi compinche friki cienzudo del grupo, y un amigo magnífico pese a la tendencia ermitaña. Y Víctor, esa pequeña paradoja (marxista-capitalista, progre-taurino, empático-bruto) hecha persona que tanto me ha enseñado. También a las maravillosas personas que he conocido por ellos: Andrea, Stephy, Irene, Lourdes, Gema. Y a ti Miriam, gracias por 4 años de ensueño, y por darme la oportunidad de demostrarme lo que valgo. Un abrazo también a Jose, Benito, Jenny, Víctor y a toda esa alboratada y bondadosa familia. A los que no he podido mencionar, que sepáis que os tengo en mi mente, y que os agradezco todo el apoyo que me habéis dado durante todo este tiempo.

No podría haber llegado donde estoy sin el apoyo incondicional y amor ilimitado de mi familia. Mamá, gracias por... todo. Gracias por tantas conversaciones en la cocina, por exigirme y por darme con la verdad en la cara cuando tocaba, por tu cariño eterno, por tus mensajes para asegurarte de que estoy bien, por enseñarme gran parte de lo que sé sobre la vida, y sí, también por comprobar continuamente que mi pelo está bien. Papá, gracias por animarme siempre a pensar a lo grande, por enseñarme a ser competitivo y a no dejar de exigirme a mí mismo, por compartir esas "películas de chinos", y por cuidarme todos y cada uno de los día a través de tu comida. Clara, ¡hermana! Me siento tan afortunado de tenerte... Me alegro de que alguien como tú me saque unos años, porque tenerte de brújula me ha ayudado muchísimo siempre. Admiro todo lo que cuidas a aquellos que te rodean, tanto a través del cariño como de la exigencia, y espero poder devolver una parte de ese amor que irradias constantemente. ¡Cuñao! No miento cuando digo que siempre he admirado tu iniciativa y lo adaptable que eres. Antonio siempre el primero en pie, y si surge un problema, se hacen los apaños necesarios para poder superarlo. Ojalá se me haya pegado una parte de ti, y poder seguir creciendo a tu lado. ¡Ana y Álvaro! Mi pareja de ángel y demonio (intercambiables!). Todo tiempo con vosotros es un tesoro, y me siento orgulloso y privilegiado de poder veros crecer día a día.

Chen, disfruto hablar contigo infinito, y adoro poder compartir tu humor; Paco, gracias por compartir conmigo todo tu conocimiento y pasión; Elio, eres como mi hermano pequeño, y me encanta tu forma de emocionarte e ilusionarte, y admiro muchísimo tu talento. Tantas conversaciones, tonterías, historias, cariño, and other monster summer que hemos compartido hacen que la distancia entre nosotros sea inapreciable, y me siento muy afortunado de poder contar con vosotros y de ser vuestra familia.

Gracias a todos y cada uno, tengo muchísima suerte de que hayáis formado parte de mi vida. Ahora, ¡a celebrar!

Abstract

This thesis explores the role of dynamic functional connectivity (dFC) in understanding brain function and its alterations across the Alzheimer's disease (AD) continuum. Traditional functional connectivity (FC) approaches have primarily treated brain connectivity as a static process, neglecting the dynamic nature of brain activity. This research challenges this perspective by employing magnetoencephalography (MEG) to investigate dFC, which captures time-varying interactions between different brain regions, offering potentially earlier biomarkers for AD than static functional connectivity (sFC).

The primary objectives of this thesis are to develop novel methodologies for measuring dFC and to apply these methods to understand the progression of AD. Three main studies were conducted: (1) examining dFC across the full AD spectrum using MEG, (2) investigating the relationship between blood biomarkers (p-Tau231) and dFC in cognitively intact individuals, and (3) assessing the impact of transcranial alternating current stimulation (tACS) on both dFC and sFC within the default mode network (DMN). The findings reveal several key insights:

1. **dFC Across the AD Spectrum**: The first study (Chapter 2) demonstrated a global reduction of dFC in both alpha and beta bands in mild cognitive impairment (MCI) patients, aligning with known posterior-stage disease markers. Spatial analysis showed significant dFC reductions in regions such as the orbitofrontal cortex, temporal pole, hippocampus, and cingulate cortex, which are critical to the progression of AD. These results suggest that dFC could serve as a sensitive marker for AD progression monitoring before significant cognitive decline occurs.

2. **Biomarker Modulation of dFC**: The second study (Chapter 3) found that dFC increases with higher plasma p-Tau231 levels in cognitively healthy individuals, particularly in the orbitofrontal and temporal areas. This suggests that even in the absence of cognitive symptoms, dFC alterations may indicate early pathological changes. The study highlights the complex interplay between structural and functional brain changes, underscoring dFC's potential role as an early biomarker for AD.

3. **Effects of Neurostimulation on dFC**: The third study (Chapter 4) explored the effects of personalized alpha-frequency tACS on dFC and sFC within the DMN. Results showed a reduction in sFC but no significant changes in dFC post-stimulation, indicating that while tACS affects certain connectivity metrics, its impact on the temporal dynamics of connectivity remains unclear. This points to the necessity for further studies to understand how non-invasive brain stimulation might modulate brain network dynamics and its potential therapeutic implications for AD.

Overall, this thesis establishes the importance of considering brain connectivity as a dynamic phenomenon, particularly in the context of neurodegenerative diseases like AD. It provides evidence that dFC can offer unique insights into the early stages of AD, potentially serving as a biomarker for its early diagnosis and monitoring. Furthermore, it suggests that interventions targeting dFC or sFC could modulate disease progression, presenting new avenues for preven-

tive strategies. The findings advocate for the continued development of dFC methodologies and their integration into clinical practice to enhance early detection and treatment of AD. This research underscores the sensitivity of MEG as a tool for detecting subtle changes in brain function, advocating for its use in both research and clinical settings to better understand and address the complexities of AD pathology. Future work should aim to refine dFC measurement techniques, expand sample diversity, and explore additional biomarkers to further elucidate the role of dynamic brain connectivity in AD.

Resumen

Esta tesis explora el papel de la conectividad funcional dinámica (dFC) en la función cerebral y sus alteraciones a lo largo del continuo de la enfermedad de Alzheimer (AD, por sus siglas en inglés). Los enfoques tradicionales de conectividad funcional (FC) han tratado la sincronía cerebral como un proceso estático, descartando su naturaleza dinámica. Esta investigación desafía esta perspectiva empleando magnetoencefalografía (MEG) para investigar la dFC, que captura las interacciones temporales entre diferentes regiones cerebrales, ofreciendo potencialmente biomarcadores más tempranos para la AD que la conectividad funcional estática (sFC).

Los objetivos principales de esta tesis son desarrollar nuevas metodologías para medir la dFC y aplicarlas para entender la progresión de la AD. Se realizaron tres estudios para (1) examinar la dFC a lo largo del espectro de la AD utilizando MEG, (2) investigar la relación entre los biomarcadores sanguíneos (p-tau231) y la dFC en individuos cognitivamente intactos, y (3) evaluar el impacto de la estimulación transcraneal con corriente alterna (tACS) sobre la dFC y la sFC en la red por defecto (DMN).

Los hallazgos principales son:

1. **dFC a lo largo del espectro de la AD**: El primer estudio (Capítulo 2) mostró una reducción global de la dFC en las bandas alfa y beta en pacientes con deterioro cognitivo leve (MCI). El análisis espacial reveló reducciones significativas de dFC en la corteza orbitofrontal, el polo temporal, el hipocampo y la corteza cingulada, regiones críticas para la progresión de la AD. Estos resultados sugieren que la dFC podría servir como un marcador sensible para detectar cambios tempranos de la AD antes de que ocurra un deterioro cognitivo significativo.

2. **Modulación de la dFC por biomarcadores en sangre**: El segundo estudio (Capítulo 3) encontró que la dFC aumenta con niveles más altos de p-Tau231 en plasma en individuos sanos, especialmente en las áreas orbitofrontal y temporal. Esto indica que, incluso sin síntomas cognitivos, las alteraciones de la dFC pueden reflejar cambios patológicos tempranos. El estudio resalta la interacción entre cambios estructurales y funcionales del cerebro, subrayando el potencial de la dFC como biomarcador temprano para la AD.

3. **Efectos de la neuroestimulación sobre la dFC**: El tercer estudio (Capítulo 4) evaluó los efectos de la tACS a la frecuencia alfa personal sobre la dFC y sFC dentro de la DMN. Los resultados mostraron una reducción en la sFC pero no cambios significativos en la dFC después de la estimulación, sugiriendo que, aunque la tACS afecta ciertas métricas de conectividad, su efecto en la dinámica temporal sigue sin estar claro. Esto destaca la necesidad de estudios adicionales para entender cómo la estimulación cerebral no invasiva podría modular la dinámica de la red cerebral y sus posibles implicaciones terapéuticas para la AD.

En conclusión, esta tesis subraya la importancia de considerar la conectividad cerebral como un fenómeno dinámico en enfermedades neurodegenerativas como la AD. La evidencia

muestra que la dFC puede ofrecer perspectivas únicas sobre las etapas tempranas de la AD, potencialmente sirviendo como biomarcador para el diagnóstico temprano y el monitoreo de la misma. Además, sugiere que las intervenciones dirigidas a la dFC o sFC podrían influir en la progresión de la enfermedad, presentando nuevas estrategias preventivas. Los hallazgos apoyan el desarrollo continuo de metodologías de dFC y su integración en la práctica clínica para mejorar la detección temprana y el tratamiento de la AD. Esta investigación demuestra la sensibilidad de la MEG como herramienta para detectar cambios sutiles en la función cerebral, defendiendo su uso tanto en investigación como en entornos clínicos para abordar mejor la patología de la AD. Futuros trabajos deben centrarse en refinar las técnicas de medición de dFC, ampliar la diversidad muestral y explorar biomarcadores adicionales para entender mejor el papel de la conectividad cerebral dinámica en la AD.

Contents

Agradecimientos v
Abstract viii
Resumen x
List of Figures xviii
List de Tables xx
Abbreviatures & acronyms xxi

1 General introduction **1**
1.1 Background 1
1.2 Brain and neuronal activity: static or dynamic? 4
1.2.1 Brain cells, synapse and action potential 4
Central nervous system cell types and cell states 4
The action potential 5
Synapse 6
Dynamic activity at the microscale 8
1.2.2 Macroscopic electrophysiological activity 10
Brain oscillatory activity 11
Dynamics of rhythmic activity 13
1.2.3 Neuronal networks in the brain 14
1.3 Dynamic functional connectivity 17
1.3.1 Introduction to functional connectivity 17
Amplitude envelope correlation (AEC) 17
Phase-locking value (PLV) 19
Volume conduction, source leakage and connectivity 20
1.3.2 The problem with classical measures of functional connectivity 21
1.3.3 Introduction to dynamic functional connectivity 23
Sliding window analysis 24
Event-based analysis 28
Time-modeling approaches 31
1.3.4 Proposed methodologies in this thesis 33
Recurrence matrix dFC 33
Entropy dFC 35
1.4 Alzheimer's Disease 37
1.4.1 Introduction to AD 37

1.4.2 AD neuropathology . . . 39
Amyloid beta (Aβ) . . . 39
Tau proteinopathy . . . 42
Additional neuropathological factors . . . 43
1.4.3 AD and functional connectivity . . . 43
AD and changes in sFC . . . 44
AD and changes in dFC . . . 46
1.5 Introduction to MEG . . . 49
1.5.1 MEG versus other neuroimaging techniques . . . 50
1.5.2 Physiological origin of the MEG signal . . . 51
1.5.3 The MEG system . . . 52
1.5.4 MEG data acquisition . . . 54
1.5.5 MEG data preprocessing . . . 55
Signal space separation . . . 55
Artifact removal . . . 56
1.5.6 Source reconstruction . . . 57
The forward problem . . . 58
The inverse problem . . . 59
1.6 Research framework . . . 61
1.6.1 Research context and aims . . . 61
1.6.2 Research objectives and hypothesis . . . 62
Study 1: '*Dynamics of Brain Connectivity across the Alzheimer's Disease Spectrum: a magnetoencephalography study*' . . . 62
Study 2: '*Dynamic functional connectivity is modulated by the amount of p-Tau231 in blood in cognitively intact participants*' . . . 62
Study 3: '*Individual alpha frequency tACS reduces functional connectivity across the default mode network*' . . . 63

References **65**

2 Dynamics of Brain Connectivity across the Alzheimer's Disease Spectrum **91**
2.1 Objectives and hypotheses . . . 91
2.2 Introduction . . . 92
2.3 Materials and methods . . . 94
2.3.1 Participants . . . 94
Neuropsychological assessment . . . 95
2.3.2 Magnetic Resonance Imaging . . . 96
2.3.3 MEG data acquisition . . . 96
2.3.4 MEG processing and source reconstruction . . . 97
2.3.5 Dynamic functional connectivity . . . 97
dFC calculation . . . 97
Whole-brain dFC . . . 98
Spatial dFC analysis . . . 99
2.3.6 Statistical analysis . . . 99
Whole-brain dFC . . . 99

Spatial dFC analysis . . . 100
Neuropsychological, volumetric and DTI FA correlations . . . 100
2.4 Results . . . 100
2.4.1 Sample demographics and neuropsychological assessment . . . 100
2.4.2 Whole-brain dFC is reduced along the AD spectrum . . . 101
2.4.3 Localization of dFC changes along the AD continuum . . . 101
2.4.4 dFC correlates with cognitive performance along the AD continuum and in MCI . . . 103
2.5 Discussion . . . 104
2.6 Conclusion . . . 108

References **109**

3 Dynamic functional connectivity is modulated by the amount of p-Tau231 in blood in cognitively intact participants **117**
3.1 Objectives and hypotheses . . . 117
3.2 Introduction . . . 118
3.3 Materials and methods . . . 119
3.3.1 Participants . . . 119
3.3.2 Plasma p-tau231 determination . . . 120
3.3.3 AD family history . . . 121
3.3.4 Apolipoprotein E genetic evaluation . . . 121
3.3.5 Magnetic resonance imaging . . . 121
3.3.6 MEG data acquisition . . . 122
3.3.7 MEG preprocessing and source reconstruction . . . 122
3.3.8 Functional connectivity . . . 123
3.3.9 Statistical analyses . . . 124
Spatial FC analysis . . . 124
Risk factor linear regressions . . . 125
3.4 Results . . . 125
3.4.1 Sample demographics and variables of interest . . . 125
3.4.2 dFC increases along with p-tau231 values over orbitofrontal and temporal areas . . . 126
3.4.3 dFC is related to p-tau231 levels, sFC, and fractional anisotropy . . . 127
3.5 Discussion . . . 127
3.6 Conclusion . . . 130

References **133**

4 Individual alpha frequency tACS reduces functional connectivity across the default mode network **139**
4.1 Objectives and hypotheses . . . 139
4.2 Introduction . . . 140
4.3 Materials and methods . . . 141
4.3.1 Study design . . . 141

4.3.2 Participants . . . 141
4.3.3 MEG Data acquisition . . . 142
4.3.4 MEG preprocessing and source reconstruction . . . 142
4.3.5 Neurostimulation . . . 143
4.3.6 Functional connectivity . . . 143
Static functional connectivity . . . 144
Dynamic functional connectivity . . . 144
4.3.7 Statistical analyses . . . 144
4.3.8 Simulation of tACS phase-shifts effects on sFC . . . 145
4.4 Results . . . 146
4.4.1 Sample demographics and adverse tACS effects . . . 146
4.4.2 DMN's sFC decreases through tACS, while dFC increases in both *stim* and *sham* . . . 146
4.4.3 tACS prominently decreases sFC at posterior-posterior and antero-posterior hub links of the DMN . . . 149
4.4.4 Static functional connectivity of posterior areas correlate with power change . . . 149
4.4.5 Simulating tACS-induced phase disparities explain reductions in sFC 150
4.5 Discussion . . . 151
4.6 Conclusion . . . 155

References **157**

5 Conclusions **163**
5.1 Main conclusions . . . 163
5.2 Limitations and future directions . . . 167
5.3 Final remarks . . . 168
5.4 Ideas finales . . . 169

References **171**

Appendices **175**

A Supplementary material for Chapter 2 **177**
A.1 Supplementary tables . . . 177
A.2 Supplementary Figures . . . 182

B Supplementary material for Chapter 3 **183**
B.1 Supplementary tables . . . 183

C Supplementary material for Chapter 4 **185**
C.1 Supplementary tables . . . 185
C.2 Supplementary instructions . . . 188

List of Figures

1.1 Representative trace of an action potential 6
1.2 Tripartite synapse 8
1.3 MEG spectra and alpha topography. 12
1.4 The triple network. 15
1.5 Amplitude envelope correlation (AEC) calculation. 18
1.6 Phase locking value (PLV) calculation. 20
1.7 Usual procedure for the calculation of static functional connectivity (sFC). . 22
1.8 Number of studies published per year on functional connectivity and dynamic functional connectivity. 23
1.9 Summary of the main techniques derived from the sliding window methodology. 26
1.10 Steps in frame-based and microstate analysis. 29
1.11 Calculation of the recurrence matrix (C). 34
1.12 Seed-based recurrence matrix. 35
1.13 FC entropy calculation. 36
1.14 AD continuum and evolution according to the amyloid hypothesis. 39
1.15 Staging of Aβ accumulation in AD. 41
1.16 Staging of the NFT accumulation in AD. 42
1.17 The "X" model of AD. 45
1.18 Progression of sFC and dFC over the AD continuum. 47
1.19 Representation of the different neuroimaging techniques according to their temporal and spatial resolution. 51
1.20 MEG components. 53
1.21 MEG acquisition protocol. 54
1.22 Magnetic fields interfering with the MEG signal. 55

2.1 Depiction of the methods used in this Chapter 2. 98
2.2 Whole-brain dynamicity comparisons between healthy control (HC), subjective cognitive decline (SCD) and mild cognitive impairment (MCI) groups. 101
2.3 Results of the CBPT analyses for seed-based dynamicity. 102
2.4 Correlations between whole-brain dynamicity and MMSE, eTIV-normalized hippocampal volume and the left Cingulum fractal anisotropy. 104

3.1 Depiction of the methods used in Chapter 3. 123
3.2 Clusters of significant association between dFC and p-tau231. 126
3.3 Correlation between dFC and linear regression model predictors. 128

4.1 tACS maximal electric field distribution. 143
4.2 DMN AEC-c sFC decreases due to tACS. 147
4.3 DMN AEC-c dFC increases in both *stim* and *sham* groups. 148
4.4 DMN links showing a significant decrease in AEC-c sFC after tACS. 149
4.5 Negative correlations between AEC-c sFC ratio in posterior areas and IAF ± 2 Hz relative power ratio. 150
4.6 Results of the simulation of the effect of phase-shift tACS on FC. 151
4.7 Orthogonal components of the electric field with respect to the white-matter surface. 153

5.1 Progression of sFC and dFC over the AD continuum, after the results reported in this thesis. 165

A.1 Violin plots depicting whole-brain dynamicity in the stable MCI (sMCI) and progressive MCI (pMCI) groups. 182

C.1 Example of a filtered artificial signal between 8 and 12 Hz. 189
C.2 Combined signals at in-phase stimulation (top), and out-of-phase (π phase difference, bottom) stimulation. 191
C.3 Relation between PLV and AEC and the phase difference between stimulation sinusoids. 193

List of Tables

2.1 Sample demographics, neuropsychological test scores, and anatomic and white matter parameters. 95
2.2 Correlation results between whole brain dynamicity and neuropsychological, anatomic and diffusion-weighted imaging (DWI) parameters in the alpha band. 105
2.3 Correlation results between whole brain dynamicity and neuropsychological, anatomic and diffusion-weighted imaging (DWI) parameters in the beta band. 106

3.1 Sample demographics. 120

4.1 Sample demographics. 146

A.1 Sample demographics of the stable MCI (sMCI) and progressive MCI (pMCI) participants. 177
A.2 Complete statistical report on the whole-brain dynamicity between HC and SCD linear regression models. 178
A.3 Complete statistical report on the whole-brain dynamicity between HC and MCI linear regression models. 178
A.4 Complete statistical report on the whole-brain dynamicity between SCD and MCI linear regression models. 179
A.5 Complete statistical report from the stable MCI (sMCI) and progressive MCI (pMCI) linear regressions. 179
A.6 List of the regions of interest (ROI) of the AAL atlas contained in the significant cluster found between the HC and MCI groups in the alpha band. 180
A.7 List of the regions of interest (ROI) of the AAL atlas contained in the significant cluster found between the HC and MCI groups in the beta band. 181

B.1 Linear regression results for the model number 1 ($dFC\ 1 + Age + sFC$). . . 183
B.2 Linear regression results for the model number 2 ($dFC\ 1 + p - tau231 + sFC$). 183
B.3 Linear regression results for the model number 2 ($dFC\ 1 + p - tau231 + sFC + FAfmi$). 184

C.1 Distribution of reported adverse effects of tACS by group. 185
C.2 Complete statistical report for the sFC and dFC comparisons at the DMN. . 185
C.3 Complete statistical report for the links between the areas of the DMN for AEC-c. 186

C.4 Complete statistical report for the links between the areas of the DMN for ci-PLV. 187

Abbreviations & acronyms

AAL Automatic Anatomical Labelling

ACC Anterior cingulate cortex

AD Alzheimer's disease

ADHD Attention deficit hyperactivity disorder

AEC Amplitude envelope correlation

AEC-c Leakage corrected amplitude envelope correlation

Aβ Amyloid-beta

ALFF Amplitude of low frequency fluctuations

APP Amyloid precursor protein

APOE Apolipoprotein E

BOLD Blood-oxygenation level-dependent

C Recurrence matrix

C3N Center for Cognitive and Computational Neuroscience

CAT Computed axial tomography

CBPT Cluster-based permutation test

CEN Central executive network

CGC Cingulate gyrus part of the cingulum

ci-PLV Corrected imaginary phase locking value

CNS Central nervous system

CSF Cerebrospinal fluid

COWAT Controlled Oral Word Association Test

CTB Centro de Tecnología Biomédica

d Cohen's d

dFC Dynamic functional connectivity

DMN Default mode network

DWI Diffusion-weighted imaging

Dyn Dynamicity

E/I Excitation/Inhibition

ECoG Electrocorticography

EEG Electroencephalography

EKG Electrocardiogram

EOG Electrooculogram

eTIV Estimated total intracranial volume

FAQ Functional Assessment Questionnaire

FA Fractional anisotropy

FC Functional connectivity

fMRI Functional magnetic resonance imaging

fNIRS functional near-infrared spectroscopy

GABA Gamma-aminobutyric acid

GDS Geriatric Depression Scale

GFP Global field power

HC Healthy controls

Hip Hippocampus

HIS Hachinski Ischemic Score

HMM Hidden Markov model

HPI Head position indicator

IAF Individual alpha frequency

ICA Independent component analysis

ICN Intrinsic connectivity network

ILF Inferior longitudinal fasciculus

IPG Inferior parietal gyrus

ISV Inter-subject variability

LCMV Linearly constrained minimum variance

LTD Long-term depression

LTP Long-term potentiation

MCI Mild cognitive impairment

MEG Magnetoencephalography

MMSE Mini Mental State Examination

MNI Montreal Neurological Institute

MoCA Montreal Cognitive Assessment

MRI Magnetic resonance imaging

MSR Magnetically shielded room

MTL Medial temporal lobe

mPFC Medial prefrontal cortex

NIA-AA National Institute on Aging and Alzheimer's Association

NIBS Non-invasive brain stimulation

NFT Neurofibrillary tangles

PET Positron emission tomography

PCA Principal component analysis

PCU Precuneus

PCC Posterior cingulate cortex

PLV Phase locking value

pMCI Progressive mild cognitive impairment

p-Tau Hyperphosphorylated tau protein

PPA Point process analysis

PSEN1 Presenilin-1

PSEN2 Presenilin-2

PTSD Post-traumatic stress disorder

Rectus Gyrus rectus

RF Radio frequency

ROI Region of interest

ROAST Realistic vOlumetric-Approach-based Simulator for Transcranial electric stimulation

S Shannon entropy

SCD Subjective cognitive decline

sEEG Stereoelectroencephalography

sFC Static functional connectivity

SFG Superior frontal gyrus

SNP Single nucleotide polymorphism

SN Salience network

SNR Signal-to-noise ratio

SOBI Second-order blind identification

SPECT Single-photon emission computed tomography

SQUID Superconducting quantum interference device

SSS Signal space separation

std Standard deviation

sMCI Stable mild cognitive impairment

SVD Single value decomposition

tACS Transcranial alternating current stimulation

tSSS Temporally extended signal space separation

TVDN Time-varying dynamic network

UCM Universidad Complutense de Madrid

UPM Universidad Politécnica de Madrid

WHO World Health Organization

WMS Wechsler Memory Scale

Chapter 1

General introduction

1.1 Background

Functional connectivity (FC), defined as the interdependence of spatially separate brain activities (Van Diessen et al., 2015), is a fundamental concept in network neuroscience, the emerging field that views the brain as a complex system composed of interconnected networks, where cognitive functions arise from the dynamic interplay between distributed neural populations (Bassett and Sporns, 2017). These networks are characterized by a set of nodes (specific brain regions) and edges (the connections between them), encompassing both structural connections and functional connections, which are patterns of synchronized activity that allow for coordinated network functioning. The study of functional connectivity has been pivotal in understanding the brain's network architecture, as well as for revealing how different regions communicate and how these interactions underpin cognitive processes (Friston, 1994).

FC research has been essential in characterizing normal brain function and investigating changes due to various conditions. For instance, FC has been used to study developmental changes in brain activity like maturation and aging (Sala-Llonch et al., 2015; Stevens, 2016), as well as alterations in brain function associated with neurological diseases and disorders such as epilepsy, Parkinson's disease, and ADHD among others(Ives-Deliperi and Butler, 2021; Kowalczyk et al., 2022). These investigations have provided valuable insights into the neural basis of these conditions, allowing for a better understanding of their underlying mechanisms and potential interventions.

Despite its importance, most studies on FC share a methodological limitation based on a common assumption: they treat FC as a stationary process (Núñez et al., 2019). Typically, these studies segment neuroimaging signals into uniform time intervals, compute FC within each segment, and then average these estimates over time. This approach, known as static functional connectivity (sFC), assumes that brain connectivity patterns remain constant over the period of observation, thus disregarding any temporal fluctuations in the signal. This assumption seems counterintuitive, considering that the brain, the most complex organ known to humans, is inherently dynamic (De Pasquale et al., 2010; Rabinovich et al., 2012). Its

components and mechanisms, from neurons and synapses to large-scale oscillatory patterns, exhibit significant variability and adaptability in very small time scales, as discussed throughout this introduction.

Research focusing on the temporal variations in FC, referred to as dynamic functional connectivity (dFC), has started to gain traction. However, studies in this area remain relatively few, comprising only about 5% of the total research on FC. Even fewer studies have utilized electrophysiological methods, such as electroencephalography (EEG) or magnetoencephalography (MEG), to investigate dFC, as opposed to functional magnetic resonance imaging (fMRI), despite these methods' superior temporal resolution and ability to directly measure neuronal activity. This is particularly surprising given the potential of these techniques to provide more detailed insights into the temporal dynamics of brain networks.

This gap in research is especially relevant in the context of Alzheimer's disease (AD), a neurodegenerative disorder responsible for 60% to 80% of dementia cases. AD is characterized by the accumulation of amyloid-beta (Aβ) plaques and neurofibrillary tangles (NFTs) of hyperphosphorylated tau, leading to cortical degeneration and cognitive decline (Jack et al., 2018; Mattsson et al., 2019). Prior studies on AD have observed distinct patterns in sFC across the disease continuum: an initial phase of increased synchronization (hypersynchronization) during the preclinical stages and the initial accumulation of Aβ (García-Colomo et al., 2024; López-Sanz et al., 2017; Maestú et al., 2021; Nakamura et al., 2017; Ramírez-Toraño et al., 2021), followed by reduced connectivity (hyposynchrony) as the disease progresses to the dementia stage (De Haan et al., 2012; Pusil, López, et al., 2019). These findings suggest that the observed network alterations in AD could reflect underlying changes in dFC, which might provide earlier and more nuanced biomarkers for disease detection and monitoring.

While there exist some studies on dFC and AD, these are centered on the late stages of the AD continuum and identify a generalized decline in dFC (Córdova-Palomera et al., 2017; D. T. Jones et al., 2012; Li et al., 2019; Núñez et al., 2019). To shed light on the dynamics of FC during the pre-dementia stages and study where in the brain these changes in dFC were more prominent, we performed, to the best of our knowledge, the first electrophysiological study covering the whole pre-dementia spectrum (Chapter 2). Additionally, we proposed a new methodology to measure dFC both at a global and individual source scale through the correlation of connectivity matrices at different time-points.

The shift towards a biological conception of AD in recent years has led to the definition of a continuum that begins well before the emergence of any cognitive symptoms, associated with the accumulation of Aβ and tau NFTs, as previously explained (Jack et al., 2018). These changes can emerge up to 20 years before the diagnosis, and induce cumulative functional and anatomical alterations in the brain. At the time the disease is diagnosed by currently generalized clinical standards, brain damage is too extensive, hampering any success from ongoing potential treatments. This underscores the importance of noninvasive early diagnosis tools to identify individuals entering the AD continuum, and motivates the work in Chapter 3, part of a Spanish Government funded project titled *"Study of the anatomical-functional connectome of relatives of Alzheimer's patients: a proposal for early cognitive and lifestyle intervention"* (RTI2018-098762-B-C31). In this second study, we compared the capability of sFC and dFC to perform an early detection of alterations associated to AD by exploring its

correlation with p-tau231 levels, a blood biomarker used as a proxy for Aβ accumulation, in a sample of cognitively unimpaired adults (Chapter 3).

Finally, given the pathological nature of the changes observed in both sFC and dFC (Maestú et al., 2021), and the dire need for potential treatments to prevent the advance of the disease, we explored in Chapter 4 the possibility to externally modulate sFC and dFC in a pilot study applying tACS at the individual alpha frequency (IAF) in healthy participants over the default mode network (DMN), a key network in the progression of AD (Mattsson et al., 2019; Menon, 2011). This work was performed under a second Spanish Government funded project titled *"Efficacy of combined cognition and neuromodulation intervention in relatives of AD and elderly with SCQ: cognition, genetics and MRI"* (PID2021-122979OB-C21).

In what follows, we will introduce the theoretical and methodological framework in which this thesis' experimental studies are founded. Importantly, all the experiments were conducted using MEG, a non-invasive functional neuroimaging technique that captures small magnetic fields produced by intracellular currents in the brain (Hämäläinen et al., 1993). Its optimal combination of a fair spatial resolution (centimeters) and an excellent temporal (milliseconds) make this technique adequate for the investigation of fast dynamics in brain connectivity, the main topic of this thesis.

1.2 Brain and neuronal activity: static or dynamic?

1.2.1 Brain cells, synapse and action potential

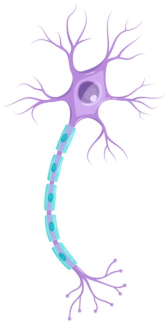
The brain is the most complex organ known to humans to date. 171 thousand million cells are part of it, of which 86 thousand million are neurons (Azevedo et al., 2009). These neurons, at the same time, are connected to each mainly through synapses, amounting to approximately 164 billion ($164 * 10^{12}$ synapses, Tang et al., 2001). It is the intricate relationship between these simple components that generates the highly complex activity characterizing our brain.

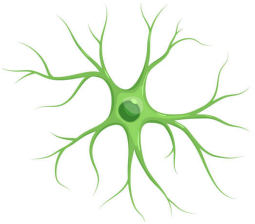
This section describes the nature of the main protagonists of the ecosystem of the brain, as well as the basic mechanisms of neuronal communication, e.g. action potentials and synapses. Furthermore, we will demonstrate that even at this elemental dimension, there exists rapid dynamic behaviour that shapes higher-order brain activity.

Central nervous system cell types and cell states

The central nervous system (CNS) is a complex network of cells that work together to control and coordinate bodily functions and responses to external stimuli. The CNS comprises the brain, the main character of this thesis, and spinal cord, serving as the primary control center for the body. The functionality of the CNS is attributed to the diverse cell types it contains, each playing a unique and vital role, and exhibiting complex relationships among them. These cells include neurons, the primary signaling units, and various glial cells such as astrocytes, oligodendrocytes, and microglia (Snell, 2010). Additionally, cerebrovascular cell types contribute to the maintenance of the blood-brain barrier and overall CNS homeostasis.

Neurons are the principal cells within the CNS responsible for transmitting information via electrical and chemical signals. Each neuron is composed of a soma (cell body), dendrites, and an axon. The dendrites receive synaptic inputs from other neurons, which are integrated within the soma and subsequently transmitted along the axon to other neurons or effector cells. Neuronal communication occurs through the combination of action potentials and synapses, where neurotransmitters are released to traverse the synaptic cleft, enabling signal propagation to the next neuron. This intricate signaling mechanism will be further explained later in the text, and underpins all CNS activities, ranging from fundamental reflexes to complex cognitive processes.

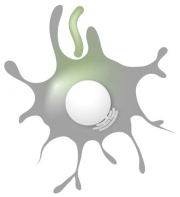




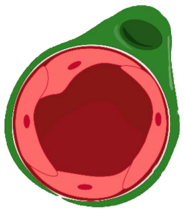
Astrocytes, star-shaped glial cells, perform a myriad of supportive functions within the CNS. They regulate the extracellular ionic balance, provide structural scaffolding for neurons, and participate in the repair and scarring processes post-injury. Astrocytes are pivotal in the formation and maintenance of the blood-brain barrier, a selective permeability barrier that protects the CNS from potentially harmful blood-borne substances while facilitating the transport of essential nutrients.



Oligodendrocytes are a type of glial cell primarily responsible for myelination within the CNS. These cells synthesize the myelin sheath, a lipid-rich layer that insulates axons and augments the velocity and fidelity of electrical signal transmission. Unlike Schwann cells in the peripheral nervous system, each oligodendrocyte can myelinate multiple axons. Myelination is crucial for rapid nerve impulse conduction, facilitating swift and coordinated responses to stimuli.



Microglia serve as the resident immune cells of the CNS, acting as the primary defenders against pathogens and injury. These small, highly dynamic cells continuously surveil the CNS environment, ready to respond to any signs of damage or infection. Upon detecting a threat, microglia activate and perform phagocytosis of debris, and release cytokines to modulate the inflammatory response. Furthermore, microglia are involved in synaptic pruning during development and neuroplasticity.



Cerebrovascular cell types, including endothelial cells, pericytes, and smooth muscle cells, are integral to the CNS vasculature. Endothelial cells constitute the lining of blood vessels, contributing to the blood-brain barrier which meticulously regulates the exchange of substances between the blood-stream and the brain parenchyma. Pericytes, embedded in the capillary walls, contribute to blood-brain barrier integrity, regulate cerebral blood flow, and participate in angiogenesis. Smooth muscle cells encircle larger blood vessels and control vessel constriction and dilation, thereby ensuring proper cerebral perfusion and oxygenation.

While these are the cell types contributing the most to the cell count of the CNS, this system consists of a highly heterogeneous array of cell types, each with essential roles that sustain the system's functionality and integrity. Transcriptomically derived cell type taxonomies in the adult brain consistently reveal a hierarchical organization of cell types, with about 170 differentiated cell types just in the brain (Zeng, 2022). A comprehensive understanding of these principal cell types and their interactions is fundamental to elucidating the operational mechanisms and adaptive responses of the central nervous system.

The action potential

Neurons are the primary signaling units of the CNS, and as such they generate and propagate action potentials. Action potentials were firstly theorized by Emil du Bois-Reymond in 1841, and then recorded by Hodgkin and Huxley on giant squid axons in 1939 (Hodgkin and Huxley, 1939). In neurons, action potentials play a central role in cell–cell communication by providing for the propagation of signals along the neuron's axon toward synaptic buttons situated at its end. These signals can then connect with other neurons at synapses, or to motor cells or glands.

An action potential is a rapid, transient change in the membrane potential of a neuron, initiated when the membrane potential reaches a certain threshold, typically around -55 mV

(Hodgkin and Huxley, 1952). This process is driven by the orchestrated opening and closing of voltage-gated ion channels. At rest, a neuron maintains a resting membrane potential of approximately -70 mV, primarily due to the differential distribution of ions, particularly sodium (Na+) and potassium (K+), across the neuronal membrane and the activity of the sodium-potassium pump. Upon sufficient excitatory stimulation, voltage-gated Na+ channels open, allowing an influx of Na+ ions, which depolarizes the membrane. If the threshold potential is reached (Figure 1.1A), a rapid depolarization phase occurs, peaking around +30 mV (Figure 1.1B and C).

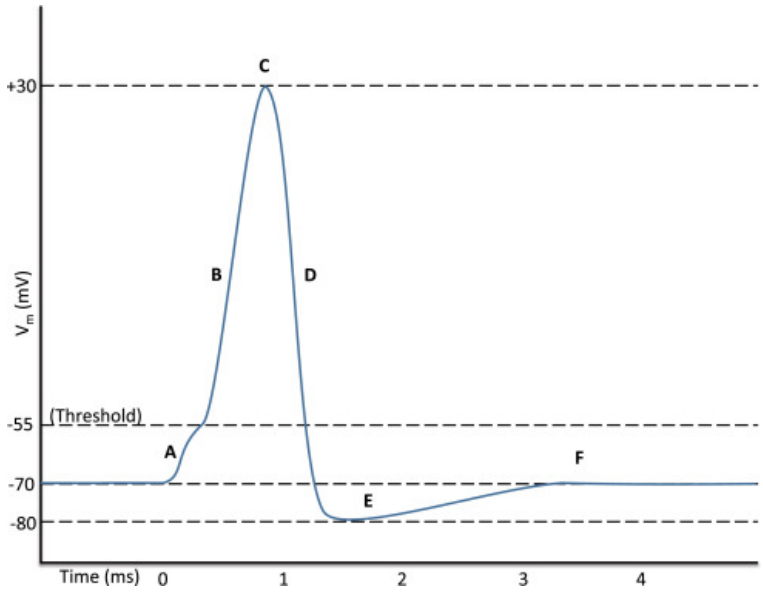


Figure 1.1: Representative trace of an action potential, adapted from Kotermanski and Cascio, 2023.

Subsequently, the Na+ channels close, and voltage-gated K+ channels open, permitting K+ ions to exit the cell. This repolarizes the membrane, bringing the potential back towards the resting level (Figure1.1D). Often, an overshoot, known as hyperpolarization, occurs due to prolonged K+ channel activity, temporarily making the membrane potential more negative than the resting state (Hodgkin and Huxley, 1952, Figure1.1E). The neuron then returns to its resting potential through the action of the sodium-potassium pump and closure of the K+ channels (Figure 1.1F).

The amplitude of an action potential is often thought to be independent of the amount of current that produced it. In other words, larger currents do not create larger action potentials. Therefore, action potentials are said to be all-or-none signals, since either they occur fully, or they do not occur at all.

Synapse

Action potentials travel along the neuron's axon toward the synaptic buttons situated at its ends, where the impulse is transmitted to the next neuron through the synapse, a term coined by Charles Sherrington in 1897 (Foster, 1897). Synapses constitute the fundamental

communication points between neurons in the nervous system, playing a crucial role in enabling rapid and direct communication and creating neuronal circuits.

At a synapse (Figure 1.2), the presynaptic neuron (the sending neuron) and the postsynaptic neuron (the receiving neuron) come into close proximity, separated by a small gap called the synaptic cleft. In most synapses, the presynaptic part is located on an axon, while the postsynaptic part is located on a dendrite or soma, and astrocytes support synaptic function through the regulation of ion concentration in the extracellular space or the uptake and release of neurotransmitters (Südhof, 2021).The process of synaptic transmission begins when an action potential travels down the presynaptic neuron and reaches its end. This arrival triggers the opening of voltage-gated calcium channels, allowing calcium ions to flow into the neuron. The influx of calcium ions causes synaptic vesicles, which are filled with neurotransmitters, to merge with the presynaptic membrane and release their contents into the synaptic cleft. Once released, neurotransmitters diffuse across the synaptic cleft and bind to specific receptors on the postsynaptic neuron. This binding initiates a postsynaptic potential in the postsynaptic neuron, which can either depolarize or hyperpolarize its cell membrane, depending on the type of synapse involved. This process of neurotransmitter release and binding is central to neural communication.

Hence, synapses can be classified based on their effects on the postsynaptic neuron. Excitatory synapses cause depolarization of the postsynaptic membrane by triggering the opening of Na+ ion channels, making it more likely for the neuron to fire an action potential. Glutamate is the primary neurotransmitter involved in these excitatory synapses in the CNS, followed by acetylcholine or epinephrine. Inhibitory synapses, on the other hand, cause hyperpolarization of the postsynaptic membrane, mainly by the release of gamma-aminobutyric acid (GABA), which binds to postsynaptic receptors that open Cl- ion channels, allowing its entrance to the neuron, or K+ channels, triggering their release from the cell, consequently decreasing the membrane potential, making it less likely for the neuron to fire an action potential.

The brain's functionality heavily relies on a balance between excitatory and inhibitory synapses and neurons. This balance in the connectivity pattern of the microconnectome is crucial for proper synaptic activity, information processing, and maintaining overall brain homeostasis. Interestingly, while the relative percentage of inhibitory neurons is much smaller than excitatory neurons in the cortex (Kajiwara et al., 2021), inhibitory neurons exhibit a higher controlling ability over other neurons, particularly in topological mechanisms, making them relatively more influential than excitatory neurons. This influence is especially notable in the deeper layers of the cortex, where inhibitory neurons are observed to be located at more central positions in the cortical microconnectome, and therefore playing a key role in sustaining brain homeostasis (Kajiwara et al., 2021). Furthermore, the balance between inhibition and excitation in the brain varies across different levels of the cortical hierarchy, as there is a gradual scaling down of the inhibition/excitation ratio from feedforward to feedback pathways, indicating a dynamic balance that adjusts according to the functional demands of different cortical areas (D'Souza et al., 2016).

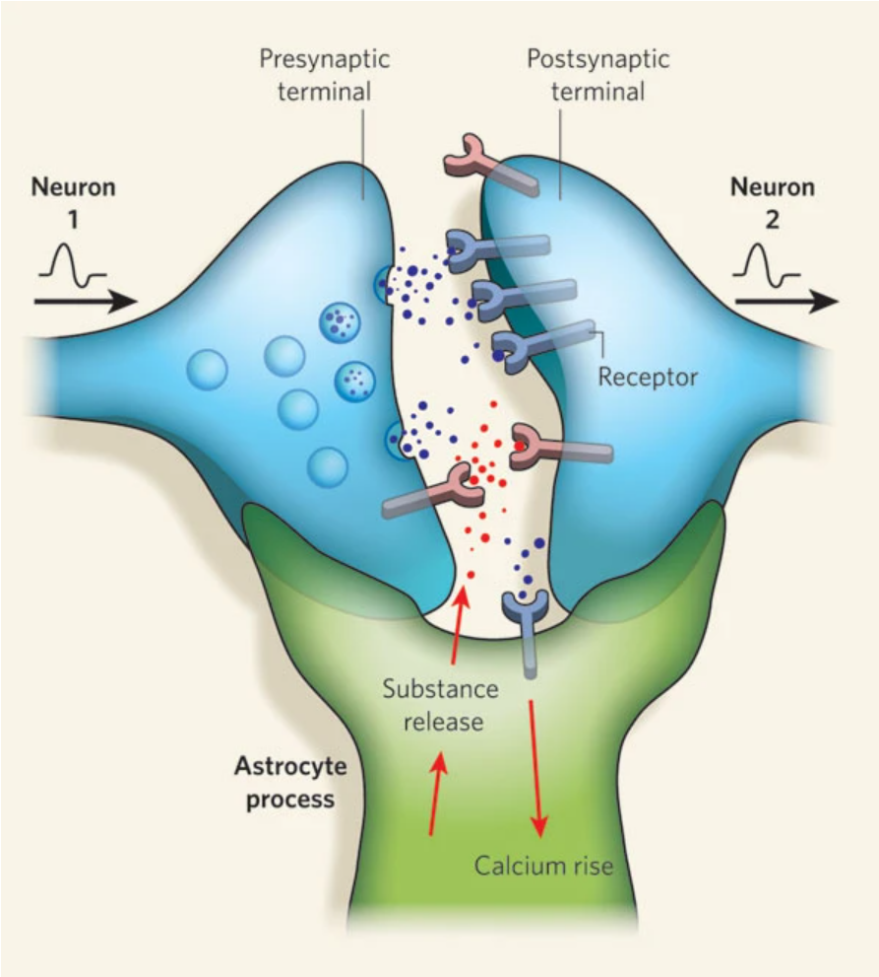


Figure 1.2: Tripartite synapse, as represented in N. J. Allen and Barres, 2009.

Dynamic activity at the microscale

While the basic elements and mechanisms of neuronal communication presented in the previous sections have been extensively studied and characterized over the years, there remains a vast frontier of discovery. Particularly, the dynamic behavior of these elements is an area of special interest for further research. The intricate and rapid changes in neuronal activity, synaptic plasticity, and network dynamics are still not fully understood. Modern techniques and technologies are continually uncovering new aspects of how these components interact and adapt in real-time, highlighting that our understanding of brain communication is far from complete. This ongoing research is crucial for unraveling the complexities of higher-order brain functions and the underlying mechanisms that drive cognition, behavior, and neurological health.

Even if not entirely known, dynamic behaviours of the earlier described cells and mechanisms have been observed, and can be classified according to their diverse time-scales:

- **Immediate to short-term changes**: In the order of milliseconds to seconds, these changes mostly involve alterations in receptor dynamics, or extracellular ion or neuro-

transmitter concentrations. For instance, the kinetics of ion channels, such as sodium and potassium channels, can be rapidly modulated through phosphorylation or binding of modulatory molecules. This allows for quick adjustments in response to synaptic inputs or neuromodulatory signals. Activity-dependent modifications such as cumulative sodium channel inactivation or potassium channel activation can alter the refractory period almost instantaneously following a burst of action potentials(G.-S. Yi et al., 2016), or change the resonance frequency of a neuron after sub-threshold stimulation (Lau and Zochowski, 2011).

Another example involves the role of astrocytes in synaptic modulation. Although not electrically active, astrocytes exhibit a form of excitability by dynamic changes in intracellular calcium levels, which allow them to detect synaptic activity, which may trigger glutamate exocytosis or release of gliotransmitters on a millisecond time scale, modulating synapse excitability and conditioning impulse response from neighboring neurons (Calì et al., 2008).

- **Medium-Term Changes**: Spanning seconds to minutes, intracellular calcium dynamics play a crucial role in this category. Calcium influx during action potentials can activate calcium-dependent potassium channels, which contribute to the afterhyperpolarization phase. This modulation can persist for several seconds, affecting the relative refractory period and the overall excitability of the neuron during this timeframe (Delvendahl et al., 2019; Kuznetsova et al., 2008).

  Furthermore, this category also includes cell state transitions, the cell capacity to dynamically change its genetic expression, transitioning to different phenotypical conditions (Zeng, 2022). Neuronal activation in the hippocampus and the medial prefrontal cortex during contextual fear conditioning is linked to subsequent memory formation, and has now been associated with an induction of a proteostasis response in both neuronal and non-neuronal cell types, product of a genetic expression modulation through a cell state change (Stott et al., 2021). Interestingly, these adaptations were detected as soon as 30 minutes after the fear-conditioning stimuli, highlighting the rapid response that both neuronal and glial cells present.

- **Long-Term Changes**: These changes occur over minutes to hours or longer, and often involve changes in synapse strength, gene expression and protein synthesis, happening usually due to cell state transitions. Long-term neuromodulatory effects are especially relevant in memory formation processes. Importantly, long-term synaptic modulations include long-term potentiation (LTP) and long-term depression (LTD), widely considered the major cellular mechanisms that underlie learning and memory (Cooke and Bliss, 2006). LTP is an activity-dependent and persistent enhancement of synapse strength, able to produce a long-lasting increase in signal transmission between neurons following brief trains of high frequency stimulation of a monosynaptic pathway, while LTD produces an activity-dependent reduction in the efficacy of neuronal synapses induced by low-frequency repetitive stimulation. The early phase of these processes occurs within minutes to a few hours after the activity-dependent induction, involving rapid biochemical changes at the synapse, such as the phosphorylation of proteins and the insertion or removal of receptors in the postsynaptic membrane. On the other hand,

late-phase LTP and LTD last from several hours to days or even a lifetime. It involves more stable changes, including alterations in gene expression and protein synthesis, leading to structural changes in the synapse (Deperrois and Graupner, 2020).

Memory formation also involves processes of neuronal recruitment at the hippocampus. The mechanism begins with clusters of hippocampal CA1 neurons presenting double-stranded DNA breaks and perinuclear release of DNA fragments after learning. Following these events, surrounding neurons transition to an inflammatory phenotype, eliciting a cascade of learning-induced molecular events in discrete neuronal clusters undergoing double-stranded DNA damage and repairment through toll-like receptor 9 pathways, resulting in neuronal recruitment to memory circuits, occurring just a few hours after the learning task (Jovasevic et al., 2024).

The complex dynamics underlying the very elemental units of the brain constitute the grounds upon which mesoscale and macroscale brain activity are based, and let us grasp the foundations of high-order dynamic behaviour.

1.2.2 Macroscopic electrophysiological activity

The development of the current electrophysiological techniques used to investigate brain activity falls back to the XVIII century, when Luigi Galvani forged the link of two previously separated concepts: electricity and physiology.

For macroscopic brain electrophysiological recordings, the path was continued by Richard Caton, who published in 1875 experiments on the brains of dogs and apes in which bare unipolar electrodes were placed either on the surface of both hemispheres or one electrode on the cerebral cortex and the other on the surface of the skull, measuring current with a galvanometer (Berger, 1929), and laying the groundwork for the following researchers on brain electrophysiology. He was followed in the investigation of electrical currents on the surface of animal brains by Adolf Beck, Vladimir Vladimirovich Pravdich-Neminsky, Napoleon Cybulski and Jelenska-Macieszyna. However, it took 50 years from Richard Caton's experiments for the first recordings of the electrical activity arising from the human brain by Hans Berger in 1924. Berger also invented the technique of electroencephalography (EEG), with which he firstly described the different waves or rhythms that were present in the normal and abnormal brain, such as the alpha wave rhythm, also known as "Berger's wave", and its suppression when the subject opened the eyes, also known as the alpha blockade (İnce et al., 2021). By enabling the direct measurement of electrical activity in the brain, EEG has provided unprecedented insights into brain function, revolutionizing both clinical practice and scientific research.

EEG signal is thought to be primarily produced by the postsynaptic potentials of pyramidal neurons in the cerebral cortex that are positioned perpendicularly to the brain's surface. In order to create a measurable EEG signal at the scalp it is estimated that between 10000 to 100000 neurons need to fire synchronously in a coordinated manner while being parallel to each other, so that the associated postsynaptic potentials achieve spatio-temporal summation (Murakami and Okada, 2006).

Brain oscillatory activity

As Berger reported, the recordings of the electrical activity at the scalp revealed oscillatory patterns. These signals, measured as a function of time, can also be represented in the frequency domain through the Fourier transform. Basically, the Fourier transform decomposes a time-domain variable in the sum of a discrete collection of sinus signals, each with a different amplitude depending on its contribution to the original signal (Nussbaumer and Nussbaumer, 1982). Afterwards, the contributions of each of these sinus signals can be plotted against their frequency (in other words, how many times the sine oscillates in a second, measured in Hertz). This representation is called the power spectrum, and as we mentioned earlier, it depicts the contribution of each frequency to the power of the original signal. Research revealed that the power spectrum of cortical activity in humans showed peaks within specific frequency bands (Mazaheri et al., 2018). Figure 1.3A shows a typical EEG power spectrum measured during a resting-state eyes-closed recording, featuring a dominant peak in the alpha-band [8–12] Hz, usually distributed over occipital areas, as shown in Figure 1.3B. EEG oscillatory activity has been investigated between 1 Hz and 100 Hz, and its power spectrum is typically divided into the so-called classical frequency bands: delta [0.5–4] Hz, theta [4–8] Hz, alpha/mu [8–12] Hz, sometimes further subdivided as low alpha [8–10] Hz and high alpha [10–12] Hz, beta [12–30] Hz , and gamma (>30 Hz). Although there are no one-to-one mappings between oscillatory activity in a given frequency band and a cognitive process, these frequency bands have nevertheless been associated with distinct processes and cognitive activities (Jensen and Mazaheri, 2010):

- **Delta (1-4 Hz)**: Delta activity is the slowest and is most prominent during deep, restorative sleep (slow-wave sleep). Delta waves have been shown to decrease across the lifespan, being the predominant waveforms of infants, and showing a strong decline in the mid-forties. By the age of about 75, stage four sleep and delta waves may be entirely absent (Colrain et al., 2010). Delta activity is typically less prominent during waking states but has also been associated with internal attention processes and motivation and (Jiang et al., 2021).
- **Theta (4-8 Hz)**: theta frequency band is a prominent oscillatory activity, whose putative role depends on the neuroanatomical source of the activity. Theta arising from medial frontal regions has been associated with working memory maintenance and updating (Scheeringa et al., 2009), together with error processing. Theta activity arising from sources in the medial temporal lobe, such as the hippocampus, has been associated with episodic memory (Lega et al., 2016), and frontal theta in general has been found to correlate with cognitive workload (Chikhi et al., 2022).
- **Alpha (8-12 Hz)**: Alpha waves are prominent when an individual is awake but in a relaxed and calm state, often with its eyes closed, showing activity that is most intense over the occipital lobe and posterior regions (Buzsáki, 2006). The spontaneous emergence of alpha in task-irrelevant areas and its correlation with cognitive performance has led to the hypothesis of functional inhibition, which states that alpha activity in task-irrelevant areas is key for optimal performance as it allocates processing resources for task-relevant regions (Jensen and Mazaheri, 2010), with other reports linking it to attention and the active maintenance of working memory representations (S. Palva and

Palva, 2007). Abnormalities in resting-state alpha oscillations have been consistently observed in pathological conditions. For instance, a reduction in relative alpha power has been described along the Alzheimer's disease continuum (Babiloni et al., 2009) as well as in other dementias (Van Straaten et al., 2012).

- **Beta (12-30 Hz)**: Beta oscillations are strongly associated with motor preparation and sensorimotor processing, as they are suppressed prior to and during movement changes (Van Ede et al., 2017). However, beta activity has also been associated with working memory maintenance and clearing (Schmidt et al., 2019).
- **Gamma (30-100 Hz)**: Gamma waves are the fastest brainwaves and constitute the main physiological basis of bottom-up information processing and integration of perceptual information. In the sensory cortex, gamma power increases with sensory drive, and with a broad range of cognitive phenomena, including perceptual grouping and attention (Jia and Kohn, 2011). Interestingly, fast-spiking GABA inhibitory interneurons are known to be crucial, with their activity being both necessary and sufficient to generate gamma (Bartos et al., 2007; Cardin et al., 2009).

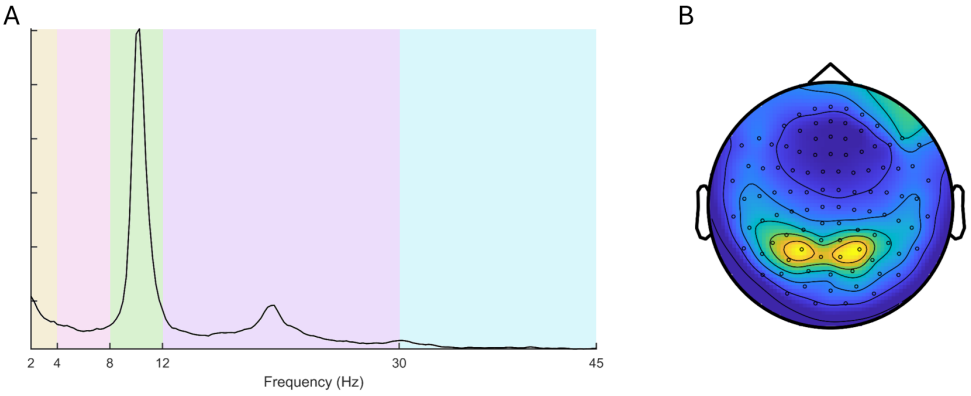


Figure 1.3: MEG spectra and alpha topography. (A) Representative resting state eyes-closed MEG power spectrum. The colour represents the frequency range of the classical frequency bands: delta (yellow), theta (pink), alpha (green), beta (purple), and gamma (blue). (B) 2-dimensional topographic distribution of the alpha-band power.

Significant interactions also occur across frequency bands, which could facilitate the integration, coordination, and regulation of neuronal activity (J. M. Palva and Palva, 2018). Notably, the power within the gamma band is embedded within the phases of both theta and alpha oscillations, meaning that both theta and alpha oscillations play roles in coordinating neural activity in higher frequency bands (Bonnefond et al., 2017). The relationship between gamma power and alpha phase is linked to the gating of information flow between regions and the active inhibition of unnecessary couplings for a given task (Bonnefond et al., 2017). In contrast, theta-gamma coupling might reflect the integration and coordination of working and episodic memory processes and attention allocation (Kim et al., 2015; Lega et al., 2016). Therefore, both the activity within individual frequency bands and the coordination of activity across different frequency bands are crucial for information processing and cognitive functions. The phase and frequency of these oscillations heavily depend on the time constants of the neural

circuits and systems from which they originate. Even minor changes in these time constants, due to age, injury, or disease, could significantly impact cognition (Karahan et al., 2022).

Dynamics of rhythmic activity

Whilst some of these 'rhythms' reflect genuinely sustained oscillatory activity, it has been raised that others may be better described as spectrally specific transient events (Quinn et al., 2019). This perspective relies on a detailed understanding of the nature of the rhythm in the unaveraged, unfiltered time-domain signal, and would be essential for the interpretation of the cellular and network level mechanisms underlying neurophysiological data (S. R. Jones, 2016). However, studies on oscillatory brain activity usually apply many levels of filtering and averaging to time series data and rely in static or trial-averaged estimates of power, and what was previously observed as a persistent oscillatory may be an artefact of averaging temporally variable, short-lived events across many trials. In this light, rhythmic activity may be better characterized by measures of temporal dynamics, such as the duration, rate, or amplitude of transient events, as they occur at the level of single trials.

For example, this perspective is evident in various research studies on the 12–30 Hz beta band. Visual attention correlates with increased beta activity, characterized by 300–1000 ms bursts that propagate through the visual stream (Wróbel, 2000). Similarly, in the motor cortex, single-trial analyses of beta power reveal motor task responses lasting several seconds, potentially constructed from bursts of less than 150 ms in both cortical and sub-cortical regions (Feingold et al., 2015). Moreover, the rate, timing, and duration of these bursts predict somatosensory and motor performance (Shin et al., 2017), indicating that the variability in these burst parameters during single trials likely represents more than just noise. Transient gamma activity, on the other hand, has been linked to working memory maintenance, especially in early ages. During brain maturation, gamma power during the maintenance-phase of memory tasks was observed to decrease, and these reductions were associated to a decrease in the gamma bursting events (McKeon et al., 2023).

Interestingly, memory encoding has been associated to sustained increases in the amplitude of neuronal oscillations in the alpha and theta frequency bands over parietal and temporal cortices, mediated by transient bursts of oscillatory activity in these frequency bands (Montez et al., 2009). Moreover, a pattern of decreased autocorrelations of alpha activity in Alzheimer's disease patients was discovered during short and intermediate time scales during a memory task. This means that alpha burst distribution has a more random temporal distribution, which correlated with the performance of the participants. Particularly interesting is that Alzheimer's disease did not influence the oscillation amplitude in the alpha band, suggesting that neuronal activity temporal structure could be at least as important as the magnitude of the oscillations as a marker of pathophysiology and, possibly, for mnemonic operations (Montez et al., 2009). To conclude, it has been observed that these changes in transient oscillatory activity can be observed even in the resting state. During 15-minute long EEG recording, decreases in the alpha and beta power over time, and increases of the power of delta and theta across almost all electrodes were observed (Maltez et al., 2004).

These examples of significant changes in electrophysiological activity over short time scales underscore the importance of rhythmic dynamics for central processes such as memory

formation, motor planning, and how changes in the temporal structure of brain activity might be behind neurodevelopmental strategies or the advance of certain pathophysiological processes.

1.2.3 Neuronal networks in the brain

Understanding brain activity requires examining not only its amplitude and frequency but also its specific location within the brain. The relationship between the location of brain activity and cognitive functions has been a subject of debate since the 18th century, with two major theories emerging: localizationism and holism.

Localizationism, advocated by Franz Joseph Gall and Paul Broca, posited that specific brain functions are tied to distinct regions of the brain. Gall's theory of phrenology, although later discredited, introduced the idea that different parts of the brain are responsible for different functions. Broca's studies on aphasia, which linked language deficits to lesions in a specific area of the left frontal lobe, provided compelling evidence for localizationism (Broca, 1861). However, this view faced criticism from figures like John Hughlings Jackson and later Henry Head. Jackson argued against the strict localization of functions, pointing out that even with damage to a presumed functional center, some residual function often remains. Head, representing the holistic perspective, suggested that brain functions are not confined to isolated regions but rather result from the brain working as a whole, where the extent of damage, rather than its precise location, predicts the impact on cognitive abilities.

A middle ground between these views emerged with the theory of associationism. Karl Wernicke played a key role in developing this approach, proposing that while certain brain areas specialize in specific functions, these areas are interconnected and must work together to produce complex behaviors. Wernicke's identification of a brain region associated with the sensory aspect of language complemented Broca's findings on motor language processing (Wernicke, 1874), illustrating how interconnected regions contribute to cognitive functions. John Hughlings Jackson's hierarchical view of brain functions (York and Steinberg, 2006) and Alexander Luria's work on the involvement of multiple brain regions in various cognitive tasks further advanced associationism. Luria's model suggested that the brain operates through three functional units: a subcortical unit for general cortical activation, a second unit for processing and integrating sensory information, and a third, frontal lobe-centered unit for higher-order cognitive functions like planning and behavior regulation (Lurija, 1997).

The development of neuroimaging techniques eventually led to the modern theory of brain functional organization known as network neuroscience (Bassett and Sporns, 2017). This approach views the brain as a complex system of interconnected networks, where cognitive functions arise from the interaction of distributed neuronal populations. These networks are defined by nodes (specific brain areas) and edges (the connections between them), which include both structural connections—anatomical pathways linking brain regions—and functional connections, which are patterns of co-activation that allow for synchronized network activity. This framework accommodates the idea that brain regions can participate in multiple networks or functions, depending on their coordination with other areas.

A neurocognitive network is then a brain system dedicated to a distinct cognitive function.

Examples of such networks are the aforementioned language network, composed by the middle temporal gyrus, as well as Broca's, Wernicke's and Geschwind's areas, or the working memory network, anchored in the dorsolateral prefrontal cortex and posterior parietal cortex. These networks were initially discovered and investigated through lesion studies, even in recent times (Vaidya et al., 2019), but their anatomical precision remained relatively poor. More recently, functional magnetic resonance imaging (fMRI) activation studies have been used in the last decades to more precisely delineate the brain regions associated with specific neurocognitive networks. More specifically, analysis of resting fMRI data using independent component analysis (ICA) allows for the identification of the so-called intrinsic connectivity networks (ICNs). ICNs represent consistent patterns of strong coupling of the ongoing activity, which remain robust under different mental states. Some of the ICNs identified through fMRI studies include the auditory network, the basal ganglia, the primary and secondary visual cortices, the language network, or the sensorimotor cortex (Schöpf et al., 2010).

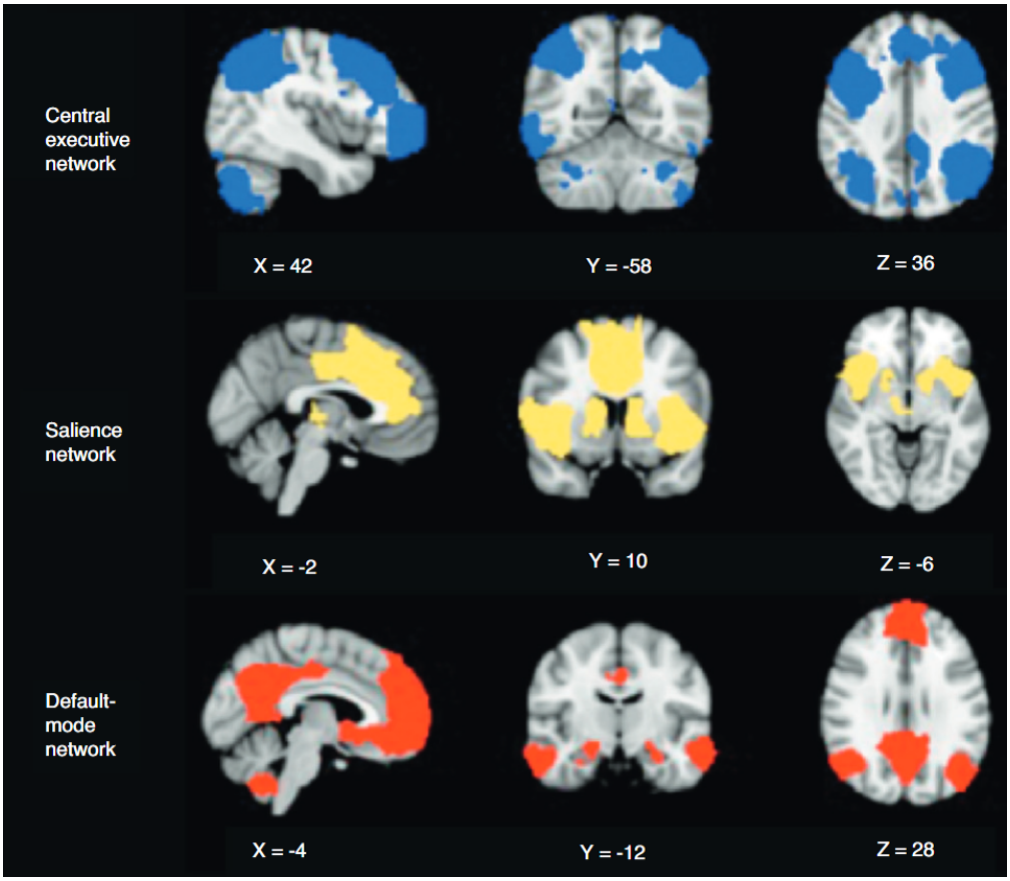


Figure 1.4: The triple network. Adapted from Menon, 2011.

From the several stable ICNs identified in the human brain, three have turned out to be of particular importance for the understanding of cognitive function and dysfunction, composing what Vinud Menon proposed to call the triple network model in 2011 (Menon, 2011; Figure 1.4): the central executive network (CEN), the salience network (SN) and the default mode network (DMN). Interestingly, these three networks show close correspondence in independent analyses of both resting and task-related neuroimaging recordings, constituting a common

framework where both intrinsic and task-based fMRI activation patterns can be studied, as well as providing useful models investigating network features of cognitive disorders.

The CEN, SN and DMN are unique networks in that they can be readily identified across an extremely wide range of cognitive tasks, and their responses increase and decrease proportionately, and often antagonistically, with general cognitive task demands. The CEN and SN typically show increases in activation during stimulus-driven cognitive and affective information processing, whereas the DMN shows decreases in activation during tasks in which self-referential and stimulus-independent memory recall is not crucial, and shows an increased activity in resting studies. According to this model, the SN, and most notably the anterior insula, would play the role of an integral hub mediating dynamic interactions between networks, and switching from the DMN, internally oriented to self-related mental processes, and engaging the CEN, involved in externally oriented attention. This way, the SN would help recruiting the target brain regions necessary to generate an appropriate behavioural response to salient stimuli, while the CEN and the DMN will mostly be anticorrelated in their activation (Menon, 2011).

Being the first to be discovered of the three networks through resting-state fMRI, the DMN is anchored in the precuneus (PCU), posterior cingulate cortex (PCC), anterior cingulate cortex (ACC), medial prefrontal cortex (mPFC), the hippocampus, also showing prominent nodes in the medial temporal lobe (MTL). Functions ascribed to this network include the episodic memory retrieval, autobiographical memory, and semantic memory related to internal thought, mainly linked to the PCC, hippocampus and the angular gyrus, while the nodes of the mPFC have been associated with self-related and social cognitive processes, value-based decision making and emotion regulation (Menon, 2011). Together, the DMN collectively comprises an integrated system for the management and integration of the different aspects of self-referential mental processes. Currently, it is known that virtually every major neurological disorder, including dementia, schizophrenia, epilepsy, anxiety, depression, autism or attention deficit hyperactivity disorder (ADHD), present with abnormalities in the co-activation patterns within the DMN. The importance of the DMN in resting state studies and in the progression of Alzheimer's disease are the reasons why the chapters of this thesis will be especially interested in the changes in connectivity patterns in it.

While the initial step in the study of network neuroscience was mainly performed through the research of co-activation patterns, usually through fMRI, the newly established concept of different brain regions being able to coordinate in space and time fostered the birth of functional connectivity, which we will discuss in depth in the next section.

The evidence presented in this section has allowed us to grasp the degree of dynamicity of brain activity at every scale of the brain, from its fundamental units, the neurons, to the organized, both temporally and spatially, activity of these neurons to bring about oscillatory activity observed through EEG and MEG. But, what about the behaviour of neuronal networks?

1.3 Dynamic functional connectivity

The rise of network neuroscience, driven by the works of Ramón y Cajal (Ramón Y Cajal, 1909) and Lorente de Nó (Lorente De Nó and Honrubia, 1966) on neuronal circuits, shifted the focus of neuroscience towards identifying the areas involved in different cognitive processes as well as understanding the communication mechanisms among them. The study of this communication is denoted as connectomics or brain connectivity, which can be separated in two main fields: anatomical connectomics, focusing on the physical connections between neuronal ensembles, e.g. the tracts of white matter joining different areas of the brain; and functional connectivity (FC), described for the first time in 1994 by Friston and his colleagues as "the temporal correlation of a neurophysiological index measured in different brain areas" (Friston, 1994). This section delves on the definition of FC, the current methodologies to estimate it and, very importantly, the contradiction between the static approaches found in recent literature to calculate FC and the fast changes that happen in the brain at every different size scale, as presented in the section 1.2, which make FC inherently dynamic. The efforts in literature to study and estimate the dynamicity of FC, also called dynamic FC (dFC), will be commented, and the proposed methodologies in this thesis will be then presented.

1.3.1 Introduction to functional connectivity

Functional connectivity is defined as the temporal correlation between spatially remote neurophysiological events (Van Diessen et al., 2015), expressed as deviation from statistical independence across these events in distributed neuronal groups and areas. This definition captures the idea that drives the study of the brain since the end of the 20th century: different areas collaborate to fulfill specific tasks, and this interaction is persistent over time. The connectivity between two regions cannot be accurately calculated, since that would require us to have the complete knowledge of the two separate systems. However, it can be estimated by means of the synchronization of their activity. The neurophysiological events to be related, or the "neurophysiological index" mentioned by Friston, indicate the open definition for the approaches at calculating FC. We can differentiate five main types of FC: linear synchronization, phase synchronization, general synchronization, Granger causality-based metrics, and information theory metrics; for a complete review in this topic, see Niso et al., 2013; Van Diessen et al., 2015. The studies under this thesis used two main FC metrics: amplitude envelope correlation, a linear synchronization parameter; and the phase locking value, falling under the phase synchronization category.

Amplitude envelope correlation (AEC)

Linear synchronization between two parameters implies a linear relation between them, meaning that one can be modeled as an escalated version of the other, with some noise contribution. Being the transformation from one signal to another completely linear, this kind of synchronization parameters are easy to compute. Correlation, the part of the signal that can be explained by the other, would fall under this category, and is equal to the ratio of the shared energy and the total energy between time series.

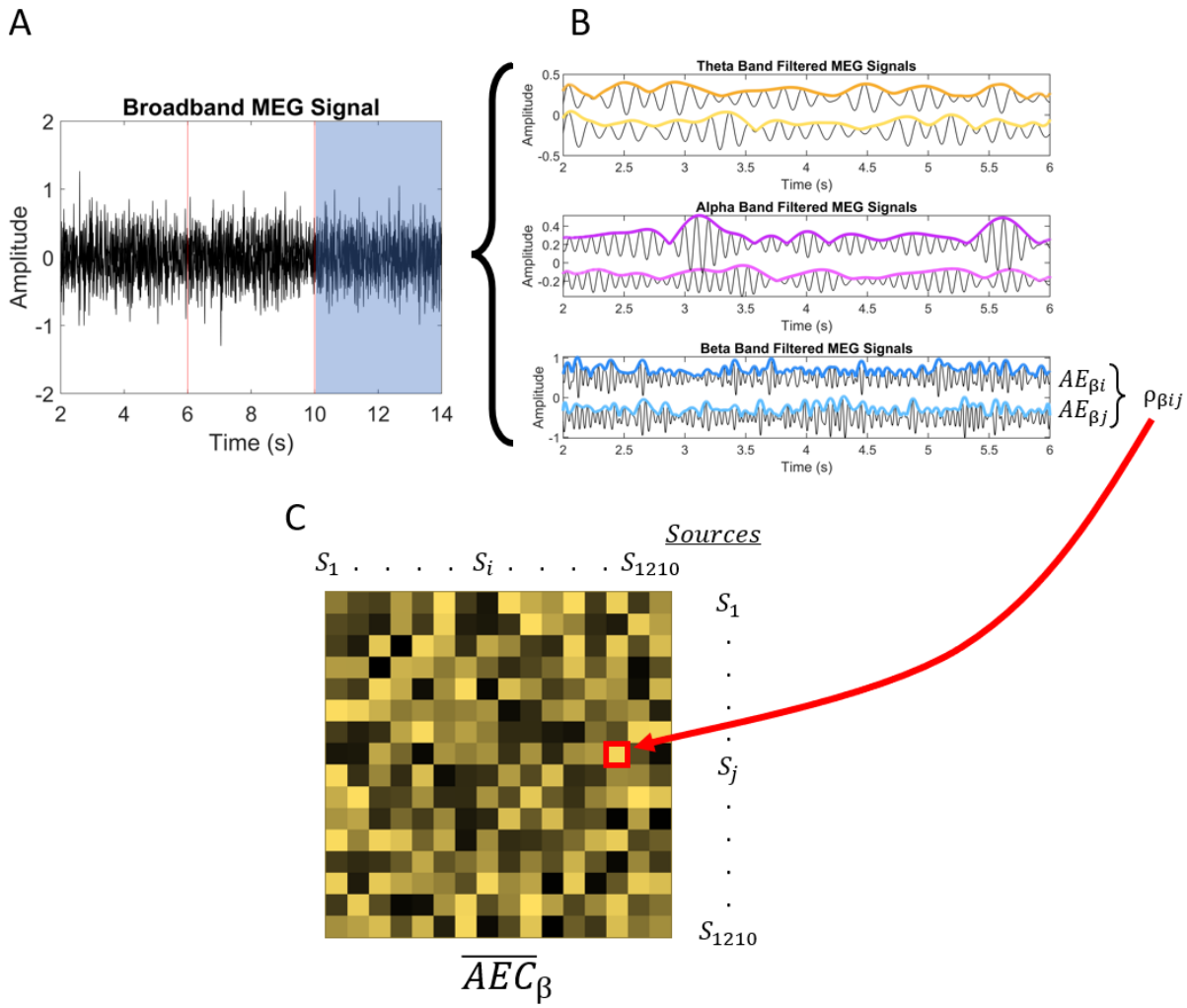


Figure 1.5: Amplitude envelope correlation (AEC) calculation. (A) MEG signals are filtered in the frequency bands of interest, and the envelope is then extracted through the Hilbert transform (B). (C) Finally, the correlation between each pair of envelopes in each temporal segment is calculated.

The envelope of a neural oscillating signal is the smooth curve outlining its extremes, effectively capturing the variations in amplitude over time. It is particularly relevant in neuroscience, given that it represents the low frequency modulations of power of neuronal oscillations, which has been linked to underlying physiological and cognitive processes previously in the text. Recently, the correlation between amplitude envelopes of band-limited signals, also known as amplitude envelope correlation (AEC; Bruns et al., 2000), has been increasingly utilized in resting-state connectivity analyses, showing spatial patterns of synchrony that resemble those shown in fMRI-based ICNs (Brookes et al., 2012; Hipp and Siegel, 2015), especially over alpha and beta frequency bands (Cabral et al., 2014). Interestingly, studies have found that these interactions might spontaneously arise from time-delayed network interactions between gamma-band oscillators in a border regime (Cabral et al., 2014).

It is possible to obtain the envelope of a real-valued, band-limited MEG signal, $x(t)$, through

its transformation into its corresponding analytical signal $x_a(t)$ using the Hilbert transform (Gabor, 1946):

$$x_a(t) = x(t) + ix_H(t) = A_x(t)e^{i\Phi_x(t)}, \tag{1.1}$$

where $A_x(t)$ and $\Phi_x(t)$ are the instantaneous amplitude and phase of $x_a(t)$, respectively:

$$A_x(t) = \sqrt{x(t)^2 + x_H(t)^2} \tag{1.2}$$

$$\Phi_x(t) = arctan(\frac{x_H(t)}{x(t)}), \tag{1.3}$$

and $x_H(t)$ is the Hilbert transform of $x(t)$, defined as (Gabor, 1946):

$$x_H(t) = \frac{1}{\pi} P.V. \int_{-\infty}^{+\infty} \frac{x(\tau)}{t-\tau} d\tau, \tag{1.4}$$

where $P.V.$ is Cauchy's principal value.

Once the envelopes from different time-series have been obtained, the AEC between the time series $x(t)$ and $y(t)$ is calculated through their correlation:

$$AEC_{xy} = \rho(A_x(t), A_y(t)) = \frac{cov(A_x(t), A_y(t))}{\sigma(A_x(t)) \cdot \sigma(A_y(t)}, \text{ if } \sigma(A_x(t)) \cdot \sigma(A_y(t) > 0, \tag{1.5}$$

where $cov(X, Y)$ is the covariance between X and Y, and $\sigma(X)$ is the standard deviation of X. As a note, since envelopes are calculated after band-pass filtering above 0 Hz, the upper and lower envelopes of the signal are symmetric, and so all AEC calculations are carried out with the upper envelope of each time series.

Phase-locking value (PLV)

Phase synchronization, on the other hand, occurs when two oscillators, $x(t)$ and $y(t)$, synchronize their instantaneous phases (Equation 1.3) over time (Rosenblum et al., 1996), which is represented as the phase-locking condition:

$$\Delta\Phi(t) = |\Phi_x(t) - \Phi_y(t)| \leq constant, \tag{1.6}$$

Importantly, the signal's phase can only be correctly estimated through the Hilbert transform if the oscillator behind the produced signal is isolated. Thus, these metrics can only be

estimated after band-pass filtering the signal, so there is no non-linear mixing of phases from two oscillators at different frequencies.

One of the most popular methods for estimating phase synchrony is the phase-locking value (PLV; Lachaux et al., 1999). PLV estimates the distribution of the relative phase, $\Delta\Phi(t)$, over a goniometric circumference, calculating the PLV as the module of the resulting vector of averaging all separate phase difference vectors. If $x(t)$ and $y(t)$ are strongly coupled, their relative phase will be approximately constant and will cluster over the same area of the unit circle, leading to a PLV approaching a value of 1. When the signals are desynchronized, the relative phase will be randomly distributed across the whole unit circle, the average vector will have a small module, and thus PLV will be close to 0 (Bruña et al., 2018, Figure 1.6). PLV is defined as (Mormann et al., 2000):

$$PLV_{xy} = \frac{1}{T}\left|\sum_{t=1}^{T} e^{-i(\Phi_x(t)-\Phi_y(t))}\right|, \tag{1.7}$$

where T is the total number of samples or data length.

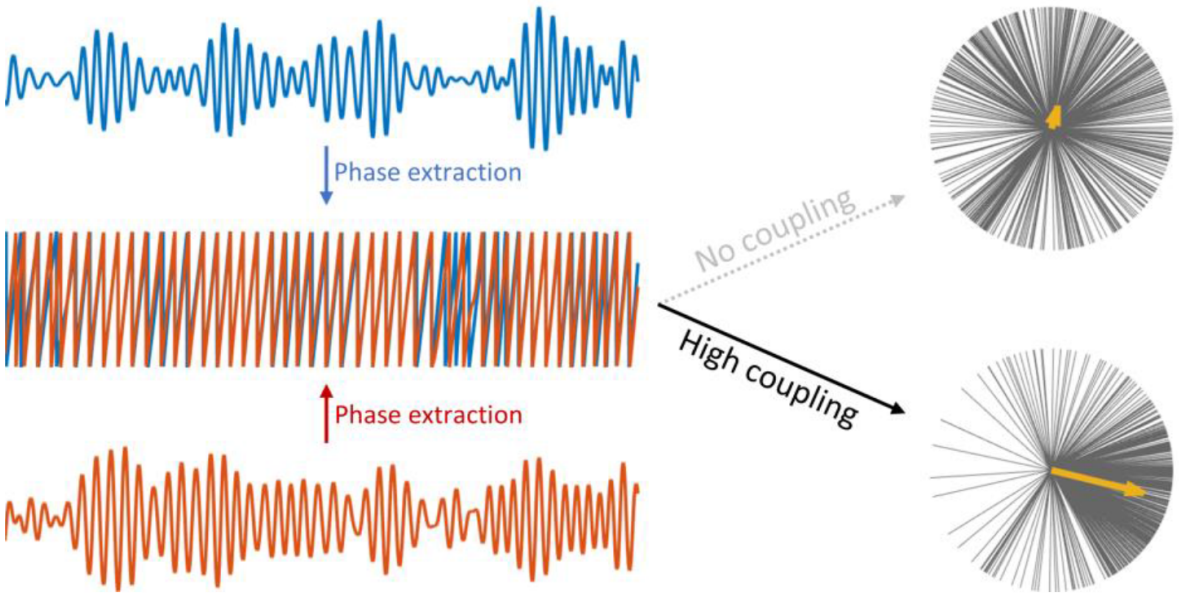


Figure 1.6: Phase locking value (PLV) calculation., extracted from Bruña Fernández, 2019.

Volume conduction, source leakage and connectivity

One of the problems that arise when calculating FC in EEG and MEG signals in sensor-space is volume conduction. This refers to the possibility that the activity from a single source may be recorded by multiple channels. The source-space equivalent to volume conduction is source leakage, the phenomenon in which the activity from the same original source is

artificially distributed across multiple sources in the brain, due to the ill-posed nature of MEG inverse problem, causing some spatial blurring. These events generate the so called "zero-lag" synchronization, which in linear synchronization translates into correlating the same signal represented in two different sources, and in phase synchronization yields a stable relative phase between signals around 0. While brain connectivity at zero-lag is possible, and its relevance has already been discussed in literature (Finger et al., 2016), it is not straightforward to differentiate physiological zero-lag connectivity from spurious zero-lag connectivity due to volume conduction or source leakage.

To tackle this problem, different connectivity measures have been defined that are insensible to zero-lag synchronization.

Regarding AEC, Colclough et al., 2015 proposed the application of a symmetrical multivariate orthogonalization of time-series before the calculation of the amplitude envelopes, referred to as leakage corrected AEC (AEC-c), eliminating any possible effect from volume conduction or source leakage. This methodology is implemented in the experiments of this thesis.

On the other hand, Bruña et al. defined a zero-lag insensitive PLV parameter called the corrected imaginary PLV (ci-PLV, Bruña et al., 2018):

$$ci - PLV_{xy} = \frac{|\Im(PLV_{xy})|}{\sqrt{1 - (\Re(PLV_{xy}))^2}}, \tag{1.8}$$

where $\Im(PLV_{xy})$ and $\Re(PLV_{xy})$ are the imaginary and real part of the PLV between $x(t)$ and $y(t)$, respectively. This connectivity measure dismissed the zero-lag connectivity contribution, and corrects the connectivity of close to zero-lag interactions.

1.3.2 The problem with classical measures of functional connectivity

Using the FC measures mentioned in the last section, researchers have helped advance and expand the knowledge on the brain function in both healthy and diseased condition, with most contributions coming from fMRI, EEG and MEG studies. More specifically, FC studies have determined that virtually everyone has intrinsic functional networks, and that those FC spatial patterns described in healthy participants are interestingly replicated in every clinical condition (Zhang et al., 2021). For example, resting FC between the major nodes of the DMN is patently present in patients with amyotrophic lateral sclerosis (Mohammadi et al., 2009), autism spectrum disorder (Cherkassky et al., 2006), schizophrenia (Zhou et al., 2007) and even in some patients in vegetative state (Boly et al., 2009), and even recent works have confirmed that the similarities in FC networks between healthy and psychiatric populations are much greater that any inter-group differences that are found (Spronk et al., 2021). In this direction, the already mentioned triple network model has proven as an excellent foundation towards the understanding of brain physiology and disease (Menon, 2011). Additionally, FC studies also have allowed us to characterize the developmental trajectory

of brain function across the human lifespan, essential when considering that many clinical disorders are neurodevelopmental or neurodegenerative in nature.

However, most research articles on resting-state functional connectivity published to this day share an assumption in their methodology: that functional connectivity is a stationary process. A stationary process is defined as a stochastic process whose unconditional joint probability distribution does not change over time. Therefore, parameters such as mean and variance do not change over time as well. Mathematically, a stationary process is defined as the following: let X_t be a stochastic process and let $F_X(x_{t_1+\tau}, ..., x_{t_n+\tau})$ represent the cumulative distribution function of the unconditional (in other words, with no reference to any particular starting value) joint distribution of X_t at times $t_1 + \tau, ..., t_n + \tau$. If so, X_t is strictly or strongly stationary if (Park, 2018):

$$F_X(x_{t_1+\tau}, ..., x_{t_n+\tau}) = F_X(x_{t_1}, ..., x_{t_n}) \text{ for all } \tau, t_1, ..., t_n \in \mathbb{R} \text{ and for all } n \in \mathbb{N} > 0 \quad (1.9)$$

Given that τ does not affect $F_X(\cdot)$, F_X is independent of time. Examples of stationary processes are white noise or Bernoulli schemes.

In FC studies, this translates to a common methodology to estimate FC (Figure 1.7). Firstly, the whole time series is divided into uniform time segments, usually selected as to have a representative number of events to be studied and enough time segments so that the resulting estimation is also representative of the underlying stochastic process. Afterwards, those segments containing artifacts are discarded, and FC is estimated independently in each of the segments, yielding one value per time-segment. Finally, these separate estimations are averaged, resulting in the final estimation of the FC that will be used in further statistical between-group or intra-group comparisons.

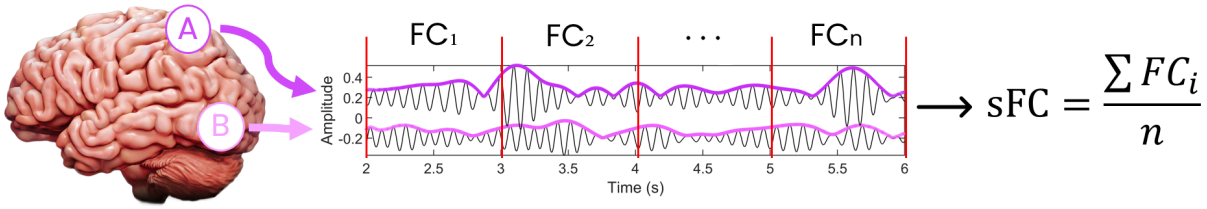


Figure 1.7: Usual procedure for the calculation of static functional connectivity (sFC). The original signal is divided into uniform temporal segments, from which the FC is calculated separately, and then averaged over time.

For example, in a typical electrophysiological study of resting-state data, approximately 5-minute EEG/MEG recordings are available. If we wanted to study FC in the alpha frequency band, we could then divide the already filtered signal in 4-second segments, which would contain each at least 32 oscillations in this frequency band (using the lower bound of the frequency band: $8Hz \cdot 4s = 32 oscillations$), and 75 signal segments.

The assumption of stationarity provides a convenient framework in which to examine and interpret results. However, after seeing in section 1.2 how every single element and component

in the brain, independently from anatomical or functional scale, has a highly dynamic behaviour, is this assumption supported by evidence?

1.3.3 Introduction to dynamic functional connectivity

The FC estimations obtained through the assumption of stationarity are referred to as static FC (sFC) throughout this thesis. Approaches built upon this assumption have produced a wealth of literature expanding our knowledge of large-scale brain networks. Nevertheless, sFC measures could merely represent an average across a complex spatio-temporal phenomena, discarding temporal information contained in the signals. Transient information would be lost, and what has been typically regarded as inter-subject variability might be in fact averaged FC temporal variability. At the same time, there is a possibility that while sFC spatial patterns are highly reproducible across health and disease, the transient coordinated activity is altered in the latter states, for example.

Given the known dynamic and condition-dependent nature of brain activity (De Pasquale et al., 2010; Rabinovich et al., 2012) it is natural to expect that FC estimated derived from neuroimaging data will exhibit variation over time. As a matter of fact, it has been proven that sFC changes due to task demands (Fornito et al., 2012; Han et al., 2017), learning (Gupta et al., 2021; Mehrkanoon et al., 2016), or during consciousness state transitions such as sleep (Bouchard et al., 2019; Tagliazucchi, Von Wegner, Morzelewski, Borisov, et al., 2012) or anesthesia (Nallasamy and Tsao, 2011). Furthermore, while inter-subject variation of FC might be expected due to its correlation to different individual characteristics (IQ, personality..., Adelstein et al., 2011; Bruzzone et al., 2022), within-subject FC has also been shown to vary between different scans in the same session (Garcés et al., 2016; Meindl et al., 2010) and even at faster time-scales of seconds or milliseconds (D. T. Jones et al., 2012; Tewarie et al., 2019).

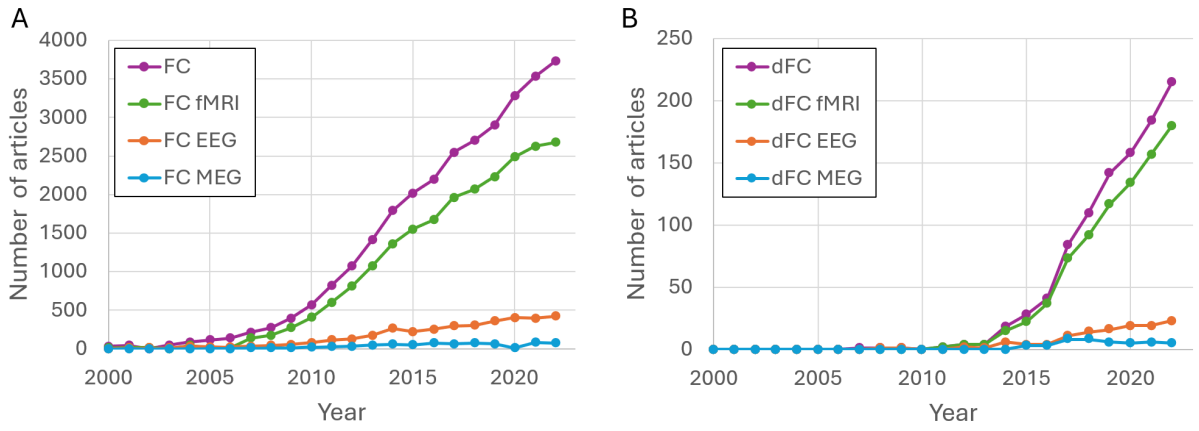


Figure 1.8: Number of studies published per year in the PubMed database associated with (A) functional connectivity and (B) dynamic functional connectivity. The graphs break down the total count of articles (purple) by neuroimaging technique: fMRI (green), EEG (orange), MEG (blue).

Since these initial findings, and in opposition to sFC, a consequent body of research has rapidly blossomed to investigate the so-called dynamic FC (dFC), with the objective of

shedding light over the behaviour of FC over time. While attracting more and more interest over the years, there is still a great breach between the number of research articles using sFC measures compared to those whose concern lies in the temporal dimension of FC, serving Figure 1.8, extracted from the PUBMED [1] database, as a broad example of this asymmetry. Importantly, this Figure also depicts another relevant event in this field: most research around both sFC and dFC has been performed through fMRI, while electrophysiological neuroimaging techniques, such as EEG and MEG have lagged behind. This strikes as a surprising fact especially for dFC, given the highly fast mechanisms underlying brain function and the higher temporal resolution of these latter techniques, which would make them the most adequate to assess dFC.

At this stage, it is important to further define dFC here, since this terminology may be interpreted in various ways. For example, dynamic fluctuations in brain connectivity exist in resting-state conditions, but attempts to characterize these changes during the execution of specific cognitive tasks, which show different methodologies, have also emerged (Gonzalez-Castillo and Bandettini, 2018; O'Neill et al., 2017; Simony et al., 2016). Also, one may argue that resting-state dFC itself exists at different time scales. While most reports, including those in this thesis, are concerned with the changes that happen over the course of seconds, there exists temporal evolution of brain connectivity at slower time scales of hours (Carrasco-Gómez et al., 2021; Orban et al., 2020) to months (Choe et al., 2015), driven by various factors ranging from learning, gene expression or disease. This thesis will focus on studying resting-state dFC through MEG at the time scale of seconds.

In spite of its recent inclusion in the scientific scenery, attempts to resolve resting-state dFC in a meaningful way have been spreading over a wide spectrum of methodological variants. Stemming from the most straightforward methodology, the sliding window technique, a myriad of procedures for estimating dFC has been developed in the field, from time-frequency analysis, to graph theory, or spatial and temporal clustering. Nonetheless, methodologies extending this initial framework have also emerged in recent years. These additional techniques can be grouped in event-based analysis, and methodologies performing analytical modeling of time of FC.

Sliding window analysis

The simplest analytical strategy to investigate dFC consists in segmenting the neuroimaging time series into a set of temporal windows, inside which the pairwise FC is estimated. The input data to sliding window analysis is then a set of timecourses representing either sensor- or source-space signals, be it BOLD or electrophysiological measures. Then a temporal window, defined by its length W, is selected, and within the temporal interval it spans (initially, from $t = 0$ to $t = W$), FC is computed between each pair of timecourses. Then, the window is shifted by a fixed step T, and FC is estimated again in the interval $[1 + T, W + T]$. T can take a number in the interval $[1, W]$, determining the amount of overlap between successive windows. The process is iterated until the window reaches the end of the original set of time series, obtaining in turn a connectivity matrix timecourse. Given a sufficient number of timepoints inside each window warrantying a robust FC estimation, any FC metric that

[1] https://pubmed.ncbi.nih.gov/

could be applied over an entire scan can be used in sliding window analysis.

Due to its simplicity and straightforward application, the sliding window framework has been enthusiastically welcomed in the scientific community, and has been applied to shed light over the relation between functional brain dynamics and cognition performance (Cohen, 2018; Elton and Gao, 2015), how the former is affected by different disorders, such as schizophrenia (Sakoğlu et al., 2010; Sanfratello et al., 2019), epilepsy (Pang et al., 2022), depression (S. Sun et al., 2024) or ADHD (Ahmadi et al., 2021), and how it compares to other structural brain measures (W. H. Lee and Frangou, 2017; Liégeois et al., 2016).

The uncomplicated approach of sliding window analysis obviously carries some shortcomings. First of all, the choice of the window length W has been a matter of debate inside the scientific community for a long time. On the one hand, the window length should be long enough to allow for a robust estimation of FC and to be able to assess the lowest frequencies of interest in the signal. On the other hand, potentially interesting transient changes in connectivity can only be detected with short enough window lengths (Hutchison et al., 2013). Previous studies have suggested a window length of 30-60 seconds for fMRI studies (Preti et al., 2017), while electrophysiological neuroimaging techniques can shorten the windows size to 2-4 seconds to be able to detect genuine fluctuations in FC (Liuzzi et al., 2019). Additionally, it is difficult to interpret the existence of variability alone just from an isolated connectivity matrix timecourse, and in fact this would not be enough to be able to state the presence of true dFC, since similar fluctuations can arise when applying a sliding window analysis to non-stationary processes such as white noise (Zalesky and Breakspear, 2015). Consequently, an appropriate statistical testing procedure has to be taken, either by comparing the dynamic behaviour of connectivity of a sample against a null distribution (obtained from surrogate data, for example), or by formally testing specific hypotheses such as searching for group differences or testing a possible correlation between dFC and another external parameter.

Starting from this basic approach, a wide variety of methodologies have moved in different directions, to obtain more refined dFC assessments (Figure 1.9):

- Summary dFC quantification

  Once the estimation of whole brain dFC has been performed after the application of the sliding window, summary measures that quantify dFC in connectivity timecourses can be calculated. The most popular summary variables include the standard deviation (std, Kucyi and Davis, 2014; Núñez et al., 2019; G. Yi et al., 2022), coefficient of variation ($CVAR(X) = \frac{std(X)}{\overline{X}}$, Gonzalez-Castillo et al., 2014), skewness and kurtosis (Fallahi et al., 2021; Wens et al., 2019), the ratio of windows with significantly different connectivity than the sFC (Hindriks et al., 2016), or the amplitude of low frequency fluctuations for fMRI studies (ALFF, Qin et al., 2015), defined as the total signal power within the low-frequency range (0.01–0.08 Hz). While these parameters might not be as informative as those presented in the next points, these measures have dominated over the early literature around dFC for their ability to compress the increased information generated by the sliding window approach, which helps in the interpretation of the results.

  Another popular approach in this direction is the application of graph theory methodol-

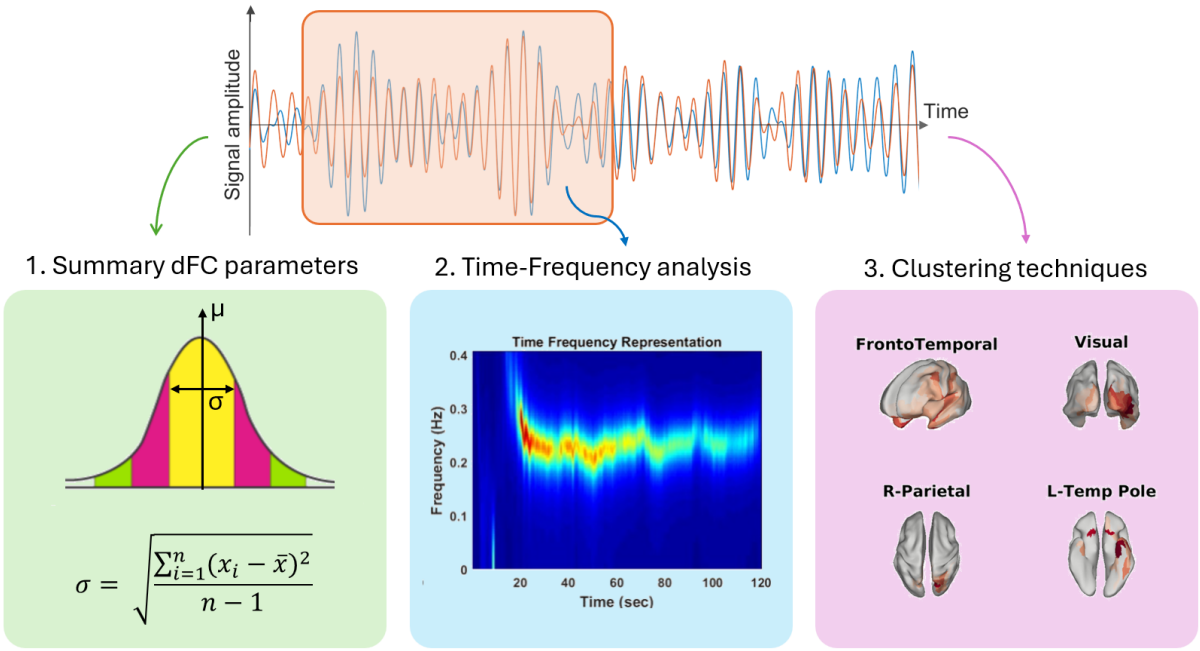


Figure 1.9: Summary of the main techniques derived from the sliding window methodology. Images extracted and modified from Giannakakis et al., 2019; Tait and Zhang, 2022.

ogy separately to each windowed connectivity matrix. This yields timecourses of graph parameters, characterizing the dynamic evolution of the architecture and information flow of the brain functional network. Moreover, the dependence between different graph parameters can be now modeled. Following this direction, Tagliazuchi et al. found that strong fluctuations over time occur over diverse graph metrics (Tagliazucchi, Von Wegner, Morzelewski, Brodbeck, and Laufs, 2012), revealing a continuous functional reorganization of the brain. The use of parameters such as the efficiency, a measure of the cost of one signal to travel from one brain region to another, or the modularity, which quantifies the extent to which a network is separated into a set of compact communities, offer a promising perspective on the dynamics of network integration and segregation (Cao et al., 2015).

- Time-frequency analyses

  A key limitation of sliding window techniques is that the window size selected is usually fixed. This window size restricts the time- and frequency-scale of the subsequent analysis, and is hopefully in equilibrium to provide both robust FC estimation and sensitivity to dynamic changes. Time-frequency analyses circumvent the need to select a fixed window, providing a multi-resolution approach that adapts the size of the window to that of the natural time-scale of the frequencies of interest in the signal. High frequencies (which elicit faster changes) are assessed with short windows, while progressively slower frequencies are analyzed with progressively longer windows. This is especially relevant knowing that electrophysiological oscillatory brain activity can be subdivided into different frequency bands with physiological underlying implications. In the fMRI case, the BOLD signal limits the temporal resolution of the analyses at hand, due to the

hemodynamic response function. FC calculated through fMRI is usually driven by fluctuations in the range of [0.01 - 0.1] Hz, while higher frequencies are contaminated by physiological noise (Preti et al., 2017). However, Zuo et al. revealed a spatially inhomogeneous frequency distribution within this narrow interval (Zuo et al., 2010). A setback from time-frequency analyses is the vast amount of information they produce (a time-frequency map per each pair of regions) when applying it to multiple subjects and brain areas, thus needing posterior handling to summarize the output along dimensions of interest.

One example of time-frequency analysis for dFC estimation is the application of the wavelet transform coherence (Torrence and Compo, 1998), providing an enriching perspective on coherence across multiple time-scales, which might be especially interesting for exploratory analyses. Through this analysis one may characterize, for instance, the dominant frequencies at which regions or networks display consistent FC, as well as how it evolves over time, as Chang and Glover did to discover that DMN-CEN anti-correlations appeared to be transient, rather than stable, phenomenon (Chang and Glover, 2010). While not as popular as other dFC techniques, principally in fMRI studies, it has been applied to assess the effect of caffeine intake on interhemispheric dFC (Rack-Gomer and Liu, 2012), to reveal a pattern of global stability in major depression disorder patients (Demirtaş et al., 2016), or to investigate the dynamics of absence seizures in epilepsy (Ieracitano et al., 2017). Ironically, this method can be useful to revert back to a sliding window methodology, to find the optimum window size for a specific analysis (Filippi et al., 2019).

- Clustering

  This set of techniques decompose dFC timecourses through matrix factorization methodologies, such as k-means clustering, principal component analysis (PCA) or ICA (Preti et al., 2017), which allows a summarization of the obtained dFC patterns in a smaller set of connectivity states. Each of these techniques applies a different criterion to obtain dFC states, and so the interpretation of the results obtained changes considerable from one to another. For example, they can either divide the timecourse into separate states, or define a set of states that contribute to the total FC network at each time point. The input for these kinds of algorithms consists in the concatenation of vectorized connectivity timecourses across subjects. Therefore, these states will not describe dFC at the individual level, but the group of subjects included in the study.

  K-means clustering was introduced by Allen et al., in 2014 (E. A. Allen et al., 2014), and has been repeatedly adopted by other researchers since (Shakil et al., 2016; Tait and Zhang, 2022), and allows identification of recurring connectivity patterns, called cluster centroids, mutually exclusive in time. Each of these cluster centroids also presents both positive and negative values, indicating correlated and anti-correlated regions, respectively. Conceptually similar methodologies can be found in hierarchical clustering (Yang et al., 2014) or community modularity approaches (Yu et al., 2015). The most important drawback from these kind of techniques is the arbitrary selection of the number of states to be found, which can significantly influence the statistical power and interpretation of the results (Ikotun et al., 2023).

In an alternative framework, Yaesoubi et al., 2015 proposed the application of temporal ICA (tICA) to obtain states that instead of maximizing spatial independence, were maximally mutually temporally independent. In this case, tICA allows a temporal overlap between different components, which will now have also a temporal dynamic interpretability. A similar output is obtained through PCA or single value decomposition (SVD, Leonardi et al., 2013) approaches, while temporal states are orthogonal by definition and maximize the variance in the concatenated dFC matrix. Careful interpretation is needed for analyzing the dFC patterns obtained via these methods, given that the obtained sign of the different states is arbitrary, and their real contribution is the result of combining them with their weight of temporal contribution. Additionally, small modifications in the processing pipeline can make a great difference in the result interpretation (Preti et al., 2017)

It is also important to remark that the aforementioned techniques are usually combined in different steps. For example, one could extract dFC states applying tICA over graph parameter timecourses or calculate the std of the time-frequency output time series at specific frequencies.

Event-based analysis

The sliding window approach has the implicit assumption that the spontaneous brain activity is characterized by a slow (second scale), but ever changing temporal dynamics. But an alternative view was proposed by Tagliazucchi and colleagues, explaining that the relevant information of resting-state FC can actually be extracted from discrete events or short periods of time in what is denominated a point process analysis (PPA, Tagliazucchi et al., 2011). This analysis only includes relevant time points, and would theoretically contain the same information as a full timecourse analysis. This has been shown both in fMRI by the same group (Tagliazucchi et al., 2016) or using electrophysiological recordings(Tait and Zhang, 2022), yielding the well-known ICNs.

This raises the question: how are the relevant points from the signal retrieved? This inquiry is especially relevant in resting-state studies, where, in opposition to task-based recordings, do not have locking or reference points to be used. However, these time-frames do exist, as revealed by research on resting-state periods following the learning of a task, where task-driven activity patterns could be found by a matching process and served as a marker of memory consolidation (Guidotti et al., 2015), the ability of inter-trial events to predict risk-taking in subsequent task trials (Pedroni et al., 2017), or the robust detection of arousal level fluctuations with electrophysiological recordings by matching templates with single frame activity (Chang et al., 2016). A potential explanation behind the spontaneous occurrence of this short periods of relevant activity could originate from the presence of neuronal avalanching activity (Lombardi et al., 2016). Typically, points from the signal are selected as relevant for subsequent analyses based their signal-to-noise ratio (SNR) and topographic stability, meaning that fMRI timecourses or EEG/MEG global field power (GFP) time series reaching a certain threshold are selected as reference time frames, but there might also rely on FC parameter timecourses (Figure 1.10). Furthermore, these time points can be extracted using the whole set of sensors/sources, or from a specific region of interest (ROI) seed-based activity.

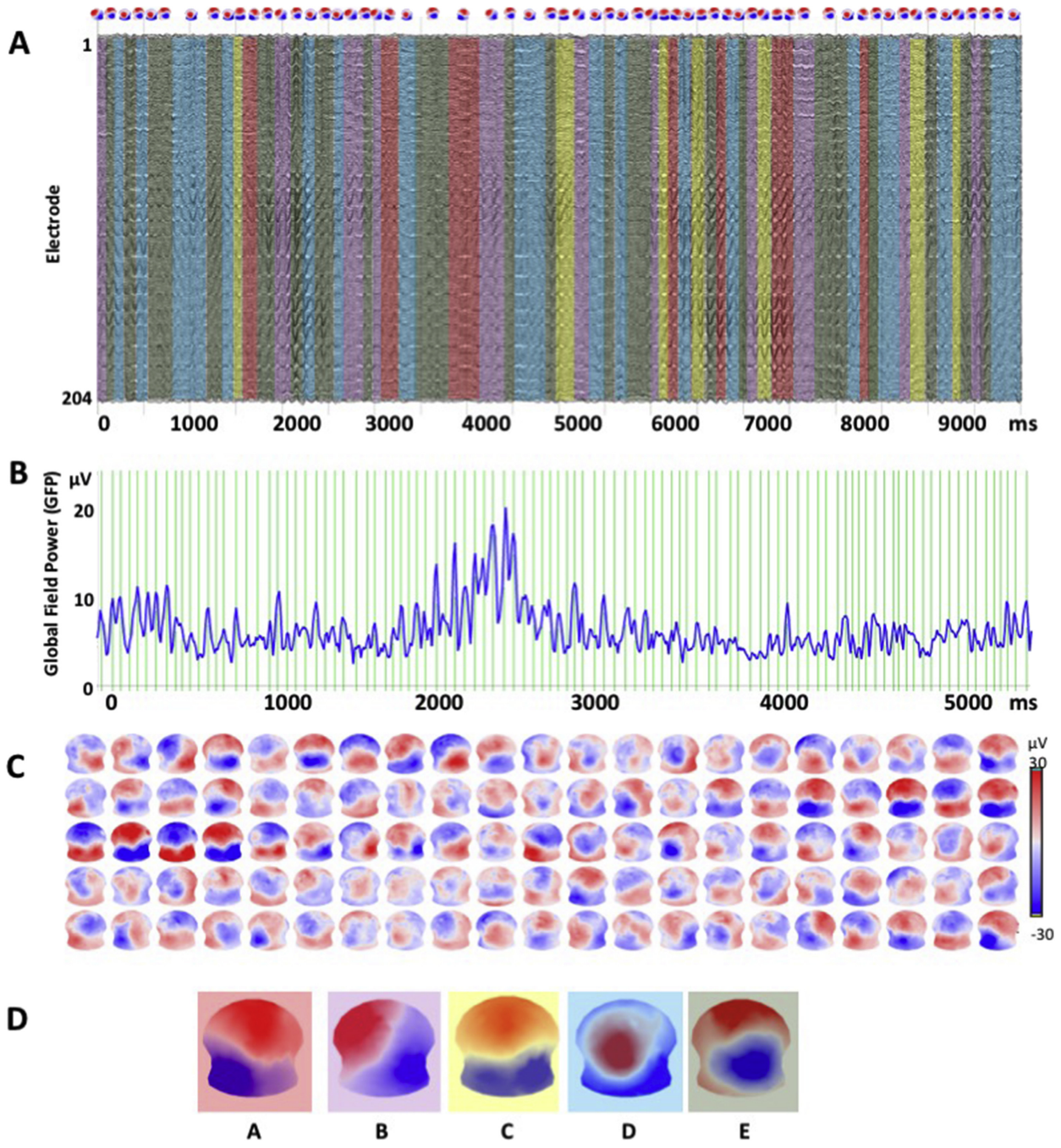


Figure 1.10: Steps in frame-based and microstate analysis. Extracted from Michel and Koenig, 2018. (A) 10-sec eyes-closed EEG recording from 204 electrodes. (B) Global Field Power (GFP) curve of the first 5 s of this EEG file. The GFP peaks, used for the subsequent frame-based analysis, are marked by vertical lines. (C) Topographical maps at consecutive GFP peaks. (D) Spatial k-means cluster analysis of the maps at GFP peaks of the whole EEG file, which revealed that 5 cluster maps optimally explained this data. These maps are then backfitted to the original EEG in (A) and each time point is labeled with the cluster map that correlated best. The period that each of the cluster maps covered is indicated in (A) by color bars.

Once the relevant time points have been identified, co-activation maps are extracted and then grouped by clustering algorithms such as the ones presented before: hierarchical, k-means

clustering or ICA. The result is again a set number of stable co-activation maps across time and subjects, which is then backfitted to the original timecourses to obtain the temporal distribution of each of the state maps. From this analysis we obtain spatial information from the distribution of correlation and anti-correlation areas of each of the co-activation maps, and temporal information which is usually summarized in terms of duration and occurrence likelihood of each of the extracted states. Remarkably, since this kind of analysis is not limited by the lower temporal resolution of the sliding window approach (windows of 30-60 s in fMRI studies and 3-4 in EEG/MEG studies), research using these techniques have found that these co-activation states have an average duration of 5-10 seconds when analyzing fMRI data (Karahanoğlu and Van De Ville, 2015), and 50-200 ms in electrophysiology studies (Tait and Zhang, 2022), providing a new insights on dFC with respect to previous studies performed with the sliding window methodology.

Examples from these new perspectives include the efforts of Liu and Duyn, who were able to demonstrate that the DMN, instead of activating as a whole as stationary approaches had revealed previously, was just partially recruited at specific moments, following a structured organization (X. Liu and Duyn, 2013). Through the computation of fMRI connectivity from a seed on active and inactive timepoints, Di and Biswal were able to compute co-activation and, interestingly, co-deactivation maps, highlighting the different information contained in both activation and deactivation events (Di and Biswal, 2015). Regarding the electrophysiology counterpart, EEG microstate analysis and the subsequent relation of those microstates to FC patterns, has been applied to study dFC. EEG microstates are robust and highly reproducible (Michel and Koenig, 2018) and have been associated to fMRI sFC and dFC (Abreu et al., 2021; Yuan et al., 2012). Moreover, they have been related to changes in cognitive domains and consciousness states (Guan et al., 2022; J. Xu et al., 2020; Zappasodi et al., 2019), and have already demonstrated their potential usefulness in clinical settings for understanding and detecting neurological disorders (Andreou et al., 2014; H. Liu et al., 2021; Tait et al., 2020). In a recent work, Tait and Zhang extended this microstate framework to MEG, adapting the methodology to overcome the lack of reference of MEG signals and the arbitrary source flipping (Tait and Zhang, 2022). Not only that, but they were able to reliably detect 10 microstates in resting-state MEG recordings, as opposed to the typical 4 microstates identified in EEG microstate studies, with consistent dFC implications and meaningful differences when compared to auditory-task MEG recordings.

This shift from a temporal window perspective to the analysis of single frames of activity has multiple advantages and contraindications. On the one hand, these techniques considerably reduce the analysis data load, a real issue when dealing with highly dimensional data as the one extracted from fMRI and EEG/MEG, and essential for current large-scale acquisition efforts (P. M. Thompson et al., 2020). Additionally, it favours data-driven, atlas-free analyses, which are not common in the sFC/dFC field. The exclusion of time points with smaller amplitude, comes as a double-edged sword, as it is true that these are more likely to be corrupted by noise, but at the same time might hold important information discarded through this approach: a considerable part of the results from these studies are based on interpolation, and might be oversimplifying the underlying processes (Gärtner et al., 2015; Koenig and Brandeis, 2016). On the other hand, the arbitrary choice of a significance threshold for relevant frame identification and the usual neglecting of negative events are important shortcomings

from this approach (Preti et al., 2017). Finally, relying on clustering techniques both comes with lights and shadows, as these techniques are good at detecting patterns and summarizing information, at the same time discarding some other possibly relevant information, and also work under some additional assumptions and arbitrary parameters.

In conclusion, this kind of analysis offers a promising perspective complementary to that of sliding window techniques, and is especially adequate for assessing very fast changes in FC.

Time-modeling approaches

The third approach included in this review is founded on the idea that we can find recurrent activity patterns in the brain, repeatedly occurring over time, and that those patterns are able to capture the evolution of FC better than analysis relying only on spatial FC patterns. In other words, while previous analyses each window or data frame was *a priori* independent from the rest, in this modality of techniques it is assumed that when a system is in a state, it will not evolve randomly, and will instead be conditioned by the present state and the previous ones in time towards a specific direction.

This means that we need to include explicit temporal models in the analysis process, see what model parameters fit best the recorded data, and draw conclusions. An early example from this methodology includes the work of Majeed et al., who developed a creative approach for finding repeated temporal sequences of spatial distributions in resting-state fMRI data in a data-driven manner, finding that the DMN and the attention network were opposed in activity levels and recurrently inverted their signs approximately every 20 seconds (Majeed et al., 2011). Another premature instance is the job of Guidotti et al., who had a significantly improved performance at discriminating the brain activity during two different tasks when applying a template matching a sequence of frames than when using single frames of spatial distribution (Guidotti et al., 2015). Nonetheless, while these are useful examples to see the relevant conditioning of previous activity in the evolution of FC, current literature methodology goes far beyond that used in these examples.

Understanding and effectively capturing time conditioning on FC is anything but easy which explains the scarce attempts at doing so in literature. One of the first approaches at time modeling stemmed from the hypothesis that FC evolution had to be continuous and smooth, thus modeling the transitions between FC at contiguous time points and constraining the solution space for the model accordingly. This can be achieved by restricting FC in a window or frame depending on the FC values of previous instances through regularization matrices (for the Alzheimer's Disease Neuroimaging Initiative et al., 2016), or the application of Kalman filtering techniques. In the latter case, the dependence between two brain activity time series is modeled through a third coefficient, equivalent to our FC parameter, which will depend both on the conjoined behaviour of both signals, and the previous values of the coefficient. The algorithm behind the Kalman filter will optimize the equilibrium between data-fitting accuracy and smoothness of the FC coefficient across time, and has proven a valuable tool to study resting-state dynamics (Ghumare et al., 2018; Kang et al., 2011). While this initial strategy is valuable, a smooth modeling of FC might not be the most adequate for an accurate description of the phenomenon of FC evolution. We already know that sudden network configuration changes occur, which require fast, and therefore not smooth, reorganizations of

brain functional architecture.

Overcoming the need of assumptions on the evolution of FC, another set of techniques has become popular among the scientific community: methodologies that parameterize the changes in FC over models that explicitly understand brain activity inside a sequential progression over different states. This way, no *a priori* hypotheses on the system dynamics are imposed and, depending on the evolution of FC or coactivation patterns, the model parameters are generated, even allowing multiple dynamic systems to coexist.

The most popular example in this category of methods are the Hidden Markov models (HMMs), a statistical model in which an observable process F (our FC parameter) is dependent on a hidden Markov process M (a finite set of neurophysiological states) in a known way. Since M cannot be observed, it is "hidden", the objective is to infer the state of M from the timecourses of F. An additional requirement of HMMs is that the outcome of F at time $t = t_0$ must be influenced exclusively by the outcome of M at $t = t_0$, and that the outcomes of both M and F at $t < t_0$ must be conditionally independent of F at $t = t_0$ given M at $t = t_0$. An HMM is characterized by $\lambda = (\pi, A, B)$, where π is the initial state probabilities, A is the state transition probabilities (how likely is state M_i to transition to M_j at a specific time), and B are the observation probabilities. To deal with multiple sensor/sources and the number of observations, neuroscience research typically uses an extension of HMMs, the multivariate Gaussian HMM (MGHMM), combining the HMM methodology with a multivariate Gaussian estimation for modelling the observation space (Duc and Lee, 2019). To solve the MGHMM model, the Baum-Welch algorithm (Liporace, 1982) or Bayesian variational algorithms (Vidaurre et al., 2017) can be used, for example.

Nevertheless, there exists a wide variety of modifications or additional steps to HMMs in literature to interpret the results or to model more complex dependencies between HMM states, granting HMMs an infinite spectrum of opportunities to investigate dFC. For example, Vidaurre et al., 2017 applied hierarchical clustering to demonstrate a hierarchically organization of network transitions, which were also subject-specific. In another work, Ou et al., 2015 applied an HMM to the output data of a sliding window analysis to model state dynamics in controls and post-traumatic stress disorder (PTSD) patients, finding that the latter showed lower state transitions, with a tendency to not disengage to a state linked to negative mood. Another example is the work of Seedat et al., 2020, who proposed the use of HMMs to identify transient spectral bursts of beta activity linked to a motor task, later deriving the brief functional connectivity profiles linked to those bursts.

While the use of HMMs comes with multiple advantages, as presented before, they also come with certain limitations. The main limitations are the need of large volumes of data for a proper model inference, which is sometimes impossible to obtain in neuroscience, as well as its dependency from the initial set of state probabilities, risking suboptimal solutions, or the assumption of conditional independence from past data, while previous microstate studies have observed non-Markovian transitions in them (Tait and Zhang, 2022). Furthermore, the model's reliance on pre-defined state numbers can limit its flexibility, often requiring extensive parameter tuning and cross-validation to avoid poor generalization (Duc and Lee, 2019).

Time-modeling approaches enable the incorporation of previously unaccounted complex

features for the understanding of the evolution of FC, and thus also constitute a promising pathway in the study of dFC.

1.3.4 Proposed methodologies in this thesis

The proposed techniques used in each of the chapters of this thesis are framed in the category of sliding window techniques, basing their quantification of FC dynamics on the FC timecourses obtained after segmenting the signals in different time portions. The reason behind this decision is that previous laboratory research on AD evaluates sFC through a sliding window process, firstly dividing the MEG signal in 4 second segments, then calculating the FC in each of those, and finally averaging the measures over all time epochs to obtain an sFC estimate. Being this the case, we base our dFC measures on the same sliding window paradigm given that (1) we want to obtain dFC measures comparable to sFC parameters as calculated in other articles from our lab, (2) we want to rely on as few assumptions as possible for the computation of dFC, being these the first efforts in the laboratory focusing on the dynamics of FC, and (3) 4-second windows have been deemed as appropriate to detect dFC changes in previous literature (Liuzzi et al., 2019). The methods proposed for assessing dFC in this thesis are based on the use of **recurrence matrices** and the **entropy quantification** of FC timecourses, both at the level of ROIs, i.e. grouping of sources according to a predefined atlas, and at source-level.

Recurrence matrix dFC

As we have previously explained, sFC was estimated by dividing the original MEG signals in uniform time segments of 4-seconds (N = total number of segments), then calculating either AEC-c or ci-PLV in each of the segments, and averaging FC parameters over time (Figure 1.7). However, for the sake of studying dFC, we calculated the correlation between the connectivity matrices corresponding to each segment. This is usually labeled in literature as the recurrence matrix (C) (Núñez et al., 2021; Tewarie et al., 2019), and represents the similarity of connectivity distributions over time, as represented in Figure 1.11. Importantly, to maintain a uniform representation of the data of all subjects, we made sure that the same number of continuous segments were used for dFC calculations in all subjects. Each of the C_{ij} terms of the recurrence matrix represents the correlation of all connectivity terms of the connectivity matrix of segment i with those of the connectivity matrix of segment j, resulting in a matrix of dimensions $N \times N$. The Fisher Z-transformation, defined as the was subsequently applied to these matrices, to prevent any skewness in the calculated distribution (Hotelling, 1953):

$$z(r) = \frac{1}{2} \ln \left(\frac{1+r}{1-r} \right) = atanh(r), \tag{1.10}$$

where ln is the natural logarithm function, r is the sample correlation coefficient, and $atanh$ is the inverse hyperbolic tangent function.

To improve the interpretability of the obtained parameter, we defined the "Dynamicity" (Dyn) as the following:

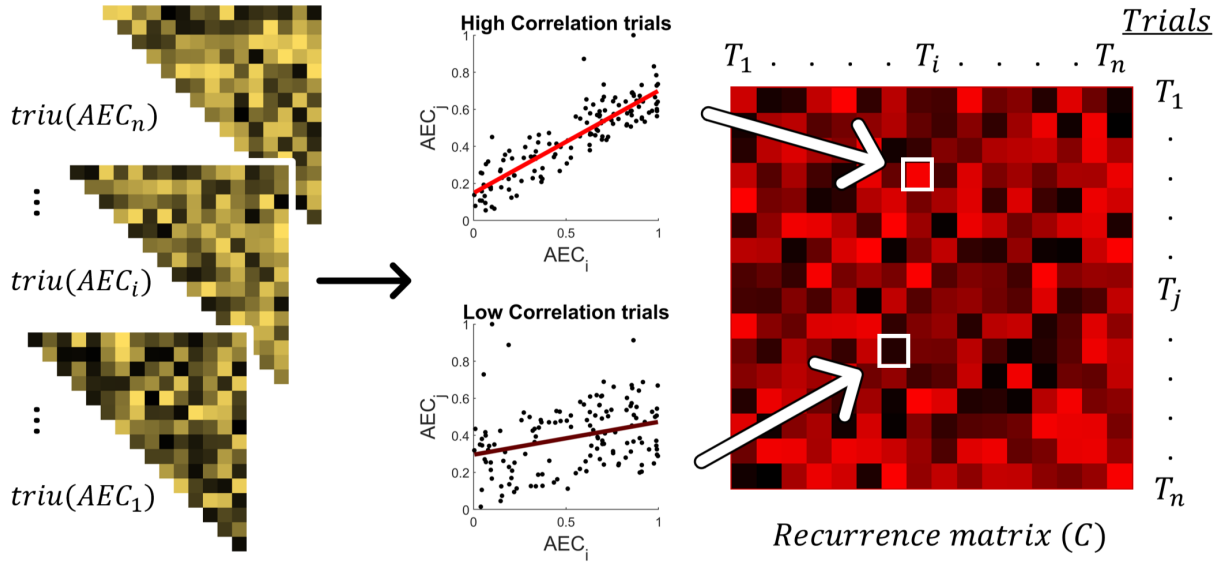


Figure 1.11: Calculation of the recurrence matrix (C). .

$$Dyn = \frac{\overline{triu(atanh(0.99)) - triu(atanh(C))}}{atanh(0.99)}, \tag{1.11}$$

where the operator triu is the upper triangle matrix selector, the operator $\overline{x}$ is the average if x, and C is the recurrence matrix.

This parameter would range from 0 to 1, where 0 represents complete stationarity while 1 would represent a complete lack of temporal correlation among connectivity matrices. Note that we use the inverse hyperbolic function of 0.99 instead of 1 for normalization, since the inverse hyperbolic tangent of 1 is infinite.

Seed-based recurrence Using the whole connectivity matrix to derive recurrence matrices means we cannot derive spatial information in this manner. To perform a data-driven analysis of the spatial distribution of changes in dFC through recurrence matrices, we propose the methodology we called "seed-based recurrence matrix". While all terms in the connectivity matrix are used to calculate the correlation of each segment with the others in a recurrence matrix, the seed-based recurrence matrix separates that process for each of the sources, as shown in Figure 1.12.

Being M the total number of sources, the calculation of the seed-based recurrence matrix for source i would follow these steps:

1. The vector of $M-1$ connectivity terms between the source i and the rest of the sources is extracted for each time segment.
2. The correlation between each segment connectivity vector is calculated.

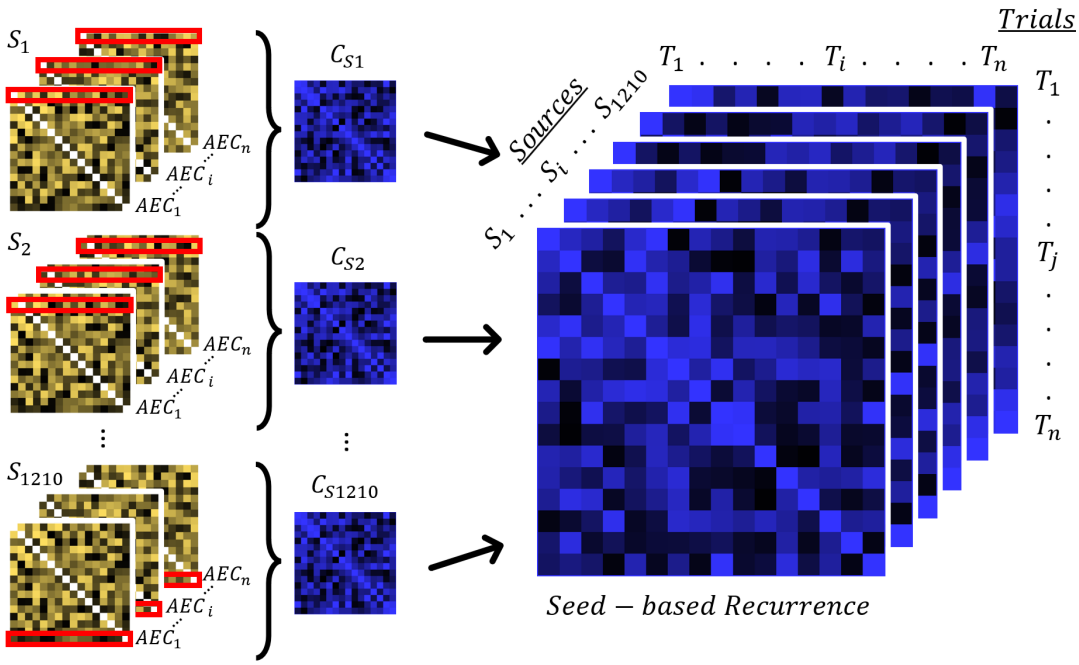


Figure 1.12: Seed-based recurrence matrix. The seed-based recurrence matrix would then be transformed to dynamicity values.

Done over all sources, the resulting seed-based recurrence matrix would have dimensions $M \times N \times N$. Importantly, M should be large enough to obtain robust correlation estimations, which is the case for MEG source-space analyses present in this thesis, where 1210 cortical sources are included. Once again, the Fisher Z-transformation was applied to the data to favor the normality of the distribution and the result was subtracted from the inverse hyperbolic tangent of 0.99, and normalized by the same number, as in Equation 1.11, obtaining a vector of M dynamicity values per subject, which can be subsequently used in source-space MEG analyses.

Entropy dFC

Again, we start from the series of connectivity matrices corresponding to each time segment (dimensions $M \times M \times N$), this time averaging them over the second dimension. The resulting matrix, of dimensions $M \times N$ is called the connectivity nodal strength over time, representing the average connectivity of each cortical source position with all the other sources across time. Then we can investigate dFC by quantifying the sample entropy of the time series in each of the sources by means of histograms with linearly spaced bins (Figure 1.13, Shannon, 1948).

Firstly, to determine the optimal number of bins for the creation of histograms in our dataset, we followed the guidelines exposed by Knuth (Knuth, 2019) for each of the sources' connectivity strength time series in all our participants. In both Chapters 3 and 4, after applying it over all sources we kept the median of the resulting calculations, obtaining an optimal number of $B = 11$ bins. Secondly, and again to assure comparability between subjects, we defined the minimum and maximum values for the binning procedure in each cortical source by

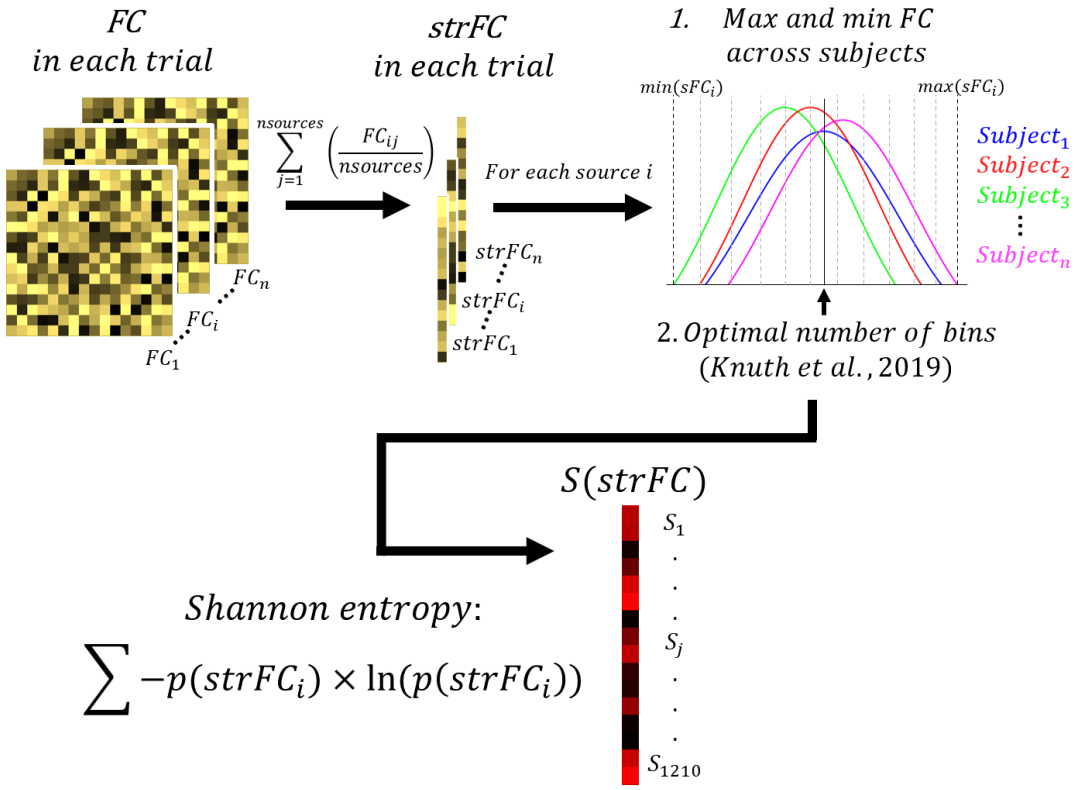


Figure 1.13: FC entropy calculation..

calculating the minimum and maximum value of the connectivity strength of a cortical source across all participants. Finally, following the optimal binning procedure, the Shannon entropy (S) was calculated (Shannon, 1948):

$$S(FC) = -\sum_{i=1}^{B} p(FC_i) \times \ln(p(FC_i)) \tag{1.12}$$

where FC is the connectivity nodal strength of a specific source, ln is the natural logarithm, and $p(FC_i)$ is the estimated probability that a connectivity value in FC falls inside the bin i.

After applying this procedure to each source in each subject, we obtain a dFC entropy value for each of the M sources that creates an entropy dFC vector for each of the subjects, again ready for further source-space MEG analyses.

1.4 Alzheimer's Disease

Dementia is a syndrome characterized by persistent cognitive impairments, such as difficulties with memory, language, reasoning, and problem-solving, that interfere with daily life, as defined by the World Health Organization[2]. The leading cause of dementia is Alzheimer's disease (AD), which accounts for 60 to 80% of all cases ("2024 Alzheimer's disease facts and figures", 2024), followed by frontotemporal dementia, vascular dementia, dementia with Lewy bodies, and Parkinson's disease. The World Health Organization (WHO) estimated that approximately 55 million people live with AD or another dementia worldwide, and predicted that number to triple by 2050 ("2024 Alzheimer's disease facts and figures", 2024). The number of dementia cases registered in the Spanish National Health System (BDCAP, Base de Datos de Clínicos de Atención Primaria; Portal Estadístico del Ministerio de Sanidad[3]) was 489.364.

1.4.1 Introduction to AD

AD is a neurodegenerative disease characterized by a progressive deterioration of memory, first discovered by Alois Alzheimer in 1907 (Alzheimer, 1907), after studying the case of Auguste Deter at the Frankfurt asylum from 1901 to 1906, when Auguste died. The early symptomatology of AD typically involves problems encoding new memories, apathy, and depression, followed afterwards by communication difficulties, spatio-temporal disorientation, mood disorders, and finally troubles for speaking, swallowing, and walking. Severely limiting the independence of the patients suffering from it, AD has an incredibly substantial burden on family members, friends, and professional caregivers, not only from the economical perspective, as unpaid dementia caregiving in the US was estimated to amount to 346.6 thousand million dollars in 2023 ("2024 Alzheimer's disease facts and figures", 2024), but also for increased risk for emotional distress and negative mental and physical health outcomes. AD is among the top five causes of death in Europe, accounting for around 5% of all deaths, and is also a major cause of disability and morbidity (Deuschl et al., 2020).

AD can present in two different forms: early-onset (autosomal dominant) or late-onset (sporadic). The early-onset form of AD, while accounting for only 1% of the cases, and its mechanisms are far better characterized, and are caused by the autosomal-dominant inheritance. The genetic mutations are located in the gene coding the amyloid precursor protein (APP), and the presenilin-1 (PSEN1) and presenilin-2 (PSEN2) genes, responsible for coding presenilin-1 and presenilin-2 proteins (Goate et al., 1991; Levy-Lahad et al., 1995; Sherrington et al., 1995). On the other hand, the mechanisms of late-onset AD are more complex and still not completely understood, involving interactions between genetic, environmental, and epigenetic variables. The main risk factors for late onset AD are age, a collection of genetic polymorphisms, and a family history of AD ("2024 Alzheimer's disease facts and figures", 2024). The risk of AD increases exponentially with age, with prevalences ranging from 5% percent of people aged 65 to 74, 13.2% of people aged 75 to 84, and 33.4% of people aged 85 or older have AD ("2024 Alzheimer's disease facts and figures", 2024), with

[2] https://www.who.int/news-room/fact-sheets/detail/dementia
[3] https://pestadistico.inteligenciadegestion.sanidad.gob.es/publicoSNS/

the incidence doubling every 6.3 years. Of the many genes that increase the risk of AD, the apolipoprotein E (APOE) gene, coding a protein for blood cholesterol transportation, has the strongest impact ("2024 Alzheimer's disease facts and figures", 2024). The APOE gene has three major alleles ($\epsilon 2$, $\epsilon 3$, and $\epsilon 4$) that confer different levels of risk: the $\epsilon 2$ allele lowers the risk by half, whereas the $\epsilon 4$ allele increases it three- (one copy) to 14-fold (two copies) (Yamazaki et al., 2019). Finally, a family history of AD is also associated with an increased AD risk. This risk factor combines known (i.e., APOE) and unknown genetic factors with other intrafamilial variables, such as lifestyle and nutrition. This means that through the modification of certain health and lifestyle variables, such as cardiovascular health, physical activity, education, and social and cognitive engagement throughout life we might be able to reduce the risk of AD ("2024 Alzheimer's disease facts and figures", 2024).

One of the current major challenges faced by the international community is the proper diagnosis of the late-onset disease. Until recently, AD stood as a clinical entity which could only be definitely diagnosed post-mortem, while living patients are labeled as possible or probable cases of AD, based on their clinical presentation and evolution of symptoms. Therefore, AD diagnosis was restricted to individuals presenting dementia (Jack et al., 2018). However, evidence has indicated that an amnestic multidomain type of dementia, the common phenotype of AD, is not exclusively associated with AD pathophysiology, and that approximately 10% to 30% of individuals clinically diagnosed with AD actually do not show any underlying AD pathology (Jack et al., 2018). These events led the National Institute on Aging and Alzheimer's Association (NIA-AA) to propose in 2018 the redefinition of AD diagnosis criteria based on its biology and pathophysiology, rather than on its clinical profile (Jack et al., 2018), establishing the pathological hallmarks of AD as the accumulation of extracellular amyloid-beta (Aβ) in Aβ plaques, and intracellular neurofibrillary tangles (NFTs) of hyperphosphorylated tau protein (p-Tau). These underlying pathological alterations are thought to begin up to 20 years before any clinical manifestations emerge ("2024 Alzheimer's disease facts and figures", 2024). Consequently, the brain has already suffered extensive damage when cognitive symptoms arise, which might be the reason behind the unsuccessful attempts at designing a valid pharmacological treatment for AD. This has motivated a recent shift in the focus of AD research, now prioritizing the identification of early changes that might lead to the development of this form of dementia.

The AD continuum The biological definition of AD allowed to extend the development timeline of AD to periods where no cognitive symptoms are present, bringing about the definition of the so-called AD continuum, which includes individuals ranging from cognitively unimpaired to suffering from dementia. This spectrum spans three distinct stages: preclinical AD, MCI, and dementia due to AD (Figure 1.14). In the preclinical stage, individuals show the first evidence of AD physiopathology while their cognitive performance is within the normal range. This stage includes a subset of preclinical patients who may report a perceived subjective cognitive decline (SCD), that is not discernible in a neuropsychological evaluation (Jessen et al., 2014). Although not everyone presenting SCD goes on to advance along the AD continuum, their risk to do so is higher than individuals at their age without SCD (Mitchell et al., 2014). Mild cognitive impairment (MCI) constitutes the prodromal stage in the AD spectra, and includes individuals with evidence of AD neuropathology, and

objective cognitive impairment, but preserved daily independence ("2024 Alzheimer's disease facts and figures", 2024). MCI can be further divided depending on the affected cognitive domain, yielding clinical diagnosis of amnestic MCI if there exists an isolated impairment of memory, or multidomain amnestic MCI if additional cognitive domains, such as language, are altered simultaneously. The annual conversion rate from MCI to AD is estimated to be 18.5% (Ghanem et al., 2024). Finally, in the dementia stage, the accumulated neurodegeneration from earlier phases reaches a critical point, leading to a progressive decline in cognitive functioning. As a result, individuals with dementia gradually lose the ability to perform daily tasks and eventually become unable to live independently. This stage can be further separated into mild, moderate, and severe dementia.

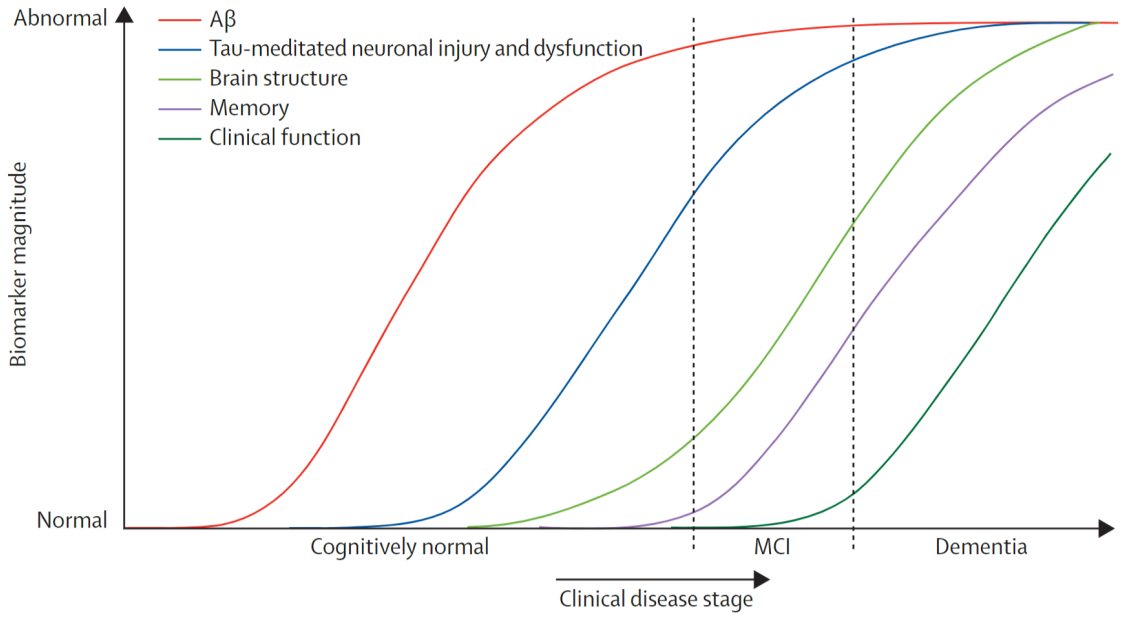


Figure 1.14: AD continuum and evolution according to the amyloid hypothesis. Evolution of the biomarkers associated with the hallmarks of AD according to the amyloid hypothesis. In this model, Aβ accumulation, NFTs presence, and cortical atrophy take place years before the onset of cognitive symptoms. Reproduced from Jack et al., 2010.

1.4.2 AD neuropathology

While the age of onset differs from the two exposed AD variants, both forms of the disease share their clinical and pathological evolution, and their development is strongly associated to a higher production and accumulation of Aβ and tau protein in the brain (Palop and Mucke, 2010).

Amyloid beta (Aβ)

Over the last decades, a wealth of studies has provided evidence for the involvement of Aβ aggregates in the development of the disease, which favoured the amyloid hypothesis as the dominant model in AD research (Karran and De Strooper, 2022). This hypothesis stems from the amyloidogenic pathway processing of the APP in the cell membrane, which derives

in the increased production of Aβ. In this pathway, the APP is sequentially cleaved by the β- and γ-secretase enzymes. The β-secretase severing produces a large extracellular domain (secreted APP-β) and a membrane-bound C99 fragment. This fragment is then cleaved by the γ-secretase, giving rise to a variety of extracellular Aβ monomers (Koo and Squazzo, 1994). Under normal physiological conditions, both APP and Aβ play protective roles. For instance, APP is involved in synaptic plasticity (De Frutos Lucas et al., 2023; Klevanski et al., 2015), while Aβ may be an antibacterial peptide in the CNS' innate immunity, and its aggregation might constitute a protective response against infection (Huang and Liu, 2020). However, if the production and clearance of these monomers become unbalanced, they begin to pathologically aggregate, leading to the formation of oligomers, fibrils, and eventually, neuritic plaques. The amyloid hypothesis is supported by important evidence such as the identifications of the previously mentioned mutations in the APP, PSEN1, and PSEN2 genes, linked to the increased expression of Aβ species (Sherrington et al., 1995), as well as the high levels of mutant APP displayed by transgenic mice which also suffered many of the pathological hallmarks of AD (Bornemann and Staufenbiel, 2000).

While the initial research efforts focused on the neurotoxic effects of Aβ plaques, research indicates that Aβ oligomers, formed by the aggregation of Aβ monomers in a previous stage to plaque formation, are more toxic than these (Busche et al., 2012; Hector and Brouillette, 2021). The presence of Aβ oligomers results in a cascade of downstream of biochemical failures, triggering alterations in neural signaling, synaptic function and neural network activity, eventually leading to neuronal loss (Gonzales et al., 2022; J. Liu et al., 2019). The pathways involved in this biochemical cascade are still being investigated, but research suggests that Aβ oligomers induce membrane alterations which result in calcium dysregulation, mitochondrial damage, generation of reactive oxygen species, abnormal tau phosphorylation, and even a further accumulation and aggregation of Aβ (Huang and Liu, 2020). Of relevance for the thesis is the influence of Aβ oligomers on the neuronal excitation/inhibition (E/I) balance (Maestú et al., 2021), an important physiological entity that shapes brain function, consequently altering other electrophysiological parameters, including brain synchrony, which will be discussed further in a future section. On the one hand, moderate concentrations of Aβ enhance excitatory neuronal activity, which in turn favour a greater release of Aβ, thus entering a vicious positive feedback loop. This effect is thought to be a result of Aβ's influence on presynaptic N-methyl-D-aspartate (NMDA) receptors (J. Liu et al., 2019), along with an increase in calcium influx. Furthermore, Aβ has also been linked to the silencing or impairment of inhibitory neurons, with evidence from animal models and human patients consistently showing GABAergic neuronal dysfunction and impaired GABA secretion (Mattson, 2020; Y. Xu et al., 2020), resulting in an additional increase in neuronal excitability. Lastly, non-neural populations, such as the astroglia, are also influenced by the concentration of Aβ, which in turn can further contribute to the excitability of the system, for instance, through the release of astroglial glutamate.

While Braak and Braak obtained a stepwise progression model of Aβ deposition through classical histological studies (H. Braak and Braak, 1991), more recent research, performed with 18F-florbetapir positron emission tomography (PET) reveal a different progression (Figure 1.15). In their work, Mattsson et al., 2019 longitudinally followed individuals across the whole AD continuum, modeling the pattern of Aβ accumulation over time considering levels

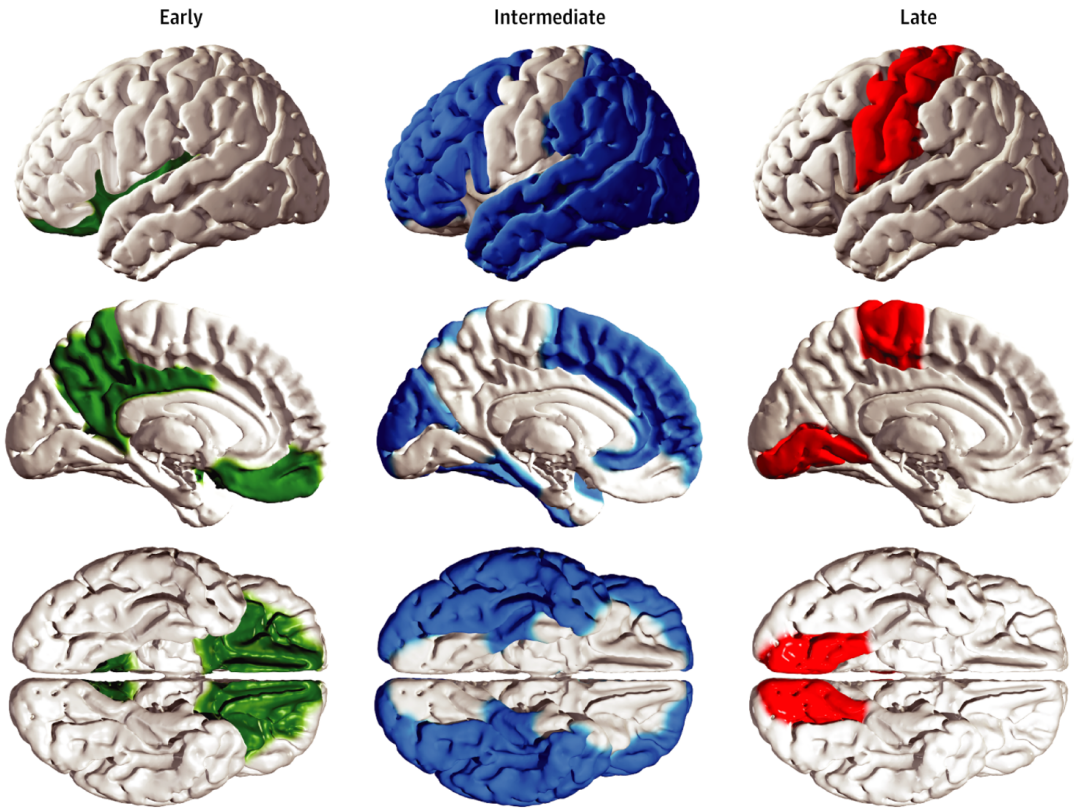


Figure 1.15: Staging of Aβ accumulation in AD according to Mattsson et al., 2019.

of Aβ on both PET and cerebrospinal fluid (CSF). Inclusion of CSF was relevant due to its early detection of abnormal Aβ levels compared to Aβ-PET, being the latter insensitive to soluble species of Aβ. Early accumulation regions were assessed comparing CSF+/PET- (early accumulators) against CSF-/PET- (nonaccumulators) individuals. The regions included in this category were the precuneus, posterior cingulate cortex and the orbitofrontal cortex, only the latter overlapping with Braak and Braak's stage 1. By contrast, late regions were identified comparing CSF+/PET+ (late accumulators) against early accumulators. Late Aβ deposition areas involved the para-, pre- and postcentral cortices, as well as the pericalcarine cortex, in accordance with Braak and Braak's stage 3 of late primary sensory areas affectation. The remaining areas were merged into an intermediate stage. Early accumulation stood as a significant risk factor for further Aβ deposition and progression into subsequent stages. Additionally, cognitive decline was associated with accumulation of Aβ intermediate and late regions, which is congruent with the temporal progression of biomarker levels across the AD continuum.

Despite all of this evidence, the amyloid hypothesis still has some unresolved issues, such as the presence of Aβ deposits in the brains of cognitively normal older adults (Aizenstein et al., 2008), or the clinical failure of different pharmacological therapies based on anti-amyloid agents(Doody et al., 2013; Henley et al., 2019).

Tau proteinopathy

The second hallmark of AD is the presence of tau pathology in the form of NFT made up of p-Tau (Okamura et al., 2018). Tau is a microtubule associated protein that, under physiological conditions, promotes microtubule assembly and stabilization in the axons of neurons (McGrowder et al., 2021). The action of phosphatases and kinases inside the cell maintain a balance between tau and phosphorylated tau levels, allowing for a proper transport of vesicles along the axon. Nevertheless, an irregular hyperphosphorylation of tau takes place under pathological conditions, potentially due to an impaired dephosphorylation, provoking the loss of tau affinity for the microtubules and the latter's stability. This process promotes microtubule depolymerization and damages axonal integrity and transport upon which nutrition and residue elimination processes depend, leading to neuronal loss. Additionally, hyperphosphorylated species of tau see their solubility reduced, thus increasing their aggregability, and contributing to the eventual formation of the NFTs, which can be found inside of neurons and in the interstitial fluid. Accordingly, NFT presence in AD, concomitant with neuronal death, usually has a more direct link to local neurodegeneration and, in turn, cognitive impairment than Aβ presence does (Nelson et al., 2012; Vogel et al., 2020).

Tauopathies include other neurodegenerative diseases apart from AD, but each of them is characterized by specific alterations of tau isoforms, and the degree and distribution of protein phosphorylation. In AD, NFTs comprise paired helical filaments of p-Tau (Okamura et al., 2018; Wang and Edison, 2019). Importantly, prior to the formation of NFTs, p-tau can aggregate in intermediate structures known as fibrils, which present a prion-like behaviour, inducing further phosphorylation of other tau molecules propagating the pathology. Research shows that propagation of these species is accelerated by the presence of Aβ in two different directions. Firstly, one of the downstream effects of Aβ oligomers is the phosphorylation of tau through the interaction with different kinases (Oliveira et al., 2015), which could elicit the creation of p-Tau. Secondly, the prionic nature of tau fibrils induces an activity-dependent propagation of these pathological species, spreading across synapses of functionally connected neurons, even between distant brain areas. Consequently, the increased neuronal excitability and activity originated by Aβ leads to an increase in both p-Tau generation and spreading.

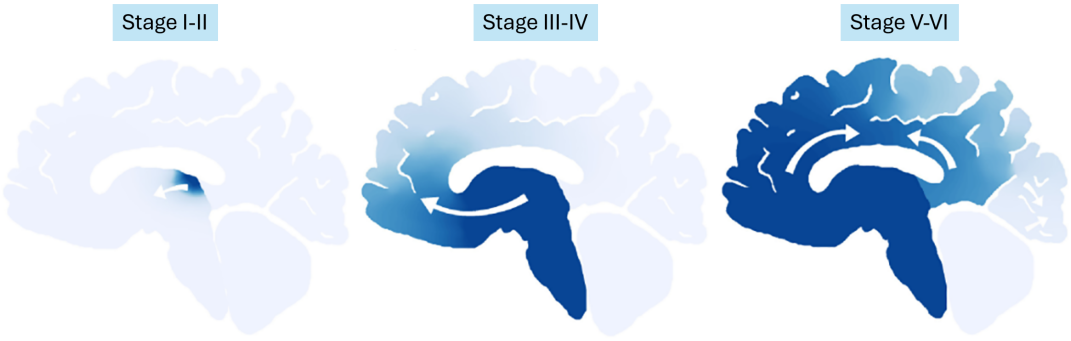


Figure 1.16: Staging of the NFT accumulation in AD according to H. Braak and Braak, 1991 and T. B. Thompson et al., 2020. Reproduced as in T. B. Thompson et al., 2020

Braak and Braak (H. Braak and Braak, 1991; H. Braak and Del Tredici, 2018) defined 6

stages of NFT propagation across the AD continuum, beginning from the entorhinal and hippocampal areas, continuing to limbic structures and culminating with the inclusion in the neocortex, first in associative regions and lastly in primary ones. Tau pathology was regarded as a late event in the AD continuum, given that NFTs, associated with neurodegeneration and cognitive decline, were only present in the late stages of the disease. Nevertheless, this evidence mentioned in the previous paragraph suggests otherwise. p-Tau species might appear as early as the initial increases in Aβ levels in regions of early accumulation (Mattsson et al., 2019), such as the precuneus and posterior cingulate cortex, a long time before the appearance of NFTs (Ashton et al., 2022; Vogel et al., 2020), and the prion-like behaviour of the propagation of tau is already being incorporated in newer models (T. B. Thompson et al., 2020, Figure 1.16).

Additional neuropathological factors

Additionally to the of Aβ and tau accumulation, cellular mechanisms behind inflammation, vascular integrity, mitochondrial function, oxidative stress, and glucose metabolism are a few of the processes that become altered from the initial stages of the disease (Scheltens et al., 2021). Chronic inflammation has brought special interest in the AD field and has been recognized as one of the major components of AD pathology (Gomez-Nicola and Boche, 2015; Onyango et al., 2021). Glial cells present a chronic pro-inflammatory phenotype in AD and accumulate around Aβ plaques and neurons with NFTs (Calsolaro and Edison, 2016; Onyango et al., 2021), exacerbating AD pathology.

1.4.3 AD and functional connectivity

Despite the advancements, the specific relationship between AD pathology and symptomatology remains unclear, which is a major setback for therapeutic research. As we have stated already, E/I balance alterations might be the missing link connecting microscale proteinopathies with large-scale network dysfunction and cognitive decline, as recently proposed in a recent review by Maestú et al., 2021. This theory is supported by evidence from multiple scales. In the microscale, Aβ plaques and soluble Aβ exert various forms of damage to the surrounding neurons, including the local reduction of dendritic spines and perisomatic GABAergic interneuron terminals (Garcia-Marin, 2009; Knafo et al., 2009, facilitating excitability and the existence of hyperactive neurons. On the other hand, p-Tau is related to changes in the cell that lead to a more generalized loss of dendritic spines and neuronal loss (Nelson et al., 2012; Vogel et al., 2020), favouring a reduction in neuronal activity or inhibition and directly translating to cognitive deficits (DeFelipe, 2015), which could explain the different neurophysiological activity patterns observed along various stages of AD. In the mesoscale we can observe the effect of these altered species of Aβ and p-Tau in neuronal circuits. In-vivo cellular-level imaging and electrophysiology studies in animal models show a significant proportion of neurons showing abnormally increased activity when in the vicinity of Aβ plaques or after local application of soluble Aβ (Busche et al., 2015; Zott et al., 2019), which is further supported by the epileptiform activity observed in electrophysiological studies in both Aβ-bearing mouse models and in AD and MCI human patients (Csernus et al., 2022; Cuesta et al., 2022; Vossel et al., 2017). Regarding the effect of p-Tau, Busche et al., 2019

revealed a tau-dependent suppression of neuronal circuits which, interestingly, was mediated by soluble species of tau rather than by NFTs, supporting the previously presented perspective of concomitance between Aβ and tau pathology, only with a different spatial progression. Other lines of research have highlighted the role of non-neuronal components in this scale, including synapse impairment by microglia and astrocytes (Hong et al., 2016; J.-H. Lee et al., 2021), alongside with myelin loss through oligodendrocytes (Chen et al., 2020). How this changes in the micro and mesoscale translate into alterations in the activity of macroscale networks is a topic of intense research, with the most common observation through electrophysiological recordings across the AD continuum being a progressive slowing of brain oscillatory activity (Fernández et al., 2006), which refers to the shift of activity from high-frequency bands (alpha, beta) to low-frequency bands (delta, theta). Interestingly, research has found an increased alpha activity in frontal areas with high Aβ depositions in preclinical stages (Nakamura et al., 2018), with subsequent decreases with progression to SCD and MCI and AD (López-Sanz et al., 2016), with these reductions in alpha power correlating with levels of p-Tau in CSF (Smailovic et al., 2018).

AD and changes in sFC

Regarding brain connectivity, of central interest for the present thesis, our research team has published several works reporting that sFC is already altered in asymptomatic adults at higher risk of developing AD. Nakamura found delta and theta-band phase hypersynchrony between the precuneus and the bilateral inferior parietal lobes in Aβ-positive healthy controls (Nakamura et al., 2017). Similarly, Ramírez-Toraño found alpha-band hypersynchrony in middle-aged HC with a family history of AD compared to those without it (Ramírez-Toraño et al., 2021), which was further exacerbated in a longitudinal follow up by García-Colomo (García-Colomo et al., 2024). Further along the AD continuum, individuals presenting SCD show hypersynchrony among regions of the parietal and occipital lobe (Kawagoe et al., 2019), and between the posterior DMN and the medial temporal lobe (Verfaillie et al., 2018). In this line, López-Sanz found a dual pattern of posterior hypo- and anterior hypersynchrony in SCD participants that was similar but more pronounced in MCI individuals (López-Sanz et al., 2017). The antero-posterior profile of hypersynchrony found in MCI patients was also reported in a previous international multicenter study (Maestú et al., 2015), and in elderly patients carriers of the APOE-ϵ4 gene allele (Cuesta et al., 2015), and at the same time predicted conversion from MCI to dementia in other studies (López et al., 2014; Pusil, López, et al., 2019). Finally, a generalized loss of network connectivity is observed once the patient progresses into AD (De Haan et al., 2012).

This hypersynchrony/hyposynchrony pattern can be better understood in the framework of the "X" model, proposed by Pusil and colleagues in 2019 (Pusil, Dimitriadis, et al., 2019, Figure 1.17). In the study, MCI patients underwent two MEG recordings, two years apart, and were classified as progressive or stable depending on whether they converted to AD or not during the follow up period, respectively. Importantly, the progressive MCI group showed a higher baseline sFC than the stable MCI group, while their roles reversed in the follow up recording: MCI patients that had converted to AD showed a collapse of synchrony in the areas that previously were hypersynchronous, and MCI patients that had not transitioned saw their synchrony increased in after two years (Pusil, López, et al., 2019). Based on this evidence,

brain hypersynchrony intuitively appears to reflect the underlying neuronal hyperactivity brought on by the propagation of Aβ species, while subsequent hyposynchrony might be caused by the neurodegeneration and neuronal loss elicited by the propagation of tau species and NFTs.

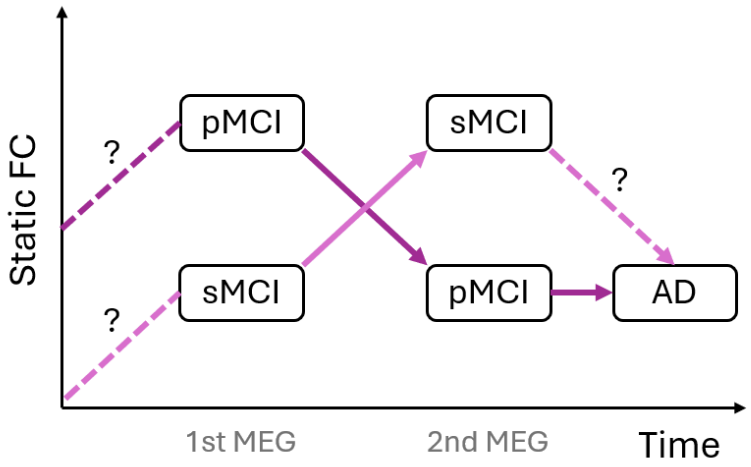


Figure 1.17: The "X" model of AD. Modified from Pusil, López, et al., 2019. sMCI: stable MCI; pMCI: progressive MCI.

To conclude, it is important to remark on the recent interest that non-invasive brain stimulation (NIBS) has accumulated as a potential alternative treatment to traditional therapeutic options. Among these, transcranial alternating current stimulation (tACS) is a non-invasive stimulation technique capable of modulating oscillatory activity in the brain and inducing neuroplasticity (Chaieb et al., 2011). Weak alternating electrical currents are applied to the scalp, reaching the brain, influencing neurons' membrane potentials and thus, influencing neuronal probability of activation (Elyamany et al., 2021). As a result, the application of tACS can induce neural entrainment (i.e. the synchronization of an oscillatory system to an external driver) at the frequency of stimulation (A. Liu et al., 2018). These techniques have been used to enhance gamma, alpha oscillations in specific brain regions (Cabrera-Álvarez et al., 2023; K. T. Jones et al., 2019; Nissim et al., 2023), as well as to increase alpha sFC in regions of the DMN (Schwab et al., 2019), both relevant events in the AD field, as depicted in the previous paragraphs. Furthermore, Cabrera-Álvarez recently developed a computational model to guide the functional decoupling of brain regions through tACS (Cabrera-Álvarez et al., 2021), which could stand as a pathway to reduce the increased sFC observed early in the AD continuum and mitigate its possible neurotoxic effects. Nevertheless, current literature around neuromodulation presents elevated variability in the methods and stimulation protocols used, yielding non-comparable results among studies and promote difficulty in extracting any generalized knowledge in the field, and more research is needed to elucidate the effect of tACS on sFC (and on dFC, since there are no studies in this direction).

AD and changes in dFC

As we already explained earlier in this text, studies on brain connectivity, including those focused on AD, have assumed until recently the stationarity of FC, missing out on the information contained in the temporal dimension of neuroimaging recordings. Given the consistency of alterations in sFC throughout the AD continuum, a novel line of research, focused on the possible dFC alterations underlying sFC changes, has become especially relevant for the disease. Most investigations involving dFC in AD have been carried out using fMRI, and a common finding in these studies is that dFC is reduced in AD patients in key networks and regions for the disease, such as the DMN (Filippi et al., 2019; Matsui and Yamashita, 2023; Zhao et al., 2022). The first study investigating dFC in AD patients was that of D. T. Jones et al., 2012, assessing the changes of a modularity metric using a sliding window analysis. They demonstrated the non-stationarity nature of brain modularity, as well as a reduction of the dwell time for connectivity states with a high contribution of posterior DMN areas in AD subjects compared to controls (D. T. Jones et al., 2012). Further supporting this findings, Schumacher et al., 2019 reported that AD patients spend more time in states of sparse connectivity, due to an inability to switch between states of low inter-network connectivity and more highly and specifically connected network configurations than controls, as seen in other posterior studies (Gu et al., 2020; Sendi et al., 2023). In another study, Córdova-Palomera et al., 2017 investigated the evolution of dFC disruptions in a wider spectrum of the AD continuum, showing alterations in patients with dementia compared to the MCI and SCD groups in terms of local dFC in the temporal, frontal-superior and DMN. These alterations indicated towards a decreased global metastability between functional states in AD patients, leading to a shrinkage of the functional "dynamic repertoire" (i.e., a smaller set of functional configurations) (Córdova-Palomera et al., 2017). In the same direction, Demirtaş et al., 2017 found again a progressive loss of brain metastability across the AD spectrum, which was additionally inversely correlated to the levels of tau CSF, while Aβ CSF levels correlated with average levels of coherence (sFC), even if this relationship only reached significance in patients with dementia.

However, the temporal resolution of fMRI is hampered by its low sampling frequency and the slow nature of the hemodynamic responses recorded, and is consequently likely to miss relevant dFC changes in the sub-second scale (Núñez et al., 2019). Electrophysiological techniques such as EEG and MEG can overcome such difficulties, both because of their higher sampling frequency and the fact that they measure the electrical activity of cortical neurons. While very scarce, electrophysiological studies point in the same direction as those using fMRI, suggesting a decrease in dFC in the last stages of the AD continuum (Li et al., 2019; Núñez et al., 2019, but see Zhao et al., 2022). Núñez et al., 2019 found decreased variance when studying the AEC-c standard deviations in sensor-space EEG in AD patients compared to the control group in both high alpha and low beta bands, while no significant differences appeared in the MCI group. In a posterior work they applied hidden Markov models to instantaneous FC in EEG sensor-space to study meta-states dynamics in AD and MCI, and found a decrease in modularity of meta-states in both MCI and AD participants compared to controls in both alpha and low beta bands (Núñez et al., 2021), meaning that their resting-state networks were less well defined, possibly contributing to the shorter dwell times they also found in the pathological groups. Jin et al., 2023 implemented a novel time-varying dynamic-network

(TVDN) model able to study spatial and temporal contributions in the data separately to observe similar evidence. In their study, AD patients exhibited a higher spatial complexity of activation maps compared to healthy controls (HC), given the higher number of eigenmodes they displayed. At the same time, AD patients presented lower temporal dynamics, with a lower number of state transitions and increased dwell times compared to HC (Jin et al., 2023). Moreover, these spatial and temporal variations were also captured by graph metrics, and significantly enhanced classification performance between AD and HC participants. In a functional near-infrared spectroscopy (fNIRS) and EEG integrative investigation, Li et al., 2019 found weaker or suppressed dFC in the high alpha and low beta bands of AD participants (Li et al., 2019), reporting lower values for degree and clustering coefficient in the frontal pole and medial orbital regions of AD-induced brain networks. On the other hand, while not centered in dFC, other electrophysiological studies focused on other highly correlated parameters, such as entropy and dynamic changes in power, report findings in the same direction. J. Sun et al., 2020 compile, in a review, reports on decreasing complexity of the MEG/EEG signal in multiple entropy parameters in AD. Finally, Puttaert et al., 2020 applied hidden Markov models to MEG power topographies of healthy individuals and SCD, MCI, and AD participants, finding only differences in the dynamics of the control and AD groups. Similarly to the aforementioned fMRI study by D. T. Jones et al., 2012 they found that AD participants spent less time in, and switched less frequently into, states with a high contribution of the posterior DMN.

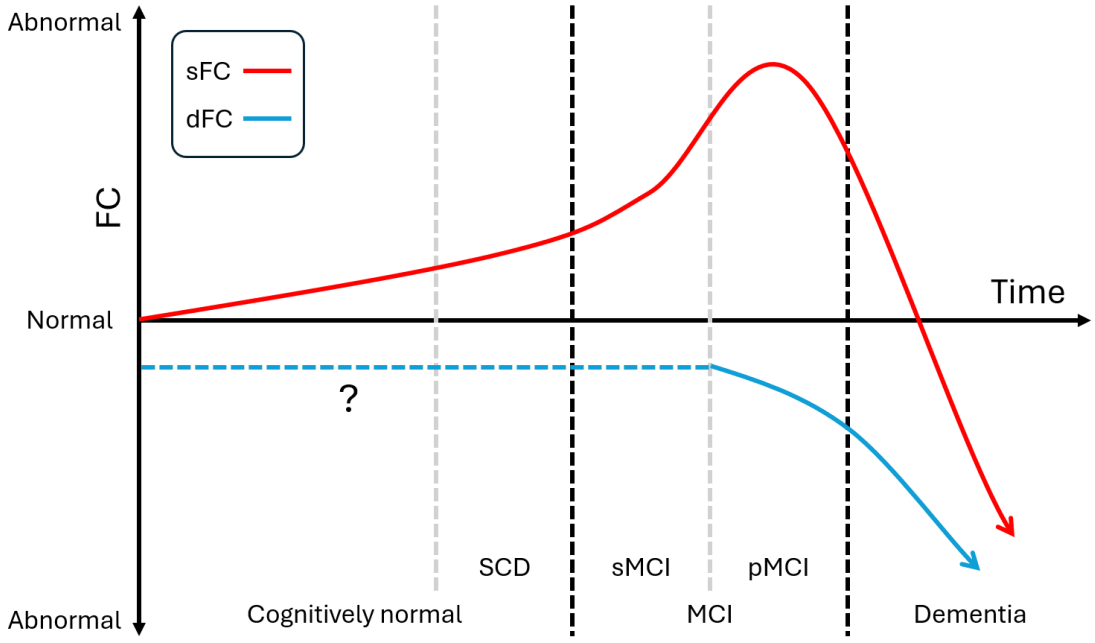


Figure 1.18: Progression of sFC and dFC over the AD continuum. While sFC studies span the whole AD continuum, dFC research has not addressed its evolution over the early stages in the AD continuum.

From the studies above one can infer that, starting from the MCI stage, dFC decreases with the progression of the disease, with MCI/AD patients showing a less differentiated profile of connectivity over time, and having difficulties in transitioning out of sparse connectivity states.

Nevertheless, characterization of dFC across the pre-dementia stages in the AD continuum is still lacking in literature, as depicted in Figure 1.18, especially in the electrophysiology field which, as we will see, might be the most adequate to assess fast dFC. Does dFC decrease monotonically across the whole AD continuum? How are these dFC measures related to structural connectivity estimates, cognitive performance scores, or early detection biomarkers? Is dFC a valid candidate for early detection of AD? Is it possible to externally modulate sFC or dFC? This thesis addresses these questions throughout the chapters that comprise it, extending the current knowledge on dFC, and more specifically about dFC in Alzheimer's disease.

1.5 Introduction to MEG

Neuroimaging refers to the discipline that deals with the in vivo depiction of both anatomy and operation of the CNS. Nowadays, nearly one hundred years after H. Berger discovered EEG (Berger, 1929), multiple neuroimaging techniques exist and allow for the investigation of the spatio-temporal aspects of brain activity and their connection to health and disease. These techniques have each their own shortcomings and strengths, and often convey complementary information. Thus, the preferred neuroimaging modality for a study must be determined by the particular research question to be answered and the level of invasiveness warranted. Neuroimaging techniques are usually classified in two main categories: structural and functional.

Structural neuroimaging pursues visualizing and studying the diverse brain structures and identify any alterations that may affect them, such as tumors, hemorrhage, or blood clots. Briefly, computed axial tomography (CAT, Hounsfield, 1980) takes advantage of the differential attenuation of X-ray beams across cranial and brain tissues to create detailed images of the brain where areas with a higher X-ray attenuation (e.g., bone) appear white, while soft tissues look darker. This technique is often applied to detect acute subarachnoid hemorrhages, trauma, and various forms of fractures. It is a safe and rapid technique, although invasive due to radiation exposure and the potential side effects of contrast agents used.

Magnetic resonance imaging (MRI) is a technique that uses a combination of radio frequency (RF) pulses and strong magnetic fields to create three-dimensional images of the brain (Rinck and European Magnetic Resonance Forum, 2019). Firstly, a strong external magnetic field, in the range of 1T to 7T, is applied to align hydrogen nuclei found in bodily tissues, producing a net magnetization in the direction of the applied field. Afterwards, an RF pulse is sent to increase the energy of the protons, enabling them to move into higher energy states. As a consequence, a change in the magnetization takes place, depicted as a 90-degree flip. After the RF pulse is switched off, the magnetization returns to its former equilibrium, and protons release energy in a tissue-specific manner, producing RF signals that are used to build the MRI image. MRI is frequently used to detect edema, infarction, and demyelination, as well as to measure brain volumetrics. Since MRI does not use any ionizing radiation, its use is favoured against computed tomography when both modalities could yield the same information. Importantly, a number of patients experience claustrophobia and may require sedation or shorter MRI protocols.

Additionally, diffusion-weighted imaging (DWI) is a specific MRI protocol that uses the diffusion of water molecules to generate contrast in MRI scans (Le Bihan and Breton, 1985), which may be considered a proxy for white matter integrity. In a DWI image, each voxel is represented by an ellipsoid describing the magnitude, degree of anisotropy, and directionality of the diffusing molecules. In an isotropic medium such as cerebrospinal fluid, water molecules move due to diffusion and can move at equal rates in all directions, while diffusion rates in anisotropic tissues vary depending on the direction in which it is measured. For example, diffusion in neurons is fast along the length of the axon, and slower perpendicularly across it. This representation enables quantitative analyses of white matter integrity, including fractional anisotropy (FA), a scalar measure of the degree of anisotropy in a given voxel.

Reduced axonal myelination and a decreased number of axons, signs of axon degeneration and damage, reduce FA, as there are fewer obstacles against water motion (Manto and Habas, 2016).

Meanwhile, functional neuroimaging techniques measure direct or indirect brain activity. Among them, Single-photon emission computed tomography (SPECT) and PET measure the nuclear decay of unstable atoms in the brain, which are embedded into radiopharmaceutical agents. During SPECT and PET, a radiotracer is injected into the patient, which accumulates in the area of interest. Gamma rays are produced by gamma-decay (SPECT) or through electron-positron annihilation after a positive beta decay event (PET). Then, gamma cameras capture the released gamma rays, which are used to produce brain images. These techniques are frequently used to study brain disorders characterized by metabolic alterations, including stroke, epilepsy, AD, and tumors. Moreover, they can be used both in structural (e.g., Aβ deposition mapping using Pittsburg compound B as a radiotracer) and in functional approaches (e.g., brain metabolism monitoring using 18F fluorodeoxyglucose). These techniques are, nevertheless, highly invasive and pose several risks, including radiation exposure and allergic responses.

Functional MRI (fMRI) exploits the differential magnetic properties of oxygenated (diamagnetic) and deoxygenated (paramagnetic) hemoglobin to create blood-oxygenation level-dependent (BOLD) images. As such, fMRI is a surrogate measure of brain activity that, instead of brain activity itself, detects the hemodynamic changes, including blood flow and oxygenation, elicited by local activations. This technique, as already mentioned in previous sections, has been used in neuroscience research to map the brain structures underlying specific cognitive processes (e.g., memory, perception, or language). Other clinical applications of fMRI also include the pre-surgical management of brain tumors, aiming to pinpoint brain function and reduce the chance of function loss.

Finally, electrophysiological techniques yield a direct measure of the brain's electrochemical activity. This category comprises both non-invasive and extremely invasive modalities. Non-invasive modalities include EEG, which measures the electric potential at the scalp using an array of electrodes placed on top of it, and MEG, which measures the magnetic field produced by neurons at the cortex using a helmet of sensors placed a few centimeters away from the head. Both of these techniques are used in neuroscience research for the most part, although they are also applied in clinical settings, where they can be used for localizing epileptic seizures, diagnosing sleep disorders, or assessing the depth of anesthesia, coma, or brain death. On the contrary, invasive modalities, such as electrocorticography (ECoG), which places an intracranial electrode grid onto the exposed surface of the brain, or stereoelectroencephalography (sEEG), which uses depth electrodes surgically implanted into the brain tissue, are exclusively applied in the clinic, usually to precisely identify epileptogenic zones before a resection.

1.5.1 MEG versus other neuroimaging techniques

Figure 1.19 represents the aforementioned functional neuroimaging techniques according to their spatial and temporal resolution, as well as invasiveness. While MEG lags behind

fMRI and other invasive techniques regarding spatial resolution, it overcomes that of EEG, given the uniform magnetic susceptibility of brain tissues, which allows for magnetic field to propagate without distortion until they reach the MEG sensors. At the same time, MEG has an excellent temporal resolution along with the other electrophysiological techniques, exceeding by multiple orders of magnitude that of fMRI, SPECT or PET. Additionally, its low invasiveness and convenience makes MEG an ideal technique for research. During the MEG experiments presented in this thesis, participants just needed to sit, close their eyes, and relax, which was essential for encouraging people to take part in the studies. Overall, MEG reflects a balanced combination of both spatial and temporal resolution, which is adequate for the investigation of fast dynamics in brain connectivity, the main topic of this thesis.

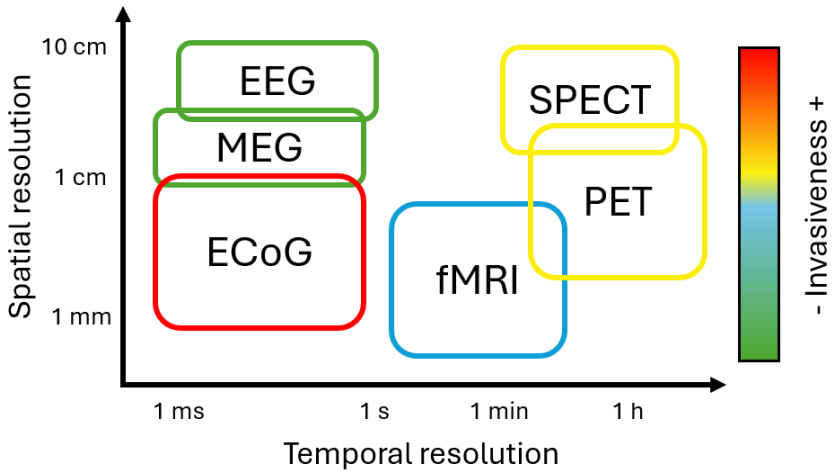


Figure 1.19: Representation of the different neuroimaging techniques according to their temporal and spatial resolution.

1.5.2 Physiological origin of the MEG signal

In the section 1.2 we already presented the fundamental units of the brain, the neurons, as well as how they communicate through the action potential, the mechanism with which a neuron form a transient, rapid change in membrane potential, and synapses, the chemical interface between two neurons. Presynaptic potentials trigger the release of neurotransmitters into the synaptic cleft, which in turn act over the receiving neuron by altering the selective permeability of its membrane. This creates a postsynaptic potential which, as we discussed, can be excitatory or inhibitory, depending on the ion channel affected and the direction of its flow. If the postsynaptic neuron receives an excitatory impulse and reaches the critical threshold of -55 mV, then a new action potential will start and propagate along the axon to the next cell.

There are important differences between postsynaptic potentials and action potentials which make the former the more likely source of MEG signals (Hämäläinen et al., 1993). In order to produce a measurable MEG signal, a minimum of around 10,000 to 100,000 neurons must be simultaneously active, or rather, contribute to the signal through spatio-temporal

summation (Murakami and Okada, 2006). Action potentials are much faster compared to postsynaptic potentials ($\tilde{1}$ millisecond vs. tens of milliseconds) and are consequently less likely to synchronize across a large population of neurons. Not only that, but action potentials are represented by current quadrupoles, while postsynaptic potentials are best described as current dipoles. Current quadrupoles produce magnetic fields that decay much faster with distance than current dipoles (r^{-3} vs. r^{-2}). All of these reasons lead to assuming the contribution of action potentials to MEG signal negligible.

The spatio-temporal summation needed to generate a measurable MEG signal also requires a non-arbitrary spatial distribution of neurons, so that their individual contributions do not cancel out. Neurons have to be parallel to each other, and perpendicular to the cortex surface (Spruston, 2008). Pyramidal neurons in the cortical layer V, which also have long apical dendrites, fulfill this condition (Lopes da Silva, 2013). The length of the apical dendrites favours the temporal convergence of postsynaptic potentials, while their parallel arrangement allows the spatial summation of the individual magnetic fields. Consequently, pyramidal neurons are considered the main generators of MEG signal.

1.5.3 The MEG system

The synchronous activity of tens of thousands of pyramidal neurons still produces a minute magnetic field, in the order of hundreds of femtoTeslas (fT, 10^{-15} T). Furthermore, environmental magnetic noise, such as the Earth's magnetic field, are several orders of magnitude larger, ranging from 24 to 64 μT (Finlay et al., 2010). The MEG system overcomes these obstacles through magnetic shielding from environmental interferences, and extremely sensitive magnetic sensors.

Proper shielding is provided by a magnetically shielded room (MSR). The MEG system is installed inside this room, which is crucial to reduce to a minimum the influence of magnetic fields generated by alternating current in cables and other devices, large moving magnetic bodies (e.g. a car) or the Earth. MSRs comprise multiple layers of highly magnetically permeable materials, such as mu-metal or perm-alloy, which deviate external magnetic fields through them, keep these external magnetic fields from penetrating into the much less permeable interior of the room. As a result, an MSR achieves an attenuation factor of 40 dB, even at low frequencies (Gratta et al., 2001).

In order to detect the minuscule magnetic fields produced by neural currents MEG systems use superconducting quantum interference device (SQUID) sensors (Supek and Aine, 2014). A SQUID consists of a superconducting ring with two Josephson junctions (i.e. thin layers of a non-superconducting material between two superconducting semi-rings). The functioning of the SQUID is based on three main principles:

1. The Meissner effect (Meissner and Ochsenfeld, 1933), the phenomenon by which the magnetic field is expelled from a superconductor.
2. The magnetic flux quantization, described as the constraint that the magnetic flux in a superconductor ring must be an integer multiple of the flux quantum ($\Phi = n\Phi_0$, where $\Phi_0 = 2.07fWb$).

3. The Josephson effect (Josephson, 1962), the quantum tunneling taking place in a Josephson junction, given that the current does not exceed that junction's critical current that would make it resistive again.

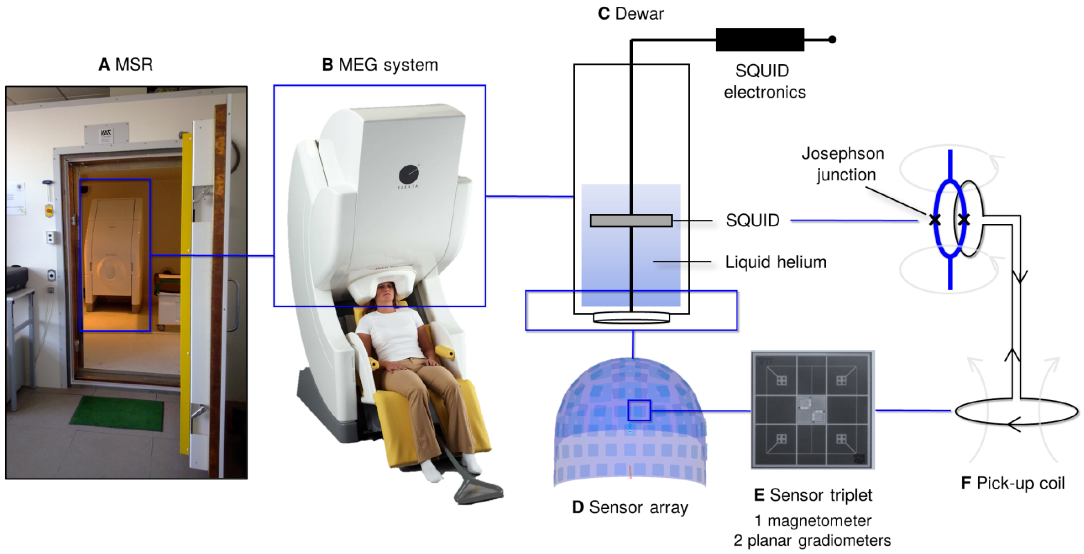


Figure 1.20: MEG components. (A) MSR. (B) Elekta's Neuromag MEG system. (C) Dewar vase containing liquid helium. (D) MEG helmet and sensor array. (E) Elekta's Neuromag sensor triplet comprises one magnetometer and two planar gradiometers. (F) A pick-up coil from a magnetometer captures the magnetic flux, which is then transformed and applied to the SQUID.

In a direct current SQUID (dc-SQUID), a constant current (bias current) is applied to the superconducting loop, which splits and passes through the two Josephson junctions. When an external magnetic field is applied, it threads the superconducting loop, creating a magnetic flux. As a consequence of Lenz's Law, an induced supercurrent is generated opposing change in magnetic flux, which will be added to the bias current in one side of the loop and oppose it on the other side, creating a phase difference between the Josephson junctions. This induced current limits the bias current that can flow through the ring without surpassing the critical current of the Josephson Junction. Since the current is maintained constant in this kind of SQUIDs, what changes with magnetic flux has to be voltage. Thus, dc-SQUIDs can be thought of as flux-to-voltage converters, where the voltage is a function of the applied magnetic field with a period equal to Φ_0. Its sensitivity is related to the magnetic flux that passes through the ring, which in turn is proportional to its enclosed area. Since the device area is too small (just a few square millimeters), the SQUID is not directly used to measure the magnetic field, and is instead captured by a flux transformer consisting of a larger pick-up coil and an input coil inductively coupled to the SQUID. The MEG system employed in our laboratory presents two different pick-up coils: magnetometers and planar gradiometers, measuring direct magnetic flux and the difference in magnetic flux from two areas in the same plane, respectively. In order to keep the SQUIDs in a superconductive state, these are placed inside a Dewar vase filled with liquid helium. Figure 1.20 shows a diagram of the different components of an MEG system.

1.5.4 MEG data acquisition

MEG data used in this thesis was collected at the Center for Cognitive and Computational Neuroscience (C3N), located at the time in the Centro de Tecnología Biomédica (CTB, Madrid, Spain). The MEG system used was a 306 channels (102 magnetometers, 206 planar gradiometers) Vectorview Elekta Neuromag (Helsinki, Finland), installed inside an MSR (VacuumSchmelze GmbH, Hanau, Germany). Data from Chapter 2 was recorded between 2013 and 2019 by some other colleagues and kindly provided, while data from Chapters 3 and 4 was recorded at the beginning of this thesis project, between 2019 and 2021.

Before any MEG recording, we took some time to welcome the participants and inform them about the MEG and the protocol that would be followed next, after which they voluntarily agreed to take part in the experiment by signing an informed consent. The participant is then asked to put apart any metallic objects on them that might interfere with the MEG signal (e.g. zippers, keys, bras, glasses, phones, make up). Importantly, those participants with metallic implants, braces, pacemakers, prostheses or other irremovable metallic sources are often excluded from MEG experiments, as their demagnetization is in most cases impossible.

The participant would sit afterwards so that we could apply four head position indicator (HPI) coils to the participant's scalp (two to the forehead and two to the mastoids). These HPI coils, when activated, generate a magnetic field at frequencies outside of those of interest for our studies, between 200 Hz and 250 Hz, which allows tracking of the position of the head during the recording. Additionally, to control for eye blinks and movement and heart activity, we also placed electrodes to obtain electrooculogram (EOG) and electrocardiogram (EKG) signals. For that purpose, we set a pair of electrodes above and below the participant's left eye and another pair diagonally across the chest, respectively. Both sets of electrodes were arranged in bipolar montages. Finally, another electrode was placed on the left earlobe, serving as ground. This configuration is depicted in Figure 1.21. Lastly, we used a FASTRAK 3D digitizer (Polhemus, Colchester, Vermont) to obtain a 3D representation of the participant's head shape. More specifically, we digitized approximately 400 points over the scalp, as well as three fiducial points (the bilateral preauricular points and the nasion), and the position of the HPI coils.

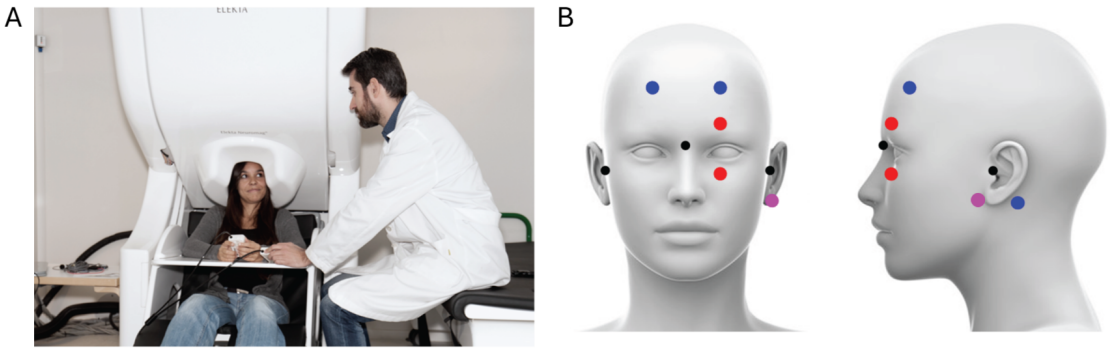


Figure 1.21: MEG acquisition protocol. (A) MEG participant in the room. (B) Position of fiducials (black), EOG electrodes (red), ground electrode (pink), and HPI coils (blue). Extracted from Suárez Méndez, 2024.

Now that the participant is prepared, we asked them to sit quietly and still in the MEG system while closing their eyes. We recorded 5 minutes of spontaneous electrophysiological activity while the participants rested awake with their eyes closed. If any sign of drowsiness was perceived, participants were alerted through a microphone. MEG raw data was acquired at a sampling rate of 1000 Hz with an online anti-aliasing band-pass filter between 0.1 and 330 Hz.

1.5.5 MEG data preprocessing

MEG raw data is contaminated by a combination of external (i.e. environmental) and internal (i.e. physiological) magnetic noise, as depicted in Figure 1.22. Examples of external noise are the Earth's magnetic field, or the magnetic noise produced by the power line (50 Hz and its harmonics in Europe). While the MSR greatly attenuates external noises, post-acquisition processing, such as the signal space separation (SSS) method (Taulu et al., 2003), is used to improve the SNR of the recordings.

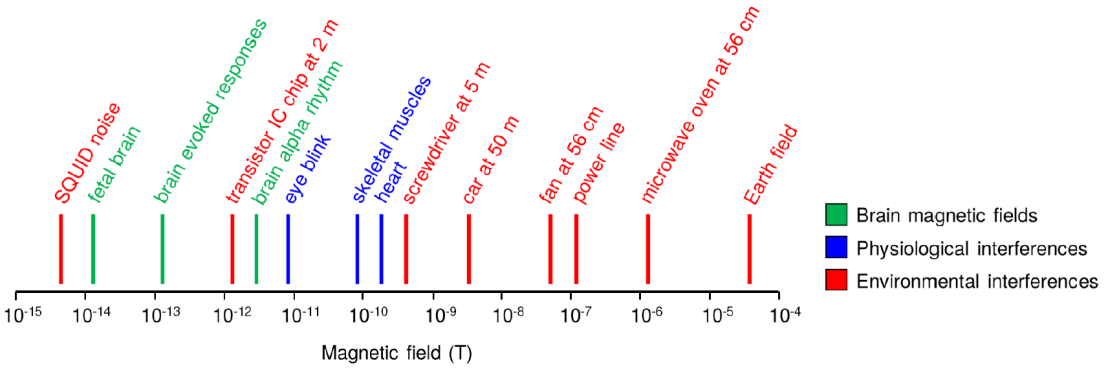


Figure 1.22: Magnetic fields interfering with the MEG signal. Brain magnetic fields of interest, in green, lie at the bottom of the scale. Extracted from Suárez Méndez, 2024.

On the other hand, the participant is the primary source of internal contamination, whether by bringing magnetic components inside the room, or through physiological artifacts, which would include cardiac, ocular and muscular artifacts.

The MEG pre-processing pipeline presented across these lines handles each of these different types of magnetic spurious signals, obtaining clean MEG signals adequate for posterior quantitative analysis.

Signal space separation

Elekta MEG systems undergo the SSS method as its first denoising step (Taulu and Simola, 2006). This method is based on the quasi-static approximation of Maxwell's equations for electromagnetism, a reasonable assumption due to the low frequencies of neuronal activity of interest (below 100 Hz, Hämäläinen et al., 1993). Maxwell's equations can be then simplified by omitting their temporal derivatives (Suárez Méndez, 2024), and as a result the magnetic field at any sensor can be represented as a linear combination of two harmonic expansions, each corresponding to two subspaces: signals generated by sources outside of the sensor array,

being consequently external interfering sources, and inside the sensor array (i.e. internal physiological sources). The sensor array itself is placed in a source-free volume.

In our experiments, we actually used a spatio-temporal extension of this method, known as the temporally extended SSS (tSSS, Taulu and Hari, 2009). This methodology also removes the contribution of sources that, by error, were temporarily located in the internal source volume, but show a strong correlation with sources in the external volume. The tSSS method was applied through the software MaxFilter (Elekta Neuromag, Helsinki, Finland), with a correlation limit of 0.9 and a window length of 10 seconds.

Artifact removal

After the application of the tSSS method, the MEG signal is clean from external noise. However, physiological interference coming from the participant or electronic noise coming from the MEG system still needs to be eliminated. During the artifact removal phase, which will identify, label and eliminate mainly cardiac artifacts, ocular artifacts, muscular artifacts, and system artifacts.

Cardiac or EKG artifacts are the results of the magnetic fields generated by the electrical activity at the heart. In a resting state, the heart beats between 60 to 100 times per minute. Its periodic depolarization generates magnetic activity which causes visible distortions in the MEG signal (Jousm??ki and Hari, 1996). Cardiac artifacts are characterized as a sequence of short pulses occurring periodically at the heart rate. In a previous section we explained that two EKG electrodes are placed on the participant's torso to facilitate their detection.

Ocular or EOG artifacts happen due to three different eye movements: eyeball movement, saccades and blinking. However, it is the latter the one responsible for the largest amplitude deflections in the MEG signal. Again, to facilitate the detection of ocular artifacts, EOG electrodes are set above and below the participant's left eye.

Muscular artifacts in MEG signal are the product of muscle contraction, and are characterized by their high-frequency nature. For example, the frontalis muscle, involved in bow wrinkling, causes artifactual activity to appear around 30-40 Hz, while posterior and neck muscles (e.g. trapezius, sternocleidomastoid) produce artifacts at frequencies higher than 100 Hz (Kumar et al., 2003).

Finally, system artifacts usually take the shape of a "jump" in the signal, and are created by transient electronic instabilities, failing to control the state of a SQUID sensor during the MEG recording, or calibration errors. This kind of artifacts are identified as abrupt single-channel shifts in the MEG signal.

The pre-processing pipeline were programmed for MATLAB (MATLAB R2021b, Mathworks, Inc.), and uses the Fieldtrip toolbox for signal processing (Oostenveld et al., 2011). It consisted of 4 main steps:

1. Bad channel elimination: channels with several events of system artifacts are deemed as "bad channels", and are thus eliminated and reconstructed from the activity of the surrounding channels, due to the high redundancy of the MEG signal(Garcés et al., 2017).

2. Automatic artifact detection and review: artifact detection was performed via the automatic artifact-detection algorithm implemented in Fieldtrip, and then visually inspected to discard false positives and label undetected artifact events in the signal. While muscle and jump artifacts are labelled for removal, EOG and EKG artifacts are treated differently, given their high occurrence. Directly removing EOG and EKG artifact would yield a low quantity of MEG trials to work with, so we have to eliminate their independent contribution to the MEG signal.

3. Independent Component Analysis (ICA): to eliminate EOG and EKG artifacts from the MEG signal and ICA procedure based on the second-order blind identification (SOBI, Belouchrani et al., 1997) was applied. This method is able to separate the MEG signal into its "unmixed" statistically independent components. Since EKG and EOG artifacts are consistent in shape across the whole MEG signal, they are typically easily isolated through ICA. By visually inspecting the resulting components, it is often straightforward to identify EOG and EKG contributions, which are then eliminated from the original signal, generating a MEG time series which is clean from both EOG and EKG artifacts.

4. Signal segmentation: the clean MEG signal is then divided into 4-second segments with no overlap. Those segments still containing muscle or jump artifacts are discarded for posterior analyses. Importantly, when extracting these segments, additional 2-second signal portions are included before and after the signals as padding, so that there is no border effect on the central 4-second segment after filtering. A 4-second segment length was used in all the studies of this thesis, since previous literature addressing the frequency bands under study work have described relevant sFC features in the AD continuum with 4-second windows (García-Colomo et al., 2024; López-Sanz et al., 2017; Ramírez-Toraño et al., 2021), and this window length is in the recommended range for the estimation of fluctuations in FC of resting state networks (Liuzzi et al., 2019).

At the end of this process, we have obtained a set of clean MEG trials ready to be used for further analyses. Importantly, all studies in this thesis use exclusively the data from magnetometers from this point of the pipeline on. This is justified by the data dimensionality reduction happening after tSSS application, making magnetometer and gradiometer information to be highly redundant (Garcés et al., 2017).

1.5.6 Source reconstruction

The clean MEG data obtained after its pre-processing is still in sensor-space. That is, each time series of the MEG signal corresponds to the signal recorded at each sensor. While this data can be directly used for further analyses, working in sensor-space has important limitations. Firstly, the activity generated from a unique source can be captured simultaneously by multiple nearby sensors, leading to spurious results, such as a false perception of synchrony among these sensors (i.e. source mixing). Additionally, the location of these sensors lacks any anatomical or physiological significance, and it would be difficult to relate results obtained to brain regions or physiological mechanisms. The process of source reconstruction allows us to infer the distribution of cortical sources within the brain volume that produced the experimental recordings.

The process of source reconstruction can be seen as taking some measures that have undergone a (in principle, known) set of processing steps and try to recreate the original information. By that definition, it falls inside the set of inverse problems (Aster et al., 2018). But before solving an inverse problem, it is essential to precisely identify the set of processes that the original information underwent, which, in out specific case, translates to handling how the MEG signal arises from a specific source distribution, also known as solving the forward model. Thus, source reconstruction involves two main steps: the forward and the inverse problem. As the reader may anticipate, there exists a myriad of source reconstruction methodologies, each with its own strengths and caveats (Hallez et al., 2007), but the discussion around this topic is out of this thesis' scope.

The forward problem

For MEG, the forward problem is solved by calculating the elicited magnetic field outside of the head by some current distribution within the brain. For that purpose, we first define the source model, which consists in defining a distribution of sources in the brain with a given orientation, as well as modelling the different tissues in the head and their magnetic properties.

While the experiment in Chapter 4 is based on a template, the experiments in Chapters 2 and 3 utilize the individual T1-weighted MRI scans for personalized source reconstruction. In the latter case, the source model is established in the Montreal National Institute (MNI) space, a commonly used template in neuroscience obtained by averaging 152 T1-MRIs of healthy subjects, using a uniform 3D grid with 10 mm spacing positioning the sources. These sources were then identified based on the automated anatomical labeling atlas (Tzourio-Mazoyer et al., 2002), resulting in 1210 cortical sources distributed across 80 regions of interest. This source model was then linearly transformed to each individual T1-weighted scan.

At the same time, we need another model assessing how the magnetic field propagates across different kinds of tissue. Modeling the human head as a spherically symmetric conductor and current densities as current dipole achieves an analytic solution for the forward problem of calculating the magnetic field from a given source. Although modeling the inner skull surface as a sphere may seem an oversimplification, most heads fit reasonably well inside a sphere centered 5 cm above the plane defined by the MEG fiducials (Hansen et al., 2010). Nevertheless, multiple methods have been developed that increase the precision of this approximation. Throughout this thesis we used the corrected-sphere method proposed by Nolte, 2003, which uses a series of spherical harmonic functions to refine the spherical solution and improve the overlapping of the head model to the inner skull surface. The MRI scans are segmented using SPM12 software (*Statistical Parametric Mapping*, 2007), creating a brain mask of grey matter, white matter, skull, CSF, and scalp. These brain segmentations helped in building realistic single-shell head models for each participant. These models, combined with the personalized MNI source models, facilitated the generation of a lead field using the aforementioned modified spherical solution.

The lead field operator relates each current dipole to the sensor output, and depends on the positions of the head relative to the sensor array, the current dipole distribution (the source model), and the head model. In matrix form, for all sensor outputs and source inputs we can

understand the lead field through the following equation:

$$M = L \cdot Q, \tag{1.13}$$

where M and Q would be the sensor- and source-space time-series, respectively, and L would be the lead field matrix of dimensions $n_{sensors} \times n_{sources}$.

The inverse problem

Once the relationship between source-level activity and sensor-space recordings has been established through the solving of the forward problem, we have to deal with the inverse problem, i.e. inferring the distribution of current dipole sources that that have produced the recorded signals in the sensors. However, the MEG inverse problem is usually described as ill-posed, meaning that there exists an infinite number of source-level distributions that could explain the observed sensor-level measurements. One of the reasons behind this is that the number of sources is larger than the number of sensors (thousands vs hundreds), making the lead field matrix in $M = LQ$ non-invertible. Finding a solution to the inverse problem is not straightforward, but is possible after imposing a number of constraints on the sources. Basically, the objective is finding the inverse operator W that satisfies the following equation:

$$\widehat{Q} = W^T M \tag{1.14}$$

Where $\widehat{Q}$ are the reconstructed current-dipole sources.

Again, while several methods have been developed to tackle the MEG inverse problem, we will describe beamforming, one of the main methodologies applied among research literature, and the one chosen across the different studies of this thesis. For a review on other inverse problem methodologies, see Awan et al., 2019; Bruña Fernández, 2019.

Beamforming is an inverse solution that approximates the activity of each current-dipole source as a linear combination of sensor measurements. Beamformers are spatial filters which maximize the sensitivity of the whole sensor array in one direction, then selectively rejecting the rest of directions. The activity of a single current-dipole placed in r can be estimated through beamforming as:

$$\widehat{q}_r(t) = W_r^T M(t), \tag{1.15}$$

where $\widehat{q}_r(t)$ is the 3-component current dipole estimation at r along each axis, W_r is the $n_{sensors} \times 3$ inverse operator at r, and $M(t)$ are the sensor time series. From Equation 1.13 we can see that the sensor recordings elicited by a given current-dipole at r, $q_r(t)$ can be defined as:

$$M(t) = L_r q_r(t), \tag{1.16}$$

where L_r is the lead field matrix of dimensions $n_{sensors} \times 3$.

Thus, we can substitute Equation 1.16 in Equation 1.15, and see that an ideal spatial filter W_r should be designed so that signals from $r' = r$ are allowed to pass, while signals from other locations ($r' \neq r$) are blocked:

$$\widehat{q}_r(t) = W_r^T L_r q_r(t) W_r^T L_r = \begin{cases} 1, & \text{for } r' = r \\ 0, & \text{for } r' \neq r \end{cases} \tag{1.17}$$

That is, the matrix product of the beamformer spatial filter W and the lead field matrix L must be the identity matrix: $W^T \cdot L = I$

However, if the data is spatially oversampled, as in the case of MEG recordings, many values of W fulfill Equation 1.17, and such ideal filter cannot be built in real life. A realistic solution proposed by Van Veen and Buckley, 1988 is the linearly constrained minimum variance (LCMV) beamformer, which minimizes source variance while preserving the unit gain at $r' = r$:

$$\min_{W_r} \left\{ tr(W_r^T C W^T) \right\}, \text{ subject to } W_r^T L_r = 1, \tag{1.18}$$

where C is the data covariance matrix. Consequently, the LCMV inverse operator is defined as:

$$W_{LCMV} = (L_r^T C^{-1} L_r)^{-1} L_r^T C^{-1} \tag{1.19}$$

One of the caveats of the LCMV procedure is that it depends on the estimation of C. If the sensor measurements are not large or clean enough, or if C is not invertible (which happens after applying tSSS), it is necessary to regularize it. This regularization implies substituting C by $(C + \lambda I)$ in Equation 1.19, where λ is the regularization parameter. In our studies, this regularization parameter was set to 1%.

With the inverse problem solved, we have obtained source-reconstructed MEG time-series, the base ingredient of any MEG source-space analysis.

1.6 Research framework

The different sections of this thesis' introduction have tried to convey that (1) every functional mechanism of the brain, from the micro-scale to the macro-scale, is dynamic, (2) but FC has been traditionally calculated through static approaches, discarding any information contained in its temporal dimension; (3) this context is especially important in AD, where consistent sFC alterations have been observed, but dFC still has to be characterized in earlier stages of the AD continuum, (4) a feat that can be performed through electrophysiological studies. Therefore, the central question around which the research work of this thesis revolves is: Can dFC, as measured by MEG, monitor the progression and even perform early detection of AD?

1.6.1 Research context and aims

The Center for Cognitive and Computational Neuroscience (C3N) hosts and has hosted several research lines responsible for the cross-sectional and longitudinal assessment of approximately 800 participants along the AD continuum. The studies of Chapters 2, 3 and 4 have utilized MEG recordings acquired at the C3N, with additional neuroimaging, neuropsychological and chemical assessments specific to each experiment.

The Center for C3N has focused over the last decade on the characterization of synaptic dysfunction and network alterations in preclinical and prodromal AD using MEG (Spanish Ministry of Economy and Competitiveness, and Ministry of Science and Innovation: PSI2009-14415-C03-01, PSI2012-38375-C03-01, PSI2015-68793-C3-1-R, PSI2015-68793-C3-2-R, PSI2015-68793-C3-3-R). In this context, and given the availability of previously recorded data from a significant number of participants across the AD pre-dementia, we performed an initial experiment to assess the progression of dFC through recurrence matrices in the available sample, locating where in the brain those changes are more prominent. Additionally, we studied the relationship between the obtained dFC markers and the subject's cognitive performance, structural connectivity and brain volumetrics. The first study of this thesis "*Dynamics of Brain Connectivity across the Alzheimer's Disease Spectrum: a magnetoencephalography study*", addressed in Chapter 2, presents the results from this initial assessment of dFC, which would serve as the basis for the rest of the studies. The data for these analyses was acquired from 2013 to 2018 by other colleagues, and kindly provided.

Having identified a pattern of progressive decrease of dFC along the AD spectra, we designed a new project that would aid us address the possibility of using dFC as a marker for early detection of AD. As part of this research project (RTI2018-098762-B-C31), which focused on the acquisition of follow up MEG, ophthalmologic, neuropsychology, nutrition and physical activity measurements among others in healthy adults at different risks of suffering AD, we included plasma p-tau231 determinations, a blood biomarker serving as a proxy of Aβ deposition in the brain (Ashton et al., 2021; Tissot et al., 2022). The second study of this thesis "*Dynamic functional connectivity is modulated by the amount of p-Tau231 in blood in cognitively intact participants*", presented in Chapter 3, evaluated dFC in this pre-clinical sample through the quantification of the entropy of FC timecourses, and investigated whether there was a relationship between sFC and dFC and the blood biomarker p-tau231, and if factors such as white matter integrity, APOE ϵ4 carriage, or a family history of AD also

influence dFC in this early stage. Recruiting of participants, coordination of the project and acquisition of the data for this study was performed by my colleagues Alejandra García Colomo, Alberto Nebreda and myself.

After obtaining a more complete perspective of the evolution of dFC across the whole AD continuum, we asked ourselves whether dFC and sFC could be externally influenced noninvasively, and so designed the research project (PID2021-122979OB-C21), which recruited healthy participants from the C3N to undergo personalized tACS neuromodulation and MEG recordings before and after the current stimulation. The third and last study in this thesis "*Individual alpha frequency tACS reduces functional connectivity across the default mode network*", presented in Chapter 4, evaluated the aftereffects of tACS on both sFC and dFC, and simulated the influence of the spatial distribution of neurons across the cortex on the effects of neuromodulation. During this project, we partnered with the University of Texas Health Center at Houston. Jesus Cabrera Álvarez, Alberto del Cerro León and I were in charge of recruiting the participants, coordinating the projects, and ultimately acquiring the data and administering the stimulation sessions.

1.6.2 Research objectives and hypothesis

Study 1: '*Dynamics of Brain Connectivity across the Alzheimer's Disease Spectrum: a magnetoencephalography study*'

Primary research question:

- How does dFC evolve across the pre-dementia stages of the AD continuum?

Hypotheses:

1. Progression across the AD continuum will be associated to decreased dFC, measured through MEG and the correlation of FC matrices over time.
2. Alterations in dFC will be more prominent in frontal and temporal regions of the brain, as well as in the DMN.

Secondary research question:

- Do alterations of dFC correlate with other metrics that measure the advance of the disease, such as cognitive scores, anatomical metrics, and white matter integrity markers?

Study 2: '*Dynamic functional connectivity is modulated by the amount of p-Tau231 in blood in cognitively intact participants*'

Primary research question:

- Are static or dynamic functional connectivity influenced by the amount of Aβ accumulation, measured through the blood biomarker p-tau231, in cognitively unimpaired adults?

Hypotheses:

1. Higher levels of p-tau231 will be associated with more pronounced alterations of dFC.

Secondary research question:

- Are additional risk factors (such as age, sex, APOE carriage, and family history of AD) or other metrics typically studied in AD (such as cognitive performance, brain volumetrics and white matter integrity markers) related to the observed changes in dFC?

Study 3: '*Individual alpha frequency tACS reduces functional connectivity across the default mode network*'

Primary research question:

- Can we influence dFC or sFC at the DMN through tACS at the individual alpha frequency (IAF)?

Hypotheses:

1. tACS will increase the SFC of the DMN, while decreasing dFC.
2. Changes in the sFc and dFC will correlate with changes in spectral power at the same areas.

Secondary research question:

- Does cortical folding in the cortex influence the potential effects of tACS over FC?

References

2024 Alzheimer's disease facts and figures. (2024). *Alzheimer's & Dementia*, *20*(5), 3708–3821. https://doi.org/10.1002/alz.13809

Abreu, R., Jorge, J., Leal, A., Koenig, T., & Figueiredo, P. (2021). EEG Microstates Predict Concurrent fMRI Dynamic Functional Connectivity States. *Brain Topography*, *34*(1), 41–55. https://doi.org/10.1007/s10548-020-00805-1

Adelstein, J. S., Shehzad, Z., Mennes, M., DeYoung, C. G., Zuo, X.-N., Kelly, C., Margulies, D. S., Bloomfield, A., Gray, J. R., Castellanos, F. X., & Milham, M. P. (2011). Personality Is Reflected in the Brain's Intrinsic Functional Architecture (M. Valdes-Sosa, Ed.). *PLoS ONE*, *6*(11), e27633. https://doi.org/10.1371/journal.pone.0027633

Ahmadi, M., Kazemi, K., Kuc, K., Cybulska-Klosowicz, A., Helfroush, M. S., & Aarabi, A. (2021). Resting state dynamic functional connectivity in children with attention deficit/hyperactivity disorder. *Journal of Neural Engineering*, *18*(4), 0460d1. https://doi.org/10.1088/1741-2552/ac16b3

Aizenstein, H. J., Nebes, R. D., Saxton, J. A., Price, J. C., Mathis, C. A., Tsopelas, N. D., Ziolko, S. K., James, J. A., Snitz, B. E., Houck, P. R., Bi, W., Cohen, A. D., Lopresti, B. J., DeKosky, S. T., Halligan, E. M., & Klunk, W. E. (2008). Frequent Amyloid Deposition Without Significant Cognitive Impairment Among the Elderly. *Archives of Neurology*, *65*(11), 1509. https://doi.org/10.1001/archneur.65.11.1509

Allen, E. A., Damaraju, E., Plis, S. M., Erhardt, E. B., Eichele, T., & Calhoun, V. D. (2014). Tracking Whole-Brain Connectivity Dynamics in the Resting State. *Cerebral Cortex*, *24*(3), 663–676. https://doi.org/10.1093/cercor/bhs352

Allen, N. J., & Barres, B. A. (2009). Glia—more than just brain glue. *Nature*, *457*(7230), 675–677.

Alzheimer, A. (1907). Über eine eigenartige erkrankung der hirnrinde. *Psychiatrie Psychisch-Gerichtliche Med. Allgemeine Zeitschrift für*, *64*, 146–148.

Andreou, C., Faber, P. L., Leicht, G., Schoettle, D., Polomac, N., Hanganu-Opatz, I. L., Lehmann, D., & Mulert, C. (2014). Resting-state connectivity in the prodromal phase of schizophrenia: Insights from EEG microstates. *Schizophrenia Research*, *152*(2-3), 513–520. https://doi.org/10.1016/j.schres.2013.12.008

Ashton, N. J., Benedet, A. L., Pascoal, T. A., Karikari, T. K., Lantero-Rodriguez, J., Brum, W. S., Mathotaarachchi, S., Therriault, J., Savard, M., Chamoun, M., Stoops, E., Francois, C., Vanmechelen, E., Gauthier, S., Zimmer, E. R., Zetterberg, H., Blennow, K., & Rosa-Neto, P. (2022). Cerebrospinal fluid p-tau231 as an early indicator of

emerging pathology in Alzheimer's disease. *eBioMedicine*, *76*, 103836. https://doi.org/10.1016/j.ebiom.2022.103836

Ashton, N. J., Pascoal, T. A., Karikari, T. K., Benedet, A. L., Lantero-Rodriguez, J., Brinkmalm, G., Snellman, A., Schöll, M., Troakes, C., Hye, A., Gauthier, S., Vanmechelen, E., Zetterberg, H., Rosa-Neto, P., & Blennow, K. (2021). Plasma p-tau231: A new biomarker for incipient Alzheimer's disease pathology. *Acta Neuropathologica*, *141*(5), 709–724. https://doi.org/10.1007/s00401-021-02275-6

Aster, R. C., Borchers, B., & Thurber, C. H. (2018). *Parameter estimation and inverse problems*. Elsevier.

Awan, F. G., Saleem, O., & Kiran, A. (2019). Recent trends and advances in solving the inverse problem for EEG source localization. *Inverse Problems in Science and Engineering*, *27*(11), 1521–1536. https://doi.org/10.1080/17415977.2018.1490279

Azevedo, F. A., Carvalho, L. R., Grinberg, L. T., Farfel, J. M., Ferretti, R. E., Leite, R. E., Filho, W. J., Lent, R., & Herculano-Houzel, S. (2009). Equal numbers of neuronal and nonneuronal cells make the human brain an isometrically scaled-up primate brain. *Journal of Comparative Neurology*, *513*(5), 532–541. https://doi.org/10.1002/cne.21974

Babiloni, C., Frisoni, G., Pievani, M., Vecchio, F., Lizio, R., Buttiglione, M., Geroldi, C., Fracassi, C., Eusebi, F., & Ferri, R. (2009). Hippocampal volume and cortical sources of EEG alpha rhythms in mild cognitive impairment and Alzheimer disease. *NeuroImage*, *44*(1), 123–135. https://doi.org/10.1016/j.neuroimage.2008.08.005

Bartos, M., Vida, I., & Jonas, P. (2007). Synaptic mechanisms of synchronized gamma oscillations in inhibitory interneuron networks. *Nature Reviews Neuroscience*, *8*(1), 45–56. https://doi.org/10.1038/nrn2044

Bassett, D. S., & Sporns, O. (2017). Network neuroscience. *Nature neuroscience*, *20*(3), 353–364.

Belouchrani, A., Abed-Meraim, K., Cardoso, J.-F., & Moulines, E. (1997). A blind source separation technique using second-order statistics. *IEEE Transactions on Signal Processing*, *45*(2), 434–444. https://doi.org/10.1109/78.554307

Berger, H. (1929). Über das Elektrenkephalogramm des Menschen. *Archiv für Psychiatrie und Nervenkrankheiten*, *87*(1), 527–570. https://doi.org/10.1007/BF01797193

Boly, M., Tshibanda, L., Vanhaudenhuyse, A., Noirhomme, Q., Schnakers, C., Ledoux, D., Boveroux, P., Garweg, C., Lambermont, B., Phillips, C., Luxen, A., Moonen, G., Bassetti, C., Maquet, P., & Laureys, S. (2009). Functional connectivity in the default network during resting state is preserved in a vegetative but not in a brain dead patient. *Human Brain Mapping*, *30*(8), 2393–2400. https://doi.org/10.1002/hbm.20672

Bonnefond, M., Kastner, S., & Jensen, O. (2017). Communication between Brain Areas Based on Nested Oscillations. *eneuro*, *4*(2), ENEURO.0153–16.2017. https://doi.org/10.1523/ENEURO.0153-16.2017

Bornemann, K. D., & Staufenbiel, M. (2000). Transgenic mouse models of alzheimer's disease. *Annals of the New York Academy of Sciences*, *908*(1), 260–266.

Bouchard, M., Lina, J.-M., Gaudreault, P.-O., Dubé, J., Gosselin, N., & Carrier, J. (2019). EEG connectivity across sleep cycles and age. *Sleep*, zsz236. https://doi.org/10.1093/sleep/zsz236

Braak, H., & Braak, E. (1991). Neuropathological stageing of Alzheimer-related changes. *Acta Neuropathologica*, *82*(4), 239–259. https://doi.org/10.1007/BF00308809

Braak, H., & Del Tredici, K. (2018). Spreading of Tau Pathology in Sporadic Alzheimer's Disease Along Cortico-cortical Top-Down Connections. *Cerebral Cortex*, *28*(9), 3372–3384. https://doi.org/10.1093/cercor/bhy152

Broca, P. (1861). Remarques sur le siège de la faculté du langage articulé, suivies d'une observation d'aphémie (perte de la parole). *Bulletin et Memoires de la Societe anatomique de Paris*, *6*, 330–357.

Brookes, M. J., Liddle, E. B., Hale, J. R., Woolrich, M. W., Luckhoo, H., Liddle, P. F., & Morris, P. G. (2012). Task induced modulation of neural oscillations in electrophysiological brain networks. *Neuroimage*, *63*(4), 1918–1930.

Bruña, R., Maestú, F., & Pereda, E. (2018). Phase locking value revisited: Teaching new tricks to an old dog. *Journal of Neural Engineering*, *15*(5), 056011. https://doi.org/10.1088/1741-2552/aacfe4

Bruña Fernández, R. (2019). *Simultaneous MEG/EEG recordings for the study of source domain brain connectivity in neurodegenerative diseases* [PhD Thesis]. Universidad Politécnica de Madrid. https://doi.org/10.20868/UPM.thesis.54514

Bruns, A., Eckhorn, R., Jokeit, H., & Ebner, A. (2000). Amplitude envelope correlation detects coupling among incoherent brain signals. *Neuroreport*, *11*(7), 1509–1514.

Bruzzone, S. E. P., Lumaca, M., Brattico, E., Vuust, P., Kringelbach, M. L., & Bonetti, L. (2022). Dissociated brain functional connectivity of fast versus slow frequencies underlying individual differences in fluid intelligence: A DTI and MEG study. *Scientific Reports*, *12*(1), 4746. https://doi.org/10.1038/s41598-022-08521-5

Busche, M. A., Chen, X., Henning, H. A., Reichwald, J., Staufenbiel, M., Sakmann, B., & Konnerth, A. (2012). Critical role of soluble amyloid-β for early hippocampal hyperactivity in a mouse model of Alzheimer's disease. *Proceedings of the National Academy of Sciences*, *109*(22), 8740–8745. https://doi.org/10.1073/pnas.1206171109

Busche, M. A., Kekuš, M., Adelsberger, H., Noda, T., Förstl, H., Nelken, I., & Konnerth, A. (2015). Rescue of long-range circuit dysfunction in Alzheimer's disease models. *Nature Neuroscience*, *18*(11), 1623–1630. https://doi.org/10.1038/nn.4137

Busche, M. A., Wegmann, S., Dujardin, S., Commins, C., Schiantarelli, J., Klickstein, N., Kamath, T. V., Carlson, G. A., Nelken, I., & Hyman, B. T. (2019). Tau impairs neural circuits, dominating amyloid-β effects, in Alzheimer models in vivo. *Nature Neuroscience*, *22*(1), 57–64. https://doi.org/10.1038/s41593-018-0289-8

Buzsáki, G. (2006, October). *Rhythms of the Brain*. Oxford University Press. https://doi.org/10.1093/acprof:oso/9780195301069.001.0001

Cabral, J., Luckhoo, H., Woolrich, M., Joensson, M., Mohseni, H., Baker, A., Kringelbach, M. L., & Deco, G. (2014). Exploring mechanisms of spontaneous functional connectivity in MEG: How delayed network interactions lead to structured amplitude envelopes of band-pass filtered oscillations. *NeuroImage*, *90*, 423–435. https://doi.org/10.1016/j.neuroimage.2013.11.047

Cabrera-Álvarez, J., Sánchez-Claros, J., Carrasco-Gómez, M., Del Cerro-León, A., Gómez-Ariza, C. J., Maestú, F., Mirasso, C. R., & Susi, G. (2023). Understanding the effects of cortical gyrification in tACS: Insights from experiments and computational models. *Frontiers in Neuroscience*, *17*, 1223950. https://doi.org/10.3389/fnins.2023.1223950

Cabrera-Álvarez, J., Susi, G., Sánchez-Claro, J., Carrasco, M., Cerro, A. D., Maestú, F., & Mirasso, C. (2021). A computational model to guide the functional decoupling of two

brain regions with transcranial alternating current stimulation. *Brain Stimulation*, *14*(6), 1613. https://doi.org/10.1016/j.brs.2021.10.082

Calì, C., Marchaland, J., Regazzi, R., & Bezzi, P. (2008). SDF 1-alpha (CXCL12) triggers glutamate exocytosis from astrocytes on a millisecond time scale: Imaging analysis at the single-vesicle level with TIRF microscopy. *Journal of Neuroimmunology*, *198*(1-2), 82–91. https://doi.org/10.1016/j.jneuroim.2008.04.015

Calsolaro, V., & Edison, P. (2016). Neuroinflammation in Alzheimer's disease: Current evidence and future directions. *Alzheimer's & Dementia*, *12*(6), 719–732. https://doi.org/10.1016/j.jalz.2016.02.010

Cao, Y., Cai, L., Wang, J., Wang, R., Yu, H., Cao, Y., & Liu, J. (2015). Characterization of complexity in the electroencephalograph activity of Alzheimer's disease based on fuzzy entropy. *Chaos: An Interdisciplinary Journal of Nonlinear Science*, *25*(8), 083116. https://doi.org/10.1063/1.4929148

Cardin, J. A., Carlén, M., Meletis, K., Knoblich, U., Zhang, F., Deisseroth, K., Tsai, L.-H., & Moore, C. I. (2009). Driving fast-spiking cells induces gamma rhythm and controls sensory responses. *Nature*, *459*(7247), 663–667. https://doi.org/10.1038/nature08002

Carrasco-Gómez, M., Keijzer, H. M., Ruijter, B. J., Bruña, R., Tjepkema-Cloostermans, M. C., Hofmeijer, J., & Van Putten, M. J. (2021). EEG functional connectivity contributes to outcome prediction of postanoxic coma. *Clinical Neurophysiology*, *132*(6), 1312–1320. https://doi.org/10.1016/j.clinph.2021.02.011

Chaieb, L., Antal, A., & Paulus, W. (2011). Transcranial alternating current stimulation in the low kHz range increases motor cortex excitability. *Restorative Neurology and Neuroscience*, *29*(3), 167–175. https://doi.org/10.3233/RNN-2011-0589

Chang, C., & Glover, G. H. (2010). Time–frequency dynamics of resting-state brain connectivity measured with fMRI. *NeuroImage*, *50*(1), 81–98. https://doi.org/10.1016/j.neuroimage.2009.12.011

Chang, C., Leopold, D. A., Schölvinck, M. L., Mandelkow, H., Picchioni, D., Liu, X., Ye, F. Q., Turchi, J. N., & Duyn, J. H. (2016). Tracking brain arousal fluctuations with fMRI. *Proceedings of the National Academy of Sciences*, *113*(16), 4518–4523. https://doi.org/10.1073/pnas.1520613113

Chen, W.-T., Lu, A., Craessaerts, K., Pavie, B., Sala Frigerio, C., Corthout, N., Qian, X., Laláková, J., Kühnemund, M., Voytyuk, I., Wolfs, L., Mancuso, R., Salta, E., Balusu, S., Snellinx, A., Munck, S., Jurek, A., Fernandez Navarro, J., Saido, T. C., … De Strooper, B. (2020). Spatial Transcriptomics and In Situ Sequencing to Study Alzheimer's Disease. *Cell*, *182*(4), 976–991.e19. https://doi.org/10.1016/j.cell.2020.06.038

Cherkassky, V. L., Kana, R. K., Keller, T. A., & Just, M. A. (2006). Functional connectivity in a baseline resting-state network in autism. *NeuroReport*, *17*(16), 1687–1690. https://doi.org/10.1097/01.wnr.0000239956.45448.4c

Chikhi, S., Matton, N., & Blanchet, S. (2022). Eeg power spectral measures of cognitive workload: A meta-analysis. *Psychophysiology*, *59*(6), e14009.

Choe, A. S., Jones, C. K., Joel, S. E., Muschelli, J., Belegu, V., Caffo, B. S., Lindquist, M. A., Van Zijl, P. C. M., & Pekar, J. J. (2015). Reproducibility and Temporal Structure in Weekly Resting-State fMRI over a Period of 3.5 Years (D. Margulies, Ed.). *PLOS ONE*, *10*(10), e0140134. https://doi.org/10.1371/journal.pone.0140134

Cohen, J. R. (2018). The behavioral and cognitive relevance of time-varying, dynamic changes in functional connectivity. *NeuroImage*, *180*, 515–525. https://doi.org/10.1016/j.neuroimage.2017.09.036

Colclough, G., Brookes, M., Smith, S., & Woolrich, M. (2015). A symmetric multivariate leakage correction for MEG connectomes. *NeuroImage*, *117*, 439–448. https://doi.org/10.1016/j.neuroimage.2015.03.071

Colrain, I. M., Crowley, K. E., Nicholas, C. L., Afifi, L., Baker, F. C., Padilla, M., Turlington, S. R., & Trinder, J. (2010). Sleep evoked delta frequency responses show a linear decline in amplitude across the adult lifespan. *Neurobiology of Aging*, *31*(5), 874–883. https://doi.org/10.1016/j.neurobiolaging.2008.06.003

Cooke, S. F., & Bliss, T. V. (2006). Plasticity in the human central nervous system. *Brain*, *129*(7), 1659–1673.

Córdova-Palomera, A., Kaufmann, T., Persson, K., Alnæs, D., Doan, N. T., Moberget, T., Lund, M. J., Barca, M. L., Engvig, A., Brækhus, A., Engedal, K., Andreassen, O. A., Selbæk, G., & Westlye, L. T. (2017). Disrupted global metastability and static and dynamic brain connectivity across individuals in the Alzheimer's disease continuum. *Scientific Reports*, *7*(1), 40268. https://doi.org/10.1038/srep40268

Csernus, E. A., Werber, T., Kamondi, A., & Horvath, A. A. (2022). The Significance of Subclinical Epileptiform Activity in Alzheimer's Disease: A Review. *Frontiers in Neurology*, *13*, 856500. https://doi.org/10.3389/fneur.2022.856500

Cuesta, P., Garcés, P., Castellanos, N. P., López, M. E., Aurtenetxe, S., Bajo, R., Pineda-Pardo, J. A., Bruña, R., Marín, A. G., Delgado, M., Barabash, A., Ancín, I., Cabranes, J. A., Fernandez, A., Del Pozo, F., Sancho, M., Marcos, A., Nakamura, A., & Maestú, F. (2015). Influence of the APOE ϵ4 Allele and Mild Cognitive Impairment Diagnosis in the Disruption of the MEG Resting State Functional Connectivity in Sources Space. *Journal of Alzheimer's Disease*, *44*(2), 493–505. https://doi.org/10.3233/JAD-141872

Cuesta, P., Ochoa-Urrea, M., Funke, M., Hasan, O., Zhu, P., Marcos, A., López, M. E., Schulz, P. E., Lhatoo, S., Pantazis, D., Mosher, J. C., & Maestu, F. (2022). Gamma band functional connectivity reduction in patients with amnestic mild cognitive impairment and epileptiform activity. *Brain Communications*, *4*(2), fcac012. https://doi.org/10.1093/braincomms/fcac012

De Frutos Lucas, J., Sewell, K. R., García-Colomo, A., Markovic, S., Erickson, K. I., & Brown, B. M. (2023). How does apolipoprotein E genotype influence the relationship between physical activity and Alzheimer's disease risk? A novel integrative model. *Alzheimer's Research & Therapy*, *15*(1), 22. https://doi.org/10.1186/s13195-023-01170-4

De Haan, W., Van Der Flier, W. M., Wang, H., Van Mieghem, P. F., Scheltens, P., & Stam, C. J. (2012). Disruption of Functional Brain Networks in Alzheimer's Disease: What Can We Learn from Graph Spectral Analysis of Resting-State Magnetoencephalography? *Brain Connectivity*, *2*(2), 45–55. https://doi.org/10.1089/brain.2011.0043

De Pasquale, F., Della Penna, S., Snyder, A. Z., Lewis, C., Mantini, D., Marzetti, L., Belardinelli, P., Ciancetta, L., Pizzella, V., Romani, G. L., & Corbetta, M. (2010). Temporal dynamics of spontaneous MEG activity in brain networks. *Proceedings of the National Academy of Sciences*, *107*(13), 6040–6045. https://doi.org/10.1073/pnas.0913863107

DeFelipe, J. (2015). The dendritic spine story: An intriguing process of discovery. *Frontiers in Neuroanatomy*, *9*. https://doi.org/10.3389/fnana.2015.00014

Delvendahl, I., Kita, K., & Müller, M. (2019). Rapid and sustained homeostatic control of presynaptic exocytosis at a central synapse. *Proceedings of the National Academy of Sciences*, *116*(47), 23783–23789. https://doi.org/10.1073/pnas.1909675116

Demirtaş, M., Falcon, C., Tucholka, A., Gispert, J. D., Molinuevo, J. L., & Deco, G. (2017). A whole-brain computational modeling approach to explain the alterations in resting-state functional connectivity during progression of Alzheimer's disease. *NeuroImage: Clinical*, *16*, 343–354. https://doi.org/10.1016/j.nicl.2017.08.006

Demirtaş, M., Tornador, C., Falcón, C., López-Solà, M., Hernández-Ribas, R., Pujol, J., Menchón, J. M., Ritter, P., Cardoner, N., Soriano-Mas, C., & Deco, G. (2016). Dynamic functional connectivity reveals altered variability in functional connectivity among patients with major depressive disorder. *Human Brain Mapping*, *37*(8), 2918–2930. https://doi.org/10.1002/hbm.23215

Deperrois, N., & Graupner, M. (2020). Short-term depression and long-term plasticity together tune sensitive range of synaptic plasticity (H. Cuntz, Ed.). *PLOS Computational Biology*, *16*(9), e1008265. https://doi.org/10.1371/journal.pcbi.1008265

Deuschl, G., Beghi, E., Fazekas, F., Varga, T., Christoforidi, K. A., Sipido, E., Bassetti, C. L., Vos, T., & Feigin, V. L. (2020). The burden of neurological diseases in Europe: An analysis for the Global Burden of Disease Study 2017. *The Lancet Public Health*, *5*(10), e551–e567. https://doi.org/10.1016/S2468-2667(20)30190-0

Di, X., & Biswal, B. B. (2015). Dynamic brain functional connectivity modulated by resting-state networks. *Brain Structure and Function*, *220*(1), 37–46. https://doi.org/10.1007/s00429-013-0634-3

Doody, R. S., Raman, R., Farlow, M., Iwatsubo, T., Vellas, B., Joffe, S., Kieburtz, K., He, F., Sun, X., Thomas, R. G., Aisen, P. S., Siemers, E., Sethuraman, G., & Mohs, R. (2013). A Phase 3 Trial of Semagacestat for Treatment of Alzheimer's Disease. *New England Journal of Medicine*, *369*(4), 341–350. https://doi.org/10.1056/NEJMoa1210951

D'Souza, R. D., Meier, A. M., Bista, P., Wang, Q., & Burkhalter, A. (2016). Recruitment of inhibition and excitation across mouse visual cortex depends on the hierarchy of interconnecting areas. *eLife*, *5*, e19332. https://doi.org/10.7554/eLife.19332

Duc, N. T., & Lee, B. (2019). Microstate functional connectivity in EEG cognitive tasks revealed by a multivariate Gaussian hidden Markov model with phase locking value. *Journal of Neural Engineering*, *16*(2), 026033. https://doi.org/10.1088/1741-2552/ab0169

Elton, A., & Gao, W. (2015). Task-related modulation of functional connectivity variability and its behavioral correlations: Task-Related Connectivity Variability. *Human Brain Mapping*, *36*(8), 3260–3272. https://doi.org/10.1002/hbm.22847

Elyamany, O., Leicht, G., Herrmann, C. S., & Mulert, C. (2021). Transcranial alternating current stimulation (tACS): From basic mechanisms towards first applications in psychiatry. *European Archives of Psychiatry and Clinical Neuroscience*, *271*(1), 135–156. https://doi.org/10.1007/s00406-020-01209-9

Fallahi, A., Pooyan, M., Lotfi, N., Baniasad, F., Tapak, L., Mohammadi-Mobarakeh, N., Hashemi-Fesharaki, S. S., Mehvari-Habibabadi, J., Ay, M. R., & Nazem-Zadeh, M.-R. (2021). Dynamic functional connectivity in temporal lobe epilepsy: A graph theoretical

and machine learning approach. *Neurological Sciences*, *42*(6), 2379–2390. https://doi.org/10.1007/s10072-020-04759-x

Feingold, J., Gibson, D. J., DePasquale, B., & Graybiel, A. M. (2015). Bursts of beta oscillation differentiate postperformance activity in the striatum and motor cortex of monkeys performing movement tasks. *Proceedings of the National Academy of Sciences*, *112*(44), 13687–13692. https://doi.org/10.1073/pnas.1517629112

Fernández, A., Hornero, R., Mayo, A., Poza, J., Maestú, F., & Ortiz Alonso, T. (2006). Quantitative Magnetoencephalography of Spontaneous Brain Activity in Alzheimer Disease: An Exhaustive Frequency Analysis. *Alzheimer Disease & Associated Disorders*, *20*(3), 153–159. https://doi.org/10.1097/00002093-200607000-00006

Filippi, M., Spinelli, E. G., Cividini, C., & Agosta, F. (2019). Resting State Dynamic Functional Connectivity in Neurodegenerative Conditions: A Review of Magnetic Resonance Imaging Findings. *Frontiers in Neuroscience*, *13*, 657. https://doi.org/10.3389/fnins.2019.00657

Finger, H., Bönstrup, M., Cheng, B., Messé, A., Hilgetag, C., Thomalla, G., Gerloff, C., & König, P. (2016). Modeling of Large-Scale Functional Brain Networks Based on Structural Connectivity from DTI: Comparison with EEG Derived Phase Coupling Networks and Evaluation of Alternative Methods along the Modeling Path (J. Daunizeau, Ed.). *PLOS Computational Biology*, *12*(8), e1005025. https://doi.org/10.1371/journal.pcbi.1005025

Finlay, C. C., Maus, S., Beggan, C., Bondar, T., Chambodut, A., Chernova, T., Chulliat, A., Golovkov, V., Hamilton, B., Hamoudi, M., et al. (2010). International geomagnetic reference field: The eleventh generation. *Geophysical Journal International*, *183*(3), 1216–1230.

for the Alzheimer's Disease Neuroimaging Initiative, Wee, C.-Y., Yang, S., Yap, P.-T., & Shen, D. (2016). Sparse temporally dynamic resting-state functional connectivity networks for early MCI identification. *Brain Imaging and Behavior*, *10*(2), 342–356. https://doi.org/10.1007/s11682-015-9408-2

Fornito, A., Harrison, B. J., Zalesky, A., & Simons, J. S. (2012). Competitive and cooperative dynamics of large-scale brain functional networks supporting recollection. *Proceedings of the National Academy of Sciences*, *109*(31), 12788–12793. https://doi.org/10.1073/pnas.1204185109

Foster, M. (1897). *A text-book of physiology pt. 3*. McMillan & Company.

Friston, K. J. (1994). Functional and effective connectivity in neuroimaging: A synthesis. *Human Brain Mapping*, *2*(1-2), 56–78. https://doi.org/10.1002/hbm.460020107

Gabor, D. (1946). Theory of communication. Part 1: The analysis of information. *Journal of the Institution of Electrical Engineers - Part III: Radio and Communication Engineering*, *93*(26), 429–441. https://doi.org/10.1049/ji-3-2.1946.0074

Garcés, P., López-Sanz, D., Maestú, F., & Pereda, E. (2017). Choice of Magnetometers and Gradiometers after Signal Space Separation. *Sensors*, *17*(12), 2926. https://doi.org/10.3390/s17122926

Garcés, P., Martín-Buro, M. C., & Maestú, F. (2016). Quantifying the Test-Retest Reliability of Magnetoencephalography Resting-State Functional Connectivity. *Brain Connectivity*, *6*(6), 448–460. https://doi.org/10.1089/brain.2015.0416

García-Colomo, A., Nebreda, A., Carrasco-Gómez, M., De Frutos-Lucas, J., Ramirez-Toraño, F., Spuch, C., Comis-Tuche, M., Bruña, R., Alfonsín, S., & Maestú, F. (2024). Longitudinal changes in the functional connectivity of individuals at risk of Alzheimer's disease. *GeroScience*, *46*(3), 2989–3003. https://doi.org/10.1007/s11357-023-01036-5

Garcia-Marin, V. (2009). Diminished perisomatic GABAergic terminals on cortical neurons adjacent to amyloid plaques. *Frontiers in Neuroanatomy*, *3*. https://doi.org/10.3389/neuro.05.028.2009

Gärtner, M., Brodbeck, V., Laufs, H., & Schneider, G. (2015). A stochastic model for EEG microstate sequence analysis. *NeuroImage*, *104*, 199–208. https://doi.org/10.1016/j.neuroimage.2014.10.014

Ghanem, A., Berry, D. S., Burkes, A., Grill, N., Hall, T. M., Hart, K. A., Hernandez, N. C., Chapman, S., Sharma, V. D., Huey, E. D., et al. (2024). Prevalence of and annual conversion rates to mild cognitive impairment and dementia: Prospective, longitudinal study of an essential tremor cohort. *Annals of Neurology*, *95*(6), 1193–1204.

Ghumare, E. G., Schrooten, M., Vandenberghe, R., & Dupont, P. (2018). A Time-Varying Connectivity Analysis from Distributed EEG Sources: A Simulation Study. *Brain Topography*, *31*(5), 721–737. https://doi.org/10.1007/s10548-018-0621-3

Giannakakis, G., Marias, K., & Tsiknakis, M. (2019). A stress recognition system using hrv parameters and machine learning techniques. *2019 8th International Conference on Affective Computing and Intelligent Interaction Workshops and Demos (ACIIW)*, 269–272.

Goate, A., Chartier-Harlin, M.-C., Mullan, M., Brown, J., Crawford, F., Fidani, L., Giuffra, L., Haynes, A., Irving, N., James, L., Mant, R., Newton, P., Rooke, K., Roques, P., Talbot, C., Pericak-Vance, M., Roses, A., Williamson, R., Rossor, M., ... Hardy, J. (1991). Segregation of a missense mutation in the amyloid precursor protein gene with familial Alzheimer's disease. *Nature*, *349*(6311), 704–706. https://doi.org/10.1038/349704a0

Gomez-Nicola, D., & Boche, D. (2015). Post-mortem analysis of neuroinflammatory changes in human Alzheimer's disease. *Alzheimer's Research & Therapy*, *7*(1), 42. https://doi.org/10.1186/s13195-015-0126-1

Gonzales, M. M., Garbarino, V. R., Pollet, E., Palavicini, J. P., Kellogg, D. L., Kraig, E., Orr, M. E., et al. (2022). Biological aging processes underlying cognitive decline and neurodegenerative disease. *The Journal of clinical investigation*, *132*(10).

Gonzalez-Castillo, J., & Bandettini, P. A. (2018). Task-based dynamic functional connectivity: Recent findings and open questions. *NeuroImage*, *180*, 526–533. https://doi.org/10.1016/j.neuroimage.2017.08.006

Gonzalez-Castillo, J., Handwerker, D. A., Robinson, M. E., Hoy, C. W., Buchanan, L. C., Saad, Z. S., & Bandettini, P. A. (2014). The spatial structure of resting state connectivity stability on the scale of minutes. *Frontiers in Neuroscience*, *8*. https://doi.org/10.3389/fnins.2014.00138

Gratta, C. D., Pizzella, V., Tecchio, F., & Romani, G. L. (2001). Magnetoencephalography - a noninvasive brain imaging method with 1 ms time resolution. *Reports on Progress in Physics*, *64*(12), 1759–1814. https://doi.org/10.1088/0034-4885/64/12/204

Gu, Y., Lin, Y., Huang, L., Ma, J., Zhang, J., Xiao, Y., Dai, Z., & Alzheimer's Disease Neuroimaging Initiative. (2020). Abnormal dynamic functional connectivity in Alzheimer's

disease. *CNS Neuroscience & Therapeutics*, *26*(9), 962–971. https://doi.org/10.1111/cns.13387

Guan, K., Zhang, Z., Chai, X., Tian, Z., Liu, T., & Niu, H. (2022). EEG Based Dynamic Functional Connectivity Analysis in Mental Workload Tasks With Different Types of Information. *IEEE Transactions on Neural Systems and Rehabilitation Engineering*, *30*, 632–642. https://doi.org/10.1109/TNSRE.2022.3156546

Guidotti, R., Del Gratta, C., Baldassarre, A., Romani, G. L., & Corbetta, M. (2015). Visual Learning Induces Changes in Resting-State fMRI Multivariate Pattern of Information. *Journal of Neuroscience*, *35*(27), 9786–9798. https://doi.org/10.1523/JNEUROSCI.3920-14.2015

Gupta, A., Siddhad, G., Pandey, V., Roy, P. P., & Kim, B.-G. (2021). Subject-Specific Cognitive Workload Classification Using EEG-Based Functional Connectivity and Deep Learning. *Sensors*, *21*(20), 6710. https://doi.org/10.3390/s21206710

Hallez, H., Vanrumste, B., Grech, R., Muscat, J., De Clercq, W., Vergult, A., D'Asseler, Y., Camilleri, K. P., Fabri, S. G., Van Huffel, S., & Lemahieu, I. (2007). Review on solving the forward problem in EEG source analysis. *Journal of NeuroEngineering and Rehabilitation*, *4*(1), 46. https://doi.org/10.1186/1743-0003-4-46

Hämäläinen, M., Hari, R., Ilmoniemi, R. J., Knuutila, J., & Lounasmaa, O. V. (1993). Magnetoencephalography—theory, instrumentation, and applications to noninvasive studies of the working human brain. *Reviews of Modern Physics*, *65*(2), 413–497. https://doi.org/10.1103/RevModPhys.65.413

Han, Y., Wang, K., Jia, J., & Wu, W. (2017). Changes of EEG Spectra and Functional Connectivity during an Object-Location Memory Task in Alzheimer's Disease. *Frontiers in Behavioral Neuroscience*, *11*, 107. https://doi.org/10.3389/fnbeh.2017.00107

Hansen, P., Kringelbach, M., & Salmelin, R. (Eds.). (2010, June). *MEG: An Introduction to Methods*. Oxford University Press. https://doi.org/10.1093/acprof:oso/9780195307238.001.0001

Hector, A., & Brouillette, J. (2021). Hyperactivity Induced by Soluble Amyloid-β Oligomers in the Early Stages of Alzheimer's Disease. *Frontiers in Molecular Neuroscience*, *13*, 600084. https://doi.org/10.3389/fnmol.2020.600084

Henley, D., Raghavan, N., Sperling, R., Aisen, P., Raman, R., & Romano, G. (2019). Preliminary Results of a Trial of Atabecestat in Preclinical Alzheimer's Disease. *New England Journal of Medicine*, *380*(15), 1483–1485. https://doi.org/10.1056/NEJMc1813435

Hindriks, R., Adhikari, M., Murayama, Y., Ganzetti, M., Mantini, D., Logothetis, N., & Deco, G. (2016). Can sliding-window correlations reveal dynamic functional connectivity in resting-state fMRI? *NeuroImage*, *127*, 242–256. https://doi.org/10.1016/j.neuroimage.2015.11.055

Hipp, J. F., & Siegel, M. (2015). Bold fmri correlation reflects frequency-specific neuronal correlation. *Current Biology*, *25*(10), 1368–1374.

Hodgkin, A. L., & Huxley, A. F. (1939). Action potentials recorded from inside a nerve fibre. *Nature*, *144*(3651), 710–711.

Hodgkin, A. L., & Huxley, A. F. (1952). A quantitative description of membrane current and its application to conduction and excitation in nerve. *The Journal of physiology*, *117*(4), 500.

Hong, S., Beja-Glasser, V. F., Nfonoyim, B. M., Frouin, A., Li, S., Ramakrishnan, S., Merry, K. M., Shi, Q., Rosenthal, A., Barres, B. A., Lemere, C. A., Selkoe, D. J., & Stevens, B. (2016). Complement and microglia mediate early synapse loss in Alzheimer mouse models. *Science*, *352*(6286), 712–716. https://doi.org/10.1126/science.aad8373

Hotelling, H. (1953). New Light on the Correlation Coefficient and its Transforms. *Journal of the Royal Statistical Society: Series B (Methodological)*, *15*(2), 193–225. https://doi.org/10.1111/j.2517-6161.1953.tb00135.x

Hounsfield, G. N. (1980). Computed medical imaging. *Science*, *210*(4465), 22–28.

Huang, Y.-r., & Liu, R.-t. (2020). The Toxicity and Polymorphism of β-Amyloid Oligomers. *International Journal of Molecular Sciences*, *21*(12), 4477. https://doi.org/10.3390/ijms21124477

Hutchison, R. M., Womelsdorf, T., Allen, E. A., Bandettini, P. A., Calhoun, V. D., Corbetta, M., Della Penna, S., Duyn, J. H., Glover, G. H., Gonzalez-Castillo, J., Handwerker, D. A., Keilholz, S., Kiviniemi, V., Leopold, D. A., De Pasquale, F., Sporns, O., Walter, M., & Chang, C. (2013). Dynamic functional connectivity: Promise, issues, and interpretations. *NeuroImage*, *80*, 360–378. https://doi.org/10.1016/j.neuroimage.2013.05.079

Ieracitano, C., Duun-Henriksen, J., Mammone, N., La Foresta, F., & Morabito, F. C. (2017). Wavelet coherence-based clustering of EEG signals to estimate the brain connectivity in absence epileptic patients. *2017 International Joint Conference on Neural Networks (IJCNN)*, 1297–1304. https://doi.org/10.1109/IJCNN.2017.7966002

Ikotun, A. M., Ezugwu, A. E., Abualigah, L., Abuhaija, B., & Heming, J. (2023). K-means clustering algorithms: A comprehensive review, variants analysis, and advances in the era of big data. *Information Sciences*, *622*, 178–210. https://doi.org/10.1016/j.ins.2022.11.139

İnce, R., Adanır, S. S., & Sevmez, F. (2021). The inventor of electroencephalography (eeg): Hans berger (1873–1941). *Child's Nervous System*, *37*, 2723–2724.

Ives-Deliperi, V., & Butler, J. T. (2021). Mechanisms of cognitive impairment in temporal lobe epilepsy: A systematic review of resting-state functional connectivity studies. *Epilepsy & Behavior*, *115*, 107686.

Jack, C. R., Bennett, D. A., Blennow, K., Carrillo, M. C., Dunn, B., Haeberlein, S. B., Holtzman, D. M., Jagust, W., Jessen, F., Karlawish, J., Liu, E., Molinuevo, J. L., Montine, T., Phelps, C., Rankin, K. P., Rowe, C. C., Scheltens, P., Siemers, E., Snyder, H. M., ... Silverberg, N. (2018). NIA-AA Research Framework: Toward a biological definition of Alzheimer's disease. *Alzheimer's & Dementia*, *14*(4), 535–562. https://doi.org/10.1016/j.jalz.2018.02.018

Jack, C. R., Knopman, D. S., Jagust, W. J., Shaw, L. M., Aisen, P. S., Weiner, M. W., Petersen, R. C., & Trojanowski, J. Q. (2010). Hypothetical model of dynamic biomarkers of the alzheimer's pathological cascade. *The Lancet Neurology*, *9*(1), 119–128.

Jensen, O., & Mazaheri, A. (2010). Shaping Functional Architecture by Oscillatory Alpha Activity: Gating by Inhibition. *Frontiers in Human Neuroscience*, *4*. https://doi.org/10.3389/fnhum.2010.00186

Jessen, F., Amariglio, R. E., Van Boxtel, M., Breteler, M., Ceccaldi, M., Chételat, G., Dubois, B., Dufouil, C., Ellis, K. A., Van Der Flier, W. M., Glodzik, L., Van Harten, A. C., De Leon, M. J., McHugh, P., Mielke, M. M., Molinuevo, J. L., Mosconi, L., Osorio,

R. S., Perrotin, A., ... Subjective Cognitive Decline Initiative (SCD-I) Working Group. (2014). A conceptual framework for research on subjective cognitive decline in preclinical Alzheimer's disease. *Alzheimer's & Dementia*, *10*(6), 844–852. https://doi.org/10.1016/j.jalz.2014.01.001

Jia, X., & Kohn, A. (2011). Gamma Rhythms in the Brain. *PLoS Biology*, *9*(4), e1001045. https://doi.org/10.1371/journal.pbio.1001045

Jiang, Y., Zhang, H., & Yu, S. (2021). Changes in delta and theta oscillations in the brain indicate dynamic switching of attention between internal and external processing. *4th International Conference on Biometric Engineering and Applications*, 25–31. https://doi.org/10.1145/3476779.3476784

Jin, H., Ranasinghe, K. G., Prabhu, P., Dale, C., Gao, Y., Kudo, K., Vossel, K., Raj, A., Nagarajan, S. S., & Jiang, F. (2023). Dynamic functional connectivity meg features of alzheimer's disease. *NeuroImage*, *281*, 120358.

Jones, D. T., Vemuri, P., Murphy, M. C., Gunter, J. L., Senjem, M. L., Machulda, M. M., Przybelski, S. A., Gregg, B. E., Kantarci, K., Knopman, D. S., Boeve, B. F., Petersen, R. C., & Jack, C. R. (2012). Non-Stationarity in the "Resting Brain's" Modular Architecture (Y. He, Ed.). *PLoS ONE*, *7*(6), e39731. https://doi.org/10.1371/journal.pone.0039731

Jones, K. T., Arciniega, H., & Berryhill, M. E. (2019). Replacing tDCS with theta tACS provides selective, but not general WM benefits. *Brain Research*, *1720*, 146324. https://doi.org/10.1016/j.brainres.2019.146324

Jones, S. R. (2016). When brain rhythms aren't 'rhythmic': Implication for their mechanisms and meaning. *Current Opinion in Neurobiology*, *40*, 72–80. https://doi.org/10.1016/j.conb.2016.06.010

Josephson, B. (1962). Possible new effects in superconductive tunnelling. *Physics Letters*, *1*(7), 251–253. https://doi.org/10.1016/0031-9163(62)91369-0

Jousm??ki, V., & Hari, R. (1996). Cardiac Artifacts in Magnetoencephalogram: *Journal of Clinical Neurophysiology*, *13*(2), 172–176. https://doi.org/10.1097/00004691-199603000-00008

Jovasevic, V., Wood, E. M., Cicvaric, A., Zhang, H., Petrovic, Z., Carboncino, A., Parker, K. K., Bassett, T. E., Moltesen, M., Yamawaki, N., et al. (2024). Formation of memory assemblies through the dna-sensing tlr9 pathway. *Nature*, *628*(8006), 145–153.

Kajiwara, M., Nomura, R., Goetze, F., Kawabata, M., Isomura, Y., Akutsu, T., & Shimono, M. (2021). Inhibitory neurons exhibit high controlling ability in the cortical microconnectome (D. Marinazzo, Ed.). *PLOS Computational Biology*, *17*(4), e1008846. https://doi.org/10.1371/journal.pcbi.1008846

Kang, J., Wang, L., Yan, C., Wang, J., Liang, X., & He, Y. (2011). Characterizing dynamic functional connectivity in the resting brain using variable parameter regression and Kalman filtering approaches. *NeuroImage*, *56*(3), 1222–1234. https://doi.org/10.1016/j.neuroimage.2011.03.033

Karahan, E., Tait, L., Si, R., Özkan, A., Szul, M. J., Graham, K. S., Lawrence, A. D., & Zhang, J. (2022). The interindividual variability of multimodal brain connectivity maintains spatial heterogeneity and relates to tissue microstructure. *Communications Biology*, *5*(1), 1007. https://doi.org/10.1038/s42003-022-03974-w

Karahanoğlu, F. I., & Van De Ville, D. (2015). Transient brain activity disentangles fMRI resting-state dynamics in terms of spatially and temporally overlapping networks. *Nature Communications*, *6*(1), 7751. https://doi.org/10.1038/ncomms8751

Karran, E., & De Strooper, B. (2022). The amyloid hypothesis in Alzheimer disease: New insights from new therapeutics. *Nature Reviews Drug Discovery*, *21*(4), 306–318. https://doi.org/10.1038/s41573-022-00391-w

Kawagoe, T., Onoda, K., & Yamaguchi, S. (2019). Subjective memory complaints are associated with altered resting-state functional connectivity but not structural atrophy. *NeuroImage: Clinical*, *21*, 101675. https://doi.org/10.1016/j.nicl.2019.101675

Kim, J. W., Lee, J., Kim, B.-N., Kang, T., Min, K. J., Han, D. H., & Lee, Y. S. (2015). Theta-phase gamma-amplitude coupling as a neurophysiological marker of attention deficit/hyperactivity disorder in children. *Neuroscience Letters*, *603*, 25–30. https://doi.org/10.1016/j.neulet.2015.07.006

Klevanski, M., Herrmann, U., Weyer, S. W., Fol, R., Cartier, N., Wolfer, D. P., Caldwell, J. H., Korte, M., & Müller, U. C. (2015). The APP Intracellular Domain Is Required for Normal Synaptic Morphology, Synaptic Plasticity, and Hippocampus-Dependent Behavior. *The Journal of Neuroscience*, *35*(49), 16018–16033. https://doi.org/10.1523/JNEUROSCI.2009-15.2015

Knafo, S., Alonso-Nanclares, L., Gonzalez-Soriano, J., Merino-Serrais, P., Fernaud-Espinosa, I., Ferrer, I., & DeFelipe, J. (2009). Widespread Changes in Dendritic Spines in a Model of Alzheimer's Disease. *Cerebral Cortex*, *19*(3), 586–592. https://doi.org/10.1093/cercor/bhn111

Knuth, K. H. (2019). Optimal data-based binning for histograms and histogram-based probability density models. *Digital Signal Processing*, *95*, 102581. https://doi.org/10.1016/j.dsp.2019.102581

Koenig, T., & Brandeis, D. (2016). Inappropriate assumptions about EEG state changes and their impact on the quantification of EEG state dynamics. *NeuroImage*, *125*, 1104–1106. https://doi.org/10.1016/j.neuroimage.2015.06.035

Koo, E. H., & Squazzo, S. L. (1994). Evidence that production and release of amyloid beta-protein involves the endocytic pathway. *The Journal of Biological Chemistry*, *269*(26), 17386–17389.

Kotermanski, S. E., & Cascio, M. (2023). Neuronal action potentials and ion channel allostery.

Kowalczyk, O. S., Mehta, M. A., O'Daly, O. G., & Criaud, M. (2022). Task-based functional connectivity in attention-deficit/hyperactivity disorder: A systematic review. *Biological Psychiatry Global Open Science*, *2*(4), 350–367.

Kucyi, A., & Davis, K. D. (2014). Dynamic functional connectivity of the default mode network tracks daydreaming. *NeuroImage*, *100*, 471–480. https://doi.org/10.1016/j.neuroimage.2014.06.044

Kumar, S., Narayan, Y., & Amell, T. (2003). Power spectra of sternocleidomastoids, splenius capitis, and upper trapezius in oblique exertions. *The Spine Journal*, *3*(5), 339–350. https://doi.org/10.1016/S1529-9430(03)00077-9

Kuznetsova, M. S., Higgs, M. H., & Spain, W. J. (2008). Adaptation of Firing Rate and Spike-Timing Precision in the Avian Cochlear Nucleus. *The Journal of Neuroscience*, *28*(46), 11906–11915. https://doi.org/10.1523/JNEUROSCI.3827-08.2008

Lachaux, J.-P., Rodriguez, E., Martinerie, J., & Varela, F. J. (1999). Measuring phase synchrony in brain signals. *Human Brain Mapping*, *8*(4), 194–208. https://doi.org/10.1002/(SICI)1097-0193(1999)8:4<194::AID-HBM4>3.0.CO;2-C

Lau, T., & Zochowski, M. (2011). The Resonance Frequency Shift, Pattern Formation, and Dynamical Network Reorganization via Sub-Threshold Input (M. Kaiser, Ed.). *PLoS ONE*, *6*(4), e18983. https://doi.org/10.1371/journal.pone.0018983

Le Bihan, D., & Breton, E. (1985). Imagerie de diffusion in-vivo par résonance magnétique nucléaire. *Comptes-Rendus de l'Académie des Sciences*, *93*(5), 27–34.

Lee, J.-H., Kim, J.-y., Noh, S., Lee, H., Lee, S. Y., Mun, J. Y., Park, H., & Chung, W.-S. (2021). Astrocytes phagocytose adult hippocampal synapses for circuit homeostasis. *Nature*, *590*(7847), 612–617. https://doi.org/10.1038/s41586-020-03060-3

Lee, W. H., & Frangou, S. (2017). Linking functional connectivity and dynamic properties of resting-state networks. *Scientific Reports*, *7*(1), 16610. https://doi.org/10.1038/s41598-017-16789-1

Lega, B., Burke, J., Jacobs, J., & Kahana, M. J. (2016). Slow-Theta-to-Gamma Phase–Amplitude Coupling in Human Hippocampus Supports the Formation of New Episodic Memories. *Cerebral Cortex*, *26*(1), 268–278. https://doi.org/10.1093/cercor/bhu232

Leonardi, N., Richiardi, J., Gschwind, M., Simioni, S., Annoni, J.-M., Schluep, M., Vuilleumier, P., & Van De Ville, D. (2013). Principal components of functional connectivity: A new approach to study dynamic brain connectivity during rest. *NeuroImage*, *83*, 937–950. https://doi.org/10.1016/j.neuroimage.2013.07.019

Levy-Lahad, E., Wasco, W., Poorkaj, P., Romano, D. M., Oshima, J., Pettingell, W. H., Yu, C.-e., Jondro, P. D., Schmidt, S. D., Wang, K., Crowley, A. C., Fu, Y.-H., Guenette, S. Y., Galas, D., Nemens, E., Wijsman, E. M., Bird, T. D., Schellenberg, G. D., & Tanzi, R. E. (1995). Candidate Gene for the Chromosome 1 Familial Alzheimer's Disease Locus. *Science*, *269*(5226), 973–977. https://doi.org/10.1126/science.7638622

Li, R., Nguyen, T., Potter, T., & Zhang, Y. (2019). Dynamic cortical connectivity alterations associated with Alzheimer's disease: An EEG and fNIRS integration study. *NeuroImage: Clinical*, *21*, 101622. https://doi.org/10.1016/j.nicl.2018.101622

Liégeois, R., Ziegler, E., Phillips, C., Geurts, P., Gómez, F., Bahri, M. A., Yeo, B. T. T., Soddu, A., Vanhaudenhuyse, A., Laureys, S., & Sepulchre, R. (2016). Cerebral functional connectivity periodically (de)synchronizes with anatomical constraints. *Brain Structure and Function*, *221*(6), 2985–2997. https://doi.org/10.1007/s00429-015-1083-y

Liporace, L. (1982). Maximum likelihood estimation for multivariate observations of Markov sources. *IEEE Transactions on Information Theory*, *28*(5), 729–734. https://doi.org/10.1109/TIT.1982.1056544

Liu, A., Vöröslakos, M., Kronberg, G., Henin, S., Krause, M. R., Huang, Y., Opitz, A., Mehta, A., Pack, C. C., Krekelberg, B., Berényi, A., Parra, L. C., Melloni, L., Devinsky, O., & Buzsáki, G. (2018). Immediate neurophysiological effects of transcranial electrical stimulation. *Nature Communications*, *9*(1), 5092. https://doi.org/10.1038/s41467-018-07233-7

Liu, H., Tang, H., Wei, W., Wang, G., Du, Y., & Ruan, J. (2021). Altered peri-seizure EEG microstate dynamics in patients with absence epilepsy. *Seizure*, *88*, 15–21. https://doi.org/10.1016/j.seizure.2021.03.020

Liu, J., Chang, L., Song, Y., Li, H., & Wu, Y. (2019). The role of nmda receptors in alzheimer's disease. *Frontiers in neuroscience*, *13*, 43.

Liu, X., & Duyn, J. H. (2013). Time-varying functional network information extracted from brief instances of spontaneous brain activity. *Proceedings of the National Academy of Sciences*, *110*(11), 4392–4397. https://doi.org/10.1073/pnas.1216856110

Liuzzi, L., Quinn, A. J., O'Neill, G. C., Woolrich, M. W., Brookes, M. J., Hillebrand, A., & Tewarie, P. (2019). How Sensitive Are Conventional MEG Functional Connectivity Metrics With Sliding Windows to Detect Genuine Fluctuations in Dynamic Functional Connectivity? *Frontiers in Neuroscience*, *13*, 797. https://doi.org/10.3389/fnins.2019.00797

Lombardi, F., Herrmann, H. J., Plenz, D., & De Arcangelis, L. (2016). Temporal correlations in neuronal avalanche occurrence. *Scientific Reports*, *6*(1), 24690. https://doi.org/10.1038/srep24690

Lopes da Silva, F. (2013). EEG and MEG: Relevance to Neuroscience. *Neuron*, *80*(5), 1112–1128. https://doi.org/10.1016/j.neuron.2013.10.017

López, M. E., Bruña, R., Aurtenetxe, S., Pineda-Pardo, J. Á., Marcos, A., Arrazola, J., Reinoso, A. I., Montejo, P., Bajo, R., & Maestú, F. (2014). Alpha-Band Hypersynchronization in Progressive Mild Cognitive Impairment: A Magnetoencephalography Study. *The Journal of Neuroscience*, *34*(44), 14551–14559. https://doi.org/10.1523/JNEUROSCI.0964-14.2014

López-Sanz, D., Bruña, R., Garcés, P., Camara, C., Serrano, N., Rodríguez-Rojo, I. C., Delgado, M. L., Montenegro, M., López-Higes, R., Yus, M., & Maestú, F. (2016). Alpha band disruption in the AD-continuum starts in the Subjective Cognitive Decline stage: A MEG study. *Scientific Reports*, *6*(1), 37685. https://doi.org/10.1038/srep37685

López-Sanz, D., Bruña, R., Garcés, P., Martín-Buro, M. C., Walter, S., Delgado, M. L., Montenegro, M., López Higes, R., Marcos, A., & Maestú, F. (2017). Functional Connectivity Disruption in Subjective Cognitive Decline and Mild Cognitive Impairment: A Common Pattern of Alterations. *Frontiers in Aging Neuroscience*, *9*, 109. https://doi.org/10.3389/fnagi.2017.00109

Lorente De Nó, R., & Honrubia, V. (1966). Theory of the flow of action currents in isolated myelinated nerve fibers. X. *Proceedings of the National Academy of Sciences*, *55*(2), 321–328. https://doi.org/10.1073/pnas.55.2.321

Lurija, A. R. (1997). *The working brain: An introduction to neuropsychology* (Nachdr.). Basic Books.
Aus d. Russ. übers. - Literaturverz. S. 345 - 371.

Maestú, F., de Haan, W., Busche, M. A., & DeFelipe, J. (2021). Neuronal excitation/inhibition imbalance: Core element of a translational perspective on Alzheimer pathophysiology. *Ageing Research Reviews*, *69*, 101372. https://doi.org/10.1016/j.arr.2021.101372

Maestú, F., Peña, J.-M., Garcés, P., González, S., Bajo, R., Bagic, A., Cuesta, P., Funke, M., Mäkelä, J. P., Menasalvas, E., Nakamura, A., Parkkonen, L., López, M. E., Del Pozo, F., Sudre, G., Zamrini, E., Pekkonen, E., Henson, R. N., & Becker, J. T. (2015). A multicenter study of the early detection of synaptic dysfunction in Mild Cognitive Impairment using Magnetoencephalography-derived functional connectivity. *NeuroImage: Clinical*, *9*, 103–109. https://doi.org/10.1016/j.nicl.2015.07.011

Majeed, W., Magnuson, M., Hasenkamp, W., Schwarb, H., Schumacher, E. H., Barsalou, L., & Keilholz, S. D. (2011). Spatiotemporal dynamics of low frequency BOLD fluctuations in rats and humans. *NeuroImage*, *54*(2), 1140–1150. https://doi.org/10.1016/j.neuroimage.2010.08.030

Maltez, J., Hyllienmark, L., Nikulin, V. V., & Brismar, T. (2004). Time course and variability of power in different frequency bands of eeg during resting conditions. *Neurophysiologie Clinique/Clinical Neurophysiology*, *34*(5), 195–202.

Manto, M., & Habas, C. (2016). Cerebellar disorders. In *Handbook of Clinical Neurology* (pp. 479–491, Vol. 135). Elsevier. https://doi.org/10.1016/B978-0-444-53485-9.00023-4

Matsui, T., & Yamashita, K.-i. (2023). Static and Dynamic Functional Connectivity Alterations in Alzheimer's Disease and Neuropsychiatric Diseases. *Brain Connectivity*, *13*(5), 307–314. https://doi.org/10.1089/brain.2022.0044

Mattson, M. P. (2020). Involvement of GABAergic interneuron dysfunction and neuronal network hyperexcitability in Alzheimer's disease: Amelioration by metabolic switching. In *International Review of Neurobiology* (pp. 191–205, Vol. 154). Elsevier. https://doi.org/10.1016/bs.irn.2020.01.006

Mattsson, N., Palmqvist, S., Stomrud, E., Vogel, J., & Hansson, O. (2019). Staging β-Amyloid Pathology With Amyloid Positron Emission Tomography. *JAMA Neurology*, *76*(11), 1319. https://doi.org/10.1001/jamaneurol.2019.2214

Mazaheri, A., Slagter, H. A., Thut, G., & Foxe, J. J. (2018). Orchestration of brain oscillations: Principles and functions. *European Journal of Neuroscience*, *48*(7), 2385–2388. https://doi.org/10.1111/ejn.14189

McGrowder, D. A., Miller, F., Vaz, K., Nwokocha, C., Wilson-Clarke, C., Anderson-Cross, M., Brown, J., Anderson-Jackson, L., Williams, L., Latore, L., Thompson, R., & Alexander-Lindo, R. (2021). Cerebrospinal Fluid Biomarkers of Alzheimer's Disease: Current Evidence and Future Perspectives. *Brain Sciences*, *11*(2), 215. https://doi.org/10.3390/brainsci11020215

McKeon, S. D., Calabro, F., Thorpe, R. V., De La Fuente, A., Foran, W., Parr, A. C., Jones, S. R., & Luna, B. (2023). Age-related differences in transient gamma band activity during working memory maintenance through adolescence. *NeuroImage*, *274*, 120112. https://doi.org/10.1016/j.neuroimage.2023.120112

Mehrkanoon, S., Boonstra, T. W., Breakspear, M., Hinder, M., & Summers, J. J. (2016). Upregulation of cortico-cerebellar functional connectivity after motor learning. *NeuroImage*, *128*, 252–263. https://doi.org/10.1016/j.neuroimage.2015.12.052

Meindl, T., Teipel, S., Elmouden, R., Mueller, S., Koch, W., Dietrich, O., Coates, U., Reiser, M., & Glaser, C. (2010). Test–retest reproducibility of the default-mode network in healthy individuals. *Human Brain Mapping*, *31*(2), 237–246. https://doi.org/10.1002/hbm.20860

Meissner, W., & Ochsenfeld, R. (1933). Ein neuer Effekt bei Eintritt der Supraleitf higkeit. *Die Naturwissenschaften*, *21*(44), 787–788. https://doi.org/10.1007/BF01504252

Menon, V. (2011). Large-scale brain networks and psychopathology: A unifying triple network model. *Trends in Cognitive Sciences*, *15*(10), 483–506. https://doi.org/10.1016/j.tics.2011.08.003

Michel, C. M., & Koenig, T. (2018). EEG microstates as a tool for studying the temporal dynamics of whole-brain neuronal networks: A review. *NeuroImage*, *180*, 577–593. https://doi.org/10.1016/j.neuroimage.2017.11.062

Mitchell, A. J., Beaumont, H., Ferguson, D., Yadegarfar, M., & Stubbs, B. (2014). Risk of dementia and mild cognitive impairment in older people with subjective memory complaints: Meta-analysis. *Acta Psychiatrica Scandinavica*, *130*(6), 439–451. https://doi.org/10.1111/acps.12336

Mohammadi, B., Kollewe, K., Samii, A., Krampfl, K., Dengler, R., & Münte, T. F. (2009). Changes of resting state brain networks in amyotrophic lateral sclerosis. *Experimental Neurology*, *217*(1), 147–153. https://doi.org/10.1016/j.expneurol.2009.01.025

Montez, T., Poil, S.-S., Jones, B. F., Manshanden, I., Verbunt, J. P. A., Van Dijk, B. W., Brussaard, A. B., Van Ooyen, A., Stam, C. J., Scheltens, P., & Linkenkaer-Hansen, K. (2009). Altered temporal correlations in parietal alpha and prefrontal theta oscillations in early-stage Alzheimer disease. *Proceedings of the National Academy of Sciences*, *106*(5), 1614–1619. https://doi.org/10.1073/pnas.0811699106

Mormann, F., Lehnertz, K., David, P., & E. Elger, C. (2000). Mean phase coherence as a measure for phase synchronization and its application to the EEG of epilepsy patients. *Physica D: Nonlinear Phenomena*, *144*(3-4), 358–369. https://doi.org/10.1016/S0167-2789(00)00087-7

Murakami, S., & Okada, Y. (2006). Contributions of principal neocortical neurons to magnetoencephalography and electroencephalography signals. *The Journal of Physiology*, *575*(3), 925–936. https://doi.org/10.1113/jphysiol.2006.105379

Nakamura, A., Cuesta, P., Fernández, A., Arahata, Y., Iwata, K., Kuratsubo, I., Bundo, M., Hattori, H., Sakurai, T., Fukuda, K., Washimi, Y., Endo, H., Takeda, A., Diers, K., Bajo, R., Maestú, F., Ito, K., & Kato, T. (2018). Electromagnetic signatures of the preclinical and prodromal stages of Alzheimer's disease. *Brain*, *141*(5), 1470–1485. https://doi.org/10.1093/brain/awy044

Nakamura, A., Cuesta, P., Kato, T., Arahata, Y., Iwata, K., Yamagishi, M., Kuratsubo, I., Kato, K., Bundo, M., Diers, K., Fernández, A., Maestú, F., & Ito, K. (2017). Early functional network alterations in asymptomatic elders at risk for Alzheimer's disease. *Scientific Reports*, *7*(1), 6517. https://doi.org/10.1038/s41598-017-06876-8

Nallasamy, N., & Tsao, D. Y. (2011). Functional Connectivity in the Brain: Effects of Anesthesia. *The Neuroscientist*, *17*(1), 94–106. https://doi.org/10.1177/1073858410374126

Nelson, P. T., Alafuzoff, I., Bigio, E. H., Bouras, C., Braak, H., Cairns, N. J., Castellani, R. J., Crain, B. J., Davies, P., Tredici, K. D., Duyckaerts, C., Frosch, M. P., Haroutunian, V., Hof, P. R., Hulette, C. M., Hyman, B. T., Iwatsubo, T., Jellinger, K. A., Jicha, G. A., … Beach, T. G. (2012). Correlation of Alzheimer Disease Neuropathologic Changes With Cognitive Status: A Review of the Literature. *Journal of Neuropathology & Experimental Neurology*, *71*(5), 362–381. https://doi.org/10.1097/NEN.0b013e31825018f7

Niso, G., Bruña, R., Pereda, E., Gutiérrez, R., Bajo, R., Maestú, F., & del-Pozo, F. (2013). HERMES: Towards an Integrated Toolbox to Characterize Functional and Effective Brain Connectivity. *Neuroinformatics*, *11*(4), 405–434. https://doi.org/10.1007/s12021-013-9186-1

Nissim, N., Pham, D. V., Poddar, T., Blutt, E., & Hamilton, R. (2023). The impact of gamma transcranial alternating current stimulation (tACS) on cognitive and memory processes

in patients with mild cognitive impairment or Alzheimer's disease: A literature review. *Brain Stimulation*, *16*(3), 748–755. https://doi.org/10.1016/j.brs.2023.04.001

Nolte, G. (2003). The magnetic lead field theorem in the quasi-static approximation and its use for magnetoencephalography forward calculation in realistic volume conductors. *Physics in Medicine and Biology*, *48*(22), 3637–3652. https://doi.org/10.1088/0031-9155/48/22/002

Núñez, P., Poza, J., Gómez, C., Rodríguez-González, V., Hillebrand, A., Tewarie, P., Tola-Arribas, M. Á., Cano, M., & Hornero, R. (2021). Abnormal meta-state activation of dynamic brain networks across the Alzheimer spectrum. *NeuroImage*, *232*, 117898. https://doi.org/10.1016/j.neuroimage.2021.117898

Núñez, P., Poza, J., Gómez, C., Rodríguez-González, V., Hillebrand, A., Tola-Arribas, M. A., Cano, M., & Hornero, R. (2019). Characterizing the fluctuations of dynamic resting-state electrophysiological functional connectivity: Reduced neuronal coupling variability in mild cognitive impairment and dementia due to Alzheimer's disease. *Journal of Neural Engineering*, *16*(5), 056030. https://doi.org/10.1088/1741-2552/ab234b

Nussbaumer, H. J., & Nussbaumer, H. J. (1982). *The fast fourier transform*. Springer.

Okamura, N., Harada, R., Ishiki, A., Kikuchi, A., Nakamura, T., & Kudo, Y. (2018). The development and validation of tau PET tracers: Current status and future directions. *Clinical and Translational Imaging*, *6*(4), 305–316. https://doi.org/10.1007/s40336-018-0290-y

Oliveira, J. M., Henriques, A. G., Martins, F., Rebelo, S., & Da Cruz E Silva, O. A. (2015). Amyloid-β Modulates Both AβPP and Tau Phosphorylation. *Journal of Alzheimer's Disease*, *45*(2), 495–507. https://doi.org/10.3233/JAD-142664

O'Neill, G. C., Tewarie, P. K., Colclough, G. L., Gascoyne, L. E., Hunt, B. A., Morris, P. G., Woolrich, M. W., & Brookes, M. J. (2017). Measurement of dynamic task related functional networks using MEG. *NeuroImage*, *146*, 667–678. https://doi.org/10.1016/j.neuroimage.2016.08.061

Onyango, I. G., Jauregui, G. V., Čarná, M., Bennett, J. P., & Stokin, G. B. (2021). Neuroinflammation in Alzheimer's Disease. *Biomedicines*, *9*(5), 524. https://doi.org/10.3390/biomedicines9050524

Oostenveld, R., Fries, P., Maris, E., & Schoffelen, J.-M. (2011). FieldTrip: Open Source Software for Advanced Analysis of MEG, EEG, and Invasive Electrophysiological Data. *Computational Intelligence and Neuroscience*, *2011*, 1–9. https://doi.org/10.1155/2011/156869

Orban, C., Kong, R., Li, J., Chee, M. W. L., & Yeo, B. T. T. (2020). Time of day is associated with paradoxical reductions in global signal fluctuation and functional connectivity (B. Seymour, Ed.). *PLOS Biology*, *18*(2), e3000602. https://doi.org/10.1371/journal.pbio.3000602

Ou, J., Xie, L., Jin, C., Li, X., Zhu, D., Jiang, R., Chen, Y., Zhang, J., Li, L., & Liu, T. (2015). Characterizing and Differentiating Brain State Dynamics via Hidden Markov Models. *Brain Topography*, *28*(5), 666–679. https://doi.org/10.1007/s10548-014-0406-2

Palop, J. J., & Mucke, L. (2010). Amyloid-β–induced neuronal dysfunction in Alzheimer's disease: From synapses toward neural networks. *Nature Neuroscience*, *13*(7), 812–818. https://doi.org/10.1038/nn.2583

Palva, J. M., & Palva, S. (2018). Functional integration across oscillation frequencies by cross-frequency phase synchronization. *European Journal of Neuroscience*, *48*(7), 2399–2406. https://doi.org/10.1111/ejn.13767

Palva, S., & Palva, J. M. (2007). New vistas for α-frequency band oscillations. *Trends in Neurosciences*, *30*(4), 150–158. https://doi.org/10.1016/j.tins.2007.02.001

Pang, X., Liang, X., Zhao, J., Wu, P., Li, X., Wei, W., Nie, L., Chang, W., Lv, Z., & Zheng, J. (2022). Abnormal Static and Dynamic Functional Connectivity in Left and Right Temporal Lobe Epilepsy. *Frontiers in Neuroscience*, *15*, 820641. https://doi.org/10.3389/fnins.2021.820641

Park, K. I. (2018). *Fundamentals of Probability and Stochastic Processes with Applications to Communications*. Springer International Publishing. https://doi.org/10.1007/978-3-319-68075-0

Pedroni, A., Gianotti, L. R. R., Koenig, T., Lehmann, D., Faber, P., & Knoch, D. (2017). Temporal Characteristics of EEG Microstates Mediate Trial-by-Trial Risk Taking. *Brain Topography*, *30*(1), 149–159. https://doi.org/10.1007/s10548-016-0539-6

Preti, M. G., Bolton, T. A., & Van De Ville, D. (2017). The dynamic functional connectome: State-of-the-art and perspectives. *NeuroImage*, *160*, 41–54. https://doi.org/10.1016/j.neuroimage.2016.12.061

Pusil, S., Dimitriadis, S. I., López, M. E., Pereda, E., & Maestú, F. (2019). Aberrant MEG multi-frequency phase temporal synchronization predicts conversion from mild cognitive impairment-to-Alzheimer's disease. *NeuroImage: Clinical*, *24*, 101972. https://doi.org/10.1016/j.nicl.2019.101972

Pusil, S., López, M. E., Cuesta, P., Bruña, R., Pereda, E., & Maestú, F. (2019). Hypersynchronization in mild cognitive impairment: The 'X' model. *Brain*, *142*(12), 3936–3950. https://doi.org/10.1093/brain/awz320

Puttaert, D., Coquelet, N., Wens, V., Peigneux, P., Fery, P., Rovai, A., Trotta, N., Sadeghi, N., Coolen, T., Bier, J.-C., Goldman, S., & De Tiège, X. (2020). Alterations in resting-state network dynamics along the Alzheimer's disease continuum. *Scientific Reports*, *10*(1), 21990. https://doi.org/10.1038/s41598-020-76201-3

Qin, J., Chen, S.-G., Hu, D., Zeng, L.-L., Fan, Y.-M., Chen, X.-P., & Shen, H. (2015). Predicting individual brain maturity using dynamic functional connectivity. *Frontiers in Human Neuroscience*, *9*. https://doi.org/10.3389/fnhum.2015.00418

Quinn, A. J., Van Ede, F., Brookes, M. J., Heideman, S. G., Nowak, M., Seedat, Z. A., Vidaurre, D., Zich, C., Nobre, A. C., & Woolrich, M. W. (2019). Unpacking Transient Event Dynamics in Electrophysiological Power Spectra. *Brain Topography*, *32*(6), 1020–1034. https://doi.org/10.1007/s10548-019-00745-5

Rabinovich, M. I., Friston, K. J., & Varona, P. (Eds.). (2012, July). *Principles of Brain Dynamics: Global State Interactions*. The MIT Press. https://doi.org/10.7551/mitpress/9108.001.0001

Rack-Gomer, A. L., & Liu, T. T. (2012). Caffeine increases the temporal variability of resting-state BOLD connectivity in the motor cortex. *NeuroImage*, *59*(3), 2994–3002. https://doi.org/10.1016/j.neuroimage.2011.10.001

Ramírez-Toraño, F., Bruña, R., De Frutos-Lucas, J., Rodríguez-Rojo, I. C., Marcos De Pedro, S., Delgado-Losada, M. L., Gómez-Ruiz, N., Barabash, A., Marcos, A., López Higes, R., & Maestú, F. (2021). Functional Connectivity Hypersynchronization in Relatives of

Alzheimer's Disease Patients: An Early E/I Balance Dysfunction? *Cerebral Cortex*, *31*(2), 1201–1210. https://doi.org/10.1093/cercor/bhaa286

Ramón Y Cajal, S. (1909). *Histologie du système nerveux de l'homme & des vertébrés*. Maloine. https://doi.org/10.5962/bhl.title.48637

Rinck, P. A., & European Magnetic Resonance Forum (Eds.). (2019). *Magnetic resonance in medicine: A critical introduction: The basic text book of the European Magnetic Resonance Forum* (12th completely revised edition). Books on Demand.

Rosenblum, M. G., Pikovsky, A. S., & Kurths, J. (1996). Phase Synchronization of Chaotic Oscillators. *Physical Review Letters*, *76*(11), 1804–1807. https://doi.org/10.1103/PhysRevLett.76.1804

Sakoğlu, Ü., Pearlson, G. D., Kiehl, K. A., Wang, Y. M., Michael, A. M., & Calhoun, V. D. (2010). A method for evaluating dynamic functional network connectivity and task-modulation: Application to schizophrenia. *Magnetic Resonance Materials in Physics, Biology and Medicine*, *23*(5-6), 351–366. https://doi.org/10.1007/s10334-010-0197-8

Sala-Llonch, R., Bartrés-Faz, D., & Junqué, C. (2015). Reorganization of brain networks in aging: A review of functional connectivity studies. *Frontiers in psychology*, *6*, 663.

Sanfratello, L., Houck, J., & Calhoun, V. (2019). Relationship between MEG global dynamic functional network connectivity measures and symptoms in schizophrenia. *Schizophrenia Research*, *209*, 129–134. https://doi.org/10.1016/j.schres.2019.05.007

Scheeringa, R., Petersson, K. M., Oostenveld, R., Norris, D. G., Hagoort, P., & Bastiaansen, M. C. (2009). Trial-by-trial coupling between eeg and bold identifies networks related to alpha and theta eeg power increases during working memory maintenance. *Neuroimage*, *44*(3), 1224–1238.

Scheltens, P., De Strooper, B., Kivipelto, M., Holstege, H., Chételat, G., Teunissen, C. E., Cummings, J., & Van Der Flier, W. M. (2021). Alzheimer's disease. *The Lancet*, *397*(10284), 1577–1590. https://doi.org/10.1016/S0140-6736(20)32205-4

Schmidt, R., Herrojo Ruiz, M., Kilavik, B. E., Lundqvist, M., Starr, P. A., & Aron, A. R. (2019). Beta Oscillations in Working Memory, Executive Control of Movement and Thought, and Sensorimotor Function. *The Journal of Neuroscience*, *39*(42), 8231–8238. https://doi.org/10.1523/JNEUROSCI.1163-19.2019

Schöpf, V., Kasess, C., Lanzenberger, R., Fischmeister, F., Windischberger, C., & Moser, E. (2010). Fully exploratory network ICA (FENICA) on resting-state fMRI data. *Journal of Neuroscience Methods*, *192*(2), 207–213. https://doi.org/10.1016/j.jneumeth.2010.07.028

Schumacher, J., Peraza, L. R., Firbank, M., Thomas, A. J., Kaiser, M., Gallagher, P., O'Brien, J. T., Blamire, A. M., & Taylor, J.-P. (2019). Dynamic functional connectivity changes in dementia with Lewy bodies and Alzheimer's disease. *NeuroImage: Clinical*, *22*, 101812. https://doi.org/10.1016/j.nicl.2019.101812

Schwab, B. C., Misselhorn, J., & Engel, A. K. (2019). Modulation of large-scale cortical coupling by transcranial alternating current stimulation. *Brain Stimulation*, *12*(5), 1187–1196. https://doi.org/10.1016/j.brs.2019.04.013

Seedat, Z. A., Quinn, A. J., Vidaurre, D., Liuzzi, L., Gascoyne, L. E., Hunt, B. A., O'Neill, G. C., Pakenham, D. O., Mullinger, K. J., Morris, P. G., Woolrich, M. W., & Brookes, M. J. (2020). The role of transient spectral 'bursts' in functional connectivity: A

magnetoencephalography study. *NeuroImage*, *209*, 116537. https://doi.org/10.1016/j.neuroimage.2020.116537

Sendi, M. S., Zendehrouh, E., Ellis, C. A., Fu, Z., Chen, J., Miller, R. L., Mormino, E. C., Salat, D. H., & Calhoun, V. D. (2023). The link between static and dynamic brain functional network connectivity and genetic risk of Alzheimer's disease. *NeuroImage: Clinical*, *37*, 103363. https://doi.org/10.1016/j.nicl.2023.103363

Shakil, S., Lee, C.-H., & Keilholz, S. D. (2016). Evaluation of sliding window correlation performance for characterizing dynamic functional connectivity and brain states. *NeuroImage*, *133*, 111–128. https://doi.org/10.1016/j.neuroimage.2016.02.074

Shannon, C. E. (1948). A Mathematical Theory of Communication. *Bell System Technical Journal*, *27*(3), 379–423. https://doi.org/10.1002/j.1538-7305.1948.tb01338.x

Sherrington, R., Rogaev, E. I., Liang, Y., Rogaeva, E. A., Levesque, G., Ikeda, M., Chi, H., Lin, C., Li, G., Holman, K., Tsuda, T., Mar, L., Foncin, J.-F., Bruni, A. C., Montesi, M. P., Sorbi, S., Rainero, I., Pinessi, L., Nee, L., … St George-Hyslop, P. H. (1995). Cloning of a gene bearing missense mutations in early-onset familial Alzheimer's disease. *Nature*, *375*(6534), 754–760. https://doi.org/10.1038/375754a0

Shin, H., Law, R., Tsutsui, S., Moore, C. I., & Jones, S. R. (2017). The rate of transient beta frequency events predicts behavior across tasks and species. *eLife*, *6*, e29086. https://doi.org/10.7554/eLife.29086

Simony, E., Honey, C. J., Chen, J., Lositsky, O., Yeshurun, Y., Wiesel, A., & Hasson, U. (2016). Dynamic reconfiguration of the default mode network during narrative comprehension. *Nature Communications*, *7*(1), 12141. https://doi.org/10.1038/ncomms12141

Smailovic, U., Koenig, T., Kåreholt, I., Andersson, T., Kramberger, M. G., Winblad, B., & Jelic, V. (2018). Quantitative EEG power and synchronization correlate with Alzheimer's disease CSF biomarkers. *Neurobiology of Aging*, *63*, 88–95. https://doi.org/10.1016/j.neurobiolaging.2017.11.005

Snell, R. S. (2010). *Clinical neuroanatomy*. Lippincott Williams & Wilkins.

Spronk, M., Keane, B. P., Ito, T., Kulkarni, K., Ji, J. L., Anticevic, A., & Cole, M. W. (2021). A Whole-Brain and Cross-Diagnostic Perspective on Functional Brain Network Dysfunction. *Cerebral Cortex*, *31*(1), 547–561. https://doi.org/10.1093/cercor/bhaa242

Spruston, N. (2008). Pyramidal neurons: Dendritic structure and synaptic integration. *Nature Reviews Neuroscience*, *9*(3), 206–221. https://doi.org/10.1038/nrn2286

Statistical Parametric Mapping. (2007). Elsevier. https://doi.org/10.1016/B978-0-12-372560-8.X5000-1

Stevens, M. C. (2016). The contributions of resting state and task-based functional connectivity studies to our understanding of adolescent brain network maturation. *Neuroscience & Biobehavioral Reviews*, *70*, 13–32.

Stott, R. T., Kritsky, O., & Tsai, L.-H. (2021). Profiling DNA break sites and transcriptional changes in response to contextual fear learning (B. Yao, Ed.). *PLOS ONE*, *16*(7), e0249691. https://doi.org/10.1371/journal.pone.0249691

Suárez Méndez, I. (2024). *Caracterización de condiciones prevalentes en el envejecimiento mediante magnetoencefalografía* [doctoral thesis]. Universidad Complutense de Madrid [Publication Title: Characterization of prevalent conditions in aging using magnetoencephalography].

Südhof, T. C. (2021). The cell biology of synapse formation. *The Journal of cell biology*, *220*(7).

Sun, J., Wang, B., Niu, Y., Tan, Y., Fan, C., Zhang, N., Xue, J., Wei, J., & Xiang, J. (2020). Complexity Analysis of EEG, MEG, and fMRI in Mild Cognitive Impairment and Alzheimer's Disease: A Review. *Entropy*, *22*(2), 239. https://doi.org/10.3390/e22020239

Sun, S., Yan, C., Qu, S., Luo, G., Liu, X., Tian, F., Dong, Q., Li, X., & Hu, B. (2024). Resting-state dynamic functional connectivity in major depressive disorder: A systematic review. *Progress in Neuro-Psychopharmacology and Biological Psychiatry*, *135*, 111076. https://doi.org/10.1016/j.pnpbp.2024.111076

Supek, S., & Aine, C. J. (Eds.). (2014). *Magnetoencephalography: From Signals to Dynamic Cortical Networks*. Springer Berlin Heidelberg. https://doi.org/10.1007/978-3-642-33045-2

Tagliazucchi, E., Balenzuela, P., Fraiman, D., Montoya, P., & Chialvo, D. R. (2011). Spontaneous BOLD event triggered averages for estimating functional connectivity at resting state. *Neuroscience Letters*, *488*(2), 158–163. https://doi.org/10.1016/j.neulet.2010.11.020

Tagliazucchi, E., Siniatchkin, M., Laufs, H., & Chialvo, D. R. (2016). The Voxel-Wise Functional Connectome Can Be Efficiently Derived from Co-activations in a Sparse Spatio-Temporal Point-Process. *Frontiers in Neuroscience*, *10*. https://doi.org/10.3389/fnins.2016.00381

Tagliazucchi, E., Von Wegner, F., Morzelewski, A., Borisov, S., Jahnke, K., & Laufs, H. (2012). Automatic sleep staging using fMRI functional connectivity data. *NeuroImage*, *63*(1), 63–72. https://doi.org/10.1016/j.neuroimage.2012.06.036

Tagliazucchi, E., Von Wegner, F., Morzelewski, A., Brodbeck, V., & Laufs, H. (2012). Dynamic BOLD functional connectivity in humans and its electrophysiological correlates. *Frontiers in Human Neuroscience*, *6*. https://doi.org/10.3389/fnhum.2012.00339

Tait, L., Tamagnini, F., Stothart, G., Barvas, E., Monaldini, C., Frusciante, R., Volpini, M., Guttmann, S., Coulthard, E., Brown, J. T., Kazanina, N., & Goodfellow, M. (2020). EEG microstate complexity for aiding early diagnosis of Alzheimer's disease. *Scientific Reports*, *10*(1), 17627. https://doi.org/10.1038/s41598-020-74790-7

Tait, L., & Zhang, J. (2022). MEG cortical microstates: Spatiotemporal characteristics, dynamic functional connectivity and stimulus-evoked responses. *NeuroImage*, *251*, 119006. https://doi.org/10.1016/j.neuroimage.2022.119006

Tang, Y., Nyengaard, J. R., De Groot, D. M., & Gundersen, H. J. G. (2001). Total regional and global number of synapses in the human brain neocortex. *Synapse*, *41*(3), 258–273. https://doi.org/10.1002/syn.1083

Taulu, S., & Simola, J. (2006). Spatiotemporal signal space separation method for rejecting nearby interference in MEG measurements. *Physics in Medicine and Biology*, *51*(7), 1759–1768. https://doi.org/10.1088/0031-9155/51/7/008

Taulu, S., & Hari, R. (2009). Removal of magnetoencephalographic artifacts with temporal signal-space separation: Demonstration with single-trial auditory-evoked responses. *Human Brain Mapping*, *30*(5), 1524–1534. https://doi.org/10.1002/hbm.20627

Taulu, S., Kajola, M., & Simola, J. (2003). Suppression of Interference and Artifacts by the Signal Space Separation Method. *Brain Topography*, *16*(4), 269–275. https://doi.org/10.1023/B:BRAT.0000032864.93890.f9

Tewarie, P., Liuzzi, L., O'Neill, G. C., Quinn, A. J., Griffa, A., Woolrich, M. W., Stam, C. J., Hillebrand, A., & Brookes, M. J. (2019). Tracking dynamic brain networks using high temporal resolution MEG measures of functional connectivity. *NeuroImage*, *200*, 38–50. https://doi.org/10.1016/j.neuroimage.2019.06.006

Thompson, P. M., Jahanshad, N., Ching, C. R. K., Salminen, L. E., Thomopoulos, S. I., Bright, J., Baune, B. T., Bertolín, S., Bralten, J., Bruin, W. B., Bülow, R., Chen, J., Chye, Y., Dannlowski, U., De Kovel, C. G. F., Donohoe, G., Eyler, L. T., Faraone, S. V., Favre, P., ... for the ENIGMA Consortium. (2020). ENIGMA and global neuroscience: A decade of large-scale studies of the brain in health and disease across more than 40 countries. *Translational Psychiatry*, *10*(1), 100. https://doi.org/10.1038/s41398-020-0705-1

Thompson, T. B., Chaggar, P., Kuhl, E., Goriely, A., & for the Alzheimer's Disease Neuroimaging Initiative. (2020). Protein-protein interactions in neurodegenerative diseases: A conspiracy theory (A. Csikász-Nagy, Ed.). *PLOS Computational Biology*, *16*(10), e1008267. https://doi.org/10.1371/journal.pcbi.1008267

Tissot, C., Therriault, J., Kunach, P., L Benedet, A., Pascoal, T. A., Ashton, N. J., Karikari, T. K., Servaes, S., Lussier, F. Z., Chamoun, M., Tudorascu, D. L., Stevenson, J., Rahmouni, N., Poltronetti, N. M., Pallen, V., Bezgin, G., Kang, M. S., Mathotaarachchi, S. S., Wang, Y.-T., ... Rosa-Neto, P. (2022). Comparing tau status determined via plasma pTau181, pTau231 and [18F]MK6240 tau-PET. *eBioMedicine*, *76*, 103837. https://doi.org/10.1016/j.ebiom.2022.103837

Torrence, C., & Compo, G. P. (1998). A Practical Guide to Wavelet Analysis. *Bulletin of the American Meteorological Society*, *79*(1), 61–78. https://doi.org/10.1175/1520-0477(1998)079<0061:APGTWA>2.0.CO;2

Tzourio-Mazoyer, N., Landeau, B., Papathanassiou, D., Crivello, F., Etard, O., Delcroix, N., Mazoyer, B., & Joliot, M. (2002). Automated Anatomical Labeling of Activations in SPM Using a Macroscopic Anatomical Parcellation of the MNI MRI Single-Subject Brain. *NeuroImage*, *15*(1), 273–289. https://doi.org/10.1006/nimg.2001.0978

Vaidya, A. R., Pujara, M. S., Petrides, M., Murray, E. A., & Fellows, L. K. (2019). Lesion studies in contemporary neuroscience. *Trends in cognitive sciences*, *23*(8), 653–671.

Van Diessen, E., Numan, T., Van Dellen, E., Van Der Kooi, A., Boersma, M., Hofman, D., Van Lutterveld, R., Van Dijk, B., Van Straaten, E., Hillebrand, A., & Stam, C. (2015). Opportunities and methodological challenges in EEG and MEG resting state functional brain network research. *Clinical Neurophysiology*, *126*(8), 1468–1481. https://doi.org/10.1016/j.clinph.2014.11.018

Van Ede, F., Niklaus, M., & Nobre, A. C. (2017). Temporal Expectations Guide Dynamic Prioritization in Visual Working Memory through Attenuated α Oscillations. *The Journal of Neuroscience*, *37*(2), 437–445. https://doi.org/10.1523/JNEUROSCI.2272-16.2016

Van Straaten, E. C., De Haan, W., De Waal, H., Scheltens, P., Van Der Flier, W. M., Barkhof, F., Koene, T., & Stam, C. J. (2012). Disturbed oscillatory brain dynamics in subcortical ischemic vascular dementia. *BMC Neuroscience*, *13*(1), 85. https://doi.org/10.1186/1471-2202-13-85

Van Veen, B., & Buckley, K. (1988). Beamforming: A versatile approach to spatial filtering. *IEEE ASSP Magazine*, *5*(2), 4–24. https://doi.org/10.1109/53.665

Verfaillie, S. C., Pichet Binette, A., Vachon-Presseau, E., Tabrizi, S., Savard, M., Bellec, P., Ossenkoppele, R., Scheltens, P., Van Der Flier, W. M., Breitner, J. C., Villeneuve, S., Aisen, P., Anthal, E., Appleby, M., Ayranci, G., Barkun, A., Beaudry, T., Bellec, P., Benbouhoud, F., ... Yu, E. (2018). Subjective Cognitive Decline Is Associated With Altered Default Mode Network Connectivity in Individuals With a Family History of Alzheimer's Disease. *Biological Psychiatry: Cognitive Neuroscience and Neuroimaging*, *3*(5), 463–472. https://doi.org/10.1016/j.bpsc.2017.11.012

Vidaurre, D., Smith, S. M., & Woolrich, M. W. (2017). Brain network dynamics are hierarchically organized in time. *Proceedings of the National Academy of Sciences*, *114*(48), 12827–12832. https://doi.org/10.1073/pnas.1705120114

Vogel, J. W., Iturria-Medina, Y., Strandberg, O. T., Smith, R., Levitis, E., Evans, A. C., Hansson, O., Alzheimer's Disease Neuroimaging Initiative, Weiner, M., Aisen, P., Petersen, R., Jack, C. R., Jagust, W., Trojanowki, J. Q., Toga, A. W., Beckett, L., Green, R. C., Saykin, A. J., Morris, J., ... Wollmer, P. (2020). Spread of pathological tau proteins through communicating neurons in human Alzheimer's disease. *Nature Communications*, *11*(1), 2612. https://doi.org/10.1038/s41467-020-15701-2

Vossel, K. A., Tartaglia, M. C., Nygaard, H. B., Zeman, A. Z., & Miller, B. L. (2017). Epileptic activity in Alzheimer's disease: Causes and clinical relevance. *The Lancet Neurology*, *16*(4), 311–322. https://doi.org/10.1016/S1474-4422(17)30044-3

Wang, Y. T., & Edison, P. (2019). Tau Imaging in Neurodegenerative Diseases Using Positron Emission Tomography. *Current Neurology and Neuroscience Reports*, *19*(7), 45. https://doi.org/10.1007/s11910-019-0962-7

Wens, V., Bourguignon, M., Vander Ghinst, M., Mary, A., Marty, B., Coquelet, N., Naeije, G., Peigneux, P., Goldman, S., & De Tiège, X. (2019). Synchrony, metastability, dynamic integration, and competition in the spontaneous functional connectivity of the human brain. *NeuroImage*, *199*, 313–324. https://doi.org/10.1016/j.neuroimage.2019.05.081

Wernicke, C. (1874). *Der aphasische symptomencomplex: Eine psychologische studie auf anatomischer basis*. Cohn & Weigert.

Wróbel, A. (2000). Beta activity: A carrier for visual attention. *Acta Neurobiologiae Experimentalis*, *60*(2), 247–260. https://doi.org/10.55782/ane-2000-1344

Xu, J., Pan, Y., Zhou, S., Zou, G., Liu, J., Su, Z., Zou, Q., & Gao, J.-H. (2020). EEG microstates are correlated with brain functional networks during slow-wave sleep. *NeuroImage*, *215*, 116786. https://doi.org/10.1016/j.neuroimage.2020.116786

Xu, Y., Zhao, M., Han, Y., & Zhang, H. (2020). Gabaergic inhibitory interneuron deficits in alzheimer's disease: Implications for treatment. *Frontiers in neuroscience*, *14*, 660.

Yaesoubi, M., Miller, R. L., & Calhoun, V. D. (2015). Mutually temporally independent connectivity patterns: A new framework to study the dynamics of brain connectivity at rest with application to explain group difference based on gender. *NeuroImage*, *107*, 85–94. https://doi.org/10.1016/j.neuroimage.2014.11.054

Yamazaki, Y., Zhao, N., Caulfield, T. R., Liu, C.-C., & Bu, G. (2019). Apolipoprotein E and Alzheimer disease: Pathobiology and targeting strategies. *Nature Reviews Neurology*, *15*(9), 501–518. https://doi.org/10.1038/s41582-019-0228-7

Yang, Z., Craddock, R. C., Margulies, D. S., Yan, C.-G., & Milham, M. P. (2014). Common intrinsic connectivity states among posteromedial cortex subdivisions: Insights from

analysis of temporal dynamics. *NeuroImage*, *93*, 124–137. https://doi.org/10.1016/j.neuroimage.2014.02.014

Yi, G.-S., Wang, J., Li, H.-Y., Wei, X.-L., & Deng, B. (2016). Metabolic Energy of Action Potentials Modulated by Spike Frequency Adaptation. *Frontiers in Neuroscience*, *10*, 534. https://doi.org/10.3389/fnins.2016.00534

Yi, G., Wang, L., Chu, C., Liu, C., Zhu, X., Shen, X., Li, Z., Wang, F., Yang, M., & Wang, J. (2022). Analysis of complexity and dynamic functional connectivity based on resting-state EEG in early Parkinson's disease patients with mild cognitive impairment. *Cognitive Neurodynamics*, *16*(2), 309–323. https://doi.org/10.1007/s11571-021-09722-w

York, G. K., & Steinberg, D. A. (2006). An introduction to the life and work of john hughlings jackson with a catalogue raisonnØ of his writings. *Medical History, Supplement*, *26*.

Yu, Q., Erhardt, E. B., Sui, J., Du, Y., He, H., Hjelm, D., Cetin, M. S., Rachakonda, S., Miller, R. L., Pearlson, G., & Calhoun, V. D. (2015). Assessing dynamic brain graphs of time-varying connectivity in fMRI data: Application to healthy controls and patients with schizophrenia. *NeuroImage*, *107*, 345–355. https://doi.org/10.1016/j.neuroimage.2014.12.020

Yuan, H., Zotev, V., Phillips, R., Drevets, W. C., & Bodurka, J. (2012). Spatiotemporal dynamics of the brain at rest — Exploring EEG microstates as electrophysiological signatures of BOLD resting state networks. *NeuroImage*, *60*(4), 2062–2072. https://doi.org/10.1016/j.neuroimage.2012.02.031

Zalesky, A., & Breakspear, M. (2015). Towards a statistical test for functional connectivity dynamics. *NeuroImage*, *114*, 466–470. https://doi.org/10.1016/j.neuroimage.2015.03.047

Zappasodi, F., Perrucci, M. G., Saggino, A., Croce, P., Mercuri, P., Romanelli, R., Colom, R., & Ebisch, S. J. (2019). EEG microstates distinguish between cognitive components of fluid reasoning. *NeuroImage*, *189*, 560–573. https://doi.org/10.1016/j.neuroimage.2019.01.067

Zeng, H. (2022). What is a cell type and how to define it? *Cell*, *185*(15), 2739–2755. https://doi.org/10.1016/j.cell.2022.06.031

Zhang, J., Kucyi, A., Raya, J., Nielsen, A. N., Nomi, J. S., Damoiseaux, J. S., Greene, D. J., Horovitz, S. G., Uddin, L. Q., & Whitfield-Gabrieli, S. (2021). What have we really learned from functional connectivity in clinical populations? *NeuroImage*, *242*, 118466. https://doi.org/10.1016/j.neuroimage.2021.118466

Zhao, C., Huang, W.-J., Feng, F., Zhou, B., Yao, H.-X., Guo, Y.-E., Wang, P., Wang, L.-N., Shu, N., & Zhang, X. (2022). Abnormal characterization of dynamic functional connectivity in Alzheimer's disease. *Neural Regeneration Research*, *17*(9), 2014. https://doi.org/10.4103/1673-5374.332161

Zhou, Y., Liang, M., Tian, L., Wang, K., Hao, Y., Liu, H., Liu, Z., & Jiang, T. (2007). Functional disintegration in paranoid schizophrenia using resting-state fMRI. *Schizophrenia Research*, *97*(1-3), 194–205. https://doi.org/10.1016/j.schres.2007.05.029

Zott, B., Simon, M. M., Hong, W., Unger, F., Chen-Engerer, H.-J., Frosch, M. P., Sakmann, B., Walsh, D. M., & Konnerth, A. (2019). A vicious cycle of β amyloid–dependent neuronal hyperactivation. *Science*, *365*(6453), 559–565. https://doi.org/10.1126/science.aay0198

Zuo, X.-N., Di Martino, A., Kelly, C., Shehzad, Z. E., Gee, D. G., Klein, D. F., Castellanos, F. X., Biswal, B. B., & Milham, M. P. (2010). The oscillating brain: Complex and reliable. *NeuroImage*, *49*(2), 1432–1445. https://doi.org/10.1016/j.neuroimage.2009.09.037

Chapter 2

Dynamics of Brain Connectivity across the Alzheimer's Disease Spectrum

2.1 Objectives and hypotheses

O.2.1 To determine the progression of dFC across the initial stages of the AD continuum.

Hypotheses: Progression across the AD continuum will be associated to decreased dFC. Also, that MEG and the correlation of FC matrices over time are techniques sensitive enough to capture such alterations.

O.2.2 To determine the brain regions where dFC alterations are more prominent.

Hypotheses: Changes in dFC will be more prominent in frontal and temporal regions of the brain, as well as in the DMN.

O.2.3 To explore the relationship between dFC and other metrics that monitor the progression of AD, including cognitive scores, brain volumetrics, and white matter integrity.

Hypotheses: dFC will be associated with a decline in cognitive performance, brain volumetrics and white matter integrity, especially in the MCI group.

This chapter is based on the publication:

Carrasco-Gómez, M., García-Colomo, A., Cabrera-Álvarez, J., Bruña, R., Santos, A., & Maestú, F. (2024). Dynamics of Brain Connectivity across the Alzheimer's Disease Spectrum: a magnetoencephalography study. bioRxiv, 2024-03. (Under review in *Human Brain Mapping*) doi: https://doi.org/10.1101/2024.03.14.584574

2.2 Introduction

Alzheimer's disease (AD) is the most common form of dementia ("2024 Alzheimer's disease facts and figures", 2024), affecting an estimated of 32 million people worldwide. In AD, functional networks supporting cognition become altered, including activation and deactivation deficits, abnormal oscillatory activity, and synaptic failure, and leading to impaired memory, behavioral disorders, and emotional changes (Maestú et al., 2021).

One way to evaluate the integrity of neural communication in the brain is through functional connectivity (FC), the statistical dependency of distant neural activity, which has been extensively used in the study of AD. More specifically, FC changes have been described along the disease spectrum, including alterations among individuals in the dementia phase of AD (Koelewijn et al., 2017); in participants with mild cognitive impairment (MCI) (Bajo et al., 2010; Mao et al., 2021); in subjective cognitive decline (SCD) (López-Sanz et al., 2017; Viviano and Damoiseaux, 2020), a preclinical asymptomatic stage in which participants already report a decrease in their cognitive capabilities, prodromal to MCI; and even as early as in healthy adults at risk of developing dementia (García-Colomo et al., 2024; Ramírez-Toraño et al., 2021). Taken together, these studies show an inverted U-shape pattern of FC changes along the continuum of AD, finding increased FC in the early stages, followed by a decrease in connectivity later on in the continuum Pusil et al., 2019. These changes have been previously associated with the underlying pathology hallmarks of AD (Franzmeier et al., 2019; Sepulcre et al., 2017).

Notably, studies on brain connectivity have assumed, until recently, the stationarity of FC. However, the brain's functional activity, far from being static, has been described as highly dynamic, forming various functional networks that underlie complex cognition (Bola and Sabel, 2015). Consequently, by averaging over lengthy imaging recordings, transient information may be lost, and what we interpreted as inter-subject variability might in fact be averaged temporal variability. This perspective has brought attention to the field of spatiotemporal dynamics of brain networks, also called "dynamic functional connectivity" (dFC), which studies how FC evolves over time and what connectivity profiles arise. It has been proven that dFC changes dynamically in response to different contexts or stimuli, even in the resting-state (Núñez et al., 2019).

Given the consistency of the changes in static FC (sFC) throughout the continuum of AD, a novel line of research, focused on the possible dFC alterations underlying sFC changes, has become especially relevant for the disease. Most investigations involving dFC in AD have been carried out using functional magnetic resonance imaging (fMRI). A common finding in these studies is that dFC is reduced in AD, in key networks and regions for the disease, such as the DMN (Matsui and Yamashita, 2023). Additionally, some studies have also reported such a decrease in dFC among MCI participants in regions like the precuneus, which correlated with cognitive performance (Córdova-Palomera et al., 2017; Gu et al., 2020; Zhao et al., 2022). Likewise, Jones et al. found a reduction of time spent in connectivity states with a high contribution of posterior DMN areas among AD patients (Jones et al., 2012), and Schumacher et al. reported that AD patients spend more time in states of sparse connectivity, due to an inability to switch between states of low inter-network connectivity and more highly and

specifically connected network configurations than controls (Schumacher et al., 2019). For a review of fMRI findings about dFC in AD, see Filippi et al., 2019 and Matsui and Yamashita, 2023.

However, the temporal resolution of fMRI is hampered by its low sampling frequency and the slow nature of the hemodynamic responses recorded, and is consequently likely to miss relevant dFC changes in the sub-second scale (Núñez et al., 2019). Electrophysiological techniques such as electroencephalography (EEG) and magnetoencephalography (MEG) are able to overcome such difficulties, both because of their higher sampling frequency and the fact that they measure the electrical activity of cortical neurons. While very scarce, electrophysiological studies point in the same direction as those using fMRI, suggesting a decrease in dFC in the last stages of the AD continuum (Li et al., 2019; Núñez et al., 2019). Núñez et al. found decreased variance when studying the leaked-corrected amplitude envelope (AEC-c) correlations in sensor-space EEG in AD patients compared to the control group in both high alpha and low beta bands, while no significant differences appeared in the MCI group (Núñez et al., 2019). In a posterior work they applied hidden Markov models to instantaneous FC in EEG sensor-space to study meta-states dynamics in AD and MCI, and found a decrease in modularity of meta-states in both MCI and AD participants compared to controls in both alpha and low beta bands (Núñez et al., 2021), meaning that their resting-state networks were less well defined, possibly contributing to the shorter dwell times they also found in the pathological groups. In a functional near-infrared spectroscopy (fNIRS) and EEG integrative investigation, Li et al. found weaker or suppressed dFC in the high alpha and low beta bands of AD participants, reporting lower values for degree and clustering coefficient in the frontal pole and medial orbital regions of AD-induced brain networks (Li et al., 2019). On the other hand, while not centered in dFC, other electrophysiological studies focused on other highly correlated parameters, such as entropy and dynamic changes in power, report findings in the same direction. Sun et al. compile, in a review, reports on decreasing complexity of the MEG/EEG signal in multiple entropy parameters in AD (Sun et al., 2020). Finally, Puttaert et al. applied hidden Markov models to MEG power topographies of healthy individuals and SCD, MCI, and AD participants, finding only differences in the dynamics of the control and AD groups (Puttaert et al., 2020). Similarly to the aforementioned fMRI study by Jones et al., 2012, they found that AD participants spent less time in, and switched less frequently into, states with a high contribution of the posterior DMN.

To the best of our knowledge, no electrophysiological studies exist on the whole pre-dementia spectrum of AD that characterize the evolution of dFC in this population. Based on the presented premises, this study aims to characterize the evolution of dFC in the AD spectrum by estimating connectivity through AEC-c and correlating it over different segments of MEG data in a large cohort consisting of healthy controls, SCD participants, and both stable and progressive MCI participants. Guided by the claims of previous research, we hypothesize we will find the trend of dFC reduction earlier in the AD spectrum, as well as that these reductions to be predominant in frontal and temporal regions and in the DMN. Lastly, to wrap the interpretation of our findings, we will also study the correlation of dFC with cognitive scores, anatomical metrics, and white matter integrity markers, which we hypothesize to decline along with dFC.

2.3 Materials and methods

2.3.1 Participants

The sample for the present study consisted of 321 individuals with valid MEG resting state recordings, T1-weighted magnetic resonance imaging (MRI) scans, and a thorough neuropsychological evaluation. Of them, 143 were unimpaired older adults with no cognitive complaints, namely the healthy control (HC) group, 72 were unimpaired individuals with SCD, and 106 presented MCI.

MCI patients were diagnosed according to the National Institute on Aging-Alzheimer Association (NIA-AA) criteria (Albert et al., 2013), based on their cognitive profile. Besides meeting the core clinical criteria for MCI, patients also exhibited significant hippocampal atrophy according to the evaluation of an experienced neuroradiologist who was blinded to the clinical outcome (see also below hippocampal volumes calculation). Consequently, patients were categorized as "MCI due to AD with intermediate likelihood" (Albert et al., 2013). MCI participants underwent longitudinal assessment on their clinical progression after a mean of 2 (standard deviation of 0.5 years). They were further subdivided into 64 stable MCI (sMCI) and 42 progressive MCI (pMCI) patients, depending on their progression to probable AD in during the follow-up period (McKhann et al., 2011). The participants were recruited from different Spanish institutions and associations; namely, the "Fulbright Alumni Association", the "Asociación Española de Ingenieros de Telecomunicación", or the "Hospital Universitario Clínico San Carlos", being the last one located in Madrid.

To correctly characterize the SCD group, cognitive concerns were self-reported by the participants in an interview with clinician experts. The final group assignment was made after neuropsychological evaluation attending to a multidisciplinary consensus (by neuropsychologists, psychiatrists, and neurologists). To prevent possible confounders of SCD, problematic medication, psycho-affective disorders or other relevant medical conditions lead to the exclusion from the study. Following the recommendations made by the SCD-I-WG, all subjects were older than 60 at onset of SCD, and this onset took place within the last 5 years prior to the recruitment.

The exclusion criteria employed in this study were the followings: (1) history of psychiatric or neurological disorders or drug consumption that could affect MEG activity, such as cholinesterase inhibitors; (2) evidence of infection, infarction or focal lesions in a T2-weighted scan within 2 months before MEG acquisition; (3) history of alcoholism, chronic use of anxiolytics, neuroleptics, narcotics, anticonvulsants or sedative hypnotics; and (4) for the healthy individuals (HC and SCD groups), a score below 26 points in the MMSE. Besides, additional analyses were conducted to rule out other possible causes of cognitive decline, such as B12 vitamin deficit, diabetes mellitus, thyroid problems, syphilis, or infection by the human immunodeficiency virus.

All participants were native Spanish speakers and provided written informed consent. The Institutional Review Board Ethics Committee at Hospital Universitario San Carlos approved the study protocol, and the procedure was performed following the Helsinki Declaration and National and European Union regulations. Table 2.1 summarizes relevant demographic and

clinical information of the sample, and Table S1 compares demographics from sMCI and pMCI groups.

Table 2.1: Sample demographics, neuropsychological test scores, and anatomic and white matter parameters. Pair-wise group-level differences are shown in the right columns, with significant results after FDR correction (q = 0.05) with an asterisk. HC: healthy control; SCD: subjective cognitive decline; MCI: mild cognitive impairment; MMSE: Mini Mental State Examination; FA: fractional anisotropy.

				p-value		
	HC	SCD	MCI	HC vs SCD	HC vs MCI	SCD vs MCI
N	143	72	106	-	-	-
Sex	55M/92F	19M/63F	38M/68F	0.0620	0.8880	0.0925
Age	71.5 ± 4.0	72.1 ± 5.4	74.4 ± 5.2	0.5924	**$4.6{\cdot}10^{-6}$***	**0.0001***
MMSE	28.8 ± 1.4	28.2 ± 1.9	26.6 ± 2.6	0.1591	**$5.1{\cdot}10^{-18}$***	**$4.0{\cdot}10^{-9}$***
Delayed recall test	22.2 ± 9.5	18.7 ± 8.7	5.0 ± 6.5	0.0759	**$1.9{\cdot}10^{-36}$***	**$1.8{\cdot}10^{-25}$***
Total grey matter volume (eTIV-normalized)	0.293 ± 0.017	0.292 ± 0.016	0.280 ± 0.022	0.4818	**$1.6{\cdot}10^{-7}$***	**0.0002***
Hippocampus volume (eTIV-normalized)	0.005 ± 0.0005	0.0049 ± 0.0005	0.0045 ± 0.0007	0.0735	**$3.0{\cdot}10^{-11}$***	**$4.2{\cdot}10^{-5}$***
Left Cingulum tract FA	0.5359 ± 0.0326	0.5292 ± 0.0367	0.5194 ± 0.0336	0.1872	**0.0003***	0.0847
Right Cingulum tract FA	0.4986 ± 0.0263	0.4951 ± 0.0290	0.4889 ± 0.0280	0.3828	**0.0101***	0.1868
Left Inferior Logitudinal tract FA	0.4752 ± 0.0883	0.4897 ± 0.0241	0.4834 ± 0.0584	0.1838	0.4470	0.3987
Right Inferior Logitudinal tract FA	0.4781 ± 0.0892	0.4915 ± 0.0271	0.4874 ± 0.0599	0.2265	0.3915	0.6018

Neuropsychological assessment

To assess the general cognitive and functional status of the participants, the following set of screening questionnaires were used: The Mini Mental State Examination (MMSE, Lobo et al., 1999); the Geriatric Depression Scale–Short Form (GDS, Yesavage, 1988); the Hachinski Ischemic Score, (HIS, Rosen et al., 1980); and the Functional Assessment Questionnaire (FAQ, Pfeffer et al., 1982). After the initial screening, all subjects underwent an exhaustive neuropsychological assessment including: Direct and Inverse Digit Span tests (Wechsler Memory Scale, WMS-IV, "Wechsler Memory Scale–Fourth Edition", 2012); Immediate and Delayed logic memory component of the WMS-IV ("Wechsler Memory Scale–Fourth Edition", 2012); and Phonemic and Semantic Fluency (Controlled Oral Word Association Test, COWAT,

Benton et al., 2017). From these measures, both MMSE scores and the Delayed logic memory component of the WMS-IV were used in this study.

2.3.2 Magnetic Resonance Imaging

An individual T1-weighted MRI scan was acquired for each participant in a General Electric 1.5 T scan. A high-resolution antenna was employed, together with a homogenization phased array uniformity enhancement filter (fast spoiled gradient echo sequence, TR/TE/TI of 11.2/4.2/450 ms; flip angle of 12°; slice thickness of 1 mm, 256 × 256 matrix, and FOV of 25 cm. These images were processed using the FreeSurfer software (version 6.1.0) for automated cortical and subcortical segmentation and parcellation (Fischl, 2012).

Additionally, diffusion weighted imaging (DWI) scans were acquired using a single shot echo planar imaging sequence with a TE of 96.1 ms, a TR of 12ms; a NEX 3 for increasing the signal-to-noise ratio, a FOV of 30.7 cm (resolution of 128 x 128), and a 4 mm slice thickness. In the DWI sequence, one image had no diffusion sensitization (i.e., T2-weighted b0 images), and 25 were DWI (b = 900 s/mm2). DWI images were processed with AutoPtx for probabilistic tractography, as outlined by de Groot et al. in their paper (De Groot et al., 2013). The procedure extracted the mean fractional anisotropy (FA) for each of the tracts of interest (see next paragraph).

The volumetric and tractography measures that were included in further analyses were the total volumes (mm^3) of cortical gray matter and hippocampus, normalized by the estimated total intracranial volume (eTIV), and the FA of the cingulate gyrus part of the cingulum (CGC) and the inferior longitudinal fasciculus (ILF), due to their relevance in the early progression of the disease (Lo Buono et al., 2020).

2.3.3 MEG data acquisition

Each participant underwent a four-minute, eyes-closed, resting-state MEG scan at the Center for Biomedical Technology in Madrid, Spain. This session used a 306-sensor Elekta Neuromag system (Elekta AB, Stockholm, Sweden) to record brain activity. Additionally, ocular and cardiac activities were monitored using two sets of bipolar electrodes. To track head position, four head position indication coils were placed on the participants' scalp: two on the forehead and two on the mastoids. These coils, along with approximately 200 points of the participant's head shape, were digitized using the Fastrak 3D scan (Polhemus, Colchester, VT, USA). The coils were actively used during the recording to continuously monitor the head's position in relation to the MEG helmet. The procedure was conducted in a magnetically shielded room, and participants were advised to remain as motionless and relaxed as possible. The data were filtered in real time between 0.1 and 330 Hz and digitized at a rate of 1000 Hz. For data processing, the spatiotemporal signal space separation method (Taulu and Simola, 2006), as implemented in the Neuromag software (MaxFilter version 2.2, with a correlation of 0.90 and a time window of 10 seconds), was employed to eliminate external noise and correct for any head movements during the MEG scan.

2.3.4 MEG processing and source reconstruction

MEG data were blindly preprocessed by an electrophysiology expert using FieldTrip software (Oostenveld et al., 2011). This process involved dividing the continuous data into non-overlapping, artifact-free 4-second segments, with an extra 2 seconds of real data to each side for padding purposes. Participants who had at least 20 valid segments were selected for further analysis. Due to the high redundancy in the data after applying the signal space separation method (Garcés et al., 2017), analysis focused solely on data from the magnetometers.

Each participant's T1-weighted MRI scan was used for individual source reconstruction. The source model was established in MNI space using a uniform 3D grid with 10 mm spacing. Source positions were identified based on the automated anatomical labeling atlas (Tzourio-Mazoyer et al., 2002), resulting in 1210 cortical sources distributed across 80 regions of interest. This source model was then linearly transformed to each participant's T1-weighted scan. The scans were segmented using SPM12 software (*Statistical Parametric Mapping*, 2007), creating a brain mask. This mask aided in constructing the participants' single-shell realistic head models. These models, combined with the participants' source models, facilitated the generation of a lead field using a modified spherical solution (Nolte, 2003).

To derive time series data for each source location, a linearly constrained, minimum variance beamformer was used as the inverse model. To this end, the beamformers were computed using the covariance matrix of the data filtered between 2 and 45 Hz, with a regularization level set at 1% of the average sensor power.

2.3.5 Dynamic functional connectivity

dFC calculation

FC was estimated using the AEC with leakage correction (O'Neill et al., 2015), either between each pair of time-series in the 80 ROIS of the AAL or between the 1210 brain sources, using the absolute value of the Pearson correlation between the envelopes of the band-pass filtered time-series. Data was filtered in the theta (4-8 Hz), alpha (8-12 Hz), and beta (12-30 Hz) frequency bands through a finite impulse response filter with an order of 1800, designed with a hamming window. AEC was chosen because of its reliability, its within and between subject consistency,44 and due to its sensibility to dFC in aforementioned literature with a similar objective (Briels et al., 2020; Núñez et al., 2019, 2021).

Typically, this connectivity metric is calculated in each of the defined signal segments, and then averaged over those, obtaining the so-called static FC (Figure 2.1A). However, for the sake of studying dFC, we calculated the correlation between the connectivity matrices corresponding to each segment. This is usually labeled in literature as the recurrence matrix (C) (Núñez et al., 2021; Tewarie et al., 2019), and represents the similarity of connectivity distributions over time, as represented in Figure 2.2B. To maintain a uniform representation of the data of all subjects, the same number of segments were used for dFC calculations in all subjects. Given that the minimum number of segments among the participants was 21, we just kept the first 21 clean segments of each participant.

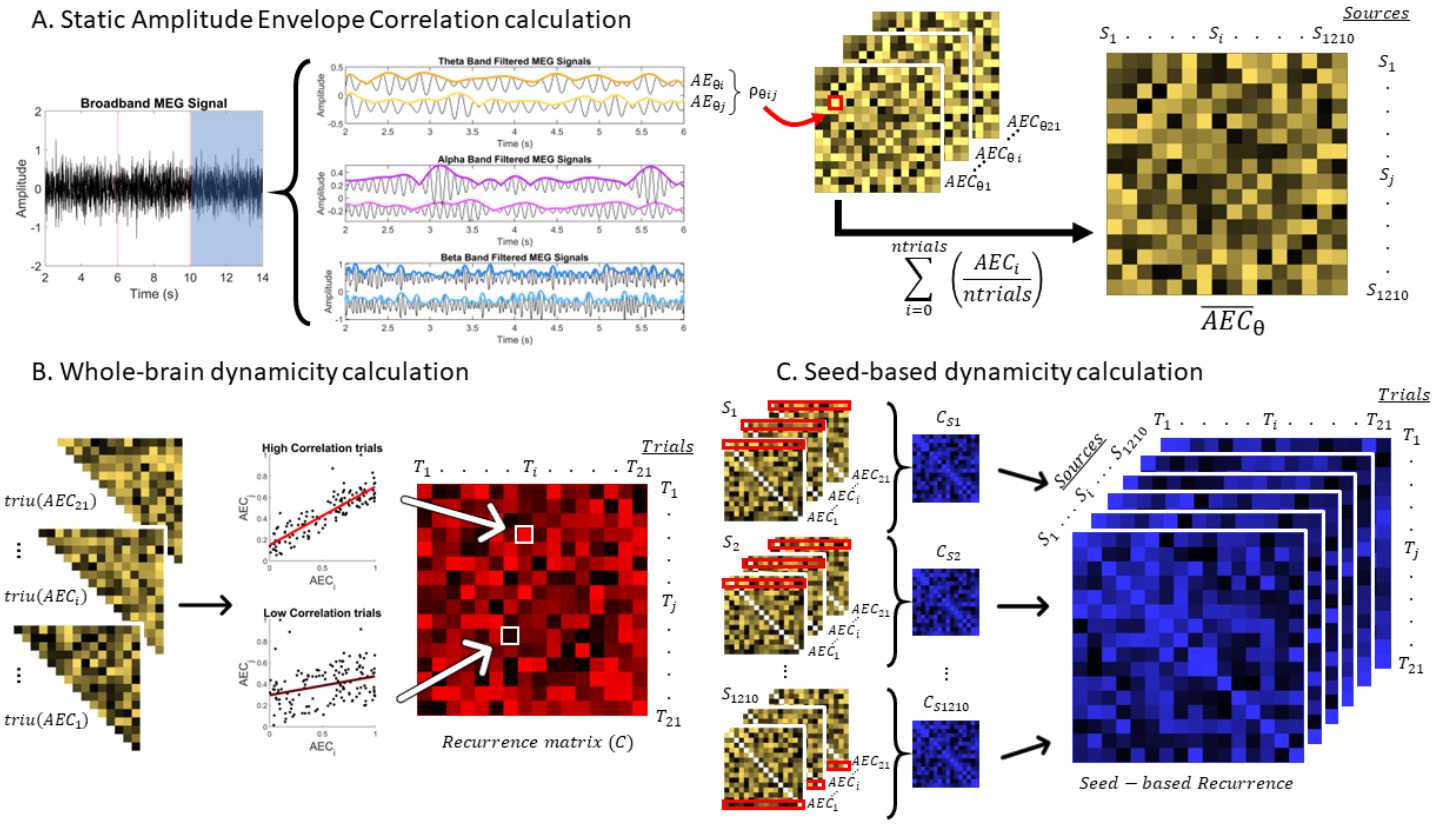


Figure 2.1: Depiction of the methods used in this study. (**A**) Description of the procedure to calculate AEC, including the signal filtering, envelope extraction through the Hilbert transform, correlation between envelopes, and averaging over trials to obtain the static functional connectivity measure of AEC. (**B**) Whole brain dynamicity calculation. Each of the AEC upper triangular matrices extracted from each signal segment of four seconds is then correlated with each other, obtaining a "number of trials" by "number of trials" recurrence matrices. The upper triangle of this matrix is then averaged to obtain a final dynamicity parameter for each subject. (**C**) Seed-based dynamicity calculation. In this case, and for each source, the connectivity of that source with the rest is extracted to obtain the recurrence matrices, obtaining a seed-based recurrence matrix of dimensions number of sources × number of trials × number of trials. Later, the upper triangle of each source recurrence matrix is averaged to get a dynamicity parameter for each of the sources, which enables us to extract spatial comparisons between groups.

Whole-brain dFC

Each of the C_n terms of the recurrence matrix represents the correlation of all connectivity terms of the connectivity matrix of segment i with those of the connectivity matrix of segment j, resulting in a matrix of dimensions number of segments × number of segments. Consequently, we obtained 321 21 s× 21 recurrence matrices, one for each subject, representing the consistency of connectivity profiles over time. The Fisher Z-transformation was subsequently applied to these matrices, to prevent any possible skewness in the calculated distribution (Hotelling, 1953). In order to acquire a parameter representing the dynamic nature of the connectivity, we calculate dynamicity (Dyn) as:

$$Dyn = \frac{\overline{triu(atanh(0.99)) - triu(atanh(C))}}{atanh(0.99)}, \tag{2.1}$$

where the operator *triu* is the upper triangle matrix selector, the operator $\overline{x}$ is the average of x, the operator *atanh* is the inverse hyperbolic tangent, equivalent to the Fisher Z-transform, and C is the recurrence matrix. This parameter would range from 0 to 1, where 0 represents complete stationarity, while 1 would represent a complete lack of temporal correlation among connectivity matrices. Note that we use the *atanh* of 0.99 instead of 1 for normalization, since the inverse hyperbolic tangent of 1 is infinite.

Spatial dFC analysis

No spatial information can be derived from the previous recurrence matrix. To perform a data-driven analysis of the spatial distribution of changes in dFC through recurrence matrices, we propose the methodology we called "seed-based recurrence matrix". While all sources are used to calculate the correlation of each segment with the others in a recurrence matrix, the seed-based recurrence matrix separates that process for each of the sources, as shown in Figure 2.1C.

For each source, the connectivity values of that source with the remaining sources are extracted, and then correlated along the different segments, obtaining a number of segments × number of segments recurrence matrix for each of the original 1210 source positions. Consequently, the seed-based recurrence matrix has a dimension of sources × number of segments × number of segments. Once again, the Fisher Z-transformation was applied to the data to favor the normality of the distribution and the result was subtracted from the inverse hyperbolic tangent of 0.99, and normalized by the same number, as in Equation 2.1. Given the number of sources used for the source reconstruction, we obtained 321 1210 × 21 × 21 seed-based recurrence matrices, one for each participant. Equally as before, we averaged the upper triangle values of the recurrence matrices of each source to finally obtain 1210 values per subject.

2.3.6 Statistical analysis

Initially, demographic characteristics were evaluated, using an independent samples t-test to compare age and neuropsychological variables, as well as a chi-square test to compare sex proportion between each of the groups.

Whole-brain dFC

Statistical analyses were carried out in a stepwise manner. Firstly, we studied whole-brain dFC across the different groups in our sample, to study whether global dFC diminishes along the AD continuum. To this end, we firstly compared the dynamicity values (Equation 2.1), between groups in each frequency band (theta, alpha and beta) through a regression analysis, introducing sex and age as covariates. FDR correction was applied to each frequency band set of comparisons through the Benjamini-Hochberg procedure (Benjamini and Hochberg, 1995),

with a q of 0.05. Any *p-values* surviving FDR were considered statistically significant, and β*-values* were used for interpreting the directionality of results.

Given that we also had the information on the progression towards AD of the participants in the MCI group, we also carried out an additional test comparing the whole-brain dFC of the participants in the sMCI and pMCI groups.

Spatial dFC analysis

The second step of our analysis aimed to study the spatial distribution of dFC changes between groups. For that purpose, the aforementioned seed-based recurrence matrices (Figure 2.1C) of each subject were used. To account for multiple comparisons, we conducted two-sided nonparametric cluster-based permutation tests (Bullmore et al., 1999), using a Montecarlo approach and an independent samples F-statistic ANOVA in each sample, including sex and age as covariates. The source-level and cluster-level significance thresholds were set to 0.05. Significant sources were grouped based on spatial contiguity, obtaining a cluster statistic defined as the sum of the individual statistics of each source in it. We conducted 10,000 permutations on the original data to create a surrogate distribution of random cluster statistics to compare with our original result. As this test was a pos-hoc analysis, it was only performed between groups that showed significant differences in global dFC (i.e., in the previous analysis). Subsequently, a post-hoc linear regression analysis comparing the seed-based dynamicity between groups at the found cluster was performed to check for the directionality of the results.

Neuropsychological, volumetric and DTI FA correlations

Finally, we investigated whether the observed changes in dFC were related to changes in cognition, brain volumetrics, and white matter integrity. To do so, we calculated Pearson's partial correlation of the dynamicity with the previously mentioned neuropsychological test scores, volumetry parameters, and tract FA in the frequency bands where statistical differences in global dFC were detected. We performed these tests both using the data from all groups as well as only from the individual groups, including sex and age as covariate in all cases. FDR correction was again applied to each frequency band set of comparisons, with a q of 0.05.

2.4 Results

2.4.1 Sample demographics and neuropsychological assessment

Sample demographics and neuropsychological test scores, as well as group-level differences, are shown in Table 2.1, and in Supplementary Table A.1 for sMCI and pMCI groups.

The age of the MCI group was significantly higher than that of both SCD and HC groups, and while sex did not significantly differ between any of the groups, p-values were close to significance, supporting the inclusion of both variables as covariates in the rest of statistical tests of the study. MCI performed significantly worse than both HC and SCD groups in all the neuropsychological tests.

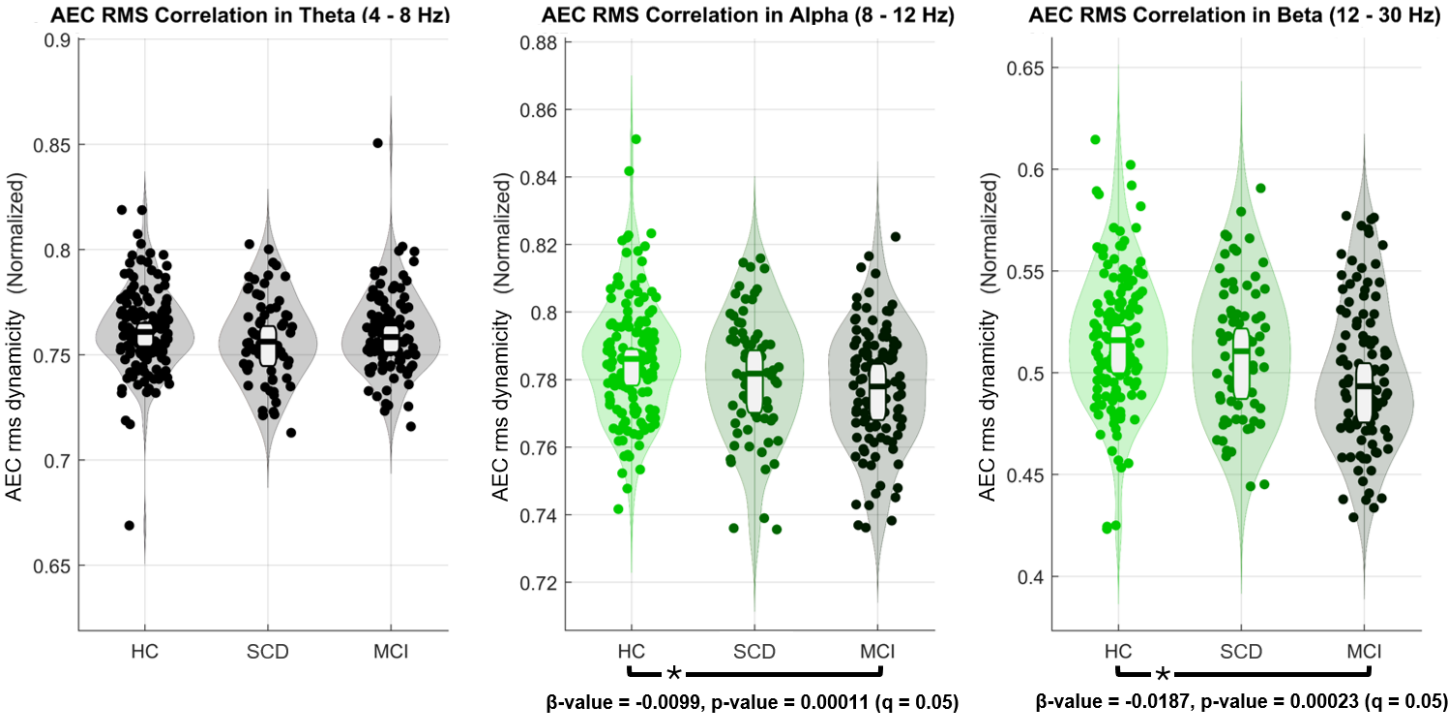


Figure 2.2: Whole-brain dynamicity comparisons between healthy control (HC), subjective cognitive decline (SCD) and mild cognitive impairment (MCI) groups. Significant differences were seen between the HC and MCI groups in the alpha (corrected p-value = 0.00015, β-value = -0.0265, Cohen's d = 0.474, q = 0.05) and beta (corrected p-value = 0.00076, β-value = -0.0135, Cohen's d = 0.506, q = 0.05). No differences were observed in the theta band or between the SCD group and the rest in any frequency band.

2.4.2 Whole-brain dFC is reduced along the AD spectrum

Whole-brain dFC was compared through dynamicity (Equation 2.1) using a linear regression test between each pair of groups, including sex and age as covariates, as shown in Figure 2.2. Dynamicity values in the HC group were significantly higher than those in the MCI group after FDR correction (q = 0.05) in both alpha (corrected p-value = 0.0002, β-value = -0.0265, Cohen's d = 0.474) and beta (corrected p-value = 0.0008, β-value = -0.0135, Cohen's d = 0.506). On the other hand, the SCD group lies in the middle, with nonsignificant differences with neither the HC nor the MCI group (all corrected p-values and β-values can be found in Supplementary Tables A.2, A.3 and A.4). Post-hoc comparisons between sMCI and pMCI groups were all non-significant, as shown in Supplementary Figure A.1 and Supplementary Table A.5.

2.4.3 Localization of dFC changes along the AD continuum

Seed-based dynamicity was compared through nonparametric CBPTs between those groups with significant differences in whole-brain dFC, namely between the HC and MCI groups in the alpha and beta frequency bands. Significant statistical differences were found in seed-based dynamicity between the HC and MCI groups in both the alpha (p-value = 0.0288) and the beta (p-value = 0.009) bands.

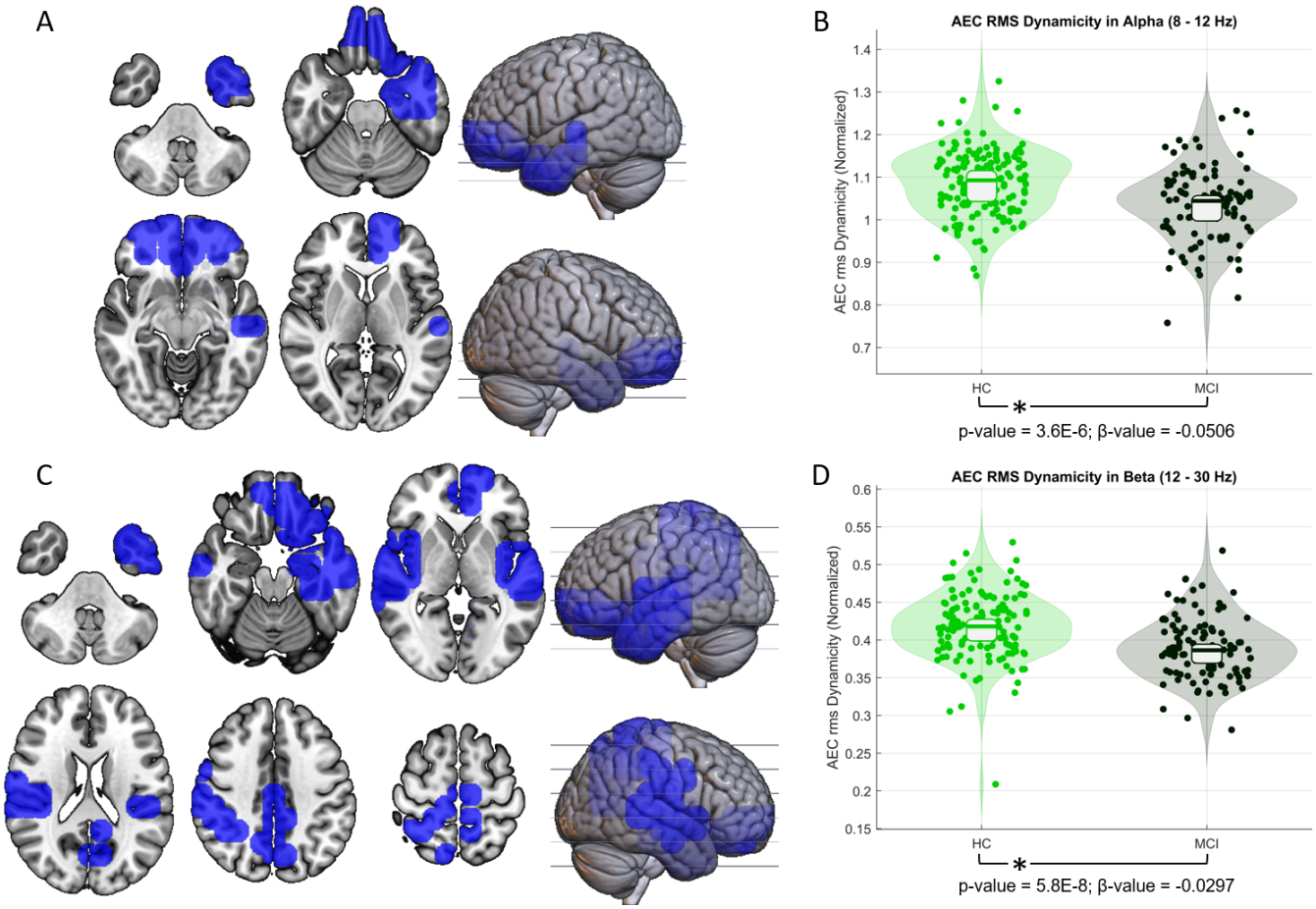


Figure 2.3: Results of the CBPT analyses for seed-based dynamicity. These comparisons were performed between those groups with significant differences in whole-brain dynamicity. Thus, CBPT tests were performed between the MCI and HC groups in the alpha and beta bands. (**A**) Significant cluster showing altered dynamic functional connectivity (dFC) in the alpha band (p-value = 0.0285). (**B**) Linear regression test results for the alpha band seed-based dynamicity values in the significant cluster depicted in A, showing a significant decrease of dFC in the MCI group (Cohen's d = 0.594). (**C**) Significant cluster showing altered dFC in the beta band (p-value = 0.0089). (**D**) Linear regression test results for the alpha band seed-based dynamicity values in the significant cluster depicted in C, showing a significant decrease of dFC in the MCI group (Cohen's d = 0.668).

The cluster showing the most notable differences in the alpha band (Figure 2.3A) included the orbital and medial-orbital areas of the frontal gyrus, the left hippocampus and parahippocampus, as well as the left temporal pole and parts of the inferior and middle temporal gyrus. A post-hoc linear regression analysis found that MCI participants showed a significant reduction in seed-based dynamicity compared to HC in this cluster (Figure 2.3B; p-value $<$ 0.0001; β-value = -0.0506; Cohen's d = 0.594). For a complete list of the AAL ROIs contained in the cluster, please see Supplementary Table A.6.

In the beta band, the cluster showing maximal differences (Figure 2.3C) comprised the left orbital and right superior frontal gyrus, left temporal pole, bilateral temporal gyrus, left hippocampus and parahippocampus, the anterior, middle, and posterior cingulate gyrus, the

precuneus, the left inferior parietal gyrus, and some parts of the calcarine fissure, fusiform gyrus, and cuneus. Again, the post-hoc linear regression analysis found a significant reduction in the MCI group compared to HC in the mentioned cluster (Figure 2.3D; p-value < 0.0001; β-value = -0.0297; Cohen's d = 0.668). For a complete list of the AAL ROIs contained in the cluster, please see Supplementary Table A.7.

2.4.4 dFC correlates with cognitive performance along the AD continuum and in MCI

Finally, we investigated the correlation between dFC and cognition, brain volume and DTI parameters, both considering the whole dataset and the individual groups. Figure 2.4 depicts correlations between dynamicity and MMSE, eTIV-normalized hippocampal volume, and fractal anisotropy of the left cingulum.

Interestingly, the MCI group showed multiple significant positive correlations, including those between dynamicity and MMSE scores, normalized hippocampus, and total grey matter volumes, and both left and right ILF tract FA. While the cingulum tracts FA did not maintain significance after FDR, both right and left tracts show a possible trend for a positive correlation with dynamicity.

At the same time, when calculating correlations with all the dataset, significant direct correlations between dynamicity and MMSE score, delayed logic recall score, normalized hippocampus and total cortical grey matter volume, and left cingulum FA were found. Both rhos and corrected p-values for all correlations calculated are shown in Tables 2.2 and 2.3, where correlations found significant after FDR are marked in bold and with an asterisk.

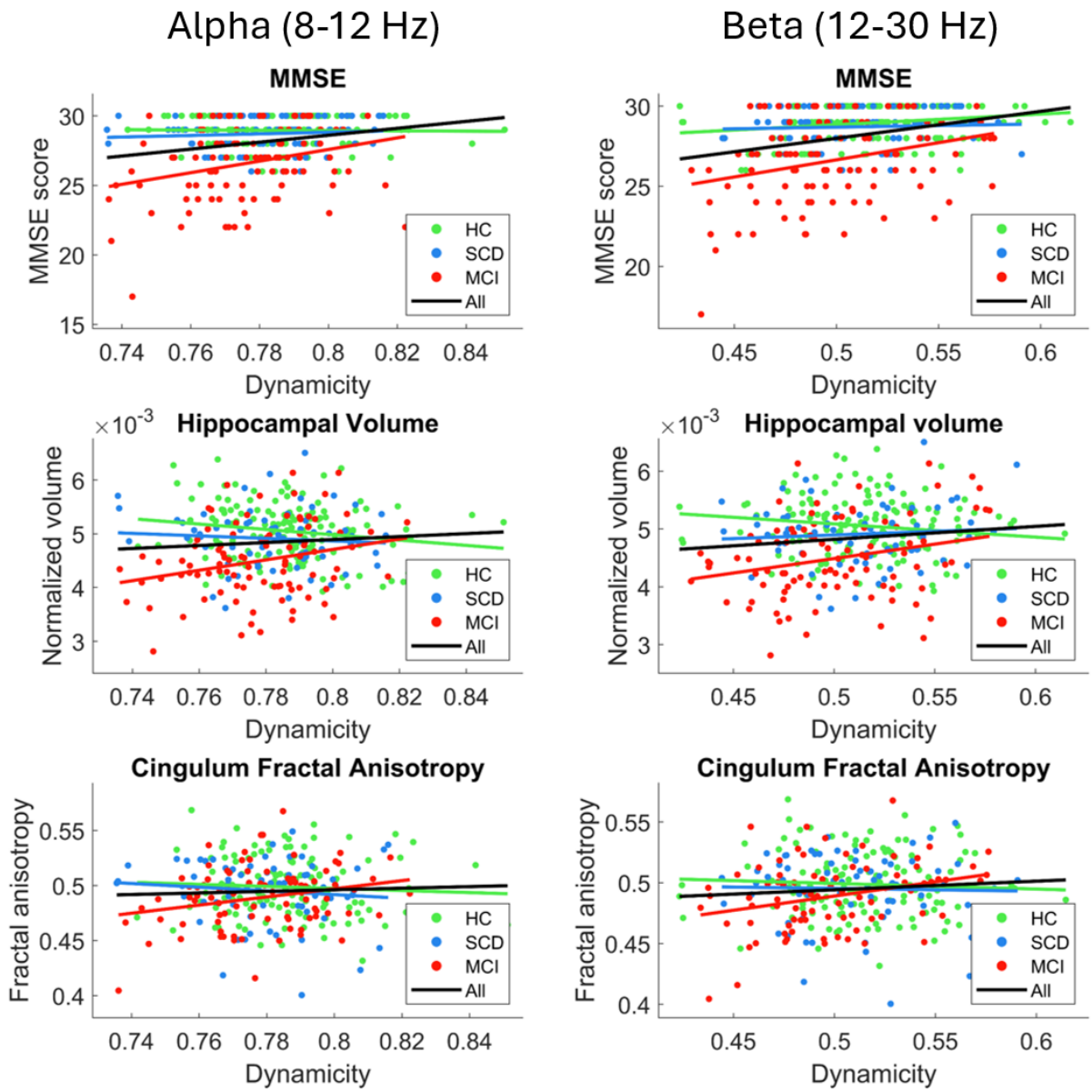


Figure 2.4: Correlations between whole-brain dynamicity and MMSE, eTIV-normalized hippocampal volume and the left Cingulum fractal anisotropy. Green corresponds to the HC group, blue to the SCD group, and red to the MCI group. The black line represents the correlation calculated when considering all subjects at the same time.

2.5 Discussion

In this pioneering study, we aimed to evaluate the evolution of dFC measured with electrophysiology over the early AD spectrum. To this end, we performed the correlation of connectivity matrices over time, both globally and at source-level, a metric simple to calculate and interpret, and that only imposes assumptions regarding the size of the sliding window used for the calculations. Finally, we studied the relationship between this metric and the cognitive and anatomical hallmarks of AD. Our findings suggest that AD progression involves

Table 2.2: Correlation results between whole brain dynamicity and neuropsychological, anatomic and diffusion-weighted imaging (DWI) parameters in the alpha band. Correlations were calculated for each group individually and then using all subjects in the sample (as indicated by the "All" column. Significant corrected p-values after FDR correction (q = 0.05) are bolded and marked with an asterisk. Column colours correspond to those assigned to each group in Figure 2.4.

	Alpha							
	HC		SCD		MCI		All	
	R	p-value	R	p-value	R	p-value	R	p-value
MMSE	0.0530	0.6084	0.0868	0.6446	0.2664	**0.0234***	0.2398	**$7.43 \cdot 10^{-5}$***
Delayed Logic Recall	0.0247	0.7725	0.0333	0.7230	0.0065	0.4756	0.1592	**0.0088***
Hippocampus volume (eTIV-normalized)	-0.0570	0.7947	-0.0297	0.8370	0.2653	**0.0234***	0.1378	**0.0175***
Total grey matter volume (eTIV-normalized)	-0.0213	0.7947	0.0871	0.6446	0.2196	**0.0356***	0.1452	**0.0140***
Left Cingulum tract FA	-0.0896	0.8457	-0.0409	0.8370	0.1746	0.0748	0.0425	0.2531
Right Cingulum tract FA	-0.0409	0.7947	-0.1058	0.8545	0.1818	0.0712	0.0394	0.2537
Left Inferior Logitudinal tract FA	0.0880	0.4844	-0.0708	0.8370	0.2047	**0.0494***	0.1038	0.0583
Right Inferior Logitudinal tract FA	0.1043	0.4844	0.1039	0.6446	0.2296	**0.0356***	0.1317	**0.0233***

a reduction in dFC, mainly in the alpha and beta bands, which is especially pronounced over orbital and temporal areas and in regions involving the DMN. In addition, the decrease in dFC is related to cognitive decline and anatomical deterioration, both when considering data from all groups and, particularly, in the MCI group. These results shed light towards the understanding of brain dynamics along the AD continuum.

Whole-brain dFC analyses displayed a reduction of dynamicity over the continuum of AD, with differences of medium effect sizes between HCs and MCIs in the alpha (Cohen's d = 0.474) and beta (Cohen's d = 0.506) frequency bands, as shown in Figure 2.2. The SCD group did not show significant differences in their whole-brain dFC in any frequency band when compared to HCs or MCIs, proving to be an intermediate state between both conditions. This dFC decreases evidence that AD progression involves a reduction in connectivity profiles over time or, in other words, an increase in the consistency of connectivity patterns. These findings are aligned with previous literature on dFC, where a shrinkage in the dynamic repertoire of connectivity is observed through electrophysiological measurements (Li et al., 2019; Núñez et al., 2019) and fMRI-based metrics Córdova-Palomera et al., 2017; Gu et al., 2020; Schumacher et al., 2019. Additionally, studies focused on brain activity entropy, which depict the quantity of information on individual nodes of activity, find a decrease in signal complexity with the advance of the pathology (Bruña et al., 2012; Cao et al., 2015; Sun et al., 2020), as well as in consciousness disorders (Ballanti et al., 2022). Remarkably, significant decreases in dynamicity between HC and MCI groups were observed specifically in the alpha

Table 2.3: Correlation results between whole brain dynamicity and neuropsychological, anatomic and diffusion-weighted imaging (DWI) parameters in the beta band. Correlations were calculated for each group individually and then using all subjects in the sample (as indicated by the "All" column. Significant corrected p-values after FDR correction (q = 0.05) are bolded and marked with an asterisk. Column colours correspond to those assigned to each group in Figure 2.4.

	Beta							
	HC		SCD		MCI		All	
	R	p-value	R	p-value	R	p-value	R	p-value
MMSE	0.2747	**0.0078***	0.0147	0.7230	0.2550	**0.0234***	0.2787	**$4.55{\cdot}10^{-6}$***
Delayed Logic Recall	0.1129	0.4844	0.0497	0.7230	0.0296	0.4164	0.1939	**0.0018***
Hippocampus volume (eTIV-normalized)	-0.0487	0.7947	0.1093	0.6446	0.2457	**0.0313***	0.1495	**0.0132***
Total grey matter volume (eTIV-normalized)	-0.0514	0.7947	0.1704	0.6446	0.3043	**0.0234***	0.1737	**0.0054***
Left Cingulum tract FA	-0.0281	0.7947	0.1388	0.6446	0.2307	**0.0356***	0.1232	**0.0301***
Right Cingulum tract FA	-0.0429	0.7947	-0.0777	0.8370	0.2246	**0.0356***	0.0574	0.1910
Left Inferior Logitudinal tract FA	0.0808	0.4844	-0.1519	0.8882	0.1193	0.1722	0.0832	0.0994
Right Inferior Logitudinal tract FA	0.0801	0.4844	0.0280	0.7230	0.0972	0.2165	0.0887	0.0901

and beta bands, agreeing with results in Núñez et al., 2019 and Li et al., 2019 even if they report differences between HCs and AD participants, while we found those earlier in the AD continuum, between the HC and MCI groups. On a related note, recent studies have observed a dilution of FC topologies in MCI and AD participants, with decreasing modularity (Núñez et al., 2021), and a blurring of frequency-dependent connectivity structure (Rodríguez-González et al., 2024). This increase in frequency and spatial network homogeneity is thought to underlie the loss of specialized and integrated networks observed in these pathologic states and, in line with our results, could contribute to the decrease in temporal variability observed in the present study.

What physiological alterations may explain these changes in dFC? Previous literature has already discussed the reduction of the dynamic repertoire of connectivity along the spectrum of AD Córdova-Palomera et al., 2017, linking it to possible alterations in white matter integrity. AD is associated with myelin aberrations both in animal models (Desai et al., 2009) and in humans (Nasrabady et al., 2018), which may occur as early as 20 years before the symptoms' onset, and has been also been connected to β-amyloid deposition (Dean et al., 2017). At the same time, several studies have drawn a connection between myelin abnormalities and brain connectivity, highlighting the importance of tract myelination, transmission speed, and the resulting coupling and synchrony patterns observed in the brain (Babaeeghazvini et al., 2021; Hunt et al., 2016). More specifically, it has been observed that the relations between structural and FC are spatial and frequency-dependent (Karahan et al., 2022; Pajevic et al.,

2014) and varies with age (Vandewouw et al., 2021). Importantly, multiple works, such as Karahan and colleagues, have established a connection between the frequency bands affected in this study and myelination distribution and white matter properties (Karahan et al., 2022). In their work, they showed negative correlations between beta sFC inter-subject variability (ISV) and myelination, with alpha sFC-ISV failing to maintain significance due to statistical corrections, and significant negative correlations between alpha and beta sFC-ISV and the hindrance of white matter pathways. Additionally, the temporal precision needed for the oscillatory coupling and phase-locking increases with oscillation frequency, leading to enhanced susceptibility to myelin degradation for higher frequency bands (Pajevic et al., 2014). Our results are aligned with all their conclusions, as we found increased effect sizes of differences over the whole-brain and source-level dFC and more widespread differences between MCI and HC groups over the beta band than in the alpha band, while not finding any result in the theta band. These events support the theory of increased vulnerability of brain coupling at higher frequencies. We also discovered significant negative correlations between whole-brain beta and alpha dFC and FA in multiple tracts, indicating a strong and important dependence between white matter degradation and network integrity in AD.

The relevance of the regions and brain networks found using seed-based dFC (including orbitofrontal and temporal areas for both alpha and beta bands, and also precuneus, IFG, anterior and posterior cingulate gyrus, and superior medial frontal gyrus for the latter) has been highlighted in former research on brain changes throughout the AD continuum, such as functional alterations (García-Colomo et al., 2024; Li et al., 2019; López-Sanz et al., 2017; Maestú et al., 2021; Ramírez-Toraño et al., 2021), volumetric atrophy observed with MRI (Blinkouskaya and Weickenmeier, 2021; Pini et al., 2016), and amyloid neuropathological disturbances measured with positron emission tomography (Mattsson et al., 2019). Interestingly, the distribution of the dFC changes found between MCI and HC correspond to multiple results in Karahan et al., 2022. Brain areas with decreased hindrance of white matter pathways display a similar distribution as the significant cluster found in the alpha band, and the location of the areas with the lowest cortical R1, e.g., with the lowest myelination, is alike the cluster found in the beta band. These areas are characterized by a lower neuronal density, large dendritic arborization, more spine density, more synapses, and higher aerobic glycolysis, which may be a neurobiological feature of the association cortices, enabling adaptable and plastic neural circuitry. These attributes might, in turn, lead to more complex FC behaviors, highlighting the importance of loss of dynamic activity in these areas along the AD continuum.

Finally, the potential of the proposed dFC marker is indicated by its significant correlations in alpha and beta with the cognitive and anatomical parameters. It is worth highlighting that those trends were found both when using the whole dataset and for the MCI group only. While correlations found in the whole dataset showcase the value of dynamicity as a possible biomarker for AD progression, it includes groups with significantly different cognitive and anatomical scores. On the other hand, MCI group correlations imply that lower dFC is related to the severity of the signs these participants show, as well as showing the link between dFC and anatomical damage due to the advance of the disease. Surprisingly, we can find studies describing significant relationships between sFC and DTI measures (Fodor et al., 2021; Vecchio et al., 2015; Zhou et al., 2015), and at the same time alternative sFC-based investigations that do not find a relationship between these two markers (Garcés et al., 2014; Gilligan et al.,

2019; Nakamura et al., 2017). Based on a relatively large sample, the correlations found in this study between dFC and white matter degradation in the pre-dementia phase of the AD continuum contrast with those reported using sFC and motivate further investigation to unveil the potential sensitivity of dFC to early structural changes in the brain.

Nevertheless, some limitations need to be noted. Firstly, the use of a sliding-window technique does not come without disadvantages. The size of the window used in this study (4 seconds) has been used in previous relevant studies determining relevant FC features in AD for the frequency bands investigated here (García-Colomo et al., 2024; López et al., 2014; López-Sanz et al., 2017; Pusil et al., 2019; Ramírez-Toraño et al., 2021), but it was not large enough to capture sufficient oscillations in the delta band, and not small enough to capture dynamic patterns in the gamma band. Future studies will address this limitation for the study of the latter frequency band, especially relevant for AD, and according to our discussion particularly vulnerable to myelin damage. While based on a large dataset, this study did not include any participant with AD, necessary to obtain a complete assessment of the entire AD spectrum. Future studies should investigate the relation of dFC with white matter integrity, sFC, and neural excitation/inhibition.

2.6 Conclusion

In conclusion, our study offers compelling evidence that dFC declines across the AD spectrum, particularly within the alpha and beta frequency bands, emphasizing its potential as a biomarker for early AD detection and progression monitoring. This decline in dFC, especially pronounced in critical brain regions involved in the default mode network, correlates with cognitive deterioration and structural brain changes, further indicating the relevance of dFC in AD, and underpinning the interconnected nature of functional, cognitive, and anatomical alterations in this disorder.

References

2024 Alzheimer's disease facts and figures. (2024). *Alzheimer's & Dementia*, *20*(5), 3708–3821. https://doi.org/10.1002/alz.13809

Albert, M. S., DeKosky, S. T., Dickson, D., Dubois, B., Feldman, H. H., Fox, N. C., Gamst, A., Holtzman, D. M., Jagust, W. J., Petersen, R. C., Snyder, P. J., Carrillo, M. C., Thies, B., & Phelps, C. H. (2013). The Diagnosis of Mild Cognitive Impairment due to Alzheimer's Disease: Recommendations from the National Institute on Aging-Alzheimer's Association Workgroups on Diagnostic Guidelines for Alzheimer's Disease. *FOCUS*, *11*(1), 96–106. https://doi.org/10.1176/appi.focus.11.1.96

Babaeeghazvini, P., Rueda-Delgado, L. M., Gooijers, J., Swinnen, S. P., & Daffertshofer, A. (2021). Brain Structural and Functional Connectivity: A Review of Combined Works of Diffusion Magnetic Resonance Imaging and Electro-Encephalography. *Frontiers in Human Neuroscience*, *15*, 721206. https://doi.org/10.3389/fnhum.2021.721206

Bajo, R., Maestú, F., Nevado, A., Sancho, M., Gutiérrez, R., Campo, P., Castellanos, N. P., Gil, P., Moratti, S., Pereda, E., & del-Pozo, F. (2010). Functional Connectivity in Mild Cognitive Impairment During a Memory Task: Implications for the Disconnection Hypothesis. *Journal of Alzheimer's Disease*, *22*(1), 183–193. https://doi.org/10.3233/JAD-2010-100177

Ballanti, S., Campagnini, S., Liuzzi, P., Hakiki, B., Scarpino, M., Macchi, C., Oddo, C. M., Carrozza, M. C., Grippo, A., & Mannini, A. (2022). EEG-based methods for recovery prognosis of patients with disorders of consciousness: A systematic review. *Clinical Neurophysiology*, *144*, 98–114. https://doi.org/10.1016/j.clinph.2022.09.017

Benjamini, Y., & Hochberg, Y. (1995). Controlling the False Discovery Rate: A Practical and Powerful Approach to Multiple Testing. *Journal of the Royal Statistical Society: Series B (Methodological)*, *57*(1), 289–300. https://doi.org/10.1111/j.2517-6161.1995.tb02031.x

Benton, A. L., Hamsher, d. S. K., & Sivan, A. B. (2017, March). Controlled Oral Word Association Test. https://doi.org/10.1037/t10132-000

Blinkouskaya, Y., & Weickenmeier, J. (2021). Brain Shape Changes Associated With Cerebral Atrophy in Healthy Aging and Alzheimer's Disease. *Frontiers in Mechanical Engineering*, *7*, 705653. https://doi.org/10.3389/fmech.2021.705653

Bola, M., & Sabel, B. A. (2015). Dynamic reorganization of brain functional networks during cognition. *NeuroImage*, *114*, 398–413. https://doi.org/10.1016/j.neuroimage.2015.03.057

Briels, C. T., Schoonhoven, D. N., Stam, C. J., de Waal, H., Scheltens, P., & Gouw, A. A. (2020). Reproducibility of EEG functional connectivity in Alzheimer's disease. *Alzheimer's Research & Therapy*, *12*(1), 68. https://doi.org/10.1186/s13195-020-00632-3

Bruña, R., Poza, J., Gómez, C., García, M., Fernández, A., & Hornero, R. (2012). Analysis of spontaneous MEG activity in mild cognitive impairment and Alzheimer's disease using spectral entropies and statistical complexity measures. *Journal of Neural Engineering*, *9*(3), 036007. https://doi.org/10.1088/1741-2560/9/3/036007

Bullmore, E., Suckling, J., Overmeyer, S., Rabe-Hesketh, S., Taylor, E., & Brammer, M. (1999). Global, voxel, and cluster tests, by theory and permutation, for a difference between two groups of structural MR images of the brain. *IEEE Transactions on Medical Imaging*, *18*(1), 32–42. https://doi.org/10.1109/42.750253

Cao, Y., Cai, L., Wang, J., Wang, R., Yu, H., Cao, Y., & Liu, J. (2015). Characterization of complexity in the electroencephalograph activity of Alzheimer's disease based on fuzzy entropy. *Chaos: An Interdisciplinary Journal of Nonlinear Science*, *25*(8), 083116. https://doi.org/10.1063/1.4929148

Córdova-Palomera, A., Kaufmann, T., Persson, K., Alnæs, D., Doan, N. T., Moberget, T., Lund, M. J., Barca, M. L., Engvig, A., Brækhus, A., Engedal, K., Andreassen, O. A., Selbæk, G., & Westlye, L. T. (2017). Disrupted global metastability and static and dynamic brain connectivity across individuals in the Alzheimer's disease continuum. *Scientific Reports*, *7*(1), 40268. https://doi.org/10.1038/srep40268

De Groot, M., Vernooij, M. W., Klein, S., Ikram, M. A., Vos, F. M., Smith, S. M., Niessen, W. J., & Andersson, J. L. (2013). Improving alignment in Tract-based spatial statistics: Evaluation and optimization of image registration. *NeuroImage*, *76*, 400–411. https://doi.org/10.1016/j.neuroimage.2013.03.015

Dean, D. C., Hurley, S. A., Kecskemeti, S. R., O'Grady, J. P., Canda, C., Davenport-Sis, N. J., Carlsson, C. M., Zetterberg, H., Blennow, K., Asthana, S., Sager, M. A., Johnson, S. C., Alexander, A. L., & Bendlin, B. B. (2017). Association of Amyloid Pathology With Myelin Alteration in Preclinical Alzheimer Disease. *JAMA Neurology*, *74*(1), 41. https://doi.org/10.1001/jamaneurol.2016.3232

Desai, M. K., Sudol, K. L., Janelsins, M. C., Mastrangelo, M. A., Frazer, M. E., & Bowers, W. J. (2009). Triple-transgenic Alzheimer's disease mice exhibit region-specific abnormalities in brain myelination patterns prior to appearance of amyloid and tau pathology. *Glia*, *57*(1), 54–65. https://doi.org/10.1002/glia.20734

Filippi, M., Spinelli, E. G., Cividini, C., & Agosta, F. (2019). Resting State Dynamic Functional Connectivity in Neurodegenerative Conditions: A Review of Magnetic Resonance Imaging Findings. *Frontiers in Neuroscience*, *13*, 657. https://doi.org/10.3389/fnins.2019.00657

Fischl, B. (2012). FreeSurfer. *NeuroImage*, *62*(2), 774–781. https://doi.org/10.1016/j.neuroimage.2012.01.021

Fodor, Z., Horváth, A., Hidasi, Z., Gouw, A. A., Stam, C. J., & Csukly, G. (2021). EEG Alpha and Beta Band Functional Connectivity and Network Structure Mark Hub Overload in Mild Cognitive Impairment During Memory Maintenance. *Frontiers in Aging Neuroscience*, *13*, 680200. https://doi.org/10.3389/fnagi.2021.680200

Franzmeier, N., Rubinski, A., Neitzel, J., Kim, Y., Damm, A., Na, D. L., Kim, H. J., Lyoo, C. H., Cho, H., Finsterwalder, S., Duering, M., Seo, S. W., Ewers, M., & for the Alzheimer's

Disease Neuroimaging Initiative. (2019). Functional connectivity associated with tau levels in ageing, Alzheimer's, and small vessel disease. *Brain*, *142*(4), 1093–1107. https://doi.org/10.1093/brain/awz026

Garcés, P., Ángel Pineda-Pardo, J., Canuet, L., Aurtenetxe, S., López, M. E., Marcos, A., Yus, M., Llanero-Luque, M., del-Pozo, F., Sancho, M., & Maestú, F. (2014). The Default Mode Network is functionally and structurally disrupted in amnestic mild cognitive impairment — A bimodal MEG–DTI study. *NeuroImage: Clinical*, *6*, 214–221. https://doi.org/10.1016/j.nicl.2014.09.004

Garcés, P., López-Sanz, D., Maestú, F., & Pereda, E. (2017). Choice of Magnetometers and Gradiometers after Signal Space Separation. *Sensors*, *17*(12), 2926. https://doi.org/10.3390/s17122926

García-Colomo, A., Nebreda, A., Carrasco-Gómez, M., De Frutos-Lucas, J., Ramirez-Toraño, F., Spuch, C., Comis-Tuche, M., Bruña, R., Alfonsín, S., & Maestú, F. (2024). Longitudinal changes in the functional connectivity of individuals at risk of Alzheimer's disease. *GeroScience*, *46*(3), 2989–3003. https://doi.org/10.1007/s11357-023-01036-5

Gilligan, T. M., Sibilia, F., Farrell, D., Lyons, D., Kennelly, S. P., & Bokde, A. L. W. (2019). No relationship between fornix and cingulum degradation and within-network decreases in functional connectivity in prodromal Alzheimer's disease (H. Zhang, Ed.). *PLOS ONE*, *14*(10), e0222977. https://doi.org/10.1371/journal.pone.0222977

Gu, Y., Lin, Y., Huang, L., Ma, J., Zhang, J., Xiao, Y., Dai, Z., & Alzheimer's Disease Neuroimaging Initiative. (2020). Abnormal dynamic functional connectivity in Alzheimer's disease. *CNS Neuroscience & Therapeutics*, *26*(9), 962–971. https://doi.org/10.1111/cns.13387

Hotelling, H. (1953). New Light on the Correlation Coefficient and its Transforms. *Journal of the Royal Statistical Society: Series B (Methodological)*, *15*(2), 193–225. https://doi.org/10.1111/j.2517-6161.1953.tb00135.x

Hunt, B. A. E., Tewarie, P. K., Mougin, O. E., Geades, N., Jones, D. K., Singh, K. D., Morris, P. G., Gowland, P. A., & Brookes, M. J. (2016). Relationships between cortical myeloarchitecture and electrophysiological networks. *Proceedings of the National Academy of Sciences*, *113*(47), 13510–13515. https://doi.org/10.1073/pnas.1608587113

Jones, D. T., Vemuri, P., Murphy, M. C., Gunter, J. L., Senjem, M. L., Machulda, M. M., Przybelski, S. A., Gregg, B. E., Kantarci, K., Knopman, D. S., Boeve, B. F., Petersen, R. C., & Jack, C. R. (2012). Non-Stationarity in the "Resting Brain's" Modular Architecture (Y. He, Ed.). *PLoS ONE*, *7*(6), e39731. https://doi.org/10.1371/journal.pone.0039731

Karahan, E., Tait, L., Si, R., Özkan, A., Szul, M. J., Graham, K. S., Lawrence, A. D., & Zhang, J. (2022). The interindividual variability of multimodal brain connectivity maintains spatial heterogeneity and relates to tissue microstructure. *Communications Biology*, *5*(1), 1007. https://doi.org/10.1038/s42003-022-03974-w

Koelewijn, L., Bompas, A., Tales, A., Brookes, M. J., Muthukumaraswamy, S. D., Bayer, A., & Singh, K. D. (2017). Alzheimer's disease disrupts alpha and beta-band resting-state oscillatory network connectivity. *Clinical Neurophysiology*, *128*(11), 2347–2357. https://doi.org/10.1016/j.clinph.2017.04.018

Li, R., Nguyen, T., Potter, T., & Zhang, Y. (2019). Dynamic cortical connectivity alterations associated with Alzheimer's disease: An EEG and fNIRS integration study. *NeuroImage: Clinical*, *21*, 101622. https://doi.org/10.1016/j.nicl.2018.101622

Lo Buono, V., Palmeri, R., Corallo, F., Allone, C., Pria, D., Bramanti, P., & Marino, S. (2020). Diffusion tensor imaging of white matter degeneration in early stage of Alzheimer's disease: A review. *International Journal of Neuroscience*, *130*(3), 243–250. https://doi.org/10.1080/00207454.2019.1667798

Lobo, A., Saz, P., Marcos, G., Día, J. L., de la Cámara, C., Ventura, T., Morales Asín, F., Fernando Pascual, L., Montañés, J. A., & Aznar, S. (1999). [Revalidation and standardization of the cognition mini-exam (first Spanish version of the Mini-Mental Status Examination) in the general geriatric population]. *Medicina Clinica*, *112*(20), 767–774.

López, M. E., Bruña, R., Aurtenetxe, S., Pineda-Pardo, J. Á., Marcos, A., Arrazola, J., Reinoso, A. I., Montejo, P., Bajo, R., & Maestú, F. (2014). Alpha-Band Hypersynchronization in Progressive Mild Cognitive Impairment: A Magnetoencephalography Study. *The Journal of Neuroscience*, *34*(44), 14551–14559. https://doi.org/10.1523/JNEUROSCI.0964-14.2014

López-Sanz, D., Bruña, R., Garcés, P., Martín-Buro, M. C., Walter, S., Delgado, M. L., Montenegro, M., López Higes, R., Marcos, A., & Maestú, F. (2017). Functional Connectivity Disruption in Subjective Cognitive Decline and Mild Cognitive Impairment: A Common Pattern of Alterations. *Frontiers in Aging Neuroscience*, *9*, 109. https://doi.org/10.3389/fnagi.2017.00109

Maestú, F., de Haan, W., Busche, M. A., & DeFelipe, J. (2021). Neuronal excitation/inhibition imbalance: Core element of a translational perspective on Alzheimer pathophysiology. *Ageing Research Reviews*, *69*, 101372. https://doi.org/10.1016/j.arr.2021.101372

Mao, Y., Liao, Z., Liu, X., Li, T., Hu, J., Le, D., Pei, Y., Sun, W., Lin, J., Qiu, Y., Zhu, J., Chen, Y., Qi, C., Su, H., & Yu, E. (2021). Disrupted balance of long and short-range functional connectivity density in Alzheimer's disease (AD) and mild cognitive impairment (MCI) patients: A resting-state fMRI study. *Annals of Translational Medicine*, *9*(1), 65–65. https://doi.org/10.21037/atm-20-7019

Matsui, T., & Yamashita, K.-i. (2023). Static and Dynamic Functional Connectivity Alterations in Alzheimer's Disease and Neuropsychiatric Diseases. *Brain Connectivity*, *13*(5), 307–314. https://doi.org/10.1089/brain.2022.0044

Mattsson, N., Palmqvist, S., Stomrud, E., Vogel, J., & Hansson, O. (2019). Staging β-Amyloid Pathology With Amyloid Positron Emission Tomography. *JAMA Neurology*, *76*(11), 1319. https://doi.org/10.1001/jamaneurol.2019.2214

McKhann, G. M., Knopman, D. S., Chertkow, H., Hyman, B. T., Jack, C. R., Kawas, C. H., Klunk, W. E., Koroshetz, W. J., Manly, J. J., Mayeux, R., Mohs, R. C., Morris, J. C., Rossor, M. N., Scheltens, P., Carrillo, M. C., Thies, B., Weintraub, S., & Phelps, C. H. (2011). The diagnosis of dementia due to Alzheimer's disease: Recommendations from the National Institute on Aging-Alzheimer's Association workgroups on diagnostic guidelines for Alzheimer's disease. *Alzheimer's & Dementia*, *7*(3), 263–269. https://doi.org/10.1016/j.jalz.2011.03.005

Nakamura, A., Cuesta, P., Kato, T., Arahata, Y., Iwata, K., Yamagishi, M., Kuratsubo, I., Kato, K., Bundo, M., Diers, K., Fernández, A., Maestú, F., & Ito, K. (2017). Early

functional network alterations in asymptomatic elders at risk for Alzheimer's disease. *Scientific Reports*, *7*(1), 6517. https://doi.org/10.1038/s41598-017-06876-8

Nasrabady, S. E., Rizvi, B., Goldman, J. E., & Brickman, A. M. (2018). White matter changes in Alzheimer's disease: A focus on myelin and oligodendrocytes. *Acta Neuropathologica Communications*, *6*(1), 22. https://doi.org/10.1186/s40478-018-0515-3

Nolte, G. (2003). The magnetic lead field theorem in the quasi-static approximation and its use for magnetoencephalography forward calculation in realistic volume conductors. *Physics in Medicine and Biology*, *48*(22), 3637–3652. https://doi.org/10.1088/0031-9155/48/22/002

Núñez, P., Poza, J., Gómez, C., Rodríguez-González, V., Hillebrand, A., Tewarie, P., Tola-Arribas, M. Á., Cano, M., & Hornero, R. (2021). Abnormal meta-state activation of dynamic brain networks across the Alzheimer spectrum. *NeuroImage*, *232*, 117898. https://doi.org/10.1016/j.neuroimage.2021.117898

Núñez, P., Poza, J., Gómez, C., Rodríguez-González, V., Hillebrand, A., Tola-Arribas, M. A., Cano, M., & Hornero, R. (2019). Characterizing the fluctuations of dynamic resting-state electrophysiological functional connectivity: Reduced neuronal coupling variability in mild cognitive impairment and dementia due to Alzheimer's disease. *Journal of Neural Engineering*, *16*(5), 056030. https://doi.org/10.1088/1741-2552/ab234b

O'Neill, G. C., Barratt, E. L., Hunt, B. A. E., Tewarie, P. K., & Brookes, M. J. (2015). Measuring electrophysiological connectivity by power envelope correlation: A technical review on MEG methods. *Physics in Medicine and Biology*, *60*(21), R271–R295. https://doi.org/10.1088/0031-9155/60/21/R271

Oostenveld, R., Fries, P., Maris, E., & Schoffelen, J.-M. (2011). FieldTrip: Open Source Software for Advanced Analysis of MEG, EEG, and Invasive Electrophysiological Data. *Computational Intelligence and Neuroscience*, *2011*, 1–9. https://doi.org/10.1155/2011/156869

Pajevic, S., Basser, P., & Fields, R. (2014). Role of myelin plasticity in oscillations and synchrony of neuronal activity. *Neuroscience*, *276*, 135–147. https://doi.org/10.1016/j.neuroscience.2013.11.007

Pfeffer, R. I., Kurosaki, T. T., Harrah, C. H., Chance, J. M., & Filos, S. (1982). Measurement of Functional Activities in Older Adults in the Community. *Journal of Gerontology*, *37*(3), 323–329. https://doi.org/10.1093/geronj/37.3.323

Pini, L., Pievani, M., Bocchetta, M., Altomare, D., Bosco, P., Cavedo, E., Galluzzi, S., Marizzoni, M., & Frisoni, G. B. (2016). Brain atrophy in Alzheimer's Disease and aging. *Ageing Research Reviews*, *30*, 25–48. https://doi.org/10.1016/j.arr.2016.01.002

Pusil, S., López, M. E., Cuesta, P., Bruña, R., Pereda, E., & Maestú, F. (2019). Hypersynchronization in mild cognitive impairment: The 'X' model. *Brain*, *142*(12), 3936–3950. https://doi.org/10.1093/brain/awz320

Puttaert, D., Coquelet, N., Wens, V., Peigneux, P., Fery, P., Rovai, A., Trotta, N., Sadeghi, N., Coolen, T., Bier, J.-C., Goldman, S., & De Tiège, X. (2020). Alterations in resting-state network dynamics along the Alzheimer's disease continuum. *Scientific Reports*, *10*(1), 21990. https://doi.org/10.1038/s41598-020-76201-3

Ramírez-Toraño, F., Bruña, R., De Frutos-Lucas, J., Rodríguez-Rojo, I. C., Marcos De Pedro, S., Delgado-Losada, M. L., Gómez-Ruiz, N., Barabash, A., Marcos, A., López Higes, R., & Maestú, F. (2021). Functional Connectivity Hypersynchronization in Relatives of

Alzheimer's Disease Patients: An Early E/I Balance Dysfunction? *Cerebral Cortex*, *31*(2), 1201–1210. https://doi.org/10.1093/cercor/bhaa286

Rodríguez-González, V., Núñez, P., Gómez, C., Hoshi, H., Shigihara, Y., Hornero, R., & Poza, J. (2024). Unveiling the alterations in the frequency-dependent connectivity structure of MEG signals in mild cognitive impairment and Alzheimer's disease. *Biomedical Signal Processing and Control*, *87*, 105512. https://doi.org/10.1016/j.bspc.2023.105512

Rosen, W. G., Terry, R. D., Fuld, P. A., Katzman, R., & Peck, A. (1980). Pathological verification of ischemic score in differentiation of dementias. *Annals of Neurology*, *7*(5), 486–488. https://doi.org/10.1002/ana.410070516

Schumacher, J., Peraza, L. R., Firbank, M., Thomas, A. J., Kaiser, M., Gallagher, P., O'Brien, J. T., Blamire, A. M., & Taylor, J.-P. (2019). Dynamic functional connectivity changes in dementia with Lewy bodies and Alzheimer's disease. *NeuroImage: Clinical*, *22*, 101812. https://doi.org/10.1016/j.nicl.2019.101812

Sepulcre, J., Sabuncu, M. R., Li, Q., El Fakhri, G., Sperling, R., & Johnson, K. A. (2017). Tau and amyloid β proteins distinctively associate to functional network changes in the aging brain. *Alzheimer's & Dementia*, *13*(11), 1261–1269. https://doi.org/10.1016/j.jalz.2017.02.011

Statistical Parametric Mapping. (2007). Elsevier. https://doi.org/10.1016/B978-0-12-372560-8.X5000-1

Sun, J., Wang, B., Niu, Y., Tan, Y., Fan, C., Zhang, N., Xue, J., Wei, J., & Xiang, J. (2020). Complexity Analysis of EEG, MEG, and fMRI in Mild Cognitive Impairment and Alzheimer's Disease: A Review. *Entropy*, *22*(2), 239. https://doi.org/10.3390/e22020239

Taulu, S., & Simola, J. (2006). Spatiotemporal signal space separation method for rejecting nearby interference in MEG measurements. *Physics in Medicine and Biology*, *51*(7), 1759–1768. https://doi.org/10.1088/0031-9155/51/7/008

Tewarie, P., Liuzzi, L., O'Neill, G. C., Quinn, A. J., Griffa, A., Woolrich, M. W., Stam, C. J., Hillebrand, A., & Brookes, M. J. (2019). Tracking dynamic brain networks using high temporal resolution MEG measures of functional connectivity. *NeuroImage*, *200*, 38–50. https://doi.org/10.1016/j.neuroimage.2019.06.006

Tzourio-Mazoyer, N., Landeau, B., Papathanassiou, D., Crivello, F., Etard, O., Delcroix, N., Mazoyer, B., & Joliot, M. (2002). Automated Anatomical Labeling of Activations in SPM Using a Macroscopic Anatomical Parcellation of the MNI MRI Single-Subject Brain. *NeuroImage*, *15*(1), 273–289. https://doi.org/10.1006/nimg.2001.0978

Vandewouw, M. M., Hunt, B. A., Ziolkowski, J., & Taylor, M. J. (2021). The developing relations between networks of cortical myelin and neurophysiological connectivity. *NeuroImage*, *237*, 118142. https://doi.org/10.1016/j.neuroimage.2021.118142

Vecchio, F., Miraglia, F., Curcio, G., Altavilla, R., Scrascia, F., Giambattistelli, F., Quattrocchi, C. C., Bramanti, P., Vernieri, F., & Rossini, P. M. (2015). Cortical Brain Connectivity Evaluated by Graph Theory in Dementia: A Correlation Study Between Functional and Structural Data. *Journal of Alzheimer's Disease*, *45*(3), 745–756. https://doi.org/10.3233/JAD-142484

Viviano, R. P., & Damoiseaux, J. S. (2020). Functional neuroimaging in subjective cognitive decline: Current status and a research path forward. *Alzheimer's Research & Therapy*, *12*(1), 23. https://doi.org/10.1186/s13195-020-00591-9

Wechsler Memory Scale–Fourth Edition. (2012, November). https://doi.org/10.1037/t15175-000

Yesavage, J. A. (1988). Geriatric Depression Scale. *Psychopharmacology Bulletin*, *24*(4), 709–711.

Zhao, C., Huang, W.-J., Feng, F., Zhou, B., Yao, H.-X., Guo, Y.-E., Wang, P., Wang, L.-N., Shu, N., & Zhang, X. (2022). Abnormal characterization of dynamic functional connectivity in Alzheimer's disease. *Neural Regeneration Research*, *17*(9), 2014. https://doi.org/10.4103/1673-5374.332161

Zhou, Y., Yu, F., Duong, T. Q., & for the Alzheimer's Disease Neuroimaging Initiative. (2015). White matter lesion load is associated with resting state functional MRI activity and amyloid pet but not FDG in mild cognitive impairment and early alzheimer's disease patients. *Journal of Magnetic Resonance Imaging*, *41*(1), 102–109. https://doi.org/10.1002/jmri.24550

Chapter 3

Dynamic functional connectivity is modulated by the amount of p-Tau231 in blood in cognitively intact participants

3.1 Objectives and hypotheses

O.3.1 To test whether dFC in cognitively unimpaired adults is influenced by the amount of Aβ accumulation, measured through the blood biomarker p-tau231.

Hypotheses: Higher levels of p-tau231 will be associated to more pronounced alterations of dFC.

O.3.2 To determine the brain regions where the influence of p-tau231 on dFC alterations is more prominent.

Hypotheses: Changes in dFC will be more prominent in the early stage Aβ accumulation regions of the brain, as defined in Mattsson et al., 2019 (Figure 1.15).

O.3.3 To explore the relationship between the observed dFC alterations, if any, and other risk factors (age, sex, APOE carriage, and family history of AD) and metrics that monitor the progression of AD (sFC, cognitive scores, brain volumetrics, and white matter integrity).

This chapter is based on the publication:

Carrasco-Gómez, M., Garcia-Colomo, A., Nebreda, A., Bruña, R., Santos, A., & Maestu, F. (2024). Dynamic functional connectivity is modulated by the amount of p-Tau231 in blood in cognitively intact participants. bioRxiv, 2024-05. (Under review in *Clinical Neurophysiology*) doi: https://doi.org/10.1101/2024.05.29.596323

3.2 Introduction

The biological conception of Alzheimer's disease (AD) led to the definition of a continuum that begins with the appearance of the pathological hallmarks of the disease but no associated clinical symptom, namely the accumulation of Aβ and tau NFTs . These changes can emerge up to 20 years before the diagnosis, which highlights the importance of early detection tools to identify individuals in this state and track the progression of the disease, along with the effect of potential interventions ("2024 Alzheimer's disease facts and figures", 2024).

Positron emission tomography (PET) and cerebrospinal fluid (CSF) biomarkers are considered poor candidates to this end, due to their high cost, invasiveness, and low accessibility. Therefore, increasing attention has been placed on blood biomarkers (Hu et al., 2019). In this vein, the recently discovered species of phosphorylated tau at threonine 231 (p-tau231) presents promising results. Abnormal levels, both in CSF and plasma, can be detected as early on as the preclinical stage. Furthermore, its levels parallel those of amyloid-beta (Aβ), tracking its changes even before Aβ-PET positivity has been achieved. Therefore, given the temporal and disease-specific association between both pathology markers, p-tau231 can be employed as a proxy of Aβ pathology (Ashton et al., 2021, 2022; Milà-Alomà et al., 2022; Suárez-Calvet et al., 2020; Tissot et al., 2022).

Neuronal dysfunction and macroscopic functional changes can also be detected in this preclinical stage. In this context, electrophysiological measures are being examined as early biomarkers, given their minimal invasiveness and ability to detect incipient alterations in brain activity (Lopes da Silva, 2013; Peraza et al., 2018). Studies addressing the changes in static functional connectivity (sFC) along the AD continuum reveal an inverted U-shaped pattern, whereby the preclinical stage is marked by increases in sFC, followed by a subsequent state of hypoconnectivity (García-Colomo, Nebreda, et al., 2024; López-Sanz et al., 2017; Nakamura et al., 2017; Pusil et al., 2019; Ramírez-Toraño et al., 2021). The initial state of hyperconnectivity has been associated with Aβ deposition, known to establish a positive feedback loop with neuronal hyperexcitability that underlies the observed hyperconnectivity (Canter et al., 2016; Schultz et al., 2017; Sepulcre et al., 2017). Furthermore, recent studies have found interesting results when exploring sFC in the alpha subfrequency bands (Engels et al., 2015; Ramírez-Toraño et al., 2021), with a special mention to García-Colomo, Nebreda, et al., 2024 where individuals at higher risk of AD showed increased sFC values, and the longitudinal increase across time in FC was associated with the Aβ and AD pathology proxy p-tau231.

Notably, resting-state activity has been broadly used in this context, in an attempt to study the organization of brain communication while avoiding inter-center bias and using comparable metrics between subjects with different levels of pathology (Van Den Heuvel and Hulshoff Pol, 2010). Functional connectivity from resting-state recordings has been typically assessed by averaging the connectivity values across the whole recording, thus providing a value of sFC, which assumes that connections and their strength are stationary over time (Hutchison et al., 2013). However, brain activity and networks are not static; rather, regions constantly connect and disconnect from each other in complex temporal dynamics even during resting state (Escrichs et al., 2021; Núñez et al., 2019). Therefore, what has been classically interpreted

as inter-subject variability or background noise, might in fact be temporal variability. Thus, capturing the changes and fluctuations in connectivity beyond classical sFC can improve the understanding of brain function. This field, dedicated to the study of spatiotemporal dynamics of brain networks, is known as "dynamic functional connectivity" (dFC). Given the relevance of early biomarkers and the alterations described in sFC as early as the preclinical stage, studying and characterizing incipient changes in dFC can aid in the understanding of the development of AD and contribute to identify individuals entering the continuum.

Most studies involving dFC in the AD continuum have been conducted using functional magnetic resonance imaging (fMRI). These consistently report a progressive reduction of dFC among mild cognitive impairment and AD patients, involving relevant regions and networks such as the precunei and default mode network (Carrasco-Gómez et al., 2024; Córdova-Palomera et al., 2017; Matsui and Yamashita, 2023). Studies addressing cognitively unimpaired individuals with AD pathology markers, however, show conflicting results, finding increases (Yang et al., 2022) and decreases (Mueller and Weiner, 2017) in dFC, this is, in the variability of FC over time, associated with the presence of Aβ. These clashing findings could be due to differences in methodology used to evaluate dFC and suggest an influence of AD pathology over dFC, which could be more sensitive to pathology from the earliest stages than sFC.

Although more appropriate to measure rapid dynamic changes in connectivity, electrophysiological studies are scarcer. Nonetheless, and similarly to fMRI, research performed in the dementia stage reveals a reduction of dFC, measured with different metrics such as variance and hidden Markov models, as well as related metrics such as entropy and dynamic changes in power (Li et al., 2019; Sun et al., 2020). Results are conflicting when considering mild cognitive impairment patients (Núñez et al., 2019, 2021) and, to the best of our knowledge, no research has been carried out addressing dFC in cognitively unimpaired individuals with AD pathology markers.

Based on the presented premises and previous results from our group, indicating a sensitivity of the subfrequencies in the alpha band to early alterations, we aim to study how dFC values in the low (8-10 Hz) and high alpha ranges (10-12 Hz) change in relation to p-tau231, a non-invasive marker of AD and Aβ pathology. Furthermore, we aim to evaluate which brain areas are most affected by this relationship. We expect to find early dFC alterations associated with the individuals' p-tau231 levels, even in the absence of AD symptomatology. Additionally, we will evaluate whether other risk factors contribute to the alteration observed in dFC.

3.3 Materials and methods

3.3.1 Participants

The present study was carried out with a sample of 73 cognitively unimpaired individuals with available plasma p-tau231 determinations, extracted from a group of 140 participants with a valid MEG recording. Volunteers for this study are part of a larger initiative ("Study of the anatomo-functional connectome of AD-relatives: an early intervention on cognition

Table 3.1: Sample demographics. The association with p-tau231 levels and the rest of the variables is shown in the two rightmost columns, displaying the independent samples t-test t-statistic and p-value for categorical values and Spearman correation's rho and p-value for continuous variables. AD: Alzheimer's disease; APOE: Apolipoprotein E; MoCA: Montreal cognitive assessment; FA: fractional anisotropy.

		p-tau231 association	
N	73	t-stat/rho	p-value
Sex	49 F/ 24 M	0,27	0,7857
Age	61.0±6.1	0,2267	0,0538
p-tau231	388.16±151.26	-	-
AD Familiar	53 FH+ / 20 FH-	-0,0948	0,9247
APOE ϵ4	21 ϵ4+ / 52 ϵ4-	-0,5357	0,5939
MOCA	28.2±1.4	0,0588	0,6239
Hippocampus volume (eTIV-normalized)	0.0053±0.0005	-0,006	0,9597
Forceps minor FA	0.3992±0.0208	-0,1093	0,3712

and lifestyles"), aimed at longitudinally following the evolution of cognitively healthy at-risk and not-at-risk individuals over time in subsequent waves. The data used for the current study belongs to the second evaluation, during which the plasma p-tau231 determination was performed.

All participants were genotyped regarding their apolipoprotein E (APOE) carriage and had an available MRI scan acquired during the baseline assessment (2 to 3 years prior) that was used for this study. During this follow-up, all participants underwent an MEG scan, a blood sample extraction for plasma markers' determination, and a thorough neuropsychological assessment to ensure a healthy cognitive status. Table 3.1 summarizes relevant demographic and clinical information of the sample.

Exclusion criteria for the current study included: (1) history of psychiatric or neurological disorders or drug consumption in the last week that could affect MEG activity; (2) family history of dementia other than Alzheimer's disease; (3) evidence of infection, infarction, or focal lesions in a T2-weighted MRI scan; (4) alcoholism or chronic use of anxiolytics, neuroleptics, narcotics, anticonvulsants, or sedative-hypnotics; (5) being younger than 50 or older than 80 years old; (6) a score in the Montreal Cognitive Assessment (MoCA) below 26; (7) unusable MEG recording or with less than 50 clean segments; (8) unavailable or unusable T1-weighted image; or (9) unavailable plasma p-tau231 determination.

The "Hospital Clínico San Carlos" Ethics Committee approved this study, and the procedure was performed following internationally accepted guidelines and regulations.

3.3.2 Plasma p-tau231 determination

Plasma p-tau231 concentration was quantified by competitive enzyme-linked immunosorbent assay, using a commercial kit (Human Phosphorylated Tau 231) (MyBioSource, Inc., USA, MBS724296), according to the manufacturer's instructions. Tests were performed in duplicate, and an automated microplate reader (Biochrom Asys UVM340, Cambridge, UK) measured

the optical density at 450 nm with MikroWin 2000 software (Berthold Technologies, Germany). Units are reported in pg/ml.

3.3.3 AD family history

Family history of AD, which constitutes a compound risk for the disease (Donix et al., 2012), was defined as having a first degree relative (direct descendants or siblings) with confirmed Alzheimer's disease. Relatives of patients were required to provide a medical report indicating the diagnosis of the patient following the NINCDS-ADRDA criteria (McKhann et al., 2011).

3.3.4 Apolipoprotein E genetic evaluation

DNA was extracted from whole-blood samples. APOE haplotype was determined by analyzing single nucleotide polymorphisms (SNPs) rs7412 and rs429358 genotypes with TaqMan assays using an Applied Biosystems 7500 Fast Real-Time PCR machine (Applied Biosystems, Foster City, CA). A genotyping call rate over 90% per plate, sample controls for each genotype, and negative sample controls were included in each assay. Three well-differentiated genotyping clusters for each SNP were required to validate results. Intra- and interplate duplicates of several DNA samples were included.

3.3.5 Magnetic resonance imaging

Each subject's T1-weighted MRI scan was acquired in a General Electric 1.5 T system. A high-resolution antenna was employed together with a homogenization Phased array Uniformity Enhancement filter (Fast Spoiled Gradient Echo sequence, TR/TE/TI = 11.2/4.2/450 ms; flip angle 12°; 1 mm slice thickness, 256 × 256 matrix and FOV 25 cm. The T1 images were processed using the FreeSurfer software (version 6.1.0) for automated cortical and subcortical segmentation and parcellation (Fischl, 2012).

Additionally, diffusion weighted imaging (DWI) scans were acquired using a single shot echo planar imaging sequence with a TE of 96.1 ms, a TR of 12000 ms; a NEX 3 for increasing the signal-to-noise ratio, a FOV of 30.7 cm (plane resolution of 128 x 128) and a 2.4 mm slice thickness, yielding an isotropic voxel of 2.4 mm3. In the DWI sequence, one image had no diffusion sensitization (i.e., T2-weighted b0 images); and 25 were DWI (b = 900 s/mm2). DWI images were processed with AutoPtx for probabilistic tractography, as outlined in De Groot et al., 2013. The procedure extracted the mean fractional anisotropy (FA) for each tract.

The volumetric and tractography measures that were included in further analyses were parameters classically studied in the literature in the progress of AD: the total volume of the bilateral hippocampi, normalized by the estimated intracranial volume (eTIV), and the FA of the forceps minor, which was chosen due to its relevance in the data-driven results obtained from the initial dFC analyses in this study.

3.3.6 MEG data acquisition

Each participant underwent a five-minute, eyes-closed, resting-state MEG scan at the Center for Biomedical Technology in Madrid (Spain) using a 306-sensor Elekta Vectorview system (Elekta AB, Stockholm, Sweden). Ocular and cardiac activity was monitored with two sets of bipolar electrodes. Head position was continuously tracked with four head position indication coils placed on the participants' forehead and mastoids. These coils, along with approximately 200 points of the head's shape, were digitized using the PolhemusFASTRAK system (Polhemus, Colchester, VT, USA). The procedure was conducted in a magnetically shielded room, and participants were advised to remain as motionless as possible. The data were filtered online between 0.1 and 330 Hz and digitized at a rate of 1000 Hz. For data processing, the spatiotemporal signal space separation method (Taulu and Simola, 2006), as implemented in the Neuromag software (MaxFilter version 2.2, with a correlation threshold of 0.90 and a correlation window of 10 seconds), was employed to eliminate external noise and adjust for any head movements during the MEG scan.

3.3.7 MEG preprocessing and source reconstruction

MEG data were blindly preprocessed by an electrophysiology expert using FieldTrip software (Oostenveld et al., 2011). This process involved dividing the continuous data into non-overlapping, artifact-free 4-second segments, with padding of 2 seconds of real data to each side of each segment. Participants who had at least 50 valid segments were selected for further analyses, given the high number of samples needed for entropy calculation (see next section). In addition, to improve the comparability across subjects, the number of segments was set to exactly 50, discarding data from those participants with more valid segments. Due to the high redundancy in the data after applying the signal space separation method (Garcés et al., 2017), only data from magnetometers were used in further analyses.

The individual T1-weighted MRI scan was used for personalized source reconstruction. The source model was established in MNI space using a uniform 3D grid with 10 mm spacing, and source positions were identified based on the automated anatomical labeling atlas (Tzourio-Mazoyer et al., 2002), resulting in 1210 cortical sources distributed across 80 regions of interest. This source model was then linearly transformed to each individual T1-weighted scan. The scans were segmented using SPM12 software (*Statistical Parametric Mapping*, 2007), creating a brain mask, which was used to construct the participants' single-shell realistic head models. This head model was combined with the individual source model for the generation of a lead field using a modified spherical solution (Nolte, 2003).

To derive the time series for each source location, a linearly constrained, minimum variance beamformer was used as the inverse method. The sensor-space data was first filtered in the low alpha (8-10 Hz) and high alpha (10-12 Hz) frequency bands through a finite impulse response filter with an order of 1800, designed with a Hamming window. After filtering, the 2-seconds of padding were discarded, to avoid edge effects in the data. The beamformers were computed using the covariance matrix of the data filtered between 2 and 45 Hz, with a regularization level set at 1% of the average sensor power.

3.3.8 Functional connectivity

FC was estimated using the amplitude envelope correlation with leakage correction (AEC-c; O'Neill et al., 2015) between the time series of each pair of the 1210 cortical sources. After orthogonalization, the absolute value of the Pearson correlation between the time series' envelopes was used. AEC was chosen because of its reliability, within and between subject consistency (Colclough et al., 2016; Liuzzi et al., 2019) and due to its sensibility to dFC in previous studies with similar objectives (Briels et al., 2020; Núñez et al., 2019, 2021).

We calculated AEC-c in each of the defined signal segments, and then averaged over those, obtaining the so-called static FC (Figure 3.1A), resulting in connectivity matrices of dimension 1210 sources × 1210 sources. Finally, we averaged the FC matrix across rows to obtain the connectivity nodal strength, which represents the average connectivity of each cortical source position with all the other sources (strAEC).

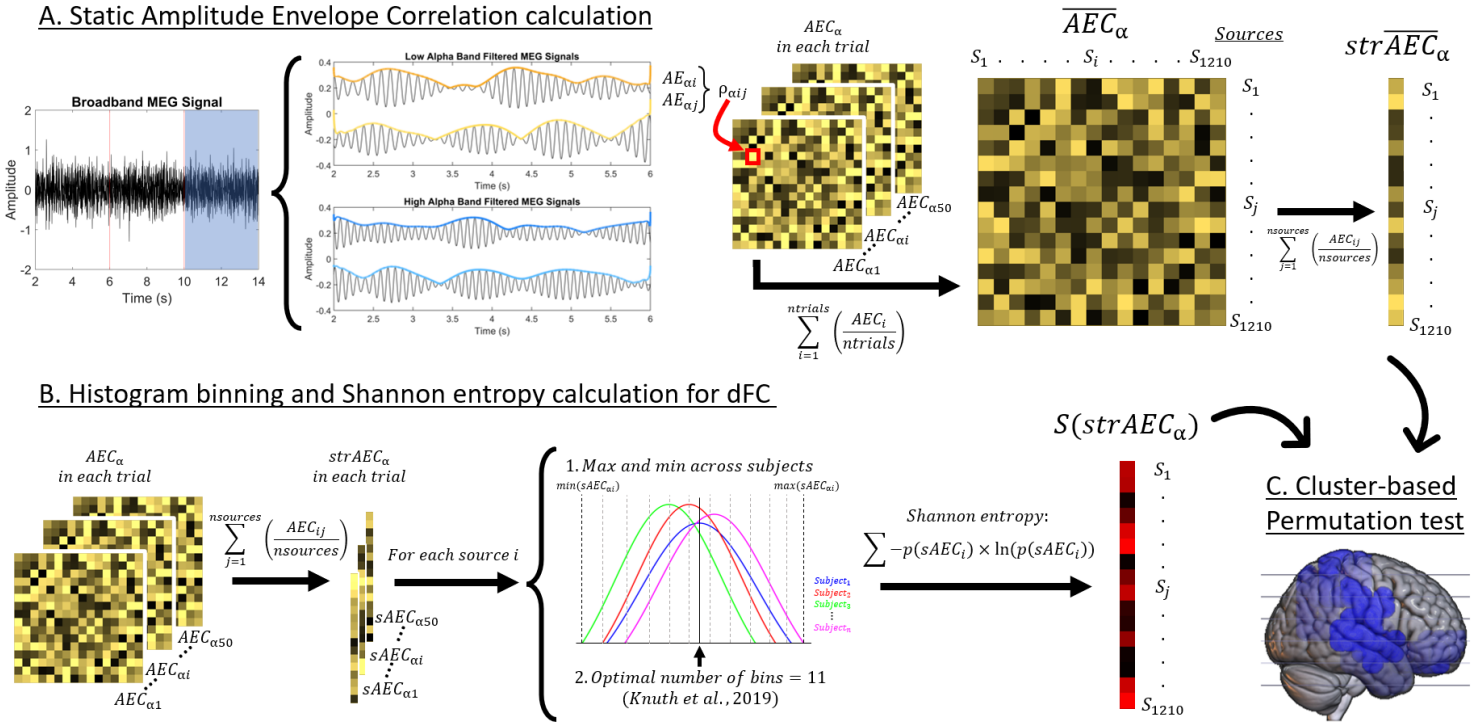


Figure 3.1: Depiction of the methods used in this study. (**A**) Description of the procedure to calculate the static AEC-c, including the signal filtering, envelope extraction through the Hilbert transform, correlation between envelopes, and averaging over trials and sources to obtain a measure of static strength (strAEC) for each source. (**B**) Description of the procedure to calculate the entropy for the nodal strength of each source position in each epoch. First, the nodal strength for each source position and epoch was calculated. We used a histogram with 11 bins to calculate Shannon entropy. This resulted in a value of entropy for each source position and participant ($S(strAEC_\alpha)$), which accounts for their dFC. (**C**) A cluster-based permutation test is used to evaluate the correlation between the p-tau231 levels and the obtained dFC and sFC values.

For the sake of studying dFC, we calculated the entropy of the series of connectivity nodal strengths for each source position prior to the segment-averaging (Figure 3.1B). First, starting from the AEC-c connectivity matrices that were not averaged across time (dimensions 1210

sources × 1210 sources × 50 segments), we averaged these matrices over the second dimension, obtaining a temporal series of connectivity strengths for each cortical source position of dimensions 1210 sources × 50 segments. Afterwards, the entropy of each of those time series was calculated by means of histograms with linearly spaced bins.

Firstly, to determine the optimal number of bins for the creation of histograms in our dataset, we followed the guidelines exposed by Knuth, 2019 for each of the sources' connectivity strength time series in all our participants. We kept the median of the resulting calculations, obtaining an optimal number of 11 bins. After that, and again to assure comparability between subjects, we defined the minimum and maximum values for the binning procedure in each cortical source by calculating the minimum and maximum value of the connectivity strength of a cortical source across all participants. Finally, following the optimal binning procedure, the Shannon entropy was calculated (Shannon, 1948):

$$S(AEC) = -\sum_{i=1}^{B} p(AEC_i) \times \ln(p(AEC_i)) \tag{3.1}$$

Where S is the entropy operator, AEC is our time series of connectivity strengths, p(AEC_i is the probability for connectivity strength to fall under bin i, ln is the natural logarithm and $nbins$ is the total number of bins. The resulting entropy vectors included one value of entropy for each of the 1210 sources, representing the level of dynamicity of the cortical source connectivity over time. In other words, each source was assigned a value which portrays how variant the FC was over time, with higher values indicating a higher variability and vice versa. Figure 3.1C depicts the calculation process of dFC parameters in this study.

3.3.9 Statistical analyses

Initially, demographic characteristics were evaluated using an independent samples t-test to compare p-tau231 levels between groups for categorical variables such as sex, APOE $\epsilon 4$ status, and AD family history. Spearman correlations were employed to assess the relationship between p-tau231 and quantitative variables, such as age, MoCA, eTIV-normalized hippocampal volume and FA at the forceps minor.

Spatial FC analysis

Statistical analyses were carried out in a data-driven, stepwise manner. Firstly, we used a cluster-based permutation test (CBPT; Bullmore et al., 1999) using a Montecarlo approach to assess which sources' sFC and dFC strength in the high alpha and low alpha range were associated with p-tau231 levels. This nonparametric analysis accounts for multiple comparisons. Two-sided, partial correlations were used to assess the relationship between sFC or dFC and p-tau231, with sex and age as covariates. The source-level and cluster-level significance thresholds were set to $\alpha = 0.05$. Significant sources were grouped based on their spatial contiguity, obtaining a cluster-level statistic defined as the sum of the individual statistics of each source within the cluster. We conducted 10000 permutations on the original data to create a surrogate distribution of random cluster-level statistics, which was then used to compare our original cluster size to the surrogate size distribution.

The clusters identified in the first step indicate brain areas showing significant correlation between sFC or dFC strength in general and levels of p-tau231. However, from this analysis alone, it is not possible to determine whether these clusters have different spatial patterns of connectivity. Therefore, we then performed a seed-based connectivity analysis, using the cluster identified in the first step as the seed. This results in a set of seed-based connectivity values for each of the source positions outside the seed. Again, we used a CBPT to identify significant partial correlations between sFC or dFC and p-tau231 levels, using sex and age as covariates. The result is a set of significant clusters of brain areas showing significant correlations with p-tau231 in their level of FC with the seed region. To obtain a single FC value for each subject, we calculated the average connectivity between the original cluster (seed) and the sources from the emerging cluster (secondary cluster), which we will refer to as the "seed-secondary cluster FC" from now on. Post-hoc Spearman partial correlation analyses were performed between the seed-secondary cluster dFC or sFC values and p-tau231 levels, using sex and age as covariates, to investigate the magnitude and directionality of the previous results.

Risk factor linear regressions

Finally, we investigated whether the observed changes in sFC or dFC were related to other risk factors aside from p-tau231 levels. To do so, we built three backwards stepwise linear regression analyses to explain the sFC or dFC of the previously found significant clusters:

- Firstly, we created a regression model including age, sex, presence of the APOE allele $\epsilon 4$, AD family history and MoCA scores. We also included sFC for dFC significant clusters and vice versa.
- Secondly, we added p-tau231 levels to the previous model to find out which parameters remained significant.
- Finally, an additional regression model was constructed from the previous one by adding factors classically studied in the continuum of AD: the eTIV-normalized hippocampal volume and fractal anisotropy of tracts related to the regions included in the clusters (i.e. the forceps minor) to the surviving factors of the previous stepwise regression analysis.

It is important to remark that we used backwards stepwise models as it was recommended in previous literature (Chatterjee and Hadi, 2012; Xu and Zhang, 2001), given that the backward procedure the model is initiated with the full variable set, inspecting the significance of all possible variables, and that this procedure is better able to handle multicollinearity than a forward method.

3.4 Results

3.4.1 Sample demographics and variables of interest

Sample demographics and variables of interest used in this study are shown in Table 3.1.

The only variable that showed an almost significant correlation with p-tau231 was age (R =

0.2267, p-value = 0.0538), supporting the inclusion of this variable as covariate in the CBPTs of the study.

3.4.2 dFC increases along with p-tau231 values over orbitofrontal and temporal areas

While sFC strength values did not correlate significantly with p-tau231 values in any of the studied frequency bands, a cluster of significant correlation between dFC and p-tau231 emerged in the low alpha frequency band (p-value = 0.0460). This cluster showed a positive correlation between dFC nodal strength and p-tau231 levels, and included parts of the right temporal pole and right inferior, middle, and superior temporal gyri, along with the right parahippocampus (Figure 3.2, yellow).

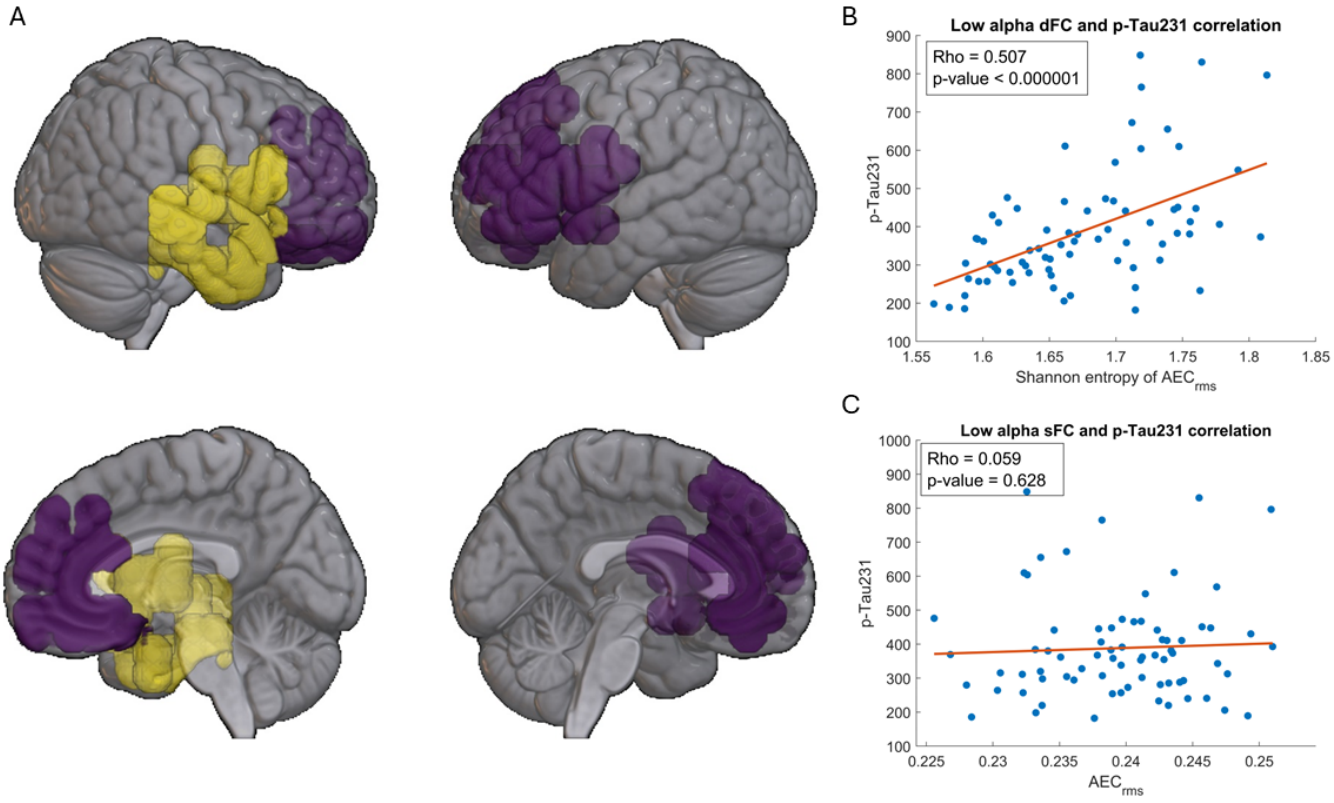


Figure 3.2: Clusters of significant association between dFC and p-tau231. (**A**) The regions that show a positive correlation between their dFC levels and p-tau231 are represented in yellow (original cluster). Marked in purple are the regions that emerge after the second cluster-based permutation test (secondary cluster), whose dFC values with the original cluster show a positive correlation with p-tau231. (**B**) Scatterplots and correlation values for the seed-secondary cluster dynamic functional connectivity (dFC; top) and static functional connectivity (sFC; bottom) with p-tau231 levels.

To better characterize this relationship, we studied the seed-based dFC of these sources with the rest of the brain in the same frequency band, using a single-sided contrast for a positive correlation between dFC and p-tau231. This analysis unveiled a unique cluster with

a significant positive correlation between p-tau231 and the dFC from the original cluster (p-value = 0.0044). This group of sources included the right and parts of the left orbitofrontal cortices, left inferior and middle frontal gyri, bilateral anterior cingulate gyrus, and left parahippocampus (Figure 3.2, purple).

Spearman partial correlations between p-tau231 levels and the seed-secondary cluster dFC and sFC and p-tau231 revealed a strongly positive correlation between dFC and p-tau231 (Rho = 0.507, p-value = $6.3 \cdot 10^{-6}$; Figure 3.2B), while the sFC did not significantly correlate with p-tau231 (Rho = 0.058, p-value = 0.6279; Figure 3.2C).

3.4.3 dFC is related to p-tau231 levels, sFC, and fractional anisotropy

Backwards stepwise linear regression models were built to explain the seed-secondary cluster dFC in the low alpha frequency band. Firstly, we evaluated the influence of the following variables on the dFC between the original and seed-based clusters: age, sex, MoCA scores, presence of the APOE allele $\epsilon 4$, AD family history, and sFC between clusters. The resulting model was significant (R-squared = 0.107, p-value = 0.0187), and only preserved two variables: age (p-value = 0.0735, β-value = 0.0021) and sFC (p-value = 0.0229, β-value = 2.77).

Subsequently, we built a second stepwise model by adding the levels of p-tau231 to find out which of the previously selected variables remained. The resulting model was significant (R-squared = 0.328, p-value = $9.0 \cdot 10^{-7}$). This model discarded age as a relevant variable for the model, preserving p-tau231 (p-value = $1.6 \cdot 10^{-6}$, β-value = 0.00021) and sFC (p-value = 0.0212, β-value = 2.43).

Finally, we added two additional factors to the previous one: eTIV-normalized hippocampal volume and FA at the forceps minor, given the location of the significant cluster. The resulting model was significant (R-squared = 0.389, p-value = $4.6 \cdot 10^{-7}$) and preserved 3 variables: p-tau231 (p-value = $3.2 \cdot 10^{-6}$, β-value = 0.00021), sFC (p-value = 0.0134, β-value = 2.65), and FA at the forceps minor (p-value = 0.0541, β-value = -0.569). A complete statistical report on the resulting linear regression models can be found in Supplementary Tables B.1, B.2, and B.3.

The correlation of the significant variables and dFC can be found in Figure 3.2B for p-tau231 (R = 0.507, p-value < 0.0001), and in Figure 3.3 for sFC (R = 0.256, p-value = 0.0290) and the FA at the forceps minor (R = -0.270, p-value = 0.0250).

3.5 Discussion

This study developed an unprecedented evaluation of the relationship between p-tau231 levels and both sFC and dFC through MEG. To this end, we calculated sFC through AEC-c and derived dFC from the entropy of the FC series over a sliding window, and calculated its spatial correlation with p-tau231 levels using non-parametric CBPTs. We found a cluster where dFC significantly and positively correlated with p-tau231 levels, located over the anterior parts of the temporal lobe and parahippocampal cortex, the orbitofrontal cortices, and bilateral anterior cingulate cortex. Moreover, we investigated which risk factors could be related to the

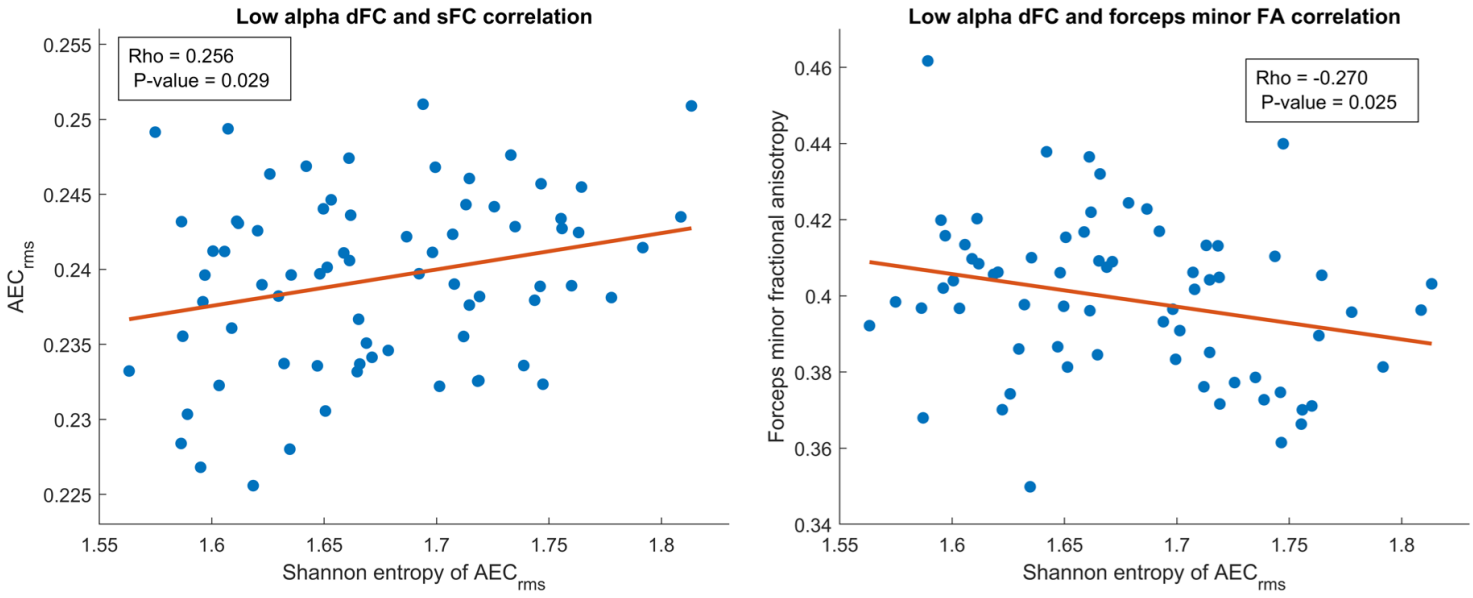


Figure 3.3: Correlation between dFC and linear regression model predictors. Scatterplot showing the positive association between dynamic functional connectivity (dFC) and static functional connectivity (sFC) of the seed-secondary cluster depicted in Figure 2 (left) and between dynamic functional connectivity of the seed-secondary cluster and the FA of the forceps minor (right).

changes observed in dFC through stepwise linear regression models. The linear regression models identified other factors influencing dFC, such as sFC and the FA of the forceps minor. These results complement and expand upon previous literature on the alterations of dFC in healthy individuals at risk of AD, addressing, for the first time, how this parameter changes in electrophysiological recordings.

The main finding from the present study is a cluster of positive correlation where the dFC values correlate with p-tau231 in the low-alpha band, as hypothesized based on previous literature (Mueller and Weiner, 2017; Yang et al., 2022). No such results emerge when addressing sFC and p-tau231. This finding is of special relevance, as dFC could constitute a more sensitive metric than sFC to early alterations associated with AD pathology, due to the detection of subtle dynamic changes traditionally considered "noise" or interpersonal variability (Battaglia et al., 2020). While previous fMRI studies in healthy individuals with AD pathology yield inconsistent results regarding the directionality of dFC changes, studies carried out addressing the prodromal and dementia stages consistently point towards a reduction of dFC, both with MEG and fMRI (Córdova-Palomera et al., 2017; Jones et al., 2012; Matsui and Yamashita, 2023). This decline is hypothesized to be another sign of the disconnection and the excitation/inhibition imbalance that characterize AD and underlie a loss of coupling strength that leads to a decrease of dFC (Núñez et al., 2019). While our results could seem inconsistent with such a trend, sFC is also known for not following a linear decline, but rather an inverted U-shaped pattern, marked by a state of hyperconnectivity in the early stages of Aβ accumulation, and hypoconnectivity later on in the continuum. The initial hyperconnectivity is caused by an underlying state of neuronal hyperexcitability that

contributes to increased Aβ deposition which, in turn, increases hyperexcitability (Maestú et al., 2021; Ranasinghe et al., 2022). In this line, previous studies by our group carried out with p-tau231 find a positive association with sFC along with centrality increases in posterior regions as predicted by theoretical and computational models of the early stages of AD (De Haan et al., 2012; García-Colomo, López-Sanz, et al., 2024; Stam, 2014). Therefore, dFC could follow an equivalent trend and experience an increase in the early stages of the disease in association with Aβ increases. Nevertheless, future research should be done to specifically address the underlying cause of the dFC increases.

The areas forming the original cluster include areas such the right temporal pole and right inferior, middle, and superior temporal gyri, along with the right parahippocampus, which show a positive relationship between dFC and p-tau231. The secondary cluster that emerged from the seed-based analysis of the original one includes regions such as the right and parts of the left orbitofrontal cortices, left inferior and middle frontal gyri, bilateral anterior cingulate gyrus, and left parahippocampus, whose dFC with the original cluster is positively associated with p-tau231. These results are congruent with previous literature, as they suggest early dFC alterations that span regions from the DMN, which is known to be especially vulnerable to AD pathology, as well as the orbitofrontal cortex, which accumulates Aβ from the earliest stages of the continuum (Li et al., 2019; Matsui and Yamashita, 2023; Mattsson et al., 2019). Moreover, a previous study carried out by Lorenzini et al. involves similar areas (Lorenzini et al., 2023). In this study of 736 healthy individuals, they evaluated the relationship between CSF Aβ levels and centrality variability. They report a decrease of centrality variability in a frontotemporal cluster encompassing areas similar to the ones that emerge in the present study. While the spatial distribution of both sets of results seems to suggest early alterations in the dynamic of frontotemporal regions, the comparability of the meaning of both sets of results in combination is hampered. More research is needed to understand the underlying neuronal cause of dFC increases and graph-theory dynamics, along with studies that link electrophysiological and fMRI dFC changes. While electrophysiological techniques might be more suitable to study dFC, fMRI has been more widely used, but results are difficult to interpret due to physiological artifacts, variation over time in both the mean and variance of the blood-oxygen-level dependent signal (Kudela et al., 2017), and different methodological differences such as the technique used to estimate dFC or the time-scale between studies. Previous investigations on multiscale entropy to assess signal complexity in AD showed that the directionality of the results depended on the time-scale for the parameter calculation, finding increased signal complexity in controls for short time-scales, and decreased for larger time-scales (Mizuno et al., 2010; Ren et al., 2020). Consequently, comparing results from different studies is intricate, and multi-analysis studies are needed to better understand the relationship between different dFC metrics and improve comparability (Torabi et al., 2024).

To better understand which factors other than p-tau231 levels influence dFC, we performed stepwise regression models. The initial model identified age and sFC as significant predictors of dFC levels. However, incorporating p-tau231 into the model resulted in the exclusion of age and enhanced the explanatory power of the model, with R-squared values increasing from 0.107 to 0.328. These findings suggest that although related, p-tau231 has an additional pathological component to that of aging, thus having a greater impact over dFC. Subsequently, two structural and classically used pathology parameters in the context of AD were included

in the model: normalized hippocampal volume and FA. Specifically, we added the FA of the forceps minor due to the location of the areas identified through the CBPTs. This resulted in the maintenance of sFC and FA of the forceps minor as predictors, alongside p-tau231, increasing the resulting R-squared of the model to 0.389. Notably, their influences on dFC are independent of p-tau231 and show significant associations with dFC both when included in the model and when addressed through separated correlation analyses: a direct association for sFC and an inverse one for the FA of the forceps minor (Figure 3.3). The inclusion of these plasma, functional, and structural variables in the models, as well as the direction of their association with dFC, suggest that the increase observed in relation to p-tau231 in frontotemporal regions is of pathological nature and begins early on. Prior research indicates that sFC increases during the initial phases of AD and in association with p-tau231 (García-Colomo, Nebreda, et al., 2024), and extensive literature links FA reductions with AD progression (Lo Buono et al., 2020). Our findings highlight a complex interplay among these biomarkers, with dFC being the only parameter correlating significantly with p-tau231. This underscores the importance of studying brain dynamics as a potential early biomarker for detection of individuals entering the AD continuum.

Some limitations must be noted. While this study seeks to develop the knowledge around the initial stages of AD, and our study is a pioneer in the follow-up of high-risk individuals within the specific age range where early pathological signs are expected to occur, a longer follow-up period is required to correctly classify cases and controls. Relevantly, this study is part of an initiative aimed at tracking these individuals for decades, with the third time point assessment already approved and funded. Further, future assessment rounds should include other standardized and widely accepted techniques to directly quantify AD pathology to adequately evaluate the relationship between connectivity parameters and the levels of pathology markers. Nonetheless, plasma p-tau231 might represent an alternative and more ecological marker that is also less invasive, widely accessible to researchers and clinicians, and more cost-efficient. On the other hand, the use of a sliding-window of a fixed size does not come without disadvantages, given that recent approaches have demonstrated that dFC can be well-described at a variety of time-scales, and there may be a mismatch between the temporal scale of the underlying fluctuations and the predefined fixed window length. However, previous literature addressing the frequency bands under study in the present work have described relevant sFC features in the AD continuum (García-Colomo, Nebreda, et al., 2024; López-Sanz et al., 2017; Ramírez-Toraño et al., 2021) with 4-second windows, which have also been recommended for the estimation of fluctuations in FC of resting state networks (Liuzzi et al., 2019). Finally, more research is needed, combining electrophysiological measures and fMRI, as well as using different dFC estimation techniques, in order to get a better understanding of the underlying neural alterations that induce the dFC changes.

3.6 Conclusion

Overall, our study takes a pioneering approach to study alterations in the dynamics of brain connectivity associated with the plasma pathology marker, p-tau231, in cognitively unimpaired individuals. Our results are innovative, as this is the first work to address dFC in healthy individuals using plasma markers and MEG. Moreover, they are consistent and

expand upon previous literature, suggesting that changes associated to AD pathology can be observed very early on using dFC, which might be more sensitive to subtle alterations than sFC, where these might be lost in the averaging process. Lastly, this early increase in dFC in frontotemporal regions appears to have a pathological nature given its relationship with other plasma, functional and structural measures.

References

2024 Alzheimer's disease facts and figures. (2024). *Alzheimer's & Dementia*, *20*(5), 3708–3821. https://doi.org/10.1002/alz.13809

Ashton, N. J., Benedet, A. L., Pascoal, T. A., Karikari, T. K., Lantero-Rodriguez, J., Brum, W. S., Mathotaarachchi, S., Therriault, J., Savard, M., Chamoun, M., Stoops, E., Francois, C., Vanmechelen, E., Gauthier, S., Zimmer, E. R., Zetterberg, H., Blennow, K., & Rosa-Neto, P. (2022). Cerebrospinal fluid p-tau231 as an early indicator of emerging pathology in Alzheimer's disease. *eBioMedicine*, *76*, 103836. https://doi.org/10.1016/j.ebiom.2022.103836

Ashton, N. J., Pascoal, T. A., Karikari, T. K., Benedet, A. L., Lantero-Rodriguez, J., Brinkmalm, G., Snellman, A., Schöll, M., Troakes, C., Hye, A., Gauthier, S., Vanmechelen, E., Zetterberg, H., Rosa-Neto, P., & Blennow, K. (2021). Plasma p-tau231: A new biomarker for incipient Alzheimer's disease pathology. *Acta Neuropathologica*, *141*(5), 709–724. https://doi.org/10.1007/s00401-021-02275-6

Battaglia, D., Boudou, T., Hansen, E. C., Lombardo, D., Chettouf, S., Daffertshofer, A., McIntosh, A. R., Zimmermann, J., Ritter, P., & Jirsa, V. (2020). Dynamic Functional Connectivity between order and randomness and its evolution across the human adult lifespan. *NeuroImage*, *222*, 117156. https://doi.org/10.1016/j.neuroimage.2020.117156

Briels, C. T., Schoonhoven, D. N., Stam, C. J., de Waal, H., Scheltens, P., & Gouw, A. A. (2020). Reproducibility of EEG functional connectivity in Alzheimer's disease. *Alzheimer's Research & Therapy*, *12*(1), 68. https://doi.org/10.1186/s13195-020-00632-3

Bullmore, E., Suckling, J., Overmeyer, S., Rabe-Hesketh, S., Taylor, E., & Brammer, M. (1999). Global, voxel, and cluster tests, by theory and permutation, for a difference between two groups of structural MR images of the brain. *IEEE Transactions on Medical Imaging*, *18*(1), 32–42. https://doi.org/10.1109/42.750253

Canter, R. G., Penney, J., & Tsai, L.-H. (2016). The road to restoring neural circuits for the treatment of Alzheimer's disease. *Nature*, *539*(7628), 187–196. https://doi.org/10.1038/nature20412

Carrasco-Gómez, M., García-Colomo, A., Cabrera-Álvarez, J., Bruña, R., Santos, A., & Maestú, F. (2024). Dynamics of brain connectivity across the alzheimer's disease spectrum: A magnetoencephalography study. *bioRxiv*, 2024–03.

Chatterjee, S., & Hadi, A. S. (2012). *Regression analysis by example* (Fifth edition). Wiley. Includes index.

Colclough, G., Woolrich, M., Tewarie, P., Brookes, M., Quinn, A., & Smith, S. (2016). How reliable are MEG resting-state connectivity metrics? *NeuroImage*, *138*, 284–293. https://doi.org/10.1016/j.neuroimage.2016.05.070

Córdova-Palomera, A., Kaufmann, T., Persson, K., Alnæs, D., Doan, N. T., Moberget, T., Lund, M. J., Barca, M. L., Engvig, A., Brækhus, A., Engedal, K., Andreassen, O. A., Selbæk, G., & Westlye, L. T. (2017). Disrupted global metastability and static and dynamic brain connectivity across individuals in the Alzheimer's disease continuum. *Scientific Reports*, *7*(1), 40268. https://doi.org/10.1038/srep40268

De Groot, M., Vernooij, M. W., Klein, S., Ikram, M. A., Vos, F. M., Smith, S. M., Niessen, W. J., & Andersson, J. L. (2013). Improving alignment in Tract-based spatial statistics: Evaluation and optimization of image registration. *NeuroImage*, *76*, 400–411. https://doi.org/10.1016/j.neuroimage.2013.03.015

De Haan, W., Mott, K., Van Straaten, E. C. W., Scheltens, P., & Stam, C. J. (2012). Activity Dependent Degeneration Explains Hub Vulnerability in Alzheimer's Disease (O. Sporns, Ed.). *PLoS Computational Biology*, *8*(8), e1002582. https://doi.org/10.1371/journal.pcbi.1002582

Donix, M., Small, G. W., & Bookheimer, S. Y. (2012). Family History and APOE-4 Genetic Risk in Alzheimer's Disease. *Neuropsychology Review*, *22*(3), 298–309. https://doi.org/10.1007/s11065-012-9193-2

Engels, M. M., Stam, C. J., Van Der Flier, W. M., Scheltens, P., De Waal, H., & Van Straaten, E. C. (2015). Declining functional connectivity and changing hub locations in Alzheimer's disease: An EEG study. *BMC Neurology*, *15*(1), 145. https://doi.org/10.1186/s12883-015-0400-7

Escrichs, A., Biarnes, C., Garre-Olmo, J., Fernández-Real, J. M., Ramos, R., Pamplona, R., Brugada, R., Serena, J., Ramió-Torrentà, L., Coll-De-Tuero, G., Gallart, L., Barretina, J., Vilanova, J. C., Mayneris-Perxachs, J., Essig, M., Figley, C. R., Pedraza, S., Puig, J., & Deco, G. (2021). Whole-Brain Dynamics in Aging: Disruptions in Functional Connectivity and the Role of the Rich Club. *Cerebral Cortex*, *31*(5), 2466–2481. https://doi.org/10.1093/cercor/bhaa367

Fischl, B. (2012). FreeSurfer. *NeuroImage*, *62*(2), 774–781. https://doi.org/10.1016/j.neuroimage.2012.01.021

Garcés, P., López-Sanz, D., Maestú, F., & Pereda, E. (2017). Choice of Magnetometers and Gradiometers after Signal Space Separation. *Sensors*, *17*(12), 2926. https://doi.org/10.3390/s17122926

García-Colomo, A., López-Sanz, D., Stam, C. J., Hillebrand, A., Carrasco-Gómez, M., Spuch, C., Comis-Tuche, M., & Maestú, F. (2024). Minimum spanning tree analysis of unimpaired individuals at risk of alzheimer's disease. *Brain Communications*, fcae283.

García-Colomo, A., Nebreda, A., Carrasco-Gómez, M., De Frutos-Lucas, J., Ramirez-Toraño, F., Spuch, C., Comis-Tuche, M., Bruña, R., Alfonsín, S., & Maestú, F. (2024). Longitudinal changes in the functional connectivity of individuals at risk of Alzheimer's disease. *GeroScience*, *46*(3), 2989–3003. https://doi.org/10.1007/s11357-023-01036-5

Hu, H., Chen, K.-L., Ou, Y.-N., Cao, X.-P., Chen, S.-D., Cui, M., Dong, Q., Tan, L., & Yu, J.-T. (2019). Neurofilament light chain plasma concentration predicts neurodegeneration and clinical progression in nondemented elderly adults. *Aging*, *11*(17), 6904–6914. https://doi.org/10.18632/aging.102220

Hutchison, R. M., Womelsdorf, T., Allen, E. A., Bandettini, P. A., Calhoun, V. D., Corbetta, M., Della Penna, S., Duyn, J. H., Glover, G. H., Gonzalez-Castillo, J., Handwerker, D. A., Keilholz, S., Kiviniemi, V., Leopold, D. A., De Pasquale, F., Sporns, O., Walter, M., & Chang, C. (2013). Dynamic functional connectivity: Promise, issues, and interpretations. *NeuroImage*, *80*, 360–378. https://doi.org/10.1016/j.neuroimage.2013.05.079

Jones, D. T., Vemuri, P., Murphy, M. C., Gunter, J. L., Senjem, M. L., Machulda, M. M., Przybelski, S. A., Gregg, B. E., Kantarci, K., Knopman, D. S., Boeve, B. F., Petersen, R. C., & Jack, C. R. (2012). Non-Stationarity in the "Resting Brain's" Modular Architecture (Y. He, Ed.). *PLoS ONE*, *7*(6), e39731. https://doi.org/10.1371/journal.pone.0039731

Knuth, K. H. (2019). Optimal data-based binning for histograms and histogram-based probability density models. *Digital Signal Processing*, *95*, 102581. https://doi.org/10.1016/j.dsp.2019.102581

Kudela, M., Harezlak, J., & Lindquist, M. A. (2017). Assessing uncertainty in dynamic functional connectivity. *NeuroImage*, *149*, 165–177. https://doi.org/10.1016/j.neuroimage.2017.01.056

Li, R., Nguyen, T., Potter, T., & Zhang, Y. (2019). Dynamic cortical connectivity alterations associated with Alzheimer's disease: An EEG and fNIRS integration study. *NeuroImage: Clinical*, *21*, 101622. https://doi.org/10.1016/j.nicl.2018.101622

Liuzzi, L., Quinn, A. J., O'Neill, G. C., Woolrich, M. W., Brookes, M. J., Hillebrand, A., & Tewarie, P. (2019). How Sensitive Are Conventional MEG Functional Connectivity Metrics With Sliding Windows to Detect Genuine Fluctuations in Dynamic Functional Connectivity? *Frontiers in Neuroscience*, *13*, 797. https://doi.org/10.3389/fnins.2019.00797

Lo Buono, V., Palmeri, R., Corallo, F., Allone, C., Pria, D., Bramanti, P., & Marino, S. (2020). Diffusion tensor imaging of white matter degeneration in early stage of Alzheimer's disease: A review. *International Journal of Neuroscience*, *130*(3), 243–250. https://doi.org/10.1080/00207454.2019.1667798

Lopes da Silva, F. (2013). EEG and MEG: Relevance to Neuroscience. *Neuron*, *80*(5), 1112–1128. https://doi.org/10.1016/j.neuron.2013.10.017

López-Sanz, D., Bruña, R., Garcés, P., Martín-Buro, M. C., Walter, S., Delgado, M. L., Montenegro, M., López Higes, R., Marcos, A., & Maestú, F. (2017). Functional Connectivity Disruption in Subjective Cognitive Decline and Mild Cognitive Impairment: A Common Pattern of Alterations. *Frontiers in Aging Neuroscience*, *9*, 109. https://doi.org/10.3389/fnagi.2017.00109

Lorenzini, L., Ingala, S., Collij, L. E., Wottschel, V., Haller, S., Blennow, K., Frisoni, G., Chételat, G., Payoux, P., Lage-Martinez, P., Ewers, M., Waldman, A., Wardlaw, J., Ritchie, C., Gispert, J. D., Mutsaerts, H. J. M. M., Visser, P. J., Scheltens, P., Tijms, B., … Wink, A. M. (2023). Eigenvector centrality dynamics are related to Alzheimer's disease pathological changes in non-demented individuals. *Brain Communications*, *5*(3), fcad088. https://doi.org/10.1093/braincomms/fcad088

Maestú, F., de Haan, W., Busche, M. A., & DeFelipe, J. (2021). Neuronal excitation/inhibition imbalance: Core element of a translational perspective on Alzheimer pathophysiology. *Ageing Research Reviews*, *69*, 101372. https://doi.org/10.1016/j.arr.2021.101372

Matsui, T., & Yamashita, K.-i. (2023). Static and Dynamic Functional Connectivity Alterations in Alzheimer's Disease and Neuropsychiatric Diseases. *Brain Connectivity*, *13*(5), 307–314. https://doi.org/10.1089/brain.2022.0044

Mattsson, N., Palmqvist, S., Stomrud, E., Vogel, J., & Hansson, O. (2019). Staging β -Amyloid Pathology With Amyloid Positron Emission Tomography. *JAMA Neurology*, *76*(11), 1319. https://doi.org/10.1001/jamaneurol.2019.2214

McKhann, G. M., Knopman, D. S., Chertkow, H., Hyman, B. T., Jack, C. R., Kawas, C. H., Klunk, W. E., Koroshetz, W. J., Manly, J. J., Mayeux, R., Mohs, R. C., Morris, J. C., Rossor, M. N., Scheltens, P., Carrillo, M. C., Thies, B., Weintraub, S., & Phelps, C. H. (2011). The diagnosis of dementia due to Alzheimer's disease: Recommendations from the National Institute on Aging-Alzheimer's Association workgroups on diagnostic guidelines for Alzheimer's disease. *Alzheimer's & Dementia*, *7*(3), 263–269. https://doi.org/10.1016/j.jalz.2011.03.005

Milà-Alomà, M., Ashton, N. J., Shekari, M., Salvadó, G., Ortiz-Romero, P., Montoliu-Gaya, L., Benedet, A. L., Karikari, T. K., Lantero-Rodriguez, J., Vanmechelen, E., Day, T. A., González-Escalante, A., Sánchez-Benavides, G., Minguillon, C., Fauria, K., Molinuevo, J. L., Dage, J. L., Zetterberg, H., Gispert, J. D., … Blennow, K. (2022). Plasma p-tau231 and p-tau217 as state markers of amyloid-β pathology in preclinical Alzheimer's disease. *Nature Medicine*. https://doi.org/10.1038/s41591-022-01925-w

Mizuno, T., Takahashi, T., Cho, R. Y., Kikuchi, M., Murata, T., Takahashi, K., & Wada, Y. (2010). Assessment of EEG dynamical complexity in alzheimer's disease using multiscale entropy. *Clinical Neurophysiology*, *121*(9), 1438–1446. https://doi.org/10.1016/j.clinph.2010.03.025

Mueller, S. G., & Weiner, M. W. (2017). Amyloid Associated Intermittent Network Disruptions in Cognitively Intact Older Subjects: Structural Connectivity Matters. *Frontiers in Aging Neuroscience*, *9*, 418. https://doi.org/10.3389/fnagi.2017.00418

Nakamura, A., Cuesta, P., Kato, T., Arahata, Y., Iwata, K., Yamagishi, M., Kuratsubo, I., Kato, K., Bundo, M., Diers, K., Fernández, A., Maestú, F., & Ito, K. (2017). Early functional network alterations in asymptomatic elders at risk for Alzheimer's disease. *Scientific Reports*, *7*(1), 6517. https://doi.org/10.1038/s41598-017-06876-8

Nolte, G. (2003). The magnetic lead field theorem in the quasi-static approximation and its use for magnetoencephalography forward calculation in realistic volume conductors. *Physics in Medicine and Biology*, *48*(22), 3637–3652. https://doi.org/10.1088/0031-9155/48/22/002

Núñez, P., Poza, J., Gómez, C., Rodríguez-González, V., Hillebrand, A., Tewarie, P., Tola-Arribas, M. Á., Cano, M., & Hornero, R. (2021). Abnormal meta-state activation of dynamic brain networks across the Alzheimer spectrum. *NeuroImage*, *232*, 117898. https://doi.org/10.1016/j.neuroimage.2021.117898

Núñez, P., Poza, J., Gómez, C., Rodríguez-González, V., Hillebrand, A., Tola-Arribas, M. A., Cano, M., & Hornero, R. (2019). Characterizing the fluctuations of dynamic resting-state electrophysiological functional connectivity: Reduced neuronal coupling variability in mild cognitive impairment and dementia due to Alzheimer's disease. *Journal of Neural Engineering*, *16*(5), 056030. https://doi.org/10.1088/1741-2552/ab234b

O'Neill, G. C., Barratt, E. L., Hunt, B. A. E., Tewarie, P. K., & Brookes, M. J. (2015). Measuring electrophysiological connectivity by power envelope correlation: A technical

review on MEG methods. *Physics in Medicine and Biology*, *60*(21), R271–R295. https://doi.org/10.1088/0031-9155/60/21/R271

Oostenveld, R., Fries, P., Maris, E., & Schoffelen, J.-M. (2011). FieldTrip: Open Source Software for Advanced Analysis of MEG, EEG, and Invasive Electrophysiological Data. *Computational Intelligence and Neuroscience*, *2011*, 1–9. https://doi.org/10.1155/2011/156869

Peraza, L. R., Cromarty, R., Kobeleva, X., Firbank, M. J., Killen, A., Graziadio, S., Thomas, A. J., O'Brien, J. T., & Taylor, J.-P. (2018). Electroencephalographic derived network differences in Lewy body dementia compared to Alzheimer's disease patients. *Scientific Reports*, *8*(1), 4637. https://doi.org/10.1038/s41598-018-22984-5

Pusil, S., López, M. E., Cuesta, P., Bruña, R., Pereda, E., & Maestú, F. (2019). Hypersynchronization in mild cognitive impairment: The 'X' model. *Brain*, *142*(12), 3936–3950. https://doi.org/10.1093/brain/awz320

Ramírez-Toraño, F., Bruña, R., De Frutos-Lucas, J., Rodríguez-Rojo, I. C., Marcos De Pedro, S., Delgado-Losada, M. L., Gómez-Ruiz, N., Barabash, A., Marcos, A., López Higes, R., & Maestú, F. (2021). Functional Connectivity Hypersynchronization in Relatives of Alzheimer's Disease Patients: An Early E/I Balance Dysfunction? *Cerebral Cortex*, *31*(2), 1201–1210. https://doi.org/10.1093/cercor/bhaa286

Ranasinghe, K. G., Kudo, K., Hinkley, L., Beagle, A., Lerner, H., Mizuiri, D., Findlay, A., Miller, B. L., Kramer, J. H., Gorno-Tempini, M. L., Rabinovici, G. D., Rankin, K. P., Garcia, P. A., Kirsch, H. E., Vossel, K., & Nagarajan, S. S. (2022). Neuronal synchrony abnormalities associated with subclinical epileptiform activity in early-onset Alzheimer's disease. *Brain*, *145*(2), 744–753. https://doi.org/10.1093/brain/awab442

Ren, P., Ma, M., Xie, G., Wu, Z., & Wu, D. (2020). Altered complexity of resting-state BOLD activity in Alzheimer's disease-related neurodegeneration: A multiscale entropy analysis. *Aging*, *12*(13), 13571–13582. https://doi.org/10.18632/aging.103463

Schultz, A. P., Chhatwal, J. P., Hedden, T., Mormino, E. C., Hanseeuw, B. J., Sepulcre, J., Huijbers, W., LaPoint, M., Buckley, R. F., Johnson, K. A., & Sperling, R. A. (2017). Phases of Hyperconnectivity and Hypoconnectivity in the Default Mode and Salience Networks Track with Amyloid and Tau in Clinically Normal Individuals. *The Journal of Neuroscience*, *37*(16), 4323–4331. https://doi.org/10.1523/JNEUROSCI.3263-16.2017

Sepulcre, J., Sabuncu, M. R., Li, Q., El Fakhri, G., Sperling, R., & Johnson, K. A. (2017). Tau and amyloid β proteins distinctively associate to functional network changes in the aging brain. *Alzheimer's & Dementia*, *13*(11), 1261–1269. https://doi.org/10.1016/j.jalz.2017.02.011

Shannon, C. E. (1948). A Mathematical Theory of Communication. *Bell System Technical Journal*, *27*(3), 379–423. https://doi.org/10.1002/j.1538-7305.1948.tb01338.x

Stam, C. J. (2014). Modern network science of neurological disorders. *Nature Reviews Neuroscience*, *15*(10), 683–695. https://doi.org/10.1038/nrn3801

Statistical Parametric Mapping. (2007). Elsevier. https://doi.org/10.1016/B978-0-12-372560-8.X5000-1

Suárez-Calvet, M., Karikari, T. K., Ashton, N. J., Lantero Rodríguez, J., Milà-Alomà, M., Gispert, J. D., Salvadó, G., Minguillon, C., Fauria, K., Shekari, M., Grau-Rivera, O., Arenaza-Urquijo, E. M., Sala-Vila, A., Sánchez-Benavides, G., González-de-Echávarri, J. M., Kollmorgen, G., Stoops, E., Vanmechelen, E., Zetterberg, H., ... Vilor-Tejedor,

N. (2020). Novel tau biomarkers phosphorylated at T181, T217 or T231 rise in the initial stages of the preclinical Alzheimer's *continuum* when only subtle changes in Aβ pathology are detected. *EMBO Molecular Medicine*, *12*(12), e12921. https://doi.org/10.15252/emmm.202012921

Sun, J., Wang, B., Niu, Y., Tan, Y., Fan, C., Zhang, N., Xue, J., Wei, J., & Xiang, J. (2020). Complexity Analysis of EEG, MEG, and fMRI in Mild Cognitive Impairment and Alzheimer's Disease: A Review. *Entropy*, *22*(2), 239. https://doi.org/10.3390/e22020239

Taulu, S., & Simola, J. (2006). Spatiotemporal signal space separation method for rejecting nearby interference in MEG measurements. *Physics in Medicine and Biology*, *51*(7), 1759–1768. https://doi.org/10.1088/0031-9155/51/7/008

Tissot, C., Therriault, J., Kunach, P., L Benedet, A., Pascoal, T. A., Ashton, N. J., Karikari, T. K., Servaes, S., Lussier, F. Z., Chamoun, M., Tudorascu, D. L., Stevenson, J., Rahmouni, N., Poltronetti, N. M., Pallen, V., Bezgin, G., Kang, M. S., Mathotaarachchi, S. S., Wang, Y.-T., … Rosa-Neto, P. (2022). Comparing tau status determined via plasma pTau181, pTau231 and [18F]MK6240 tau-PET. *eBioMedicine*, *76*, 103837. https://doi.org/10.1016/j.ebiom.2022.103837

Torabi, M., Mitsis, G. D., & Poline, J.-B. (2024). On the variability of dynamic functional connectivity assessment methods. *GigaScience*, *13*, giae009. https://doi.org/10.1093/gigascience/giae009

Tzourio-Mazoyer, N., Landeau, B., Papathanassiou, D., Crivello, F., Etard, O., Delcroix, N., Mazoyer, B., & Joliot, M. (2002). Automated Anatomical Labeling of Activations in SPM Using a Macroscopic Anatomical Parcellation of the MNI MRI Single-Subject Brain. *NeuroImage*, *15*(1), 273–289. https://doi.org/10.1006/nimg.2001.0978

Van Den Heuvel, M. P., & Hulshoff Pol, H. E. (2010). Exploring the brain network: A review on resting-state fMRI functional connectivity. *European Neuropsychopharmacology*, *20*(8), 519–534. https://doi.org/10.1016/j.euroneuro.2010.03.008

Xu, L., & Zhang, W.-J. (2001). Comparison of different methods for variable selection. *Analytica Chimica Acta*, *446*(1-2), 475–481. https://doi.org/10.1016/S0003-2670(01)01271-5

Yang, F., Jiang, X., Yue, F., Wang, L., Boecker, H., Han, Y., & Jiang, J. (2022). Exploring dynamic functional connectivity alterations in the preclinical stage of Alzheimer's disease: An exploratory study from SILCODE. *Journal of Neural Engineering*, *19*(1), 016036. https://doi.org/10.1088/1741-2552/ac542d

Chapter 4

Individual alpha frequency tACS reduces functional connectivity across the default mode network

4.1 Objectives and hypotheses

O.4.1 To observe whether sFC or dFC can be externally influenced by tACS at the individual alpha frequency (IAF), applied over occipito-parietal areas.

Hypotheses: tACS at the IAF will increase sFC at the same frequency band in the DMN, and more specifically in the precuneus.

O.4.2 To investigate if changes in sFC or dFC elicited by tACS are associated with changes in power.

Hypotheses: sFC will correlate along with power, especially in the stimulation areas.

O.4.3 To ascertain if cortical folding in the cortex influences the potential effects of tACS over FC.

This chapter is based on the publication:

Carrasco-Gómez, M., Cabrera-Álvarez, J., García-Colomo, A., del Cerro-León, A., Gómez-Ariza, C. J., Santos, A., & Maestú, F. (2024). Individual alpha frequency tACS reduces functional connectivity across the default mode network. bioRxiv, 2024-08. (Under review in *Neuromodulation: Technology at the Neural Interface*) doi: https://doi.org/10.1101/2024.08.04.606325

4.2 Introduction

The brain shows spatio-temporally organized patterns of activity even when at wakeful rest. During this resting state, the alpha rhythm (8 – 12 Hz) becomes the predominant oscillation over posterior regions (Buzsáki, 2006). The spontaneous emergence of alpha in resting state, and its correlation with performance, has led to the hypothesis that alpha reflects a functional inhibitory role that is key to the allocation of processing resources for environmental stimuli (Jensen and Mazaheri, 2010). In addition to the alpha rhythm, resting state is associated with changes in functional connectivity (FC) understood as statistical relationships between brain signals over time (Friston, 1994, 2011). These functional interactions give rise to brain networks that reflect interregional communication to support cognitive function. The default mode network (DMN) is a key functional network that is active during resting periods and deactivates during task performance (Raichle, 2011). The DMN is involved in memory processing (Menon, 2011) and includes regions such as the medial prefrontal cortex, middle temporal gyrus, the hippocampus, the posterior cingulate cortex (PCC) and the precuneus (PCU), the latter standing out as a hub of the network (Alves et al., 2019; Utevsky et al., 2014). Disruptions in both the alpha rhythms and the DMN have been associated with multiple brain diseases (Babiloni et al., 2009; Canuet et al., 2015; López-Sanz et al., 2016), therefore, their modulation constitutes a potential therapeutic avenue to explore.

Transcranial alternating current stimulation (tACS) is a non-invasive stimulation technique capable of modulating oscillatory activity in the brain and inducing neuroplasticity (Chaieb et al., 2011). Weak alternating electrical currents are applied to the scalp, reaching the brain, influencing neurons' membrane potentials and thus, influencing neuronal probability of activation (Elyamany et al., 2021). As a result, the application of tACS can induce neural entrainment (i.e. the synchronization of an oscillatory system to an external driver) at the frequency of stimulation (Liu et al., 2018). The anatomical and functional complexity of the brain makes the results of neuromodulation highly dependent on the protocol employed (Antal et al., 2008), but it has been observed that entrainment is more likely to occur if the stimulation frequency matches the frequency of the ongoing oscillation (Vogeti et al., 2022) and if the anatomy of the target region is taken into account (Aberra et al., 2020; Cabrera-Álvarez et al., 2023).

Externally applied oscillatory currents can interact with the endogenous alpha rhythm to enhance or disrupt it (De Koninck et al., 2023; Liu et al., 2018). In this line, tACS at the individual alpha frequency (IAF-tACS) has been shown to increase the power of alpha rhythm after stimulation with effects remaining up to 70 minutes after the protocol (Kasten et al., 2016; Zaehle et al., 2010). These after-effects likely involve plastic changes in neuronal circuits (Vossen et al., 2015).

Beyond these effects, cortical modulation may also influence FC. While, to the best of our knowledge, no studies have investigated the effect of tACS on dynamic FC (dFC), recent research suggests that tACS modulates static FC (sFC) in a frequency- and network-specific manner. For instance, occipito-parietal alpha stimulation during resting-state increases sFC specifically in the alpha band and in the regions of the DMN (Clancy et al., 2018; Schwab et al., 2019), which were suggested in the latter to be mediated by changes in alpha power induced

by stimulation (Clancy et al., 2018). In contrast, a 6 Hz stimulation in resting state - when the brain is typically oscillating in alpha - decreases sFC in the DMN (Abellaneda-Pérez et al., 2020), highlighting the variability in tACS effects depending on the stimulation frequency. These modulations of sFC have additionally been shown to enhance cognitive performance when increasing interregional communication through coherence (Helfrich et al., 2014; Kar et al., 2020; Polanía et al., 2012; Preisig et al., 2021; Tan et al., 2019). Therefore, tACS has become a promising tool for modulating sFC both in health and disease, and could help in understanding the nature of both sFC and dFC in a interventionist approach, rather than just observational.

In this study, we aimed to investigate the influence of a personalized IAF-tACS protocol on healthy individuals' dFC and sFC through MEG recordings. According to the aforementioned studies, we expected to find an increased sFC in the participants' DMN after the stimulation, while no direction is assumed for the changes in dFC, due to the lack of literature in the matter. To get a spatially finer analysis, we evaluate FC in the DMN, and subsequently test which links in the DMN might drive the results, if any. We implement two types of FC metrics to investigate both phase and amplitude connectivity parameters. Finally, we relate changes in FC to changes in power in the areas of interest.

4.3 Materials and methods

4.3.1 Study design

The study comprised one tACS session and three magnetoencephalography (MEG) scans, two before (*Pre1* and *Pre2* sessions) and one after the stimulation (*Post* session). We firstly recorded the electrophysiological activity of each participant through two successive 5-min eyes-closed resting-state MEG recordings, with a 10-minute interval between sessions. Two MEG recordings before the stimulation were included to account for any possible variability in the individual alpha-peak frequency (IAF) of the participants. The IAF was derived from each recording using a fast-preprocessing algorithm described in Section 4.3.4, and then averaged. Statistical analyses for the current paper were carried out using the *Pre2* data as the baseline measure since it was closer in time to the stimulation and all participants had experienced a similar situation until that point. Participants were then randomly assigned to either the real stimulation (*stim*) or placebo (*sham*) group, and received 20 min of stimulation at their own IAF with their eyes closed. Immediately after the stimulation, we performed a third MEG recording to measure its effects on the participants. We decided to use a resting-state eyes-closed paradigm given its prominent alpha activity, and previous work on the same kind of stimulation (Wang et al., 2022; Zarubin et al., 2020).

4.3.2 Participants

We recruited 27 (11 female) participants aged between 22 and 55 years from the Center for Cognitive and Computational Neuroscience (C3N) at the Complutense University of Madrid (UCM). The study included only right-handed, native Spanish-speaking participants without any prior neuropsychiatric history or metallic prostheses that could interfere with

neuroimaging and neuromodulation. Additionally, participants with indistinguishable IAF were excluded. We adhered to current guidelines and safety regulations throughout the research and obtained informed consent from each participant before their involvement.

4.3.3 MEG Data acquisition

MEG signals were acquired during 5 min of eyes-closed resting state at 1 kHz sampling rate, using 306 channels (102 magnetometers and 204 gradiometers) whole-head Elekta Neuromag system (Elekta AB, Stockholm, Sweden) located in a magnetically isolated room (VacuumSchmelze GmbH, Hanau, Germany). Using a Fastrak 3D digitizer (Polhemus, Colchester, Vermont), the positions of four head position indicator (HPI) coils attached to the scalp were defined and the shape of each participant's head relative to three anatomical locations (nasion and both preauricular points) was modeled. An online anti-aliasing filter [0.1–330 Hz] was applied during the whole session.

4.3.4 MEG preprocessing and source reconstruction

The Maxfilter software (v.2.2, correlation threshold = 0.9, time window = 10 s) was used to remove the environmental noise in the raw data, using the temporal extension of the signal space separation (tSSS) method with movement compensation (Taulu and Simola, 2006). For further analysis, only data from magnetometers was considered, given the redundancy in gradiometer data after tSSS (Garcés et al., 2017). Physiological and jump artifacts were located using the automatic Fieldtrip software (Oostenveld et al., 2011) and later reviewed by MEG signal experts. Lastly, the clean signal was divided into 4 second-segments and eye-blinks and cardiac artifacts were removed with an independent component analysis (ICA) based on SOBI (Belouchrani et al., 1997). All segments with physiological artifacts were discarded. Preprocessed MEG data was then used to carry out source localization using a Linearly Constrained Minimum Variance (LCMV) beamformer (Van Veen and Buckley, 1988). Since not all subjects had available T1 MRIs, a 1 mm resolution template of healthy adults normalized to the Montreal Neurological Institute (MNI) with a 1 mm voxel size template was used to place the sources inside the brain in a homogeneous grid of 1 cm. Next, both the template and the grid were linearly transformed to fit the head shape of each subject and a local spheres approach was used to define the leadfields and fit the headshape of each subject in the vicinity of each sensor. Using the computed leadfield and the average of all the covariance matrices for each segment, we computed the spatial filter coefficients, which were used to estimate the source-space time-series for each source in all segments. 1210 source positions belonging to 80 regions of interest defined by the automated anatomical labeling atlas (Tzourio-Mazoyer et al., 2002) were identified. The remaining sources are not part of cortical regions defined by the atlas (i.e., white matter, CSF, or subcortical regions) and thus are not considered as source generators of MEG signal (Hämäläinen et al., 1993).

To determine the IAF we used a fast-processing algorithm immediately after the acquisition of the *Pre1* and *Pre2* recordings. Some steps of the aforementioned preprocessing pipeline were omitted to obtain the IAF for the following stimulation in said frequency. Specifically, no tSSS or movement compensation method was applied, and manual revision of artifacts was skipped

as well. ICA was used to remove physiological artifacts and contaminated segments were manually removed. The power spectrum for each magnetometer was calculated using DPSS, and then averaged. The resulting spectra were visually inspected, and the frequency of the power peak in the alpha band (8–12 Hz) was defined as the IAF. The IAFs from sessions *Pre1* and *Pre2* were averaged to determine the final frequency for the neurostimulation procedure.

4.3.5 Neurostimulation

The neurostimulation sessions utilized bipolar tACS with two conductive rubber electrodes (7 cm × 5 cm) positioned at Cz (midline central) and Oz (midline occipital). A microprocessor-controlled device, the NeuroConn DC-StimulatorPlus (Neurocare, Ilmenau, Germany), was used for delivering alternating current. The electrodes were covered with sponges soaked in saline solution. For the *stim* group, stimulation at the IAF was applied during a 20-minute session with a current intensity of 3 mA peak-to-peak. In contrast, participants in the *sham* group were only exposed to stimulation during the fade-in and fade-out periods, each lasting 30 seconds. Figure 4.1 shows the maximum elicited electric field as simulated with ROAST (Huang et al., 2019). After completing the stimulation and recording protocols, participants responded to a questionnaire on potential adverse effects of tACS (Brunoni et al., 2011).

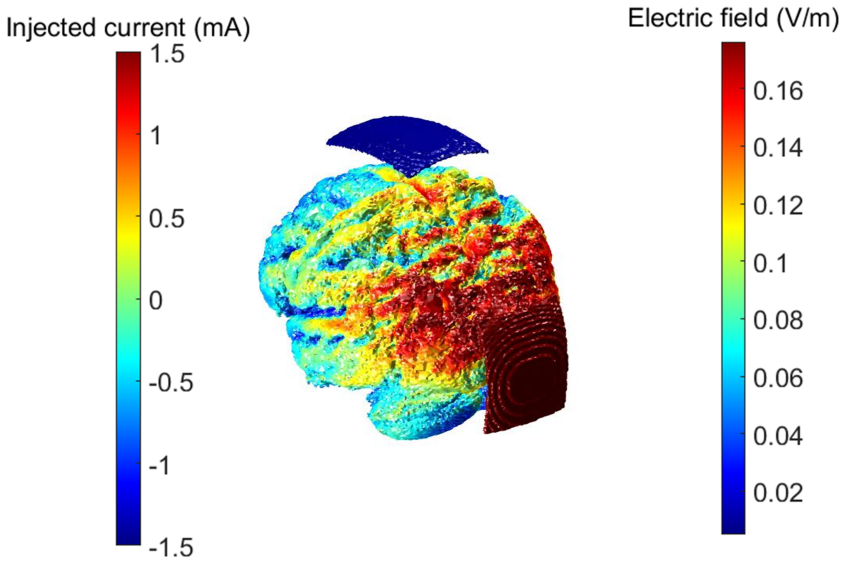


Figure 4.1: tACS maximal electric field distribution. Electric field distribution was estimated with ROAST Huang et al., 2019.

4.3.6 Functional connectivity

FC was estimated through phase and amplitude synchrony parameters after zero-phase filtering the data in the IAF ± 2 Hz frequency band through a finite impulse response filter with an order of 1800, designed with a Hamming window.

Static functional connectivity

For phase-derived connectivity, the corrected imaginary phase locking value (ci-PLV; Bruña et al., 2018) was used because of its insensitivity to volume conduction, PLV's test-retest reliability (Oostenveld et al., 2011) and ci-PLV's comparability to other phase-lag connectivity measures at group-level repeatability (Colclough et al., 2016). On the other hand, amplitude-derived connectivity was calculated through the amplitude envelope correlation with leakage correction (AEC-c; O'Neill et al., 2015) between the time series of each pair of the 1210 cortical sources. After orthogonalization, making it insensitive to volume conduction, the absolute value of the Pearson correlation between the time series' envelopes was used. AEC-c was chosen because of its reliability, and within and between subject consistency (Colclough et al., 2016). Both of these FC parameters range from 0 to 1, that is, no connectivity to full connectivity.

We calculated AEC-c and ci-PLV in each of the defined signal segments, and then averaged over those, obtaining the so-called static FC (sFC), resulting in connectivity matrices of dimension 1210 sources $\times$ 1210 sources. These matrices were then reduced to 40 ROIs $\times$ 40 ROIs by grouping sources according to their position in the automated anatomical labeling atlas (Tzourio-Mazoyer et al., 2002), resulting in 1210 cortical sources distributed across 40 regions of interest (80 unilateral regions grouped in bilateral analogues).

Dynamic functional connectivity

In order to assess dynamic FC (dFC), we calculated the entropy of the FC timecourse both for ci-PLV and for AEC-c, following the same methodology applied in Chapter 3. Importantly, instead of calculating it over the connectivity nodal strength, we obtained it for the connectivity between each pair of sources, obtaining matrices of 1210 sources $\times$ 1210 sources. Finally, and equally as for sFC parameters, the connectivity matrices were reduced to matrices of dimensions 40 ROIs $\times$ 40 ROIs.

4.3.7 Statistical analyses

Initially, demographic characteristics were evaluated, using an independent sample t-test to compare age and IAF, as well as a chi-square test to compare sex proportion between each of the groups. We also performed a baseline (*Pre2*) comparison of FC at the DMN between the *stim* and *sham* groups.

To evaluate the influence of the stimulation protocol on sFC and dFC, we performed two types of t-tests: (1) independent samples t-tests to compare the FC changes in *stim* versus *sham* groups, using a measure of their FC ratio of change; (2) repeated measures t-test to evaluate the change in FC between the *Pre2* and *Post* per experimental group.

For the former, FC ratio of change was calculated by dividing the FC of the *Post* session of each subject by that of the *Pre2* session. Next, we calculated the logarithm of the ratio to eliminate the statistical asymmetry of ratios and obtain statistical distributions centered in 0, where negative values represent decreases and positive values represent increases over recording sessions:

$$FC_{ratio} = \log\left(\frac{FC_{Post}}{FC_{Pre2}}\right) \tag{4.1}$$

As a clarification, all analyses were performed comparing *stim* vs *sham* groups, and *Post* vs *Pre2* stages, so that a positive Cohen's d or t-statistic would represent increased FC values in the *stim* group or *Post* stage.

Firstly, we evaluated the FC at the DMN, defined as including the following AAL regions (Raichle, 2015): superior frontal gyrus (SFG), gyrus rectus (Rectus), hippocampus (Hip), anterior cingulate cortex (ACC), posterior cingulate cortex (PCC), inferior parietal gyrus (IPG), and the precuneus (PCU). To do so, we carrried the aforementioned statistical comparisons for the DMN intraconnectivity (DMN-DMN), and the connectivity between the DMN and the rest of the brain (DMN-AAL). The set of tests were FDR corrected with a q = 0.1 to compensate for the multiple comparisons (Benjamini and Hochberg, 1995).

Secondly, in order to evaluate which areas of the DMN drive the differences in connectivity change between the *stim* and *sham* groups, we conducted post-hoc t-tests comparing the FC ratio at each link between any two areas belonging to the DMN. Given the high number of comparisons, post-hoc results were FDR corrected with a q of 0.1 as well.

Lastly, we aimed to study the relationship between the FC ratios and simultaneous alterations in relative power given the previously suggested capacity of tACS to alter power (Cabrera-Álvarez et al., 2023; Zaehle et al., 2010). To do this, we performed a Pearson's correlation between the FC ratio of those DMN links that showed significant differences in the stim-sham comparison after FDR correction, and the ratio of IAF ± 2Hz relative power of the regions that make up the link (e.g. supposing the ACC-PCC link's FC ratio showed significant differences between groups, the FC ratio would be correlated with the power ratio of both the ACC and PCC), independently. This analysis was carried out separately for the *stim* and *sham* groups, and their rhos were compared through a Z-test on Fisher Z-transformed correlation coefficients (Hinkle et al., 1988).

4.3.8 Simulation of tACS phase-shifts effects on sFC

We performed an ad-hoc theoretical analysis to investigate the potential effects of cortical morphology over sFC modulation. Given our current stimulation protocol and cortical folding, the neurons of certain regions may receive the stimulation in antiphase fashion, as the electric field direction may result anti-parallel to some cortical columns (i.e., hyperpolarizing) and parallel to others (Cabrera-Álvarez et al., 2023), as shown in Figure 4.7. To evaluate the effect of this phase disparities over sFC, we simulated two MEG signals through filtered white noise and calculated their initial connectivity through PLV and AEC. Afterwards, we added a sinusoidal stimulus to each of them with different phase shifts and calculated again PLV and AEC. This procedure was repeated 100 times.

A repeated measures t-test was performed to compare the connectivity values between the cases of no-stimulation, sinusoid stimulation with 0 phase shift, and sinusoid stimulation

with π phase shift. Supplementary material C.2 explains the complete methodology for the simulation process.

Table 4.1: Sample demographics. The differences in each of the demographic variables are shown in the two rightmost columns, displaying the t-statistic or chi-square statistic for continuous and categorical variables, respectively, and p-value.

		Stim	*Sham*	Stat	p-value
Age		33.4 ± 8.4	32.2 ± 9.0	0.3940	0.7302
Sex		9M / 5F	6M / 6F	0.5403	0.4623
IAF		10.3 ± 0.9	10.5 ± 1.3	-0.5741	0.5713
Pre2 DMN	sFC	0.202 ± 0.004	0.0203 ± 0.003	-0.3886	0.7010
AEC-c	dFC	1.5676 ± 0.084	1.561 ± 0.076	0.2041	0.8400
Pre2 DMN	sFC	0.169 ± 0.007	0.170 ± 0.005	-0.2887	0.7753
ci-PLV	dFC	1.666 ± 0.053	1.667 ± 0.038	-0.0790	0.9377

4.4 Results

4.4.1 Sample demographics and adverse tACS effects

Sample demographics and variables of interest used in this study are shown in Table 4.1, and reported tACS effects are depicted in Supplementary Table C.1. No statistically significant differences were observed between the groups either in demographics or tACS adverse aftereffects, or in baseline FC.

4.4.2 DMN's sFC decreases through tACS, while dFC increases in both *stim* and *sham*

To assess the effect of tACS on the DMN's FC, we performed independent samples ratio t-tests comparing the FC change between *stim* and *sham* groups. Then, we performed repeated measures t-tests to evaluate statistically the change from *Pre2* to *Post* stimulation for each group. Two spatial relationships were considered, including the DMN-DMN and the DMN-AAL. FDR correction (q = 0.1, $n_{comparisons}$ = 24) yielded a critical p-value of 0.0194.

The comparisons of the ratio of change in AEC-c sFC between experimental conditions showed a significant difference between both groups in the two spatial relationships (Figure 4.2A and 4.2B): DMN-DMN [t-stat = -2.8614, d-Cohen = -1.1257, p-value = 0.0086], and DMN-AAL [t-stat = -2.7104, d-Cohen = -1.0663, p-value = 0.0122]. Repeated-measures t-tests revealed significant decreases in AEC-c sFC between the *Post* and *Pre2* sessions in the *stim* group for each of the two spatial relationships (Figure 4.2A and 4.2B): DMN-DMN [t-stat = -3.9109, d-Cohen = -0.6383, p-value = 0.0018], and DMN-AAL [t-stat = -3.2451, d-Cohen = - 0.3966, p-value = 0.0064]. However, no significant differences were observed in the *sham* group: DMN-DMN [t-stat = 0.6828, d-Cohen = 0.1456, p-value = 0.5089]; DMN-AAL [t-stat = 1.1133, d-Cohen = 0.2365, p-value = 0.2893].

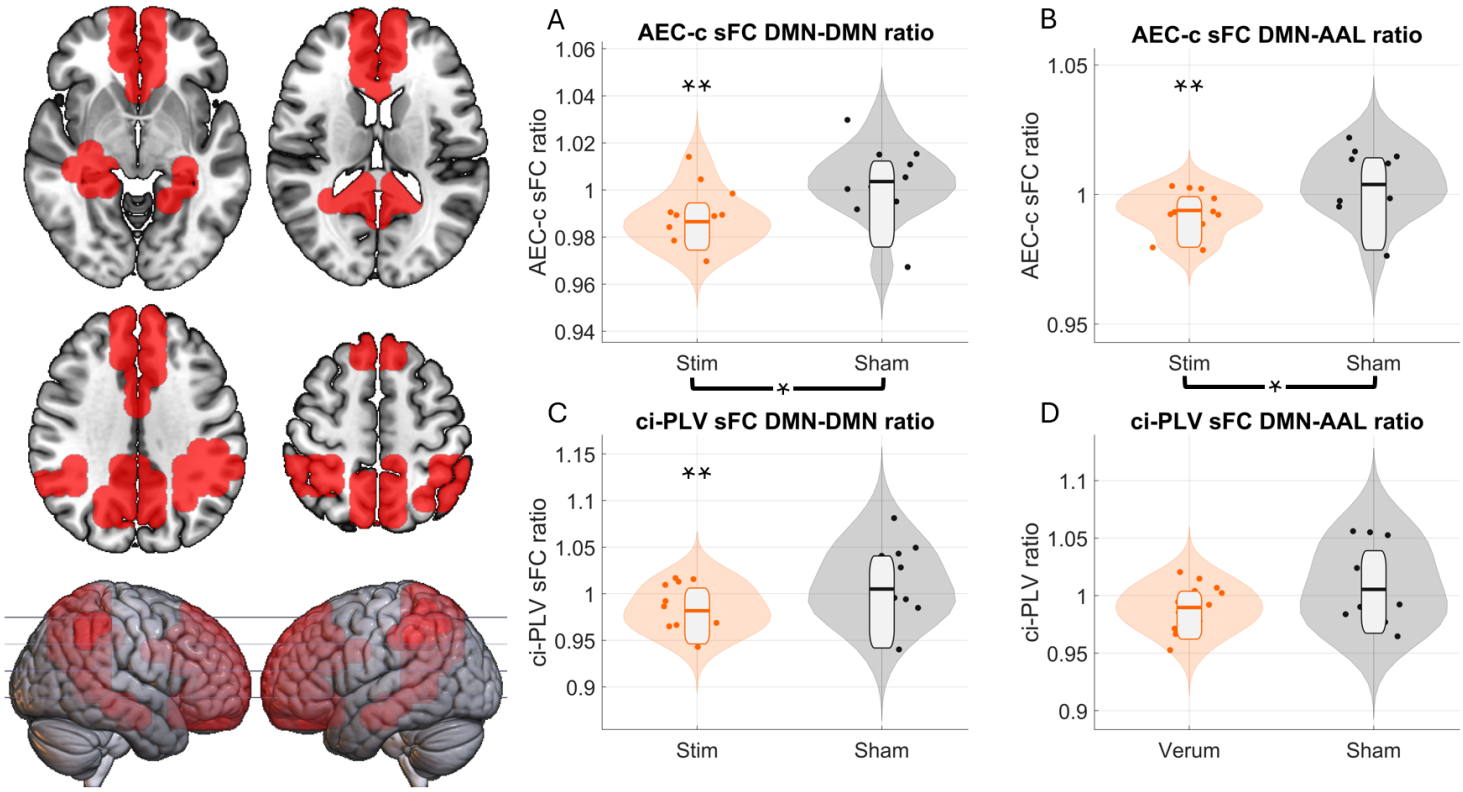


Figure 4.2: DMN AEC-c sFC decreases due to tACS. Violin plots show the *Post/Pre2* sFC ratio of DMN intraconnectivity (A and C), and between DMN and the rest of the brain (B and D). Significant reductions of sFC between the *stim* and *sham* groups were detected with AEC-c (A and B), as noted by the single asterisks (*) and the brackets below the graphs. At the same time, the *stim* group showed significant intra-group decreases of AEC-c and ci-PLV sFC for DMN intraconnectivity (A and C, respectively), and of AEC-c sFC between the DMN and the rest of the brain (B), as indicated by the double asterisks (**) above their violin plots.

Secondly, changes in the ci-PLV sFC of the *stim* group, relative to those in the *sham* group, showed decreases in the former that were close to statistical significance, both in DMN-DMN [t-stat = -2.0171, d-Cohen = -0.7935, p-value = 0.0550] and DMN-AAL [t-stat = -1.8447, d-Cohen = -0.7257, p-value = 0.0775], as depicted in Figure 4.2C and 4.2D. Repeated-measures t-tests revealed significant ci-PLV decreases between the *Post* and *Pre2* sessions in the *stim* group for DMN-DMN [t-stat = -2.6658, d-Cohen = -0.4207, p-value = 0.0194], and close to significance In the case of the DMN-AAL connectivity [t-stat = -2.0841, d-Cohen = -0.2776, p-value = 0.0574]. No significant differences were observed in the *sham* group (DMN-DMN [t-stat = 0.8127, d-Cohen = 0.2132, p-value = 0.4336]; DMN-AAL [t-stat = 0.9598, d-Cohen = 0.2091, p-value = 0.3578]).

On the other hand, a different behaviour was observed in AEC-c dFC measures. No differences were found between groups in any of the spatial configurations: DMN-DMN [t-stat = -0.4929, d-Cohen = -0.1939, p-value = 0.6265], and DMN-AAL [t-stat = 0.5449, d-Cohen = 0.2144, p-value = 0.5909]. Nevertheless, significant intra-group increases were found in both *stim* (DMN-DMN [t-stat = 3.4317, d-Cohen = 0.4755, p-value = 0.0045], and DMN-AAL [t-stat

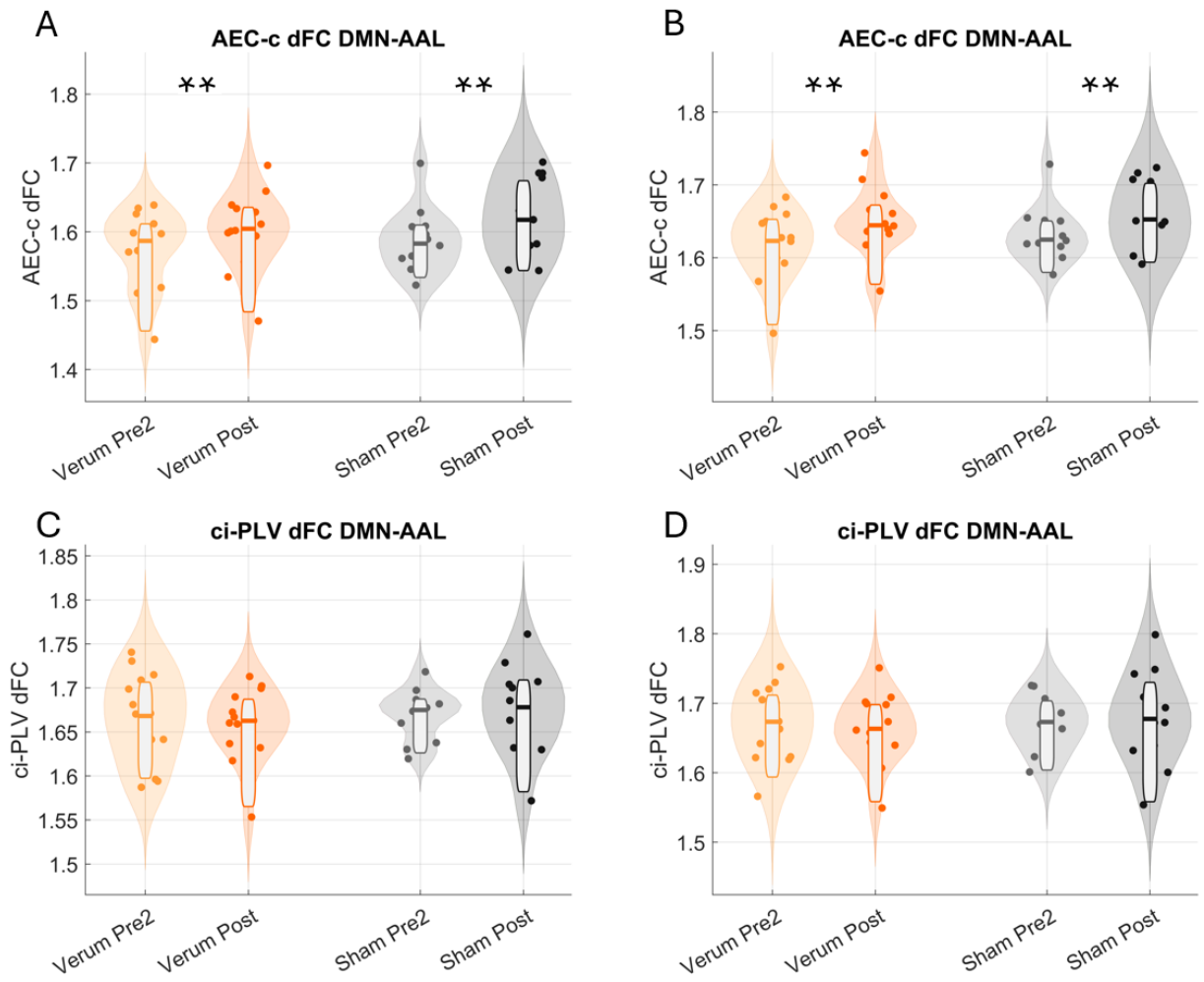


Figure 4.3: DMN AEC-c dFC increases in both *stim* and *sham* groups. Violin plots show the *Post/Pre2* sFC ratio of DMN intraconnectivity (A and C), and between DMN and the rest of the brain (B and D). Significant reductions of sFC between the *stim* and *sham* groups were detected with AEC-c (A and B), as noted by the single asterisks (*) and the brackets below the graphs. At the same time, the *stim* group showed significant intra-group decreases of AEC-c and ci-PLV sFC for DMN intraconnectivity (A and C, respectively), and of AEC-c sFC between the DMN and the rest of the brain (B), as indicated by the double asterisks (**) above their violin plots.

= 5.4827, d-Cohen = -0.6145, p-value = 0.0001]) and *sham* (DMN-DMN [t-stat = 3.2022, d-Cohen = 0.6615, p-value = 0.0084], and DMN-AAL [t-stat = 2.9012, d-Cohen = 0.5813, p-value = 0.0144]) groups, as shown in Figure 4.3A and B.

Finally, no significant differences, be it between-groups or intra-group, were found for ci-PLV dFC parameters. A complete statistical report on the results presented in this section can be found in Table C.2. Since no between-group differences were found for dFC parameters, meaning that we cannot ascertain whether tACS had an effect on dFC or not, only sFC measures were included in the following analyses.

4.4.3 tACS prominently decreases sFC at posterior-posterior and antero-posterior hub links of the DMN

Additional statistical tests were performed to identify the links of the DMN driving the decreases in sFC presented in the previous sections. Given the high number of comparisons ($n_{comparisons}$ = 28), results were FDR-corrected per connectivity measure with a q = 0.1, which yielded a critical p-value of 0.0244 for AEC-c, and no critical value for ci-PLV, since no results survived FDR.

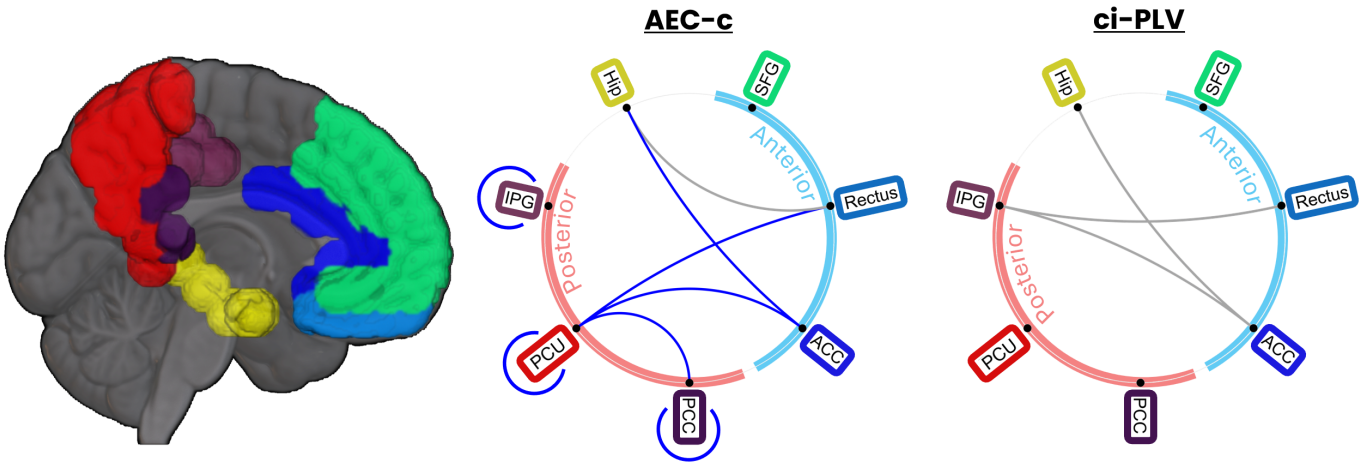


Figure 4.4: DMN links show a significant decrease in AEC-c sFC after tACS. Ratio t-tests revealed 8 DMN links showing a significant AEC-c sFC reduction and 3 showing a significant ci-PLV sFC reduction when comparing *stim* and *sham* groups. Of those, 7 AEC-c links still showed significance after FDR correction (q = 0.1), while no ci-PLV links survived. Links significant after FDR correction are indicated in blue, while those that lost significance are indicated in grey.

Out of the 28 possible links, 7 showed statistically significant differences using AEC-c including Hip-ACC, IPG-IPG, PCC-PCC, PCU-Rectus, PCU-PCC, PCU-ACC, and PCU-PCU (Figure 4.4) after FDR correction. These differences were in the same direction as reported previously (i.e., a decrease in the FC of the *stim* group). No ci-PLV link difference was significantly different after FDR. Supplementary Tables C.3 and C.4 include a complete statistical report for the 28 possible links in both connectivity metrics for AEC-c and ci-PLV, respectively.

4.4.4 Static functional connectivity of posterior areas correlate with power change

To understand the relationship between sFC and power changes elicited by the stimulation, we performed a post-hoc analysis correlating the AEC-c sFC ratio of the significant links reported in the previous section and the relative power of the IAF ± 2Hz of each area involved. This represented 11 Pearson's correlations per group, as self-connections (e.g., PCU-PCU) involved one test, while inter-regional connections (e.g., PCU-PCC) involved two.

Out of the seven links studied, two of them showed significant negative correlations between FC and power ratios in the *stim* group: PCU-PCU and PCU-PCC correlating with both

regions relative power (Figure 4.5). Nevertheless, the only case that exhibited a significantly different correlation pattern between *stim* and *sham* groups was that between the PCC-PCU's FC and the normalized power of the PCU [z-stat = -2.3703, p-value = 0.0178]. Importantly, no differences in the relative power in the IAF ± 2 Hz band were found between the *stim* and *sham* groups in any of the studied regions.

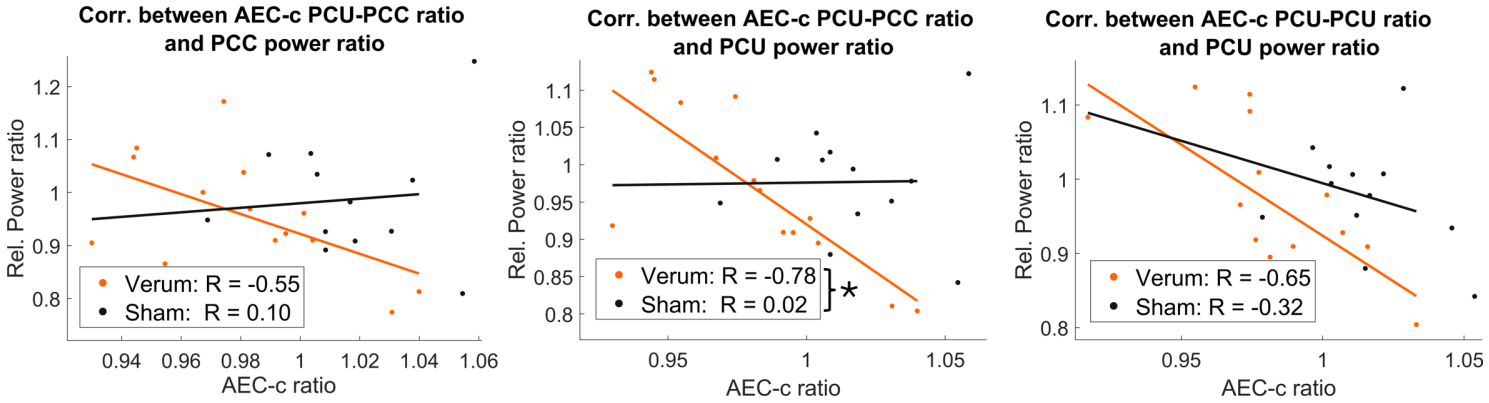


Figure 4.5: Negative correlations between AEC-c sFC ratio in posterior areas and IAF ± 2 Hz relative power ratio. Significant correlations between AEC-c and relative power in the *stim* group (orange) were found in posterior regions, while these correlations were nonsignificant in the *sham* group (black). However, only the correlation between the PCC-PCU sFC ratio and the IAF ± 2 Hz relative power ratio at the PCU was able to significantly differentiate between the *stim* and *sham* groups, as indicated by a single asterisk (*).

4.4.5 Simulating tACS-induced phase disparities explain reductions in sFC

As stated in the introduction, while we expected to observe an increase in FC after the stimulation protocol, the results showed a generalized decrease in FC in the *stim* group. In order to understand further these results, we studied the potential interaction of cortical morphology with the stimulation protocol. Given the brain cortical folding, the neurons of certain regions may receive the stimulation in anti-phase, as the electric field direction may result antiparallel to some cortical columns (i.e., hyper-polarizing effect) and parallel to others (see Figure 4.7). Therefore, we performed a theoretical experiment by introducing phase disparities in two simulated MEG signals and measuring the resulting FC.

We found that any phase shift between the stimuli deviating from 0 or 2π phase produced a decrease in connectivity both for PLV and AEC, as shown in Figure 4.6. Specifically, significant differences in connectivity values both for PLV [t-stat = 4.7082, p-value = 0.0011], and AEC [t-stat = 7.3485, p-value < 0.0001] emerged when comparing the cases of no stimulation and anti-phase stimulation (phase = π). No significant differences were found when comparing connectivity in the case of no stimulation and stimulation with in-phase sinusoids both for PLV [t-stat = -1.4465, p-value = 0.1819] and AEC [t-stat = -1.9688, p-value = 0.0805].

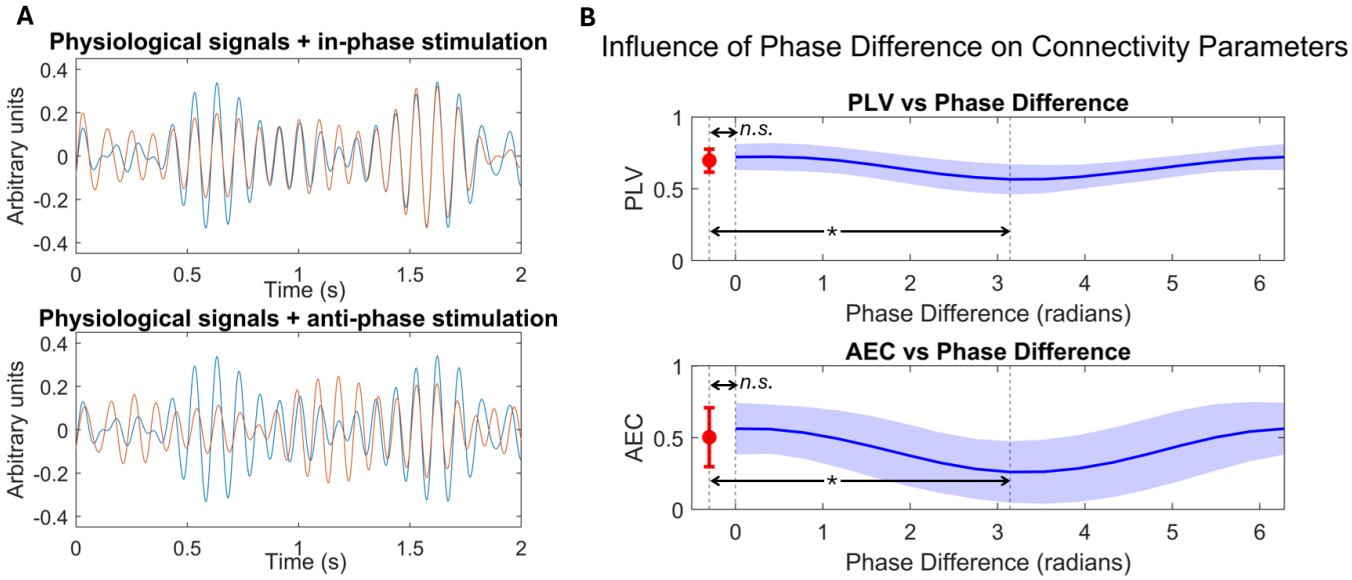


Figure 4.6: Results of the simulation of the effect of phase-shift tACS on FC. (**A**) Physiological signals being stimulated with in-phase stimulation (top), and with antiphase stimulation (bottom). (**B**) Relation between PLV and AEC and the phase difference between stimulation sinusoids. Significant reductions between antiphase stimulation and initial connectivity (red) were found and are indicated by an asterisk. N.s: non-significant.

4.5 Discussion

In this study, we assessed the influence of a parieto-occipital IAF-tACS protocol on FC measured by MEG. Both ci-PLV and AEC-c sFC and dFC were calculated, and the effect of tACS on the DMN connectivity was assessed through intra-group comparisons of FC values between *Pre2* and *Post* stimulation sessions, and between-group comparisons of *Post/Pre2* FC ratio between *stim* and *sham* groups. Between-group comparisons revealed a significantly lower AEC-c sFC ratio in the *stim* group, explained by its significant reduction between the *Pre2* and *Post* sessions. Furthermore, we studied the links of the DMN driving these results, finding a prominent decrease in AEC-c sFC over posterior areas and in the connectivity between postero-anterior hubs of the DMN. Interestingly, we found negative correlations relating the change in AEC-c sFC in posterior DMN areas and the change in power in those same areas. Finally, while no between-group difference in dFC was found, AEC-c dFC increased in both *stim* and *sham* groups between the *Pre2* and *Post* sessions. These results complement and expand previous literature by assessing the influence of personalized tACS on FC in healthy participants.

These results do not support our hypothesis of enhanced sFC after tACS, which was based on previous literature (Clancy et al., 2018; Schwab et al., 2019; Van Schouwenburg et al., 2017). On the one hand, we hypothesize that the reductions in sFC found in this study might be explained by the interaction between the electric field direction and the position of pyramidal neurons along the folded cortex. Where the electric field direction is aligned parallel to the body axis of pyramidal cells, depolarization will be elicited. Inversely, where the alignment is

antiparallel, hyperpolarisation occurs. This introduces phase disparities in the stimulation induced and its intensity (Figure 4.7).

To illustrate the possible effects of these phase disparities over both phase and amplitude sFC, we performed an ad-hoc analysis simulating the influence of tACS over physiological MEG signals. We found that any phase shift between the stimulatory sinusoids deviating from 0 or 2π phase produced a decrease in sFC both for PLV and AEC (Figure 4.6). For phase-based connectivity, the phase shift between the stimulation signals changes the spectral contribution of the stimulation frequency to the original signals, depending on the constructive or destructive interaction with the physiological signals' activity at the stimulation frequency. The differences in spectral density will result in different instantaneous frequency probability distributions for each of the signals, making it less likely for them to maintain a constant phase difference, and thus decreasing the PLV. On the other hand, the phase difference between the stimulatory sinusoid waves modifies the envelopes differently, reaching a maximum misalignment of the original physiological signals' envelopes when the phase shift is that of π, consequently reducing their AEC. The interpretation of these simulation results should be considered with caution as many assumptions have been made. For instance, we have assumed a straightforward behaviour and influence of tACS as sinusoidal signals over neuronal physiological signals, and considered white noise as a plausible proxy for neuronal activity. Nevertheless, this theoretical experiment adds to the understanding of the results obtained in this study.

An equally plausible explanation for our divergent results when compared to previous findings on sFC by others could stem from the lack of comparability in the field (Bikson et al., 2018), due to the use of different stimulation protocols, spatial targets, or means to measure the stimulation effects. The study performed by Schwab et al., 2019 reported an increase in alpha functional connectivity for occipitoparietal in-phase tACS when compared to anti-phase and jittered-phase tACS, but a *sham* group was not included, and thus our results are not comparable with theirs. Additionally, their tACS protocol was administered through HD-tACS, where the stimulation electrodes are surrounded by returning electrodes in an effort to focalize the elicited electric field. This is especially relevant, as the phase differences induced in the neural populations in the cortex would be highly different between protocols. This is the same case as in Clancy et al., 2018, which applied HD-tACS to occipito-parietal areas using the IAF as stimulation frequency, and additionally used Granger causality, a different FC parameter than ours, to measure changes in connectivity. In the work by of Van Schouwenburg et al., 2017, both increases and decreases in sFC were observed in different areas of the brain, and a second study of the same group could not replicate the results found in the first one Van Schouwenburg et al., 2018. Finally, other studies based on fMRI-FC show inconclusive results, with some finding increases in sFC after tACS stimulation (Bächinger et al., 2017; Mondino et al., 2020) and other finding sFC reductions (Abellaneda-Pérez et al., 2020; Gundlach et al., 2020). Consequently, there is a need for replication studies and a standardization of the stimulation protocols to evaluate the effects of tACS on sFC.

For a better understanding of the electrophysiological phenomena underlying the use of tACS, we conducted an additional study on the joint behaviour of sFC and power in the DMN links with significant changes after tACS. This revealed a consistent pattern of negative correlations

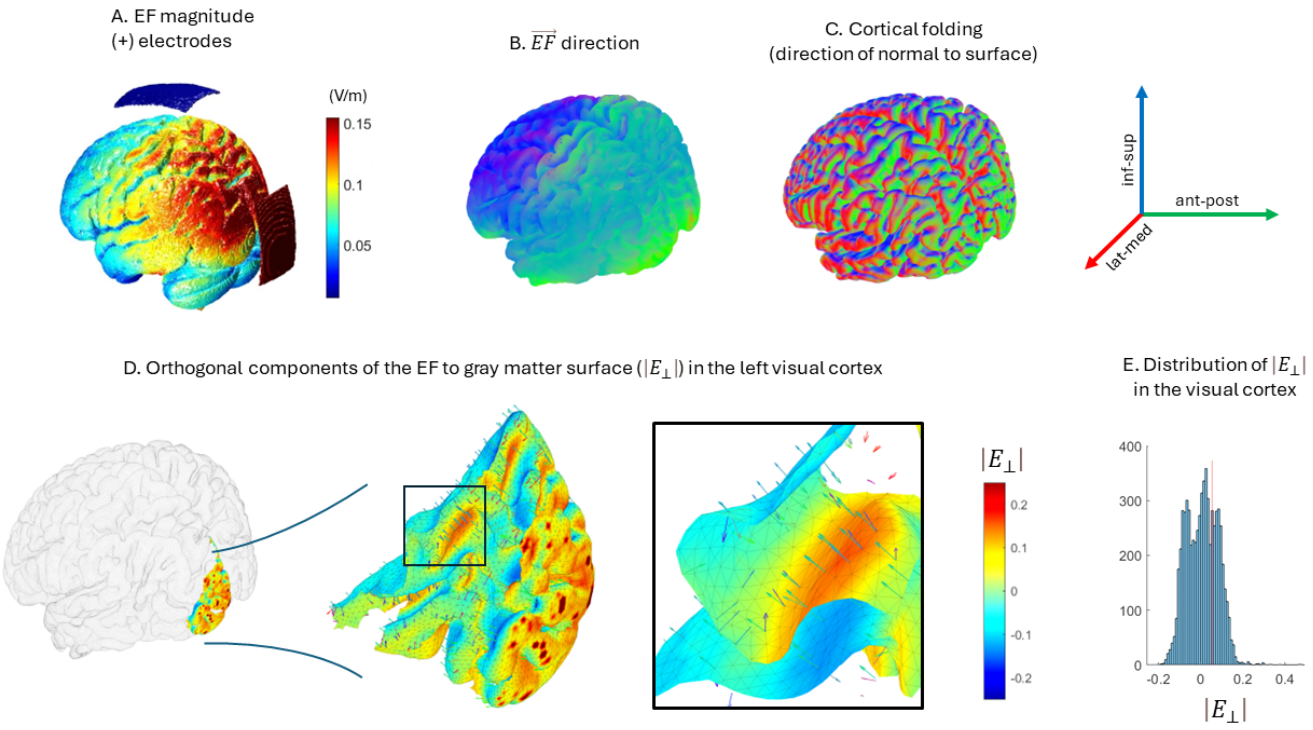


Figure 4.7: Orthogonal components of the electric field with respect to the white-matter surface. (**A**) Electrode location and electric field magnitude over the brain. B and C show the direction of both the electric field given the protocol (**B**) and the direction of the normal component to white matter surface in the folded cortex (**C**). (**D**) Distribution of orthogonal components of the electric field in the visual cortex. A sample of vectors is shown indicating both the direction of the electric field and the normal component to the surface. The surface colour indicates the magnitude of the orthogonal component (red-depolarizing, blue-hyperpolarizing). (**E**) Distribution of magnitudes of the orthogonal components of the electric field for the visual cortex. Note that in the same region coexist positive and negative values, and therefore, anti-phase stimulation effects.

between the change of AEC-c sFC in the PCU-PCC link, and power ratio of these two regions for the *stim* group. Only the correlation with the PCU's power distinguished the behaviour between the *sham* and *stim* groups, possibly due to the reduced statistical power of the sample. Aligned with the previous explanation for the sFC reductions, tACS could introduce non-uniform phase distributions in the cortex, favouring a decoupling of phases and envelopes, but still entrain the activity of the neuronal populations in the same stimulation frequency. This would consequently increase the activity within the frequency range, increasing power (Cabrera-Álvarez et al., 2023; Zaehle et al., 2010) but reducing sFC as shown previously.

The reduction of sFC in PCU-ACC and PCU-PCC sFC is of special interest in the context of Alzheimer's Disease (AD). Specifically, an early rise in sFC between these areas is found in individuals at risk of disease development due to their family history (García-Colomo et al., 2024; Ramírez-Toraño et al., 2021). Moreover, the whole DMN is affected in the disease as its function, metabolic activity and structure become altered through the course of the disease (Badhwar et al., 2017). Some of these regions, such as the PCU, behave as hubs of the network and become vulnerable to the progression of the disease (Stam, 2014). Particularly,

these regions show increased excitability and sFC in the earliest stages of Aβ accumulation, which intensifies the severity of the disease (García-Colomo et al., 2024; López-Sanz et al., 2017; Maestú et al., 2021; Ranasinghe et al., 2022). Therefore, reducing or limiting the initial increase in neuronal excitability and connectivity through a non-invasive technique such as tACS could pose as a potential preventive treatment in prodromal stages of AD. Further investigation in this direction is needed, as well as on the cognitive effects of the proposed tACS protocol.

Finally, it is also important to comment on the different behaviour observed when studying the effects of tACS on dFC. No differences were observed in ci-PLV dFC, but AEC-c dFC showed significant increases in both *stim* and *sham* groups after the stimulation, yielding non-significant between-group comparisons. Thus, our experimental design does not allow us to ascertain whether there exists an effect of tACS on dFC or not, and all we can do is consider the different possibilities behind these results. The absence of literature in this field did not facilitate in the building of hypotheses, and hinders the interpretation of these results. The observed changes could stem from a common origin in both group, such as the placebo-effect, or tiredness. On the other hand, these results might reflect a differential effect of neuromodulation, and the observed increases of dFC in the *stim* could be explained by the induced decrease in sFC observed in this same group, while the increases of dFC in the *sham* group would originate from other uncontrolled reasons. Future studies should address this problem, either increasing the sample size, or through the application of techniques that allow for the study of dFC at a lower time-scale, such as EEG microstates or Hidden Markov Models (HMMs).

Regardless, it is interesting to observe a different behaviour trend for sFC and dFC, as it equally happened in Chapter 3, where dFC was associated with changes in p-tau231 levels, while sFC was not. This supports the idea that dFC and sFC represent different physiological phenonema, and the inclusion of dFC parameters in future electrophysiological studies. Another conclusion to be drawn from these inconclusive results is that extensive research is still needed. Future studies should address whether temporal network hierarchy is an entity well preserved from external neuromodulation, the evolution trends of sFC and dFC over longer recordings and during online stimulation, and explore methodologies able to investigate dFC in shorter time scales.

Some limitations of the present experiment must be noted. Firstly, while comparable to previous studies in the field, the sample size of our experiment was modest, with a total of 26 participants. This limited the possibility of introducing potential confounding variables as covariates. Nevertheless, no significant differences in any of the demographic variables between the *sham* and *stim* groups were observed. Future studies should consider larger sample sizes to increase statistical power. Importantly, even though physiological relative IAF $\pm$ 2 Hz power was not used as a covariate, there were no significant differences in relative power between groups. Thus, the possibility for power to constitute a confounding factor in our study is slim. Secondly, the temporal length of the protocol could have induced fatigue in the participants, influencing the results in terms of power and FC (Ishii et al., 2013). Finally, it is important to note that the stimulation setup with squared patches is limited in its spatial focality, inducing current into large areas of the brain.

Our investigation lacks behavioral evaluation and consequently did not address the cognitive relevance of the findings. Also, the current literature presents elevated variability in the methods and stimulation used, yielding non-comparable results between studies. Therefore, future research should focus on standardizing methodologies, replicating previous results, including neuropsychological assessments, combining electrophysiological and fMRI measurements, as well as using personalized anatomical targeting to reduce inter-subject variability (Mikkonen et al., 2020; Miranda et al., 2018). The use of computational modeling to systematically simulate and study the differences between stimulation protocols would also contribute to knowledge convergence and experiment reproducibility in the field.

4.6 Conclusion

To conclude, this is, to the best of our knowledge, the first study assessing both offline phase- and amplitude-based sFC and dFC changes induced by personalized IAF-tACS with MEG in healthy participants. While we cannot ascertain whether tACS had a significant effect on dFC, our results suggest that IAF-tACS over occipito-parietal areas reduced AEC-c sFC and, to a lesser extent, ci-PLV sFC at the DMN. We hypothesize that this effect is mediated by the alternating in-phase and anti-phase neuromodulation that tACS produces in opposite oriented cortices, which might lead to the reduction of both phase and amplitude synchrony. Lastly, we find that the changes in sFC between posterior areas negatively correlated with power increases in the same frequency band. Our findings highlight a potential treatment for functional connectivity reduction, potentially beneficial for AD, and expand the knowledge of the possible influence of brain folding on the individual effects of tACS.

References

Abellaneda-Pérez, K., Vaqué-Alcázar, L., Perellón-Alfonso, R., Bargalló, N., Kuo, M.-F., Pascual-Leone, A., Nitsche, M. A., & Bartrés-Faz, D. (2020). Differential tDCS and tACS Effects on Working Memory-Related Neural Activity and Resting-State Connectivity. *Frontiers in Neuroscience*, *13*, 1440. https://doi.org/10.3389/fnins.2019.01440

Aberra, A. S., Wang, B., Grill, W. M., & Peterchev, A. V. (2020). Simulation of transcranial magnetic stimulation in head model with morphologically-realistic cortical neurons. *Brain Stimulation*, *13*(1), 175–189. https://doi.org/10.1016/j.brs.2019.10.002

Alves, P. N., Foulon, C., Karolis, V., Bzdok, D., Margulies, D. S., Volle, E., & Thiebaut De Schotten, M. (2019). An improved neuroanatomical model of the default-mode network reconciles previous neuroimaging and neuropathological findings. *Communications Biology*, *2*(1), 370. https://doi.org/10.1038/s42003-019-0611-3

Antal, A., Boros, K., Poreisz, C., Chaieb, L., Terney, D., & Paulus, W. (2008). Comparatively weak after-effects of transcranial alternating current stimulation (tACS) on cortical excitability in humans. *Brain Stimulation*, *1*(2), 97–105. https://doi.org/10.1016/j.brs.2007.10.001

Babiloni, C., Frisoni, G., Pievani, M., Vecchio, F., Lizio, R., Buttiglione, M., Geroldi, C., Fracassi, C., Eusebi, F., & Ferri, R. (2009). Hippocampal volume and cortical sources of EEG alpha rhythms in mild cognitive impairment and Alzheimer disease. *NeuroImage*, *44*(1), 123–135. https://doi.org/10.1016/j.neuroimage.2008.08.005

Bächinger, M., Zerbi, V., Moisa, M., Polania, R., Liu, Q., Mantini, D., Ruff, C., & Wenderoth, N. (2017). Concurrent tACS-fMRI Reveals Causal Influence of Power Synchronized Neural Activity on Resting State fMRI Connectivity. *The Journal of Neuroscience*, *37*(18), 4766–4777. https://doi.org/10.1523/JNEUROSCI.1756-16.2017

Badhwar, A., Tam, A., Dansereau, C., Orban, P., Hoffstaedter, F., & Bellec, P. (2017). Resting-state network dysfunction in Alzheimer's disease: A systematic review and meta-analysis. *Alzheimer's & Dementia: Diagnosis, Assessment & Disease Monitoring*, *8*(1), 73–85. https://doi.org/10.1016/j.dadm.2017.03.007

Belouchrani, A., Abed-Meraim, K., Cardoso, J.-F., & Moulines, E. (1997). A blind source separation technique using second-order statistics. *IEEE Transactions on Signal Processing*, *45*(2), 434–444. https://doi.org/10.1109/78.554307

Benjamini, Y., & Hochberg, Y. (1995). Controlling the False Discovery Rate: A Practical and Powerful Approach to Multiple Testing. *Journal of the Royal Statistical Society: Series B (Methodological)*, *57*(1), 289–300. https://doi.org/10.1111/j.2517-6161.1995.tb02031.x

Bikson, M., Brunoni, A. R., Charvet, L. E., Clark, V. P., Cohen, L. G., Deng, Z.-D., Dmochowski, J., Edwards, D. J., Frohlich, F., Kappenman, E. S., Lim, K. O., Loo, C., Mantovani, A., McMullen, D. P., Parra, L. C., Pearson, M., Richardson, J. D., Rumsey, J. M., Sehatpour, P., ... Lisanby, S. H. (2018). Rigor and reproducibility in research with transcranial electrical stimulation: An NIMH-sponsored workshop. *Brain Stimulation*, *11*(3), 465–480. https://doi.org/10.1016/j.brs.2017.12.008

Bruña, R., Maestú, F., & Pereda, E. (2018). Phase locking value revisited: Teaching new tricks to an old dog. *Journal of Neural Engineering*, *15*(5), 056011. https://doi.org/10.1088/1741-2552/aacfe4

Brunoni, A. R., Amadera, J., Berbel, B., Volz, M. S., Rizzerio, B. G., & Fregni, F. (2011). A systematic review on reporting and assessment of adverse effects associated with transcranial direct current stimulation. *International Journal of Neuropsychopharmacology*, *14*(8), 1133–1145. https://doi.org/10.1017/S1461145710001690

Buzsáki, G. (2006, October). *Rhythms of the Brain*. Oxford University Press. https://doi.org/10.1093/acprof:oso/9780195301069.001.0001

Cabrera-Álvarez, J., Sánchez-Claros, J., Carrasco-Gómez, M., Del Cerro-León, A., Gómez-Ariza, C. J., Maestú, F., Mirasso, C. R., & Susi, G. (2023). Understanding the effects of cortical gyrification in tACS: Insights from experiments and computational models. *Frontiers in Neuroscience*, *17*, 1223950. https://doi.org/10.3389/fnins.2023.1223950

Canuet, L., Pusil, S., Lopez, M. E., Bajo, R., Pineda-Pardo, J. A., Cuesta, P., Galvez, G., Gaztelu, J. M., Lourido, D., Garcia-Ribas, G., & Maestu, F. (2015). Network Disruption and Cerebrospinal Fluid Amyloid-Beta and Phospho-Tau Levels in Mild Cognitive Impairment. *Journal of Neuroscience*, *35*(28), 10325–10330. https://doi.org/10.1523/JNEUROSCI.0704-15.2015

Chaieb, L., Antal, A., & Paulus, W. (2011). Transcranial alternating current stimulation in the low kHz range increases motor cortex excitability. *Restorative Neurology and Neuroscience*, *29*(3), 167–175. https://doi.org/10.3233/RNN-2011-0589

Clancy, K. J., Baisley, S. K., Albizu, A., Kartvelishvili, N., Ding, M., & Li, W. (2018). Lasting connectivity increase and anxiety reduction via transcranial alternating current stimulation. *Social Cognitive and Affective Neuroscience*, *13*(12), 1305–1316. https://doi.org/10.1093/scan/nsy096

Colclough, G., Woolrich, M., Tewarie, P., Brookes, M., Quinn, A., & Smith, S. (2016). How reliable are MEG resting-state connectivity metrics? *NeuroImage*, *138*, 284–293. https://doi.org/10.1016/j.neuroimage.2016.05.070

De Koninck, B. P., Brazeau, D., Guay, S., Herrero Babiloni, A., & De Beaumont, L. (2023). Transcranial Alternating Current Stimulation to Modulate Alpha Activity: A Systematic Review. *Neuromodulation: Technology at the Neural Interface*, *26*(8), 1549–1584. https://doi.org/10.1016/j.neurom.2022.12.007

Elyamany, O., Leicht, G., Herrmann, C. S., & Mulert, C. (2021). Transcranial alternating current stimulation (tACS): From basic mechanisms towards first applications in psychiatry. *European Archives of Psychiatry and Clinical Neuroscience*, *271*(1), 135–156. https://doi.org/10.1007/s00406-020-01209-9

Friston, K. J. (1994). Functional and effective connectivity in neuroimaging: A synthesis. *Human Brain Mapping*, *2*(1-2), 56–78. https://doi.org/10.1002/hbm.460020107

Friston, K. J. (2011). Functional and Effective Connectivity: A Review. *Brain Connectivity*, *1*(1), 13–36. https://doi.org/10.1089/brain.2011.0008

Garcés, P., López-Sanz, D., Maestú, F., & Pereda, E. (2017). Choice of Magnetometers and Gradiometers after Signal Space Separation. *Sensors*, *17*(12), 2926. https://doi.org/10.3390/s17122926

García-Colomo, A., Nebreda, A., Carrasco-Gómez, M., De Frutos-Lucas, J., Ramirez-Toraño, F., Spuch, C., Comis-Tuche, M., Bruña, R., Alfonsín, S., & Maestú, F. (2024). Longitudinal changes in the functional connectivity of individuals at risk of Alzheimer's disease. *GeroScience*, *46*(3), 2989–3003. https://doi.org/10.1007/s11357-023-01036-5

Gundlach, C., Müller, M. M., Hoff, M., Ragert, P., Nierhaus, T., Villringer, A., & Sehm, B. (2020). Reduction of somatosensory functional connectivity by transcranial alternating current stimulation at endogenous mu-frequency. *NeuroImage*, *221*, 117175. https://doi.org/10.1016/j.neuroimage.2020.117175

Hämäläinen, M., Hari, R., Ilmoniemi, R. J., Knuutila, J., & Lounasmaa, O. V. (1993). Magnetoencephalography—theory, instrumentation, and applications to noninvasive studies of the working human brain. *Reviews of Modern Physics*, *65*(2), 413–497. https://doi.org/10.1103/RevModPhys.65.413

Helfrich, R. F., Knepper, H., Nolte, G., Strüber, D., Rach, S., Herrmann, C. S., Schneider, T. R., & Engel, A. K. (2014). Selective Modulation of Interhemispheric Functional Connectivity by HD-tACS Shapes Perception (O. Jensen, Ed.). *PLoS Biology*, *12*(12), e1002031. https://doi.org/10.1371/journal.pbio.1002031

Hinkle, D. E., Wiersma, W., & Jurs, S. G. (1988). Applied statistics for the behavioral sciences. 1988. *Jurs Boston: Houghton Mifflin Co.*

Huang, Y., Datta, A., Bikson, M., & Parra, L. C. (2019). Realistic volumetric-approach to simulate transcranial electric stimulation—ROAST—a fully automated open-source pipeline. *Journal of Neural Engineering*, *16*(5), 056006. https://doi.org/10.1088/1741-2552/ab208d

Ishii, A., Tanaka, M., Shigihara, Y., Kanai, E., Funakura, M., & Watanabe, Y. (2013). Neural effects of prolonged mental fatigue: A magnetoencephalography study. *Brain Research*, *1529*, 105–112. https://doi.org/10.1016/j.brainres.2013.07.022

Jensen, O., & Mazaheri, A. (2010). Shaping Functional Architecture by Oscillatory Alpha Activity: Gating by Inhibition. *Frontiers in Human Neuroscience*, *4*. https://doi.org/10.3389/fnhum.2010.00186

Kar, K., Ito, T., Cole, M. W., & Krekelberg, B. (2020). Transcranial alternating current stimulation attenuates BOLD adaptation and increases functional connectivity. *Journal of Neurophysiology*, *123*(1), 428–438. https://doi.org/10.1152/jn.00376.2019

Kasten, F. H., Dowsett, J., & Herrmann, C. S. (2016). Sustained Aftereffect of α-tACS Lasts Up to 70 min after Stimulation. *Frontiers in Human Neuroscience*, *10*. https://doi.org/10.3389/fnhum.2016.00245

Liu, A., Vöröslakos, M., Kronberg, G., Henin, S., Krause, M. R., Huang, Y., Opitz, A., Mehta, A., Pack, C. C., Krekelberg, B., Berényi, A., Parra, L. C., Melloni, L., Devinsky, O., & Buzsáki, G. (2018). Immediate neurophysiological effects of transcranial electrical stimulation. *Nature Communications*, *9*(1), 5092. https://doi.org/10.1038/s41467-018-07233-7

López-Sanz, D., Bruña, R., Garcés, P., Camara, C., Serrano, N., Rodríguez-Rojo, I. C., Delgado, M. L., Montenegro, M., López-Higes, R., Yus, M., & Maestú, F. (2016). Alpha band disruption in the AD-continuum starts in the Subjective Cognitive Decline stage: A MEG study. *Scientific Reports*, *6*(1), 37685. https://doi.org/10.1038/srep37685

López-Sanz, D., Bruña, R., Garcés, P., Martín-Buro, M. C., Walter, S., Delgado, M. L., Montenegro, M., López Higes, R., Marcos, A., & Maestú, F. (2017). Functional Connectivity Disruption in Subjective Cognitive Decline and Mild Cognitive Impairment: A Common Pattern of Alterations. *Frontiers in Aging Neuroscience*, *9*, 109. https://doi.org/10.3389/fnagi.2017.00109

Maestú, F., de Haan, W., Busche, M. A., & DeFelipe, J. (2021). Neuronal excitation/inhibition imbalance: Core element of a translational perspective on Alzheimer pathophysiology. *Ageing Research Reviews*, *69*, 101372. https://doi.org/10.1016/j.arr.2021.101372

Menon, V. (2011). Large-scale brain networks and psychopathology: A unifying triple network model. *Trends in Cognitive Sciences*, *15*(10), 483–506. https://doi.org/10.1016/j.tics.2011.08.003

Mikkonen, M., Laakso, I., Tanaka, S., & Hirata, A. (2020). Cost of focality in TDCS: Interindividual variability in electric fields. *Brain Stimulation*, *13*(1), 117–124. https://doi.org/10.1016/j.brs.2019.09.017

Miranda, P. C., Callejón-Leblic, M. A., Salvador, R., & Ruffini, G. (2018). Realistic modeling of transcranial current stimulation: The electric field in the brain. *Current Opinion in Biomedical Engineering*, *8*, 20–27. https://doi.org/10.1016/j.cobme.2018.09.002

Mondino, M., Ghumman, S., Gane, C., Renauld, E., Whittingstall, K., & Fecteau, S. (2020). Effects of Transcranial Stimulation With Direct and Alternating Current on Resting-State Functional Connectivity: An Exploratory Study Simultaneously Combining Stimulation and Multiband Functional Magnetic Resonance Imaging. *Frontiers in Human Neuroscience*, *13*, 474. https://doi.org/10.3389/fnhum.2019.00474

O'Neill, G. C., Barratt, E. L., Hunt, B. A. E., Tewarie, P. K., & Brookes, M. J. (2015). Measuring electrophysiological connectivity by power envelope correlation: A technical review on MEG methods. *Physics in Medicine and Biology*, *60*(21), R271–R295. https://doi.org/10.1088/0031-9155/60/21/R271

Oostenveld, R., Fries, P., Maris, E., & Schoffelen, J.-M. (2011). FieldTrip: Open Source Software for Advanced Analysis of MEG, EEG, and Invasive Electrophysiological Data. *Computational Intelligence and Neuroscience*, *2011*, 1–9. https://doi.org/10.1155/2011/156869

Polanía, R., Nitsche, M. A., Korman, C., Batsikadze, G., & Paulus, W. (2012). The Importance of Timing in Segregated Theta Phase-Coupling for Cognitive Performance. *Current Biology*, *22*(14), 1314–1318. https://doi.org/10.1016/j.cub.2012.05.021

Preisig, B. C., Riecke, L., Sjerps, M. J., Kösem, A., Kop, B. R., Bramson, B., Hagoort, P., & Hervais-Adelman, A. (2021). Selective modulation of interhemispheric connectivity by transcranial alternating current stimulation influences binaural integration. *Proceedings of the National Academy of Sciences*, *118*(7), e2015488118. https://doi.org/10.1073/pnas.2015488118

Raichle, M. E. (2011). The Restless Brain. *Brain Connectivity*, *1*(1), 3–12. https://doi.org/10.1089/brain.2011.0019

Raichle, M. E. (2015). The Brain's Default Mode Network. *Annual Review of Neuroscience*, *38*(1), 433–447. https://doi.org/10.1146/annurev-neuro-071013-014030

Ramírez-Toraño, F., Bruña, R., De Frutos-Lucas, J., Rodríguez-Rojo, I. C., Marcos De Pedro, S., Delgado-Losada, M. L., Gómez-Ruiz, N., Barabash, A., Marcos, A., López Higes, R., & Maestú, F. (2021). Functional Connectivity Hypersynchronization in Relatives of Alzheimer's Disease Patients: An Early E/I Balance Dysfunction? *Cerebral Cortex*, *31*(2), 1201–1210. https://doi.org/10.1093/cercor/bhaa286

Ranasinghe, K. G., Kudo, K., Hinkley, L., Beagle, A., Lerner, H., Mizuiri, D., Findlay, A., Miller, B. L., Kramer, J. H., Gorno-Tempini, M. L., Rabinovici, G. D., Rankin, K. P., Garcia, P. A., Kirsch, H. E., Vossel, K., & Nagarajan, S. S. (2022). Neuronal synchrony abnormalities associated with subclinical epileptiform activity in early-onset Alzheimer's disease. *Brain*, *145*(2), 744–753. https://doi.org/10.1093/brain/awab442

Schwab, B. C., Misselhorn, J., & Engel, A. K. (2019). Modulation of large-scale cortical coupling by transcranial alternating current stimulation. *Brain Stimulation*, *12*(5), 1187–1196. https://doi.org/10.1016/j.brs.2019.04.013

Stam, C. J. (2014). Modern network science of neurological disorders. *Nature Reviews Neuroscience*, *15*(10), 683–695. https://doi.org/10.1038/nrn3801

Tan, J., Iyer, K. K., Tang, A. D., Jamil, A., Martins, R. N., Sohrabi, H. R., Nitsche, M. A., Hinder, M. R., & Fujiyama, H. (2019). Modulating functional connectivity with non-invasive brain stimulation for the investigation and alleviation of age-associated declines in response inhibition: A narrative review. *NeuroImage*, *185*, 490–512. https://doi.org/10.1016/j.neuroimage.2018.10.044

Taulu, S., & Simola, J. (2006). Spatiotemporal signal space separation method for rejecting nearby interference in MEG measurements. *Physics in Medicine and Biology*, *51*(7), 1759–1768. https://doi.org/10.1088/0031-9155/51/7/008

Tzourio-Mazoyer, N., Landeau, B., Papathanassiou, D., Crivello, F., Etard, O., Delcroix, N., Mazoyer, B., & Joliot, M. (2002). Automated Anatomical Labeling of Activations in SPM Using a Macroscopic Anatomical Parcellation of the MNI MRI Single-Subject Brain. *NeuroImage*, *15*(1), 273–289. https://doi.org/10.1006/nimg.2001.0978

Utevsky, A. V., Smith, D. V., & Huettel, S. A. (2014). Precuneus Is a Functional Core of the Default-Mode Network. *The Journal of Neuroscience*, *34*(3), 932–940. https://doi.org/10.1523/JNEUROSCI.4227-13.2014

Van Schouwenburg, M. R., Sörensen, L. K. A., De Klerk, R., Reteig, L. C., & Slagter, H. A. (2018). No Differential Effects of Two Different Alpha-Band Electrical Stimulation Protocols Over Fronto-Parietal Regions on Spatial Attention. *Frontiers in Neuroscience*, *12*, 433. https://doi.org/10.3389/fnins.2018.00433

Van Schouwenburg, M. R., Zanto, T. P., & Gazzaley, A. (2017). Spatial Attention and the Effects of Frontoparietal Alpha Band Stimulation. *Frontiers in Human Neuroscience*, *10*. https://doi.org/10.3389/fnhum.2016.00658

Van Veen, B., & Buckley, K. (1988). Beamforming: A versatile approach to spatial filtering. *IEEE ASSP Magazine*, *5*(2), 4–24. https://doi.org/10.1109/53.665

Vogeti, S., Boetzel, C., & Herrmann, C. S. (2022). Entrainment and Spike-Timing Dependent Plasticity – A Review of Proposed Mechanisms of Transcranial Alternating Current Stimulation. *Frontiers in Systems Neuroscience*, *16*, 827353. https://doi.org/10.3389/fnsys.2022.827353

Vossen, A., Gross, J., & Thut, G. (2015). Alpha Power Increase After Transcranial Alternating Current Stimulation at Alpha Frequency (α-tACS) Reflects Plastic Changes Rather Than Entrainment. *Brain Stimulation*, *8*(3), 499–508. https://doi.org/10.1016/j.brs.2014.12.004

Wang, Y., Hou, P., Li, W., Zhang, M., Zheng, H., & Chen, X. (2022). The influence of different current-intensity transcranial alternating current stimulation on the eyes-open and eyes-closed resting-state electroencephalography. *Frontiers in Human Neuroscience*, *16*, 934382. https://doi.org/10.3389/fnhum.2022.934382

Zaehle, T., Rach, S., & Herrmann, C. S. (2010). Transcranial Alternating Current Stimulation Enhances Individual Alpha Activity in Human EEG (A. Aleman, Ed.). *PLoS ONE*, *5*(11), e13766. https://doi.org/10.1371/journal.pone.0013766

Zarubin, G., Gundlach, C., Nikulin, V., Villringer, A., & Bogdan, M. (2020). Transient Amplitude Modulation of Alpha-Band Oscillations by Short-Time Intermittent Closed-Loop tACS. *Frontiers in Human Neuroscience*, *14*, 366. https://doi.org/10.3389/fnhum.2020.00366

Chapter 5

Conclusions

5.1 Main conclusions

In this thesis we have used MEG to investigate dynamic functional connectivity and its application to Alzheimer's disease. As we explained in the General Introduction, even if every element in the brain shows a highly dynamic behaviour, functional connectivity, one of the main tools to investigate synchronized activity in the brain, has been typically treated as a stationary process, thus discarding all potential information contained in its temporal dimension. While research in this field has begun to attract interest in the scientific community, dFC studies only amount to approximately a 5% of research focused on FC. Additionally, electrophysiological research on dFC, as opposed to fMRI investigation, is very scarce, in spite to its better temporal resolution and its capability to capture direct neuronal activity. This is especially relevant in a disease such as AD, as the several reports of network alterations found along its progression through electrophysiological sFC parameters hint towards dFC changes that could potentially allow an earlier detection of the disease, or help us in further our knowledge on its nature.

Since the existing articles on dFC and AD were centered on the late stages of the AD continuum, we performed, to the best of our knowledge, the first electrophysiological study covering the whole pre-dementia spectrum (Carrasco-Gómez, García-Colomo, et al., 2024, Chapter 2), in which we proposed a new methodology to measure dFC both at a global and individual source scale through recurrence matrices. Our results showed a global reduction of dFC in the alpha and beta bands in MCI participants, as previous literature had detected in posterior stages of the disease. SCD participants were not distinguishable from either the HC or MCI groups, proving to be an intermediate state between both conditions. Furthermore, HC-MCI differences were located in relevant areas for the progression of the disease, including the orbitofrontal cortex, left temporal pole and hippocampus in both the alpha and beta frequency bands, and also in the anterior, middle and posterior cingulate cortex, bilateral temporal gyrus, and precuneus exclusively in the beta band (Figure 2.3). These areas are characterized by a lower neuronal density and myelination, large dendritic arborization, and higher glycolysis, enabling adaptable and plastic neuronal circuitry (Karahan et al., 2022), which could in turn make them more susceptible to the neuronal damage along the progression

of AD.

Finally, we also aimed to explore whether the observed changes in dFC were related to changes in cognition and anatomical markers of AD progression. The potential of the proposed dFC parameter was indicated by its significant correlations in alpha and beta with MMSE, delayed logic memory, both total grey matter volume and hippocampal volume, and fractional anisotropy of relevant tracts. It is worth highlighting that those trends were found both when using the whole dataset and for the MCI group only. While correlations found in the whole dataset showcase the value of dynamicity as a possible biomarker for AD progression, it included groups with significantly different cognitive and anatomical scores. On the other hand, MCI group correlations imply that lower dFC is related to the severity of the cognitive signs these participants show, as well as showcasing the link between dFC and anatomical damage, both in brain volumetrics and white matter integrity, due to the advance of the disease. Based on our results, we support the claim from previous research on the relevance of white matter degradation and network integrity in AD progression (Córdova-Palomera et al., 2017). Previous works have drawn a connection between tract myelination, transmission speeds and the synchrony patterns that arise in the brain (Babaeeghazvini et al., 2021; Hunt et al., 2016), especially for higher oscilaltory frequencies, where the temporal precision needed increases. Our results are aligned with these ideas, as we found increased effect sizes and more widespread differences of dFC between MCI and HC groups over the beta band than in the alpha band, while not finding any result in the theta band. Overall, the significance of this chapter lays in the proposed methodology and the evidence provided of a dFC decline across the pre-dementia stages of the AD continuum, emphasizing its potential as a biomarker for early AD detection and its reliability for AD progression monitoring.

The biological conception of AD led to the definition of a continuum that begins well before the emergence of any cognitive symptoms, associated with the appearance of the accumulation of Aβ and tau NFTs. These changes can emerge up to 20 years before the diagnosis, and induce cumulative functional and anatomical alterations in the brain (Jack et al., 2018). When the disease is diagnosed by currently generalized clinical standards, brain damage is too extensive, which hampers the success of possible treatments. This highlights the importance of noninvasive early diagnosis tools to identify individuals in the initial phase of the AD continuum. For this reason, we compared the capability of sFC and dFC for early detection of alterations associated to AD by exploring its correlation with p-tau231 levels, a blood biomarker used as a proxy for Aβ accumulation, in a sample of cognitively unimpaired adults (Carrasco-Gómez, Garcia-Colomo, et al., 2024, Chapter 3). In this work, we additionally proposed another new methodology for the estimation of dFC, based on the calculation of the Shannon entropy of FC timecourses. Our analyses revealed a cluster of brain areas whose dFC correlated positively with p-tau231 levels in blood in the low-alpha frequency band. Importantly, statistical tests did not find any significant correlation between ptau-231 and sFC, which underscores the possible increased sensitivity of dFC to early alterations due to AD pathology. The brain regions where dFC scales along with ptau-231 levels include the right temporal pole and temporal gyrus, left inferior and middle frontal gyri, and bilateral anterior cingulate cortex and parahippocampi, and are congruent with previous literature, which suggest dFC and sFC alterations across the AD continuum that span regions from the DMN, especially vulnerable to AD pathology, as well as the orbitofrontal cortex, which accumulates

Aβ from the earliest stages of the continuum (Li et al., 2019; Matsui and Yamashita, 2023; Mattsson et al., 2019; Núñez et al., 2019).

A second objective of this study was to explore the relationship between the revealed dFC alterations and other risk factors, such as age, sex, APOE ϵ4 carriage, and AD family history, and additional parameters related to AD progression, including MOCA scores, fractional anisotropy or sFC. To do so, we built backwards stepwise linear regression models, which found significant contributions of sFC and forceps minor FA to the values of dFC, independent from the influence of ptau-231. Not only that, but the pathological directionality of these correlations support the relevance of dFC alterations at this potentially very early state of AD progression. While opposite to the results found in the previous chapter, the increased values of dFC connected to the pathological nature of the correlations found with both ptau-231 and other neuroimaging parameters leads us to propose that dFC progression over the AD continuum could follow an inverted U-shape curve. According to previous work, sFC alterations across the AD spectra show this kind of evolution, marked by a state of hyperconnectivity in the early stages of Aβ accumulation, and hypoconnectivity later in the continuum (Fernández et al., 2006; García-Colomo et al., 2024; López-Sanz et al., 2017; Maestú et al., 2021; Pusil et al., 2019; Ramírez-Toraño et al., 2021). Thus, dFC could follow a similar path, only with the change from increased to decreased levels in dynamics happening earlier in the AD spectra, maybe even before subjective cognitive complaints arise (Figure 5.1). This study was the first to investigate the relationship between dFC and a blood biomarker, demonstrating the sensitivity of the proposed methodology to early alterations related to AD, as well as further proving MEG to be an excellent tool, capable to assess subtle changes in brain function even in cognitively unimpaired participants.

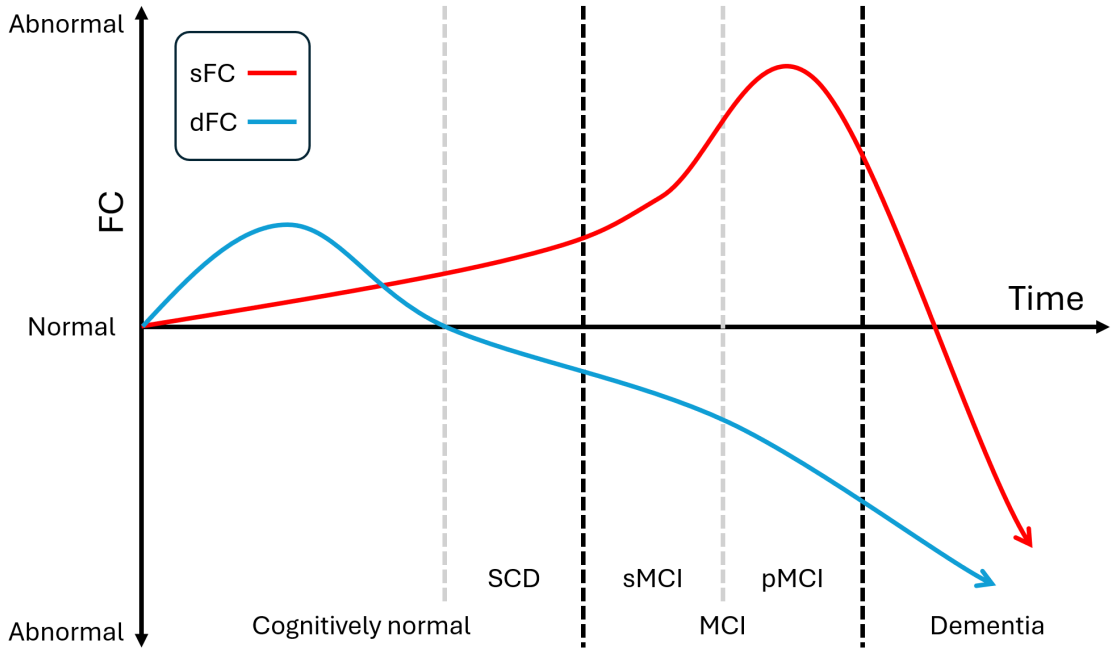


Figure 5.1: Progression of sFC and dFC over the AD continuum, after the results reported in this thesis.

With the an approximate idea of the evolution of dFC and sFC across the whole AD continuum, and given the dire need for potential treatments to prevent the advance of the disease, we investigated the possibility to externally modulate sFC and dFC in a pilot study applying tACS at the individual alpha frequency in healthy participants (Carrasco-Gómez, Cabrera-Álvarez, et al., 2024, Chapter 4). While no effect from tACS was found on dFC, we observed significant decresases in AEC-c sFC after tACS over the DMN. These differences were driven by the reduction of connectivity in posterior-posterior and posterior-anterior links between hubs of the network, such as between the PCU and PCC, and PCU and ACC. These results are of special interest in the context of AD, since early rises in sFC in participants with a family history of AD are specifically detected in these areas (García-Colomo et al., 2024; Ramírez-Toraño et al., 2021). Particularly, these regions show increased excitability and sFC linked to early accumulation of Aβ species (Mattsson et al., 2019), which in turn favour neurotoxicity and greater release of Aβ, entering a pathological positive feedback loop (Huang and Liu, 2020). Therefore, reducing or limiting the initial increase in neuronal excitability and connectivity through a non-invasive technique such as tACS could pose as an invaluable potential preventive treatment.

Nevertheless, the aforementioned increases in sFC struck us as surprising, as previous reports in literature found increased sFC after tACS application (Clancy et al., 2018; Schwab et al., 2019; Van Schouwenburg et al., 2017). We claim that these effect might arise from the interaction of cortical folding with the electrical field direction elicited by tACS, which translates into some pyramidal neurons receiving tACS oscillatory currents in-phase, and some others out-of-phase (π phase). This hypothesis was supported by a simple simulation performed in this study, which showed that phase disparities in signals with a baseline connectivity induces reduction in both phase- and envelope-based sFC, and by significant inverse correlations in the stimulation group between sFC and power changes after tACS. Finally, AEC-c dFC exhibited a different behaviour, with increases after stimulation in both the experimental and the placebo group, leading to non-significant between-group differences. While this means that we cannot ascertain whether tACS had an effect on dFC, this divergent behaviour between dFC and sFC, along with the one observed in previous chapters in this thesis, is of interest, and supports the notion of these two parameters represent different physiological phenomena, and urges us to keep including dFC parameters in future studies.

In conclusion, this thesis demonstrates the invaluable role of dFC in advancing our understanding of brain function and AD pathophysiology. Through innovative methodologies, we have successfully estimated dFC and characterized its alterations across the AD continuum, revealing both early increases and subsequent decreases in connectivity that correlate with cognitive decline and anatomical changes. Furthermore, our exploration into the potential modulation of dFC using tACS opens a promising avenue for preventive interventions targeting early sFC changes in AD. Our findings underscore the sensitivity of MEG as a neuroimaging tool, capable of detecting subtle brain activity changes in both pathological conditions and healthy individuals. Collectively, these results highlight the potential of dFC as a biomarker for early detection and monitoring of AD, paving the way for future research and clinical applications.

5.2 Limitations and future directions

The results of this thesis, while contributing and expanding knowledge on dFC in literature, are the product of a series of methodological choices and limitations. Firstly, the choice of using a sliding window approach for the studies presented here might have been limiting, and more specifically the use of 4-second windows. This window size has been used in previous relevant studies determining relevant FC features in AD for the frequency bands investigated along the different chapters (García-Colomo et al., 2024; López et al., 2014; López-Sanz et al., 2017; Pusil et al., 2019; Ramírez-Toraño et al., 2021), and its use has allowed us to compare our results to theirs. Additionally, this window size has also been recommended for the estimation of fluctuations in FC of electrophysiological resting state networks (Liuzzi et al., 2019), and has derived in robust results with relevant effect sizes and generally congruent with previous literature. Nevertheless, we considered it was not large enough to capture sufficient oscillations in the delta band, and not small enough to capture dynamic patterns in the gamma band, and this might be the reason of the absence of results in the theta band in Chapter 2. Future studies will apply other methodologies presented in the General Introduction, such as MEG microstates and HMMs, which will allow us to assess other time scales and aspects of dFC, potentially relevant in the advance of AD.

While the sample size of the study in Chapter 2 was considerably large, the sample sizes in the other studies were limited, although in line with most neuroimaging research, and especially with EEG and MEG studies to which they have been compared. Our samples lacked diversity in terms of socioeconomic status, race and ethnicity, and geographical circumstances, as most participants came from urban areas in Madrid. Furthermore, subjects with poor health and chronic conditions are less likely to take part of research (Mody et al., 2008), and consequently those participants with worse outcomes have probably been underrepresented in the studies of Chapters 2 and 3. In the particular case of Chapter 4, the exploratory nature of the pilot intervention with tACS, while harmless and without risks, forced us to perform it with healthy young participants instead of individuals in the AD continuum. Nevertheless, and after obtaining the aforementioned results, we are currently holding tACS experiments with individuals at risk of AD ($n \approx 100$), and with another MCI cohort ($n \approx 100$).

While this thesis sought to develop the knowledge on dFC around the initial stages of AD, and the study in Chapter 3 is a pioneer in the follow-up of high-risk individuals within the specific age range where early pathological signs are expected to occur, a longer follow-up period is required to correctly classify cases and controls. Relevantly, this study is part of an initiative aimed at tracking these individuals for decades, with the third time point assessment already approved and funded. Also, participants of the study in Chapter 2 lacked any assessment of AD biomarkers, such as PET Aβ imaging, CSF tau and Aβ-based analyses, or blood biomarkers, as the one used in Chapter 3. Their inclusion in future studies would help in distinguishing the progression of individuals across the preclinical spectra of the AD continuum, increase the likelihood of SCD symptoms to be AD-related, and to investigate the relationship of electrpphysiological parameters such as the ones studied in this thesis with another biological substrate of the disease. It is of special interest the inclusion of blood biomarkers, such as plasma p-tau231 or p-tau217, as they might represent an alternative and more ecological marker that is also less invasive, widely accessible to researchers and

clinicians, a reason why they were recently included in the revised criteria for AD diagnosis and staging (Jack Jr. et al., 2024). Nevertheless, it is important to note that their collection increase research costs and can make recruitment more challenging, as not all participants are accepting of such procedures.

This thesis solely focused on the use of MEG, but it does not mean other neuroimaging techniques are unsuitable for investigating dFC. EEG stands as another adequate technique to evaluate and research dFC at similar time scales as MEG, and replicating our analysis thorugh this modality would be, consequently, of a high relevance. Its increased accessibility and portability compared to MEG would make our results transferable to the clinical setting, and increase the reach of our research to other participants otherwise unavailable. On the other hand, the majority of the studies on both dFC and sFC have been performed using fMRI, a neuroimaging modality with a lower temporal resolution. The scarcity of electrophysiological studies in this field hampers the performance of hypothesis-driven research and the interpretation of results. Thus, multimodal research combining electrophysiological measures and fMRI is needed, which could enable a common reference useful for comparisons between studies performed with different neuroimaging techniques.

The most immediate future direction for this thesis is to continue the research lines proposed in Chapters 3 and 4. As a part of this work, we would like to assess the change of dFC across longitudinal data of participants at risk of AD already available at the laboratory, as well as study the further evolution of dFC in the second follow-up study in this cohort, and keep evaluating neuromodulation effects of tACS on sFC and dFC, taking at the same time additional methodological considerations. These may include evaluating test-retest reliability of the proposed dFC methodologies, study the interaction between frequency band and window size employed for the estimation of dFC, and the investigation of dFC at smaller time scales both through frame-based or time modeling techniques, or by the analysis of FC in task recordings, also available in all cohorts in our research centre.

5.3 Final remarks

1. Two new methodologies for the calculation of dFC have been proposed, one of them based on the use of connectivity recurrence matrices, and the other on the measurement of the entropy of the connectivity timecourses, allowing for the assessment of both sensor and source level analysis of dFC.
2. The dynamic nature of connectivity is reduced along the pre-dementia stage of AD, with these reductions being significant in MCI patients. Moreover, these reductions are more prominent in areas related to AD advance, and linked to $A\beta$ accumulation, and more widespread in the beta band than in the alpha band.
3. The observed decrease in dFC is associated to decline in cognitive performance, generalized neurodegeneration, and reductions of white matter integrity. These correlations were also significant inside the MCI group, meaning that dFC might be an adequate parameter to monitor the early progression of AD, as well as to assess the severity of the disease in MCI patients.

4. Nevertheless, during the initial stages of the disease, when cognitive performance remains intact, dFC increases along with levels of p-Tau231 in blood, a biomarker of $A\beta$ accumulation in the brain.
5. The areas where this positive correlation exist, mainly in the orbitofrontal cortex, temporal pole and medial superior frontal gyrus, overlap with those linked with the early accumulation of $A\beta$.
6. Increases in dFC are not only associated to elevated levels of p-Tau231, but is also linked to increases in sFC and decreases in FA, both signs of AD progression. This underscores the pathological nature of these initial increases in dFC happening in cognitively unimpaired individuals, and highlights the potential use of dFC parameters for early detection of AD.
7. While we cannot ascertain whether there exists an effect of tACS on dFC, we observed a reduction of sFC after its personalized application on parieto-occipital areas in healthy participants.
8. Through the proposed protocol we were able to reduce sFC, especially in links between antero-posterior and postero-posterior hubs of the DMN. Moreover, these reductions were paired with increases in power in the same areas.
9. These decreases in sFC might be explained by the influence of cortical gyrification on tACS, which introduces phase shifts in the induced currents at neural populations through tACS.

5.4 Ideas finales

1. Dos nuevas metodologías para la estimación de la conectividad funcional dinámica (dFC) fueron propuestas. Una de las mismas se basa en el uso de matrices de recurrencia de conectividad, mientras que la otra se fundamenta en el cálculo de la entropía de la serie temporal de valores de conectividad. Ambas metodologías permiten el análisis estadístico de la actividad cerebral a nivel de sensor y a nivel de fuente.
2. La naturaleza dinámica de la conectividad se ve reducida en la etapa pre-demencia de la enfermedad de Alzheimer (AD), siendo estas reducciones significativas en los pacientes con deterioro cognitivo leve (MCI). Adicionalmente, estas disminuciones eran más pronunciadas en regiones relacionadas con el avance de la AD, así como en áreas vinculadas a la acumulación de beta amiloide ($A\beta$).
3. La disminución observada de dFC está asociada a una reducción del rendimiento cognitivo, a la neurodegeneración generalizada del cerebro, y a un empeoramiento de la integridad de la materia blanca. Estas correlaciones fueron también significativas dentro del grupo de MCI, lo cual significa que la dFC puede ser un parámetro adecuado tanto para la monitorización del progreso temprano de la AD, así como para evaluar la severidad de la enfermedad en pacientes con MCI.
4. Sin embargo, durante los estadios iniciales de la enfermedad, en los que la habilidad

cognitiva está intacta, la dFC aumenta junto a los niveles de p-Tau231 en sangre, un biomarcador de acumulación de $A\beta$ en el cerebro.

5. Las regiones cerebrales en las que esta correlación positiva existe, principalmente la corteza orbitofrontal, el polo temporal y el giro medial superior frontal, se superponen con las áreas donde el $A\beta$ de deposita inicialmente.

6. Incrementos en la dFC no solo están vinculados a aumentos en los niveles de p-Tau231, sino que también están asociados a niveles elevados de conectividad funcional estática (sFC) y de anisotropía fraccional (FA), ambos signos del avance de la AD. Esto subraya la naturaleza patológica de estos incrementos de dFC, observados en pacientes cognitivamente sanos, y destaca el potencial uso de la dFC como marcador de detección temprana de AD.

7. Mientras que no podemos saber si existe un efecto de la estimulación transcraneal por corriente alterna (tACS) sobre la dFC, observamos una reducción de sFC tras su aplicación personalizada en participantes sanos.

8. A través del protocolo de estimulación propuesto fuimos capaces de reducir la sFC, especialmente en los links entre hubs antero-posteriores y postero-posteriores de la red por defecto (DMN). Adicionalmente, la disminución de sFC en estos links se correlacionaba con aumentos en la potencia en estas mismas áreas.

9. La disminución observada de la sFC puede ser explicada por la influencia de la girificación cortical sobre la tACS, dado que introduce diferencias de fase entre las corrientes inducidas en las neuronas.

References

Babaeeghazvini, P., Rueda-Delgado, L. M., Gooijers, J., Swinnen, S. P., & Daffertshofer, A. (2021). Brain Structural and Functional Connectivity: A Review of Combined Works of Diffusion Magnetic Resonance Imaging and Electro-Encephalography. *Frontiers in Human Neuroscience*, *15*, 721206. https://doi.org/10.3389/fnhum.2021.721206

Carrasco-Gómez, M., Cabrera-Álvarez, J., García-Colomo, A., del Cerro-León, A., Gómez-Ariza, C. J., Santos, A., & Maestú, F. (2024). Individual alpha frequency tacs reduces functional connectivity across the default mode network. *bioRxiv*, 2024–08.

Carrasco-Gómez, M., Garcia-Colomo, A., Nebreda, A., Bruña, R., Santos, A., & Maestu, F. (2024). Dynamic functional connectivity is modulated by the amount of p-tau231 in blood in cognitively intact participants. *bioRxiv*, 2024–05.

Carrasco-Gómez, M., García-Colomo, A., Cabrera-Álvarez, J., Bruña, R., Santos, A., & Maestú, F. (2024). Dynamics of brain connectivity across the alzheimer's disease spectrum: A magnetoencephalography study. *bioRxiv*, 2024–03.

Clancy, K. J., Baisley, S. K., Albizu, A., Kartvelishvili, N., Ding, M., & Li, W. (2018). Lasting connectivity increase and anxiety reduction via transcranial alternating current stimulation. *Social Cognitive and Affective Neuroscience*, *13*(12), 1305–1316. https://doi.org/10.1093/scan/nsy096

Córdova-Palomera, A., Kaufmann, T., Persson, K., Alnæs, D., Doan, N. T., Moberget, T., Lund, M. J., Barca, M. L., Engvig, A., Brækhus, A., Engedal, K., Andreassen, O. A., Selbæk, G., & Westlye, L. T. (2017). Disrupted global metastability and static and dynamic brain connectivity across individuals in the Alzheimer's disease continuum. *Scientific Reports*, *7*(1), 40268. https://doi.org/10.1038/srep40268

Fernández, A., Hornero, R., Mayo, A., Poza, J., Maestú, F., & Ortiz Alonso, T. (2006). Quantitative Magnetoencephalography of Spontaneous Brain Activity in Alzheimer Disease: An Exhaustive Frequency Analysis. *Alzheimer Disease & Associated Disorders*, *20*(3), 153–159. https://doi.org/10.1097/00002093-200607000-00006

García-Colomo, A., Nebreda, A., Carrasco-Gómez, M., De Frutos-Lucas, J., Ramirez-Toraño, F., Spuch, C., Comis-Tuche, M., Bruña, R., Alfonsín, S., & Maestú, F. (2024). Longitudinal changes in the functional connectivity of individuals at risk of Alzheimer's disease. *GeroScience*, *46*(3), 2989–3003. https://doi.org/10.1007/s11357-023-01036-5

Huang, Y.-r., & Liu, R.-t. (2020). The Toxicity and Polymorphism of β-Amyloid Oligomers. *International Journal of Molecular Sciences*, *21*(12), 4477. https://doi.org/10.3390/ijms21124477

Hunt, B. A. E., Tewarie, P. K., Mougin, O. E., Geades, N., Jones, D. K., Singh, K. D., Morris, P. G., Gowland, P. A., & Brookes, M. J. (2016). Relationships between cortical myeloarchitecture and electrophysiological networks. *Proceedings of the National Academy of Sciences*, *113*(47), 13510–13515. https://doi.org/10.1073/pnas.1608587113

Jack, C. R., Bennett, D. A., Blennow, K., Carrillo, M. C., Dunn, B., Haeberlein, S. B., Holtzman, D. M., Jagust, W., Jessen, F., Karlawish, J., Liu, E., Molinuevo, J. L., Montine, T., Phelps, C., Rankin, K. P., Rowe, C. C., Scheltens, P., Siemers, E., Snyder, H. M., ... Silverberg, N. (2018). NIA-AA Research Framework: Toward a biological definition of Alzheimer's disease. *Alzheimer's & Dementia*, *14*(4), 535–562. https://doi.org/10.1016/j.jalz.2018.02.018

Jack Jr., C. R., Andrews, J. S., Beach, T. G., Buracchio, T., Dunn, B., Graf, A., Hansson, O., Ho, C., Jagust, W., McDade, E., Molinuevo, J. L., Okonkwo, O. C., Pani, L., Rafii, M. S., Scheltens, P., Siemers, E., Snyder, H. M., Sperling, R., Teunissen, C. E., & Carrillo, M. C. (2024). Revised criteria for diagnosis and staging of alzheimer's disease: Alzheimer's association workgroup. *Alzheimer's & Dementia*, *20*(8), 5143–5169. https://doi.org/https://doi.org/10.1002/alz.13859

Karahan, E., Tait, L., Si, R., Özkan, A., Szul, M. J., Graham, K. S., Lawrence, A. D., & Zhang, J. (2022). The interindividual variability of multimodal brain connectivity maintains spatial heterogeneity and relates to tissue microstructure. *Communications Biology*, *5*(1), 1007. https://doi.org/10.1038/s42003-022-03974-w

Li, R., Nguyen, T., Potter, T., & Zhang, Y. (2019). Dynamic cortical connectivity alterations associated with Alzheimer's disease: An EEG and fNIRS integration study. *NeuroImage: Clinical*, *21*, 101622. https://doi.org/10.1016/j.nicl.2018.101622

Liuzzi, L., Quinn, A. J., O'Neill, G. C., Woolrich, M. W., Brookes, M. J., Hillebrand, A., & Tewarie, P. (2019). How Sensitive Are Conventional MEG Functional Connectivity Metrics With Sliding Windows to Detect Genuine Fluctuations in Dynamic Functional Connectivity? *Frontiers in Neuroscience*, *13*, 797. https://doi.org/10.3389/fnins.2019.00797

López, M. E., Bruña, R., Aurtenetxe, S., Pineda-Pardo, J. Á., Marcos, A., Arrazola, J., Reinoso, A. I., Montejo, P., Bajo, R., & Maestú, F. (2014). Alpha-Band Hypersynchronization in Progressive Mild Cognitive Impairment: A Magnetoencephalography Study. *The Journal of Neuroscience*, *34*(44), 14551–14559. https://doi.org/10.1523/JNEUROSCI.0964-14.2014

López-Sanz, D., Bruña, R., Garcés, P., Martín-Buro, M. C., Walter, S., Delgado, M. L., Montenegro, M., López Higes, R., Marcos, A., & Maestú, F. (2017). Functional Connectivity Disruption in Subjective Cognitive Decline and Mild Cognitive Impairment: A Common Pattern of Alterations. *Frontiers in Aging Neuroscience*, *9*, 109. https://doi.org/10.3389/fnagi.2017.00109

Maestú, F., de Haan, W., Busche, M. A., & DeFelipe, J. (2021). Neuronal excitation/inhibition imbalance: Core element of a translational perspective on Alzheimer pathophysiology. *Ageing Research Reviews*, *69*, 101372. https://doi.org/10.1016/j.arr.2021.101372

Matsui, T., & Yamashita, K.-i. (2023). Static and Dynamic Functional Connectivity Alterations in Alzheimer's Disease and Neuropsychiatric Diseases. *Brain Connectivity*, *13*(5), 307–314. https://doi.org/10.1089/brain.2022.0044

Mattsson, N., Palmqvist, S., Stomrud, E., Vogel, J., & Hansson, O. (2019). Staging β -Amyloid Pathology With Amyloid Positron Emission Tomography. *JAMA Neurology*, *76*(11), 1319. https://doi.org/10.1001/jamaneurol.2019.2214

Mody, L., Miller, D. K., McGloin, J. M., Freeman, M., Marcantonio, E. R., Magaziner, J., & Studenski, S. (2008). Recruitment and retention of older adults in aging research: (see editorial comments by dr. stephanie studenski, pp 2351–2352). *Journal of the American Geriatrics Society*, *56*(12), 2340–2348.

Núñez, P., Poza, J., Gómez, C., Rodríguez-González, V., Hillebrand, A., Tola-Arribas, M. A., Cano, M., & Hornero, R. (2019). Characterizing the fluctuations of dynamic resting-state electrophysiological functional connectivity: Reduced neuronal coupling variability in mild cognitive impairment and dementia due to Alzheimer's disease. *Journal of Neural Engineering*, *16*(5), 056030. https://doi.org/10.1088/1741-2552/ab234b

Pusil, S., López, M. E., Cuesta, P., Bruña, R., Pereda, E., & Maestú, F. (2019). Hypersynchronization in mild cognitive impairment: The 'X' model. *Brain*, *142*(12), 3936–3950. https://doi.org/10.1093/brain/awz320

Ramírez-Toraño, F., Bruña, R., De Frutos-Lucas, J., Rodríguez-Rojo, I. C., Marcos De Pedro, S., Delgado-Losada, M. L., Gómez-Ruiz, N., Barabash, A., Marcos, A., López Higes, R., & Maestú, F. (2021). Functional Connectivity Hypersynchronization in Relatives of Alzheimer's Disease Patients: An Early E/I Balance Dysfunction? *Cerebral Cortex*, *31*(2), 1201–1210. https://doi.org/10.1093/cercor/bhaa286

Schwab, B. C., Misselhorn, J., & Engel, A. K. (2019). Modulation of large-scale cortical coupling by transcranial alternating current stimulation. *Brain Stimulation*, *12*(5), 1187–1196. https://doi.org/10.1016/j.brs.2019.04.013

Van Schouwenburg, M. R., Zanto, T. P., & Gazzaley, A. (2017). Spatial Attention and the Effects of Frontoparietal Alpha Band Stimulation. *Frontiers in Human Neuroscience*, *10*. https://doi.org/10.3389/fnhum.2016.00658

Appendices

Appendix A

Supplementary material for Chapter 2

A.1 Supplementary tables

Table A.1: Sample demographics of the stable MCI (sMCI) and progressive MCI (pMCI) participants. The rightmost column show the p-values for the comparisons, and bolded and marked with an asterisk if significant.

	sMCI	pMCI	p-value
N	64	42	
Sex	20M/44F	18M/26F	0.1489
Age	73.5±5.3	75.7±4.8	0.5924
MMSE	27.0±2.4	25.9±2.9	0.1988
Delayed recall test	6.8±7.1	2.3±4.3	0.1489
Total grey matter volume (eTIV-normalized)	0.290±0.020	0.270±0.021	0.0700
Hippocampus volume (eTIV-normalized)	0.005±0.001	0.004±0.001	$\mathbf{2.7 \cdot 10^{-4}*}$
Left Cingulum tract FA	0.522±0.036	0.515±0.030	0.3838
Right Cingulum tract FA	0.491±0.028	0.486±0.028	0.1489
Left Inferior Logitudinal tract FA	0.491±0.025	0.470±0.090	0.1489
Right Inferior Longitudinal tract FA	0.496±0.028	0.471±0.091	0.1489

Table A.2: Complete statistical report on the whole-brain dynamicity between HC and SCD linear regression models. Significant FDR corrected (q = 0.05) p-values have an asterisk. SE: standard error; HC: Healthy control, SCD: Subjective cognitive decline.

		HC vs SCD			
		β-value	SE	t -Stat	p-value
Theta	Intercept	0.7213	0.0219	32.9151	$3.3{\cdot}10^{-84}$*
	Group	-0.002	0.0028	-1.0414	0.3586
	Age	0.0007	0.0003	2.1683	0.0536
	Sex	-0.0098	0.0029	-3.4344	0.0021*
Alpha	Intercept	0.7645	0.0200	38.2401	$9.4{\cdot}10^{-96}$*
	Group	-0.0037	0.0026	-1.4443	0.2002
	Age	0.0004	0.0003	1.3280	0.2387
	Sex	-0.0073	0.0026	-2.8216	0.0126*
Beta	Intercept	0.5117	0.0380	13.5039	$9.3{\cdot}10^{-30}$*
	Group	-0.0041	0.0049	-0.8455	0.4631
	Age	0.0002	0.0005	0.3281	0.7869
	Sex	-0.0118	0.0049	-2.3929	0.0333*

Table A.3: Complete statistical report on the whole-brain dynamicity between HC and MCI linear regression models. Significant FDR corrected (q = 0.05) p-values have an asterisk. Significant effects of the "Group" variable were found in the alpha and beta bands, with their corrected p-values highlighted in yellow. SE: standard error; HC: Healthy control, MCI: Mild cognitive impairment.

		HC vs MCI			
		β-value	SE	t -Stat	p-value
Theta	Intercept	0.7237	0.0197	36.7891	$2.8{\cdot}10^{-100}$*
	Group	-0.0033	0.0026	-1.2438	0.2666
	Age	0.0006	0.0003	2.2173	0.0496*
	Sex	-0.0079	0.0026	-3.1072	0.0054*
Alpha	Intercept	0.7606	0.0177	43.0197	$2.4{\cdot}10^{-114}$*
	Group	-0.0099	0.0024	-4.2026	**0.0001***
	Age	0.0004	0.0003	1.7300	0.1274
	Sex	-0.0075	0.0023	-3.2637	0.0035*
Beta	Intercept	0.5068	0.0348	14.5677	$2.7{\cdot}10^{-34}$*
	Group	-0.0187	0.0046	-4.0266	**0.0003***
	Age	0.0002	0.0005	0.5008	0.6731
	Sex	-0.0117	0.0045	-2.6009	0.0209*

Table A.4: Complete statistical report on the whole-brain dynamicity between SCD and MCI linear regression models. Significant FDR corrected (q = 0.05) p-values have an asterisk. Significant effects of the "Group" variable were found in the alpha and beta bands, with their corrected p-values highlighted in yellow. SE: standard error; SCD: Subjective Cognitive Decline, MCI: Mild cognitive impairment.

		SCD vs MCI			
		β-value	SE	t -Stat	p-value
Theta	Intercept	0.7615	0.0215	35.4265	$2.0{\cdot}10^{-80}$*
	Group	0.0018	0.0032	0.5507	0.6554
	Age	$3.5{\cdot}10^{-5}$	0.0003	0.1197	0.9307
	Sex	-0.0085	0.0033	-2.6098	0.0209*
Alpha	Intercept	0.7854	0.0195	40.2988	$6.8{\cdot}10^{-89}$*
	Group	-0.0049	0.0029	-1.6947	0.1324
	Age	$2.0{\cdot}10^{-5}$	0.0003	0.0752	0.9401
	Sex	-0.0074	0.0029	-2.5170	0.0255*
Beta	Intercept	0.5812	0.0376	15.4717	$8.3{\cdot}10^{-34}$*
	Group	-0.0110	0.0056	-1.9783	0.0774
	Age	-0.0009	0.0005	-1.6685	0.1343
	Sex	-0.0120	0.0057	-2.1213	0.0578

Table A.5: Complete statistical report from the stable MCI (sMCI) and progressive MCI (pMCI) linear regressions. No grouping variable had a significant effect after FDR correction (q = 0.05).

		sMCI vs pMCI			
		β-value	SE	t -Stat	p-value
Theta	Intercept	0.7213	0.0219	32.9151	$3.2{\cdot}10^{-46}$*
	Group	-0.0029	0.0028	-1.0414	0.9607
	Age	0.0007	0.0003	2.1683	0.8888
	Sex	-0.0098	0.0029	-3.4344	0.2729
Alpha	Intercept	0.7645	0.0200	38.2401	$5.6{\cdot}10^{-51}$*
	Group	-0.0037	0.0026	-1.4443	0.4833
	Age	0.0004	0.0003	1.3280	0.6584
	Sex	-0.0073	0.0026	-2.8216	0.1050
Beta	Intercept	0.5119	0.0379	13.5039	$1.8{\cdot}10^{-17}$*
	Group	-0.0041	0.0049	-0.8455	0.6584
	Age	0.0002	0.0005	0.3281	0.6584
	Sex	-0.0118	0.0049	-2.3929	0.2729

Table A.6: List of the regions of interest (ROI) of the Automated Anatomical Labeling (AAL) atlas Tzourio-Mazoyer et al., 2002 contained in the significant cluster found between the HC and MCI groups in the alpha band. Only the ROIs whose volume overlapped at least 10% with the cluster were included in the list. Green corresponds to frontal lobe areas, blue to temporal lobe areas and magenta to limbic lobe areas.

Area Name	% of ROI contained in the cluster	% of cluster
Left Middle Frontal gyrus, Orbital	100.00%	8.97%
Left Inferior Temporal gyrus	29.17%	8.97%
Right Middle Frontal gyrus, Orbital	85.71%	7.69%
Left Superior Frontal gyrus, Medial Orbital	100.00%	7.69%
Left Middle temporal gyrus	13.64%	7.69%
Left Inferior Frontal gyrus, Orbital	41.67%	6.41%
Right Superior Frontal gyrus, Medial Orbital	100.00%	6.41%
Left Temporal pole, Superior Temporal gyrus	50.00%	6.41%
Left Temporal pole, Middle temporal gyrus	71.43%	6.41%
Left Gyrus Rectus	50.00%	5.13%
Left Fusiform gyrus	26.67%	5.13%
Left Superior Frontal gyrus	11.11%	3.85%
Left Superior Frontal gyrus, Orbital	66.67%	2.56%
Right Superior Frontal gyrus, Orbital	66.67%	2.56%
Right Gyrus Rectus	50.00%	2.56%
Left Cingulate gyrus, Anterior part	10.53%	2.56%
Left Parahippocampus	25.00%	2.56%
Left Hippocampus	20.00%	1.28%

Table A.7: List of the regions of interest (ROI) of the Automated Anatomical Labeling (AAL) atlas contained in the significant cluster found between the HC and MCI groups in the beta band. Only the ROIs whose volume overlapped at least 10% with the cluster were included in the list. Blue corresponds to temporal lobe areas, yellow to parietal lobe areas, green to frontal lobe areas, magenta to limbic lobe areas, and red to occipital lobe areas.

Area Name	% of ROI contained in the cluster	% of cluster
Right Superior Temporal gyrus	81.48%	9.40%
Left Middle temporal gyrus	34.09%	6.41%
Left Precuneus	50.00%	5.98%
Left Superior Temporal gyrus	70.00%	5.98%
Right Postcentral gyrus	39.39%	5.56%
Left Inferior Temporal gyrus	50.00%	5.13%
Left Inferior Frontal gyrus, Orbital	66.67%	3.42%
Right Middle temporal gyrus	21.62%	3.42%
Left Cingulate gyrus, Middle part	43.75%	2.99%
Left Temporal pole, Superior Temporal gyrus	70.00%	2.99%
Left Middle Frontal gyrus, Orbital	85.71%	2.56%
Right Rolandic operculum	54.55%	2.56%
Left Insula	42.86%	2.56%
Left Calcarine fissure and surrounding cortex	30.00%	2.56%
Right Supramarginal gyrus	60.00%	2.56%
Right Paracentral lobule	75.00%	2.56%
Left Temporal pole, Middle temporal gyrus	85.71%	2.56%
Left Superior Frontal gyrus, Medial Orbital	83.33%	2.14%
Right Insula	35.71%	2.14%
Left Cingulate gyrus, Anterior part	26.32%	2.14%
Right Superior Parietal gyrus	27.78%	2.14%
Right Precuneus	23.81%	2.14%
Left Gyrus Rectus	50.00%	1.71%
Left Hippocampus	80.00%	1.71%
Left Fusiform gyrus	26.67%	1.71%
Right Inferior Parietal gyrus	36.36%	1.71%
Left Supplementary Motor area	12.50%	1.28%
Left Cingulate gyrus, Posterior part	60.00%	1.28%
Left Superior Frontal gyrus, Orbital	66.67%	0.85%
Left Rolandic operculum	40.00%	0.85%
Left Olfactory cortex	100.00%	0.85%
Right Superior Frontal gyrus, Medial Orbital	40.00%	0.85%
Left Parahippocampus	25.00%	0.85%
Left Cuneus	18.18%	0.85%
Right Heschl's gyrus	100.00%	0.85%
Right Olfactory cortex	25.00%	0.43%
Right Gyrus Rectus	25.00%	0.43%
Left Paracentral lobule	11.11%	0.43%
Left Heschls gyrus	33.33%	0.43%
Right Temporal pole, Superior Temporal gyrus	12.50%	0.43%

A.2 Supplementary Figures

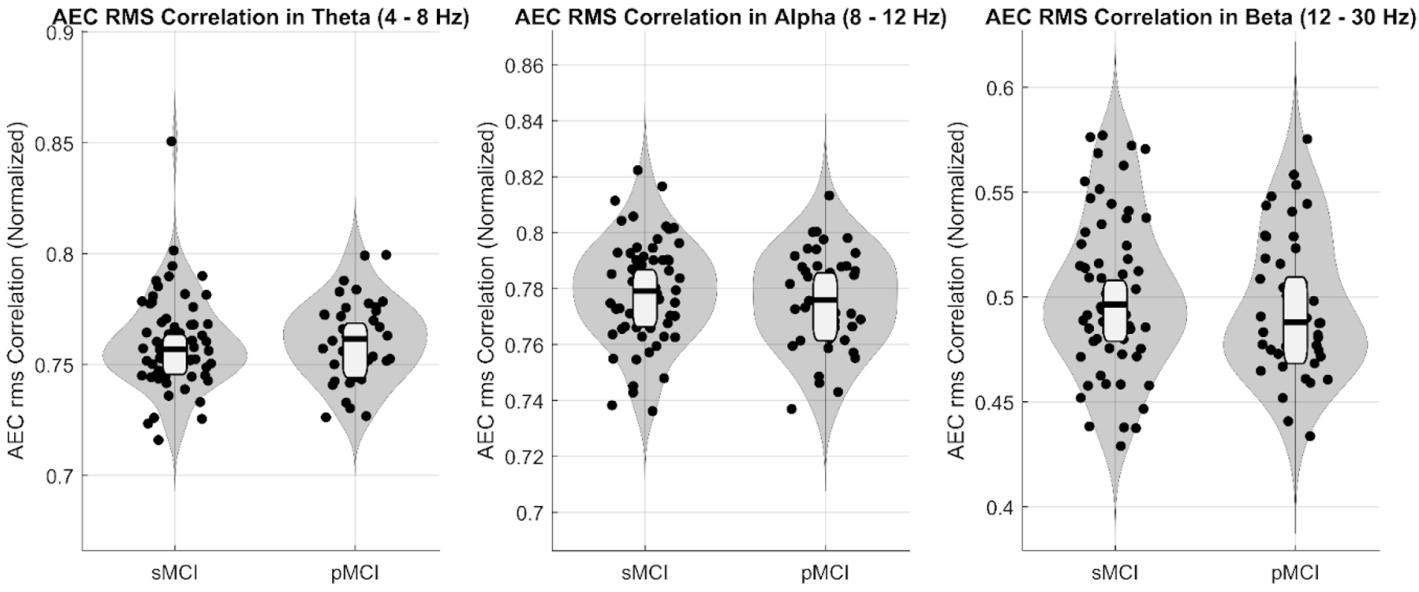


Figure A.1: Violin plots depicting whole-brain dynamicity in the stable MCI (sMCI) and progressive MCI (pMCI) groups. No significant differences were found.

Appendix B

Supplementary material for Chapter 3

B.1 Supplementary tables

Table B.1: Linear regression results for the model number 1 ($dFC\ 1 + Age + sFC$). SE stands for standard error, sFC for static functional connectivity and FA fmi for fractional anisotropy of the forceps minor.

Model 1: dFC ~ 1 + Age + sFC

	β-value	SE	t-Statistic	p-value
Intercept	0.8841	0.2961	2.9858	0.0039
Age	0.0021	0.0011	1.8169	0.0735
sFC	2.7714	1.1914	2.3261	0.0229
R-squared: 0.107, Adjusted R-Squared: 0.082				
F-statistic vs. constant model: 4.21, p-value = 0.0187				

Table B.2: Linear regression results for the model number 2 ($dFC\ 1 + p - tau231 + sFC$). SE stands for standard error, sFC for static functional connectivity and FA fmi for fractional anisotropy of the forceps minor.

Model 2: dFC ~ 1 + p-tau231 + sFC

	β-value	SE	t-Statistic	p-value
Intercept	1.010	0.2474	4.0809	0.0001
p-tau231	0.0002	$4.0{\cdot}10^{-5}$	5.2338	$1.7{\cdot}10^{-6}$
sFC	2.4373	1.0342	2.3568	0.0212
R-squared: 0.328, Adjusted R-Squared: 0.309				
F-statistic vs. constant model: 17.1, p-value = $9.0{\cdot}10^{-7}$				

Table B.3: Linear regression results for the model number 2 ($dFC\ 1 + p - tau231 + sFC + FAfmi$). SE stands for standard error, sFC for static functional connectivity and FA fmi for fractional anisotropy of the forceps minor.

Model 3: dFC ~ 1 + p-tau231 + sFC + FA fmi

	β-value	SE	t-Statistic	p-value
Intercept	1.1899	0.2838	4.1934	$8.5{\cdot}10^{-5}$
p-tau231	0.0002	$4.0{\cdot}10^{-5}$	5.0925	$3.3{\cdot}10^{-6}$
sFC	2.6564	1.0455	2.5408	0.0135
FA fmi	-0.5698	0.2905	-1.9617	0.0541

R-squared: 0.389, Adjusted R-Squared: 0.361

F-statistic vs. constant model: 13.8, p-value = $4.6{\cdot}10^{-7}$

Appendix C

Supplementary material for Chapter 4

C.1 Supplementary tables

Table C.1: Distribution of reported adverse effects of tACS by group. No significant between-group differences were observed.

	Stim	Sham	t-stat	p-value
Headache	1.28 ± 0.61	1.17 ± 0.39	0.5804	0.567
Neckache	1.07 ± 0.27	1.08 ± 0.29	-0.1091	0.914
Pain in the scalp	1 ± 0	1 ± 0	0	1
Tingling	2 ± 0.78	1.83 ± 0.72	0.5614	0.5797
Stinging sensation	1.64 ± 0.63	1.58 ± 0.67	0.2329	0.8178
Burning sensation	1.21 ± 0.43	1.25 ± 0.45	-0.2072	0.8376
Skin reddening	1 ± 0	1 ± 0	0	1
Drowsiness	2.07 ± 0.83	2.25 ± 0.75	-0.5708	0.5735
Troubled focusing	1 ± 0	1 ± 0	0	1
Mood swings	1 ± 0	1 ± 0	0	1

Table C.2: Complete statistical report for the sFC and dFC comparisons at the DMN. FDR correction (q = 0.1, $n_{comparisons} = 24$) yielded a critical p-value of 0.0194. Results from the sFC are shown in the first 4 rows, while dFC results are displayed in the last 4. Significant resultsa after FDR are bolded.

		2-sample ratio t-test			Repeated-measures t-test						
		Verum vs Sham			*Verum*			*Sham*			
	Areas	Cohen's d	t-stat	p-value	Cohen's d	t-stat	p-value	Cohen's d	t-stat	p-value	
AEC-c	DMN-DMN	-1.1257	-2.8614	**0.0086***	-0.6383	-3.9109	**0.0018***	0.1456	0.6828	0.5089	sFC
	DMN-AAL	-1.0663	-2.7104	**0.0122***	-0.3966	-3.2451	**0.0064***	0.2365	1.1133	0.2893	
ci-PLV	DMN-DMN	-0.7935	-2.0171	0.055	-0.4207	-2.6658	**0.0194***	0.2132	0.8127	0.4336	
	DMN-AAL	-0.7257	-1.8447	0.0775	-0.2776	-2.0841	0.0574	0.2091	0.9598	0.3578	
AEC-c	DMN-DMN	-0.1939	-0.4929	0.6265	0.4755	3.4317	**0.0045***	0.6615	3.2022	**0.0084***	dFC
	DMN-AAL	0.2144	0.5449	0.5909	-0.6145	5.4827	**0.0001***	0.5813	2.9012	**0.0144***	
ci-PLV	DMN-DMN	-0.3412	-0.8674	0.3943	0.0702	-0.9530	0.3580	0.1116	0.4504	0.6612	
	DMN-AAL	-0.3816	-0.9701	0.3417	-0.1581	-1.1482	0.2716	0.1054	0.5058	0.6230	

Table C.3: Complete statistical report for the links between the areas of the DMN for AEC-c. FDR correction (q = 0.1, $n_{comparisons}$ = 28) yielded a critical p-value of 0.0244. Significant results are bolded. SFG: superior frontal gyrus; ACC: anterior cingulate cortex; PCC: posterior cingulate cortex; Hip: hippocampus; IPG: inferior parietal gyrus; PCU: precuneus.

	2-sample ratio t-test		
	Stim vs Sham		
	AEC-c		
Areas	Cohen's d	t-stat	p-value
SFG-SFG	-0.3482	-0.885	0.3849
SFG-Rectus	-0.4279	-1.0876	0.2876
SFG-ACC	-0.2699	-0.6862	0.4992
SFG-PCC	-0.0237	-0.0602	0.9525
SFG-Hip	-0.5766	-1.4657	0.1557
SFG-IPG	-0.2536	-0.6446	0.5253
SFG-PCU	-0.5732	-1.457	0.1581
Rectus-Rectus	-0.0517	-0.1315	0.8965
Rectus-ACC	-0.3582	-0.9104	0.3717
Rectus-PCC	-0.1161	-0.2951	0.7705
Rectus-Hip	-0.8434	-2.1439	0.0424
Rectus-IPG	-0.5172	-1.3148	0.201
Rectus-PCU	-1.0924	-2.7768	**0.0105***
ACC-ACC	-0.4529	-1.1513	0.2609
ACC-PCC	-0.3933	-0.9998	0.3274
ACC-Hip	-0.9447	-2.4013	**0.0244***
ACC-IPG	-0.0915	-0.2326	0.8181
ACC-PCU	-1.1466	-2.9146	**0.0076***
PCC-PCC	-1.2553	-3.191	**0.0039***
PCC-Hip	-0.4275	-1.0868	0.2879
PCC-IPG	-0.5013	-1.2743	0.2148
PCC-PCU	-1.1999	-3.0501	**0.0055***
Hip-Hip	-0.6826	-1.7352	0.0955
Hip-IPG	-0.6421	-1.6322	0.1157
Hip-PCU	-0.4328	-1.1003	0.2821
IPG-IPG	-1.0074	-2.5607	**0.0172***
IPG-PCU	-0.2576	-0.6547	0.5189
PCU-PCU	-1.3268	-3.3726	**0.0025***

Table C.4: Complete statistical report for the links between the areas of the DMN for ci-PLV. No comparisons survived FDR correction (q = 0.1, $n_{comparisons} = 28$). SFG: superior frontal gyrus; ACC: anterior cingulate cortex; PCC: posterior cingulate cortex; Hip: hippocampus; IPG: inferior parietal gyrus; PCU: precuneus.

	2-sample ratio t-test		
	Stim vs Sham		
	ci-PLV		
Areas	Cohen's d	t-stat	p-value
SFG-SFG	-0.5841	-1.4847	0.1506
SFG-Rectus	-0.6596	-1.6766	0.1066
SFG-ACC	-0.7898	-2.0075	0.0561
SFG-PCC	0.0056	0.0142	0.9888
SFG-Hip	-0.3283	-0.8345	0.4122
SFG-IPG	-0.7473	-1.8995	0.0696
SFG-PCU	-0.5195	-1.3207	0.1991
Rectus-Rectus	-0.5375	-1.3662	0.1845
Rectus-ACC	-0.6513	-1.6555	0.1108
Rectus-PCC	-0.1275	-0.324	0.7487
Rectus-Hip	-0.7375	-1.8746	0.0731
Rectus-IPG	-0.9007	-2.2894	0.0311
Rectus-PCU	-0.5727	-1.4558	0.1584
ACC-ACC	-0.784	-1.9929	0.0578
ACC-PCC	-0.2482	-0.6309	0.5341
ACC-Hip	-0.8251	-2.0973	0.0467
ACC-IPG	-0.992	-2.5215	0.0187
ACC-PCU	-0.6407	-1.6287	0.1164
PCC-PCC	0.375	0.9533	0.3500
PCC-Hip	-0.2255	-0.5731	0.5719
PCC-IPG	-0.1894	-0.4816	0.6345
PCC-PCU	0.1362	0.3463	0.7321
Hip-Hip	-0.6111	-1.5533	0.1334
Hip-IPG	-0.6471	-1.6449	0.113
Hip-PCU	-0.1577	-0.4009	0.692
IPG-IPG	-0.5876	-1.4936	0.1483
IPG-PCU	-0.2485	-0.6316	0.5336
PCU-PCU	0.4566	1.1606	0.2572

C.2 Supplementary instructions

Simulation on tACS phase shift effects on functional connectivity (FC) To study the possible effects of phase disparities introduced by tACS in the brain cortex over both phase and amplitude FC, we simulated MEG signals, adding to them two stimulatory sinusoid time series with different phase shifts, and finally calculated the phase locking-value (PLV) and the amplitude envelope correlation (AEC). All the analyses were performed in MATLAB R2021B.

The complete process took the following steps:

1. Configuration for the signal's simulation.

```
% Parameters
Fs = 1000;                          % Sampling rate
T = 8;                              % Duration in seconds
filter_low = 8;                     % Lower bound of filter
filter_high = 12;                   % Upper bound of filter
filter_order = 1800;                % Filter order
sin_freq = 10;                      % Frequency of the stimulation
                                    sinusoidal signals
phases = [0, pi/8, pi/4, 3*pi/8, pi/2, 5*pi/8, 3*pi/4, 7*pi/8, pi,
9*pi/8, 5*pi/4, 11*pi/8, 3*pi/2, 13*pi/8, 7*pi/4, 15*pi/8, 2*pi];
                                    % Different phase differences
amp_sin = 0.5                       % The amplitude of the stimulation
                                    sinusoids will be 25% of the mean
                                    amplitude of the physiological
                                    signal.
amp_noise = 0.5                     % The amplitude of the noise signals
                                    will be 50% of that of the physiological
                                    signal.
```

The sampling rate, duration of the signal and the filter order were selected so that they would fit the parameters of the experimental signal and processing of the study. Given that the study is focused on the alpha band, the signals were filtered between 8 and 12 Hz, and the frequency for the stimulation sinusoids was set to 10 Hz, emulating the study setting. The phase vector included 17 values in the interval [0, 2π].

2. White noise signal generation.

```
% Generate random signals
n = Fs * T;                    % Number of samples
meg1    = randn(1, n);         % Basis for the physiological signals
meg2    = randn(1, n);         % Basis for the 1st noisy signal
meg3    = randn(1, n);         % Basis for the 2nd noisy signal
```

We generate our signals from a normal distribution centered in 0 and with a standard deviation of 1. We generate 3 signals to later create two physiological signals by combining *meg1* and *meg2*, and *meg1* and *meg3*, respectively.

3. Filtering of the signals.

```
% Filter signals between 8 and 12 Hz
d = designfilt('bandpassfir', 'FilterOrder', filter_order, ...
'CutoffFrequency1', filter_low, 'CutoffFrequency2', filter_high, ...
'SampleRate', Fs);
filtered_signal1 = filtfilt(d, meg1);
filtered_signal2 = filtfilt(d, meg2);
filtered_signal3 = filtfilt(d, meg3);
```

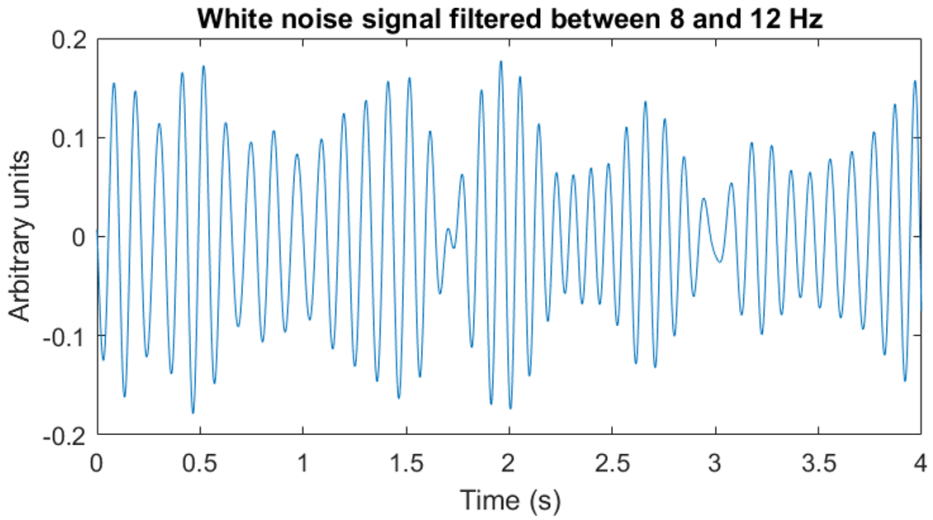


Figure C.1: Example of a filtered artificial signal between 8 and 12 Hz.

The filter is designed to have cutoff frequencies of 8 and 12 Hz, and a filter order of 1800. Then the white noise signals are zero-phased filtered using the *filtfilt* function.

4. Padding removal.

```
% Remove 2 seconds of padding (2000 samples) from the beginning and end
filtered_signal1 = filtered_signal1(2001:end-2000);
filtered_signal2 = filtered_signal2(2001:end-2000);
filtered_signal3 = filtered_signal3(2001:end-2000);
```

2 seconds are eliminated from the beginning and the end of the signal, so there is no border effect on the simulated signals.

5. Stimulation sinusoid amplitude determination.

```
% 50% peak-to-peak is 25% of amplitude
amp_sine = amp_sine * mean(abs(filtered_signal1));
```

The peak-to-peak amplitude for the stimulation sinusoids is 50% of the mean of the absolute value of the signal (necessary, since the estimated mean of the signal should be close to zero).

6. Combination of white noise signals to create two "physiological" signals.

```
% Combine together original and noisy signals
combined_signal1 = filtered_signal1 + amp_noise * filtered_signal2;
combined_signal2 = filtered_signal1 + amp_noise * filtered_signal3;
```

Then we combine the signals, so that the resulting couple of signals have some synchronization, but they still are different. Given that amp_noise is 0.5, then the resulting signals have 66.6% in common.

7. Time vector generation.

```
% Generate time vector
t = (0:length(filtered_signal1)-1) / Fs;
```

8. Initialization of the PLV and AEC vectors.

```
% Initialize arrays to store PLV and AEC values
PLV_values = zeros(1, length(phases)+1);
AEC_values = zeros(1, length(phases)+1);
```

The vector where the connectivity values are will be stored have one extra space to save the FC between the signals with no stimulation involved (baseline FC).

9. Baseline FC calculation between "physiological" signals.

```
% Calculate Phase Locking Value (PLV)
phase_diff = angle(hilbert(combined_signal1)) - ...
angle(hilbert(combined_signal2));
PLV_values(1) = abs(mean(exp(1j * phase_diff)));

% Calculate Amplitude Envelope Correlation (AEC)
envelope1 = abs(hilbert(combined_signal1));
envelope2 = abs(hilbert(combined_signal2));
AEC_values(1) = corr(envelope1', envelope2');
```

The baseline FC values are calculated from the two "physiological" signals, by calculating the average phase difference in the case of the PLV, and the correlation between the signals' envelopes in the case of the AEC.

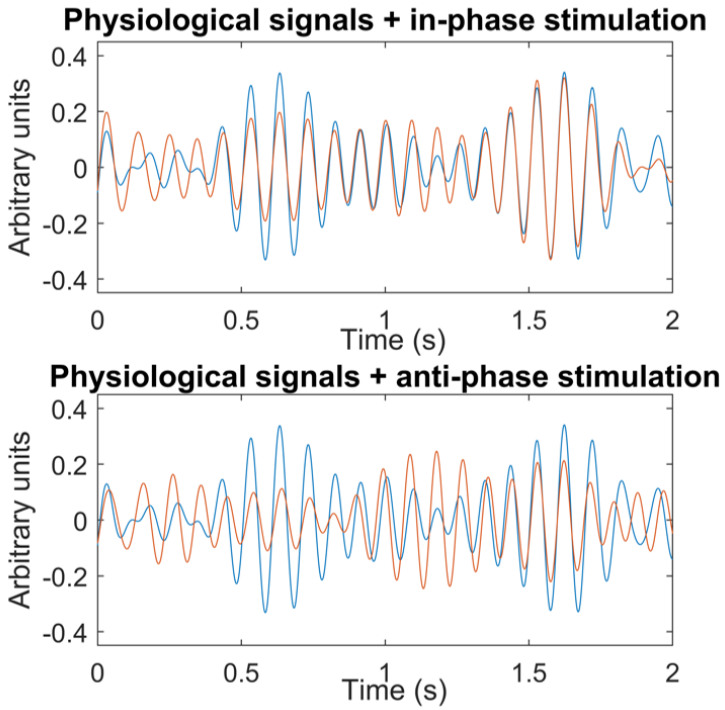


Figure C.2: Combined signals at in-phase stimulation (top), and out-of-phase (π phase difference, bottom) stimulation.

10. Loop for iterative addition of differently phase-shifted stimulation sinusoids.

A. Generation of the stimulation sinusoids.

```
% Generate sinusoidal signals with specified phase difference
    sinusoid1 = amp * sin(2 * pi * sin_freq * t);
```

```
    sinusoid2 = amp * sin(2 * pi * sin_freq * t + phases(i));
```

B. Combination of the physiological signals and the stimulation sinusoids (Figure C.2).

```
% Add sinusoidal signals to filtered signals
    combined_signal1 = filtered_signal1 + sinusoid1 ...
    + ampNoise * filtered_signal2;
    combined_signal2 = filtered_signal1 + sinusoid2 ...
    + ampNoise * filtered_signal3;
```

C. Calculation and storage of the PLV and AEC values.

```
% Calculate Phase Locking Value (PLV)
    phase_diff = angle(hilbert(combined_signal1)) - ...
    angle(hilbert(combined_signal2));
    PLV_values(i+1) = abs(mean(exp(1j * phase_diff)));

    % Calculate Amplitude Envelope Correlation (AEC)
    envelope1 = abs(hilbert(combined_signal1));
    envelope2 = abs(hilbert(combined_signal2));
    AEC_values(i+1) = corr(envelope1', envelope2');
```

This process was repeated over 100 times, so that we could obtain distributions of the influence of phase shifts over FC. Finally, repeated measures t-test were carried out between the no-stimulation condition and the in-phase stimulation (phase shift between signals = 0), and between the no-stimulation condition and the anti-phase stimulation (phase shift between signals = π), as shown in Figure C.3.

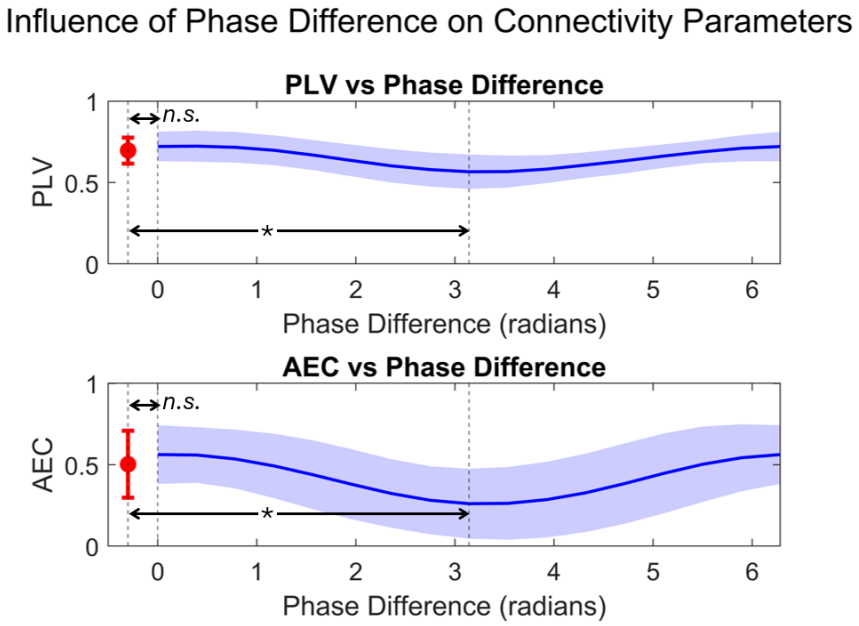


Figure C.3: Relation between PLV and AEC and the phase difference between stimulation sinusoids. Significant reductions between antiphase stimulation and initial connectivity (red) were found and are indicated by an asterisk. N.s: non-significant.